UNIVERSITY OF SOUTHAMPTON

STABILISING SHIPS FOR HELICOPTER OPERATIONS

Martyn Paul Prince

Thesis submitted in candidature for the degree of
Doctor of Philosophy

Ship Science
School of Engineering Sciences
Faculty of Engineering and Applied Science
December 2000

UNIVERSITY OF SOUTHAMPTON

ABSTRACT

FACULTY OF APPLIED SCIENCE AND ENGINEERING
SCHOOL OF ENGINEERING SCIENCES, SHIP SCIENCE

Doctor of Philosophy

STABILISING SHIPS FOR HELICOPTER OPERATIONS

by Martyn Paul Prince

Helicopter landing and its subsequent handling on warships has developed into a necessity for the operational effectiveness of modern day small naval vessels. Increasingly, there is a demand for larger helicopters to be deployed from smaller warships. With this trend, the importance of efficient landing, entrapment and handling has increased dramatically.

The overall objective of this work was to develop systems that would lead to increases in shipborne helicopter operational limits and to develop tools with which to quantify their performance.

This has been accomplished by minimising ship motions by way of a H_∞ lateral force estimator (LFE) controller. This controller exhibited improved performance over the conventional type controllers frequently used on modern day vessels. A H_∞ LFE controller has been developed that produced both good roll and LFE attenuation using a structured design approach, which out performed a classic parallel proportional integral derivative (PID) controller. The H_∞ control method proved to have advantages over more conventional approaches resulting from adaptability of the design. This benefitted the motion attenuating performance and lead to properties such as reduced fin activity at higher frequencies.

An experimental set up has been developed that was used successfully to test H_∞ roll controllers and classical frequency response roll controllers using a small scale towed ship model. The H_∞ roll controllers were found to yield similar overall roll attenuating performance in comparison to the classic controllers tested. The results from this were also used to validate a ship motion package. The software was then used to quantify the controller performances numerically.

A numerical dynamic model of a helicopter on the flight deck was developed in order to test the effects of ship motion reduction on helicopter stability. The model contains representations of non-linear oleos, tyres, wind, ship motions and decklocks and therefore can be used to determine helicopter operational limits in various conditions. Using this dynamic model, controlled ship motions were shown to reduce significantly helicopter loadings and therefore increase aircraft on deck stability, with H_∞ LFE control resulting in lower loads than classic roll control.

From these individual areas, a route has been created that allows ship roll and LFE fin controllers using various control methods to be derived, tested numerically to determine the resultant ship motions and to test the controllers overall effect on helicopter on-deck stability.

Acknowledgments

There are many people who have given me time and support throughout this project, to them I am extremely grateful.

I owe special thanks to my supervisor Philip Wilson for his continuous encouragement and guidance.

To all the staff and postgrads of the Ship Science Department (now part of the School of Engineering Sciences) for creating the working environment in which to conduct research, during my time there.

To my colleagues at the Wolfson Unit M.T.I.A. for tolerating my unusual working schedules, and the endless supply of tea.

To my parents for providing me with so much help throughout my entire education.

And finally to Marie, for her constant encouragement and support and managing to put up with me.

Contents

1 Introduction

Helicopter landing and its subsequent handling on warships has developed into a necessity for the operational effectiveness of modern day naval frigates. Increasingly, there is a demand for larger helicopters to be deployed from smaller warships, with this trend the importance of efficient landing, entrapment and handling has increased dramatically.

The most recent example of large aircraft operating from small warships involves landing the EH-101 *'Merlin'* on the flight deck of a Type 23 frigate. From previous use of the *Lynx* helicopter on these ships, a system has been adapted that suits the operations and properties of this helicopter. The differences between the *Lynx* and *Merlin* are extreme, making much of the existing practice ineffective, and probably operationally impossible with current systems. The scale of the challenge can be seen from the photograph of a Type 23 with Merlin on its flight deck in figure 1.

Small warships experience greater motions and accelerations than their larger counterparts, making aircraft landing much more difficult in an equivalent sea state. The flight deck areas are intrinsically smaller, also the hangar volumes are reduced. This makes movement of the aircraft on deck, into and in the hangar much more restricted.

Larger helicopters bring problems involving the accuracy of landing, combined with reduced manoeuvrability in the air and on the deck. Achieving accurate landings is critical due to the limited area upon the flight deck.

All this combines to make the landing and entrapment phase more time consuming and hazardous, therefore systems to improve this situation are necessary.

The overall objective of this work is to improve systems that would lead to possible increases in shipborne helicopter effectiveness, with the aim to extend current sea state limitations and to develop tools and methods with which quantify their performance. The result of this will be an increase in the safety of current practice, and to improve the overall helicopter availability to higher sea states. This extends the aircraft's use as a tactical tool.

There is a broad scope to this objective, so it has therefore been broken down into a number of key problem areas:

- Prediction of future ship motions
- Deck handling systems
- Minimisation of ship motions
- Helicopter modelling

Deck handling system improvements have not been addressed in this thesis, but work has been carried out in this field by the author, in references [1] and [2].

These areas of research not only have relevance to the use of aircraft from warships, but on a number of motion sensitive tasks for both military and civil vessels.

1.1 Scope of Work

The thesis consists of the following major sections;

1.1.1 Literature Review

A comprehensive literature review has been provided in the first section. It is hoped that it contains a fair representation of the work carried out in these fields of research, as well as introducing methods and approaches used in other related disciplines that may be utilised for this example. For instance; many of the control methods investigated have been used for autopilots and in other control areas.

It can be seen in this chapter that extensive work has been carried out previously in areas of ship motion control and modelling the ship/helicopter dynamic interface, but the area of prediction of quiescent periods and ship motions is quite limited.

1.1.2 Prediction of Quiescent Periods

These periods of time relate to a duration in which the ship motions allow safe landing of the helicopter. The larger, heavier helicopters currently being developed need longer periods, with existing predictive methods being only appropriate in particular conditions. Therefore with the increased predictive times needed, new approaches must be found.

It was considered essential, to obtain information from the sea surface, to aid the predictive process. Technology is currently being developed to measure remotely the sea surface so it was from this, combined with knowledge of sea waves that a prediction of the sea surface at a future point in time could be attempted. From this, the ship motions could be determined to within the order of accuracy needed to produce a quiescent period length forecast.

It was with this in mind, that the wavelet analysis approach was investigated, due to their properties of identifying localised signal components and non-stationary signal analysis. The limitations caused by the frequency de-

pendence of sea wave propagation in deep water made this approach difficult to implement efficiently, but other interesting properties were identified.

1.1.3 Ship Motion Control

Ship motion attentuation by way of active fin stabilisers is a method extensively used on a variety of vessel types. Almost exclusively, they are used to minimise the ship's roll motion. Lateral force estimator (LFE) has been identified as being a more significant measure of an object's stability upon a vessel, therefore minimising this acceleration at a helicopter's location on a flight deck would increase the aircraft's operation limits.

LFE stabilisation had been studied by Tang and Wilson [3]. This adopted a method broadly based on a frequency response method [4]. The results were better in reducing LFE, than that of the other roll controllers, but essentially used a trial and error procedure to optimise the controllers. This necessitated the development of a new approach to produce an LFE controller. A structured design method was needed, that would determine control coefficients using a repeatable and logical technique. This led to the use of H_∞ control, which necessitated the use of a structured approach, and guaranteed stability and robustness requirements, in the presence of modelling uncertainties. This was an important asset, as the ship model idealisation used for LFE control would be vague in areas outside the natural roll frequency range, especially due to the coupled sway and yaw components and external factors. This allowed control action outside this frequency range to be greatly reduced to avoid possible increases in ship motions resulting from unmodelled dynamics, and also diminished unwanted fin activity that could lead to excessive system wear, for example.

The H_∞ polynomial approach adopted in [5] was used as a proven starting point from which to progress the research. This led to the adoption of a similar approach, that permitted easy implementation of roll and LFE controllers. H_∞ control based methods have been proven in a number of diverse applications such as ship roll control and autopilots [6, 7], to position servo control [8] and microvibration reduction on satellites [9].

One aim of this work was to develop and outline a structured method with which to determine roll and LFE controllers. The first step in this process was to derive an idealisation of the ship dynamics, this is based on the ship system equations of motions for the anti-symmetric degrees of freedom (DOF). This provides a nominal representation of the ship roll or LFE to fin dynamics that are combined with specific weighting functions to form the augmented plant. It is on this that H_∞ control was carried out. Matlab and its toolboxes were used for this task, as they provided software

that already incorporated the complex formulations.

From this, a number of controllers were developed, which needed to be assessed for their motion attenuation performance. This task was carried out using ship motion software [10]. This was based on a standard frequency dependent strip theory resolving the anti-symmetric degrees of freedom of roll, sway and yaw. It includes the effects of controllable fins and rudders in the system equations. This was suitable for uncontrolled and roll stabilised ships. This had to be modified to accept various control formulations.

A classic roll controller was selected using the frequency response approach [4] to be used as a baseline with which to compare subsequent controllers. This also reflected the way in which roll controllers on current vessels are determined.

The H_∞ roll controllers that were developed did not out-perform the classic controller. The relative performances over the frequency range were noticeably different, with the desired reduction in fin activity at higher frequencies for the H_∞ based controller.

The LFE controller had a significant roll and LFE reducing effect, performing better than that of the classic controller. One of the major reasons the H_∞ controller exhibited good roll and LFE reducing performance, resulted from the emphasis of the control activity towards the natural roll frequency and also tended towards the low frequency range. This prevented higher frequency fin activity, which permitted a higher overall gain to be selected. A number of variations were tested and compared.

1.1.4 Experimentation

A system has been constructed and adapted with hardware and software that allows roll fin control of scaled ship models. This was considered essential, as a means of evaluating controller and fin performance. To allow the testing of controllers in an environment more akin to that experienced by the actual vessels, unconstrained by many of the limitations and approximations made in numerical approaches.

A scale model with this controllable fin set up was used to investigate both classic and H_∞ roll controllers. The different controllers produced similar roll attenuating performance. These results were also used to validate the ship motion package [10]. The program results compared well with the experimental results, providing a solid base with which to evaluate subsequent controller designs.

1.1.5 Dynamic Ship/Helicopter Modelling

The ship motion reductions alone do not provide a direct indication of the helicopter's stability, necessitating the use of a dynamic model to investigate the loadings upon the aircraft. It is not only the anti-symmetric ship motions that affect helicopter stability, but heave and pitch, aerodynamic loads and use of entrapment and handling devices all contribute.

This led to the development of a dynamic model of a helicopter on a ship flight deck. It incorporated non-linear oleo modelling, representations of tyres, aerodynamic loading, entrapment device and ship motions. This was used to evaluate the effect of various control strategies on helicopter loading and stability. From this, the safety of the helicopter on-deck can be assessed to provide a measure of its increased availability in a range of sea states. The overall motion reductions of the H_∞ controller clearly reduced helicopter loadings. The ship motions available through the ship motion software [10], could not validly be extended to high sea states due to its linear assumptions. Despite this, the motions provided do give a good indication of the controllers relative performance in more extreme sea conditions.

Helicopter operability can be improved by alternative control methods, with a H_∞ LFE controller over a classical frequency response roll controller described in this thesis. This improved operability will translate to safer helicopter operation and availability in higher sea states.

This is not only relevant to helicopters landing on ships, but for other motion sensitive activities such as weapons deployment, refuelling and many oceanographic related tasks such as the deployment and retrieval of ROVs, arrays and other instrumentation.

From these individual areas, a route has been created that allows ship roll and LFE fin controllers to be derived, tested numerically to determine the resultant ship motions, and finally to test the controllers overall effect on helicopter on-deck stability.

1.1.6 Contribution of this Research Work

This research has introduced experimental ship model testing as a means of exploring roll controller performance. In this case H_∞ roll controllers have been investigated and found to yield similar roll attenuating performance in comparison to a classic frequency response controller. This necessitated the development of an experimental set up suitable to test these roll controllers.

A H_∞ LFE controller has been designed that out performs the classic PID roll and LFE controllers in both roll and LFE reduction tested using a numerical ship motion program.

An approach has been taken to investigate the effect of ship motion controller designs on the loadings that will be experienced by a helicopter on the flight deck of a ship. This provides a method of relating controller designs to helicopter stability. This necessitated validation of an existing ship motion code using the results from the experimental tests and forming a dynamic ship helicopter model.

2 Literature Review

2.1 Prediction of Quiescent Periods

2.1.1 Discrete Wavelets

There exists a vast array of literature on wavelets and its associated areas of application, produced since the early 1990s. This has lead to an explosion of activity within the signal processing field, that has filtered down into many scientific and engineering areas.

Major contributors to the subject of wavelets in the late 1980s, were such authors as Daubechies [11] and Mallat [12], to name but a few. They produced a huge quantity of publications, on a variety of aspects relating to the formation and use of *wavelet analysis*.

It must be borne in mind that the subject of real time sea surface analysis has been relatively unexplored, therefore few publications are dedicated to the subject. For areas more akin to the objective of analysis of sea surface information the following publications were investigated.

The article by Bruce et al. [13] provides a good overview of possible applications where wavelet analysis could be and are beneficial. It has been applied to a number of diverse fields such as digital communications, remote sensing, biomedical signal processing and imaging, astronomy and numerical analysis.

The benefits of wavelet analysis over Fourier type analysis are discussed. These are primarily recognised as being the wavelets abilities in identifying discontinuities within a signal structure. This is proven by way of example, by analysing a saw tooth signal. The signal is represented by far fewer wavelet components, than Fourier components. This leads to the use of wavelets for data compression and de-noising applications. A number of commercial and public domain wavelet software packages are also outlined.

Graps [14] gives an introduction on wavelet analysis for those outside the signal processing field, describing applications to which wavelets have been used, for such examples as; data compression of fingerprint data, denoising of data such as nuclear magnetic resonance (NMR) signals and the detection of self-similar behaviour in a time series.

Jay and Flinchem [15] provide a clear marine related application for wavelet analysis. It is used to extract time varying tidal information from current meter data. This technique is of particular use for such tidal currents, as it is suitable for the analysis of non-stationary datasets. Comparisons are made with the classic signal processing tools of Fourier transforms and harmonic analysis, typically used for such applications. It is discussed that

wavelets can identify the position of an event within a tidal cycle. The benefits of wavelets are found to be in the form of a tool that can simultaneously detect wide ranges of frequencies present in tidal current data over a period of weeks or months, but also has the ability to identify characteristics within each tidal cycle ($\approx$ 12 hours).

Newland [16, 17] provides a comprehensive theoretical description of discrete wavelet analysis. Rioul and Vetterli [18] give a general overview of the wavelet field, from continuous to discrete wavelet transform techniques.

Weiss [19] is primarily concerned with the use of wavelet transforms in wideband correlation processing. This approach uses non-orthogonal continuous mother wavelets, whereas most common applications of wavelets use orthogonal functions. In the case of wideband correlation, continuous scaling and time shifting is necessary to identify clearly the returning signal with sufficient accuracy, therefore the efficiencies gained through the use of orthogonality are not achievable. The fact that the orthogonality conditions do not need to be adhered to, increases the variety of mother wavelets (defined on page 31) that may be adopted. This permits the selection of mother wavelets that suit the application. For wideband sonar or radar correlation, the transmitted signal element is used as the mother wavelet with which the returned signal is analysed. This leads to an indication of position and relative velocity of the reflecting object(s), determined from the time delay and signal scale change (Doppler shift) of the returned signal component.

Young [20] also gives a background to wavelet theory, both continuous and discrete with particular attention towards wideband correlation processing.

2.1.2 Harmonic

The harmonic wavelet was introduced by Newland in a series of work [17, 21]. This wavelet is shown to be extremely simple to implement due to the extensive use of FFT routines within the algorithm, this also leads to fast computations. As a result, this wavelet possesses some interesting advantages over other wavelet methods. The harmonic wavelet frequency discrimination is band limited, yielding position information of that disturbance within the signal. Principally these wavelets were created for applications such as vibration analysis.

Musical wavelets were a refinement of the harmonic wavelets with greater frequency band control, and have been reported in [17, 22]. These were named 'musical' due to their possible use in discriminating each note from a signal of music. It is acknowledged that, as the frequency bandwidth of a wavelet is reduced, so the precision of location discrimination is also reduced.

2.2 Lateral Force Estimator (LFE)

It has long been acknowledged that *'ship motions can impair the human operator's ability to work onboard a vessel'* [3]. This results in degradation of crew members' effectiveness, which can lead to a reduced operational efficiency of the vessel. In the case of a warship, this is critical. With increased ship motions, even simple tasks become increasingly more difficult to carry out. There is no doubt that this can be potentially dangerous and significantly reduces the efficiency of the ship's company.

Baitis et al, [23] identified a ship's lateral acceleration (known as LFE) as relating to this loss of balance experienced by crew members. The performance index known as Motion-Induced Interruption Index (MII) incorporating LFE was derived, this was used as a measure of the likelihood of task disruption. Applications based on this parameter are given in [23] and [24].

Lloyd [25] uses LFE to determine the limiting ship motions for safe helicopter operations, where it is suggested that LFE is a very good indication of a crew's motion affected performance. This is also borne out in the work of Monk [26]. Here, LFE is identified as being a motion criterion with which it is possible to reliably compare the seakeeping characteristics of warships. A maximum allowable LFE value of $1.5m/sec^2$ at the bridge was provided as an absolute limit for suitable ship characteristics. From this, it can be concluded that minimisation of LFE would lead to improved ship operation. It was from this, that Tang and Wilson [3] started their extensive work into the minimisation of LFE.

Tang and Wilson[3] investigated LFE stabilisation with both numerical studies and full scale trials. The numerical model was based on a linear strip theory approach, this made it possible to examine the effects of different control coefficients on the resultant ship motions. Using a frequency response method, a system was formed based on a conventional roll stabilisation technique [4]. This replaced the measured roll angle with a measured LFE magnitude in the fin controller transfer function. This system was initially tuned to the natural roll frequency, in the same way as for roll stabilisation. A more favourable stabilisation regime was found when the system was tuned to a lower frequency. LFE stabilisation was shown to be a feasible alternative to roll stabilisation using conventional fins.

The full scale LFE stabilisation trials did not produce any undesirable effects over the conventional roll stabilised case, provided that suitable tuning was achieved. It was suggested that LFE stabilisation causes less disruptive motions than would be encountered during roll stabilisation. Though, it was acknowledged that further validation would be needed to verify this point.

Due to the considerable interest in Rudder Roll Stabilisation (RRS), Tang and Wilson [27] also investigated the use of the rudder as an active surface to stabilise to LFE, this was named Rudder Lateral force estimator Stabilisation (RLS). It was found that RLS was made rather ineffective due to the resultant high frequency responses of the rudder. Therefore, the use of filters to reduce the high frequencies were necessary. The reduction of these frequencies had little effect upon the frequency range of interest which is in the region of the natural roll frequency. The practicality of using such filters was limited due to the phase lag induced, this has been discussed by Baitis and Schmidt [28] and Amerongen et al, [29]. Schmitke [30] also adopted low pass filters, but failed to account for the phase lag in the numerical model used, yielding favourable results, which may not be the case once the lag has been taken into consideration.

Tang and Wilson [3] introduced simple filters into the numerical model. Low pass filtering would cause phase lag, therefore phase lead compensator systems were also investigated, with the aim of counteracting the phase lag. The use of linear low pass filters and Butterworth filters were investigated to eliminate the high frequency feedback, which as predicted produced significant phase lag. All pass filters were then used as phase lead compensators. These were found to reduce the rms LFE and roll values, therefore increasing the effectiveness of the RLS system, but not to the extent of the conventional RRS approach.

Following this, Sharif [31] et al, made a comparison of LFE controller designs for rudder stabilisation, using the classic phase lead compensator, as used by [3], and another using an optimal control LQG strategy, where a cost function is adopted. This function is altered to place the emphasises on either the LFE or roll stabilisation. The optimum controller was found to out-perform the classic controller, but this was only limited to rudder stabilisation.

2.3 Fin Roll Control

Historically, there has been a vast amount of work carried out on fin roll stabilising systems, though in recent years there have been few publications upon this subject. A major contribution was provided by Dallinga [32], where the hydromechanic aspects of fin stabiliser design were investigated, in addition to simple proportional derivative (PD) control.

A number of authors have made use of alternative control algorithm design techniques, over the more conventional classic proportional integral derivative (PID) type control design approaches, such techniques include

LQG [33], fuzzy and neurofuzzy approaches [34, 35], H_∞ [5, 6]. Linear quadratic gaussian (LQG) control is a method where a performance criterion is minimised, with the optimal weights being found through simulation. A neurofuzzy method has the ability to interpolate non-linear functions, given a number of sets of gains each of which have been optimised to different operating conditions. The process can for example determine a suitable new controller given the current roll motion spectra, allowing constant gain adaptation. This is especially relevant to the problems experienced on new fast vessels, which have vastly different control demands according to the speed and sea conditions. The H_∞ approach gives the user some control over the stability and robustness requirements. This allows selective areas of the model to have more influence, relating to the user's knowledge of the initial model definition, and the desired control characteristics.

Generally, these approaches have only been tested numerically, with the extensive use of the Matlab Simulink package.

In many cases, the system dynamics are simulated using the open loop roll-fin dynamics, with the addition of external disturbances, effects of sensors and fin dynamic non-linearities. In essence, this uses the information that was utilised to design the control algorithms, to test them. So, the applicability of the simulation is dependent upon the simulated model accuracy.

In the case of a fin stabilised roll model, accurate modelling is extremely difficult. One major reason for this is the use of the uncontrolled roll dynamics describing the system which neglect the interactive effects of the fins. In control engineering simulations, the roll effect of the fins is simply added to the uncontrolled component. The use of the controlled fins alters the roll dynamics, this is dependent directly on the control coefficients used.

This fact has been borne in mind in the creation of the seakeeping software package [10], with the resultant ship motions incorporating the effects of the controlled fins and/or rudder. A detailed description of this software has been given in [3].

Hickey et al, [36] used a H_∞ approach to form control algorithms that were tested on an in service vessel. The performance of these controllers were compared to classic parallel PID configurations, with some of the new controllers providing roll reduction of a similar order to that of the classic controllers. The H_∞ controllers did not yield any undesirable fin activity during the tests. These results must be interpreted with the knowledge that the rms roll values were extremely low, of the order of 0.3° to 1.0°. The different controllers were initiated at various time intervals over the course of two voyages. It must be borne in mind that sea conditions may change drastically over a three hour period especially in a sea area such as the English Channel. More extreme conditions are needed, to provide more reliable

comparisons of different control techniques.

2.4 Rudder Roll Stabilisation (RRS)

Rudder roll stabilisation is of great interest for ship motion control in general. This is due to the large interest shown towards this approach in recent years, therefore a vast amount of research has been conducted. This has resulted in a range of different control methods being investigated.

The major benefits of RRS come from; the side force produced by the rudder acting significantly below the ship's centre of gravity, creating a large moment about the roll plane. Also the natural roll frequency is much higher than that for yaw, which allows the two motions to be decoupled. This provides a huge advantage in terms of controller design in that the steering and roll controllers can be separated.

Taggart [37] provides one of the first major publications on the effects of excessive ship roll caused by the rudder. This was experienced on a fast cargo ship, with a large rudder and a steering control system, but excessive roll due to rudder application is also apparent in many other ship types. This work highlighted the significance of the effect of the rudder, which showed it had the potential as a roll reduction mechanism.

The use of the rudder as a means of roll stabilisation was first investigated in the early seventies, by Cowley and Lambert [38, 39], Carley [40] and Lloyd [41]. These studies included numerical investigations, model tests, as well as sea trials. The model tests and numerical studies suggested the method was effective, but not as efficient at roll attenuation as tank stabilisers. The use of compensators were needed to improve the system performance of the control circuits, with roll rate feedback being recommended. Through these various studies, it was suggested that RRS was advantageous for ships with small metacentric height (GM), low roll damping and relatively long roll period. Therefore, the RRS approach was considered to be of low applicability to the majority of ship configurations in favour at that time.

The major problem determined by these studies was the destabilising effect that RRS experienced at low encounter frequencies, consistent with encounter frequencies that would be experienced at high speed in quartering seas. In such conditions the likelihood of broaching due to this instability was greatly increased. Carley [40], carried out a detailed investigation of the control characteristics using classic control theory. It was found that there was strong cross coupling between roll and yaw. This was pronounced at frequencies in the region of 0.02 Hz, with the roll motion being excited by the yaw response. As a result, it was found that RRS was only efficient

at reducing the roll in the roll natural frequency region. For frequencies outside this region, roll motion was amplified. Lloyd [41] also predicted this destabilising effect, using a numerical study based on manoeuvring equations.

From these previous investigations, the findings were rather negative towards the applicability of RRS, though this work did provide a substantial background for subsequent researchers.

Van Gunsteren [42] using full scale experiments, concluded that the RRS provided the potential for roll stabilisation in small craft, this was useful as many small vessels do not have the capacity for fin stabilisers, so using existing appendages would be of great advantage.

Research on RRS, was then investigated as a part of the integrated control system of a vessel. This was first put forward by Carley [40], where the cross coupling effects between yaw and roll were analysed, recommending an integrated control system strategy for ship motion control. Broome [43] followed this by investigating the coupling of yaw and roll in a merchant ship. It was suggested that the roll reduction by way of the rudder, was 16% of that of the fin stabilisers roll reducing effect, for the ship used in the study. Eda [44] also discussed the strong interactions between yaw, roll and the rudder at high vessel speeds.

Whyte [45] used a LQG type approach to establish the feasibility of RRS. From this work, a number of system designs were investigated, using various feedback signals to control the fins, rudder and also using a combination of the two. These were examined using both optimal and sub-optimal design. An optimal design is where all the state vectors in the state space are used in the feedback loop, whereas the sub-optimal design is where only some of the state vectors are used in this loop. It was concluded that, the roll rate constituted the most important feedback parameter from this investigation.

Baitis et al, [23] carried out an extensive research programme developing an RRS system for US Naval ships, which included sea trials. From this, it was demonstrated that RRS could be used as a roll stabilisation device, reducing the rms roll by up to 50 %. This research also pointed out roll rate as being, in general, the most appropriate feedback for simple controller designs. An important point to acknowledge is that the speed during the sea trials was 15 knots, this is outside the destabilised high speed region identified by previous authors [41, 40]. It has been suggested that it was the work of Baitis and his co-workers [23, 46] that provided the stimulus for others to follow, from the favourable results found.

Schmitke [30] carried out numerical studies of RRS using a ship motion program based on strip theory. The studies included comparisons to a fin

stabilised configuration, where the active fins gave better performance in reducing roll. It was suggested that the inadequacies of the RRS could be improved to match the fins performance by up-grading the rudder actuator dynamics, allowing the rudder to react at greater rates. It was noted that this alteration would be relatively inexpensive, in comparison to other roll reduction devices. A key viewpoint in adopting this method is the use of band pass filters. These are used to reduce the frequencies outside the natural roll frequency range. The problems with using filters are that they attenuate the input signal, and phase shifts are introduced.

The Dutch carried out an extensive research programme on RRS, using numerical studies, model tests and sea trials. These studies were carried out by Van Amerogen et al, [29] and Van der Klugt [47]. The systems exhibited problems caused by rudder rate saturation, this was the result of slow rudder servo dynamics. Through these tests, it was suggested that it was possible for roll stabilisation by way of the rudder to yield comparable performance to that of fin stabilisation, providing a rudder rate of 15 $^{\circ}/sec.$ could be achieved. During sea trials, the destabilising effects [41] were observed at high speeds in quartering seas. It was suggested that this results from the limitations of the controller. Therefore an adaptive gain control was implemented, to overcome the rate saturation issue, where suitable control gain values were achieved.

The Swedish research was concentrated around the work of Kallström, [48, 49]. It was from this work that a minimum ship speed of 10 knots was proposed, with a rudder rate of 4 deg./sec. for RRS to be effective, yielding roll reduction in general between 40% - 60%. The roll rate and acceleration were both used in the feedback control loop. This system appeared to have overcome the destabilising effects discussed previously [41], as sea trials were carried out with a 35m fast craft running at 35 knots in quartering seas, which exhibited no unstable phenomenon. Kallström [49] made extensive use of adaptive Kalman filters, where the filter coefficients are altered for different speeds and conditions, with the filter yielding roll derivatives with minimum mean square estimation error. This had the effect of smoothing the roll rates and accelerations prior to input into the adaptive roll damping regulator. From this, a prediction of the ship roll motion is determined, for which a control signal is produced to counteract the anticipated roll. The use of an adaptive controller enables the automatic adaptation of the demand signal to the current sea condition.

The Danish efforts made by Blanke et al [50], were implemented in the design of a new naval vessel, consisting of three rudders, without fin stabilisers. This concept simply substituted a set of fin stabilisers for two rudders

which in many cases would not be beneficial, with the centre rudder to be used for steering and the port and starboard rudders to be used for steering and roll reduction. From sea trials, it was found that the roll reduction in near head seas was from 50% - 60%, beam seas 95% and for quartering seas 35% - 40%. In this example the roll rate and angle were used in the feedback control loop.

The US work was principally carried out by Baitis [23, 28, 46] where extensive sea trials were conducted, along with numerical studies. It was found that rudder rate saturation proved to be the problem, which led to the adoption of a digital controller. The US Coastguard adopted the RRS method on their Hamilton class using digital control, 70% roll reductions were achieved using a modified steering system. The potential for RRS is acknowledged, suggesting a reduction of 40% rms roll is possible, using existing ship's rudder equipment through digital control. This form of control allows the implementation of rules within the controller to prevent excessive fin demands, for example.

Other contributions came from Powell [51] where it is shown that RRS can produce performance levels comparable to that of fin stabilisation, but alterations to rudder design and increased rudder slew rates are necessary. The consideration towards the use of RRS on small vessels is given, expressing clear advantages for vessels where no other active stabilising devices are possible.

A great deal of work has been passed over from other marine control systems. The following authors adopt differing control strategies to improve roll reduction.

Katebi et al, [52] investigated different feedback control configurations using LQG. Roll rate plus roll angle was found to have only minimal advantage, roll acceleration and roll angle were found to interfere with steering, with roll rate feedback providing the best results. Roberts and Braham [53] integrate the control of both the rudder and the fins using classical frequency domain control techniques, with the roll stabilisation loops being considered independently. The investigation was based on either three terms or two terms in the feedback loop. It was found that using the existing equipment of fin stabilisers and rudder, that a greater roll reduction could be achieved over that of conventional fin roll stabilisation alone.

Zhou et al [33] present a method for adaptive RRS control. The approach is based on an adaptive controller design using a LQG control strategy with a combination of Recursive Prediction Error (RPE) techniques, designed to account for non-linear roll damping. The system describes both the rudder yaw

and roll dynamics, therefore analysing a multi-variable system. The method yields simulated roll reductions up to 75%, with small course deviations, as the method controls the course keeping as well. Unfortunately, comparisons have not been made with classical control theory results. Sutton [54] uses a linguistic Self Organising Controller (SOC) to reduce roll motion in a warship by way of the rudder. The results of this analysis have been compared to that of a fuzzy rule based controller [35] to yield similar reductions. This fuzzy based controller was also found to yield favourable simulated results in comparison to a classic controller.

Tang and Wilson [27] carried out an investigation of RRS using classical control theory, before stabilising to LFE by way of the rudder. Motion amplifications were found to occur at high speed in quartering seas, these were in the same region as the destabilising effects identified by other authors, though their magnitudes were not as significant. The effect could be reduced by careful overall gain selection. Even with relatively low rudder rates, the RRS system with roll rate feedback gave numerical model roll motion reductions of between 30% and 40% at 20 knots.

After the use of H_∞ in fin stabilisation control systems, it was then applied to RRS. Combined with the limitations created by adopting conventional rudder rates, roll stabilisation to the levels achieved with fin stabilisation was not possible. By enhancing fin stabilisation with the contributions from RRS, greater roll reductions are possible.

Grimble et al, [5] propose an H_∞ polynomial approach to control the fins and the rudder for roll stabilisation. This adopts a H_∞ control technique which has been proposed for a number of ship based control applications. It is suggested that the combined fin/rudder stabilisation technique is more effective in reducing roll, than for the two devices operating independently. The H_∞ approach is used as *'it designs robust controllers that guarantee stability and performance robustness'* [5]. It was found that this approach was more effective at reducing simulated roll motions, with 85% contribution due to the fins, 15% due to the rudders. The performance data has only been compared to the unstabilised case. Following a similar approach, Agarwal [6] constructed an integrated rudder and fin stabilisation control strategy utilising the H_∞ optimisation technique. The classical RRS controller achieves greater roll reduction at the ship's natural roll frequency, but this deteriorates at the lower and higher frequencies. Whereas the H_∞ approach is more suitable across the entire frequency range. The use of the H_∞ approach in another control environment is given by Desanj et al [7] which describes a self-tuning controller, which is used as a ship auto-pilot. The paper gives a clear overview of H_∞ theory and shows a number of applications for such a

versatile control technique.

From this review of previous work it can be seen that extensive research has been made in the field of RRS, combining their stabilising effects with the fins for roll stabilisation. Attention towards the reduction of LFE has received significantly less publications. With only two parties, Tang and Wilson [3, 27] and Sharif et al [31] using LFE stabilisation, though these were only carried out using classical control and LQG control. Clearly there is a need to explore LFE stabilisation with more robust controllers, with the ability to control multiple motion attenuating surfaces. In addition, the need to develop experimental tools to test controllers derived by various control methods without the need for full scale trials warrants further investigation.

2.5 Shipborne Helicopter Dynamic Modelling

The majority of problems involved in operating helicopters from warships are directly related to the conditions that ship is working in, primarily that of wind and the sea state resulting in ship motions. The greater the wind speed, and the more extreme the ship motions, the more restricted helicopter availability becomes. Lloyd [55] was one of the first researchers to publish work directly addressing this point. Operational limits of helicopters were determined by helicopter operability algorithms, giving the maximum permissible wind speeds, directions and ship motions that the helicopter may withstand safely. The author paid particular attention to the ability of the crew to carry out helicopter associated operations. It could be seen from this analysis that a more accurate tool with which to investigate helicopter performance would aid in the safe setting of operation limits for shipborne aircraft, as well as providing a comparison for different helicopters' marine capabilities.

Val Healey [56] published the first notable paper on the subject of modelling the dynamic interface between a helicopter and a ship. Particular attention was paid to the modelling of the complex airflows around the moving flight deck, due to the capability of the simulation to represent the airborne helicopter. The paper discussed the problems of modelling such a system.

O'Reilly [57] also investigated the ship / helicopter problem, using the Energy Index method to derive the operational windows for helicopter operations. The ship motions adopted in the model where determined from a Bretschneider spectra and using response amplitude operators (RAO), combined with helicopter sliding and toppling limitations to form the parameters within the analysis. This type of approach has been progressed by Ferrier et al [58], analysing the helicopter stability upon the flight deck. The program

developed by O'Reilly has been used to investigate aircraft on-deck sliding and toppling. The oleos and tyres are combined into a formulation with the effects of aerodynamic loads and those due to the ship motions to form the helicopter system equations of motion. The results from this are also used as part of the Energy Index, this index approach is discussed in section 3.2.4.

Arney and co-workers [59, 60, 61] were one the first groups to publish numerical results from computer simulations. They carried out an extensive program of work towards the modelling of the helicopter / ship interface for the Royal Australian Navy. The first published paper discusses the dynamic modelling of the Sikorsky S-70B-2 *Seahawk* on the FFG-7 class of frigate, outlining the problems involved in the operation of helicopters from small warships.

The programme used for the modelling of the dynamic interface had evolved from a code developed at the US Naval Air Test Centre. This code has also been discussed by other authors [57, 58]. This program is said, *'to model the complex interactions in the dynamic interface between ship and helicopter'* [58]. It is formed from a mathematical model of aircraft, ship motion, airwake over the deck and undercarriage dynamics. Modelling of the recovery, assist, securing and traverse (RAST) system is also represented in this paper.

The simulation is broken down into a number of modules:-

- Ship Motion: This procedure determines the ship motions in the six degrees of freedom, from inputs of sea state, ship speed and wave direction.

- Landing Gear: The undercarriage module, this models the forces exerted by the oleos and the tyres from non-linear equations. This section accommodates brakes on and off, tyre slide and modelling of the recovery assist cable.

- Aerodynamics: The aerodynamic model consists of two sections. The first determines the airflow over the helicopter accounting for the existence of a recirculation region aft of the hangar. This section models the total wind velocity as a function of ambient wind velocity, ship speed and direction and position of the helicopter in relation to that of the ship. The second section uses the total wind velocity to derive rotor thrusts and drags and fuselage drag, with some inputs obtained from look-up tables.

- Engine and Transmission: This is the modelling of the dynamics of the engines, allowing simulations of shut-downs.

- Pilot: The pilot control inputs model possible lag and over compensation from an optimum input that a pilot would introduce, to simulate the deviations that can occur during manned flight.

- Control: These are feedback loops that model the mechanical flight controls, they link the pilot inputs to the engine and aerodynamic modules.

All of these modules are combined to form the equations of motion of the entire system.

The program considers two main areas of the dynamic interface, firstly that of the aircraft airborne, from a hover position above the flight deck, to landing on the deck. Secondly, the motions of the helicopter once on the flight deck. From this it can be seen that the model is extremely intricate, encompassing a large number of elements. This has produced a versatile model capable of analysing many different components of shipborne helicopter operation. As can be seen from the examples given [59]:-

- Delayed control inputs: the pilot input of the cyclic stick movement is delayed, with the resulting helicopter landing clearances being analysed. This is important for radome clearance, if the landing is too heavy, then it is possible that the radome will make contact with the flight deck.

- Ground Effect: When an helicopter lands on the flight deck of a ship, ground effect is present. It can be seen that the landing clearances change considerably, depending on the magnitude of this effect.

- Ship Motion: The example given involves an aircraft stationary on the flight deck, analysing the landing gear deflections and clearances. From this, hangar clearances can be ascertained.

The most recent paper [61] published by the group, outlines the new additions to the simulation of the *Seahawk* and the FFG-7 model. Particular attention is paid to the ship airwake and the helicopter undercarriage dynamics.

The ship airwake without the existence of the helicopter is studied from onboard measurements at various wind speeds and directions. A turbulence model has also been integrated within the model.

The undercarriage model includes static and dynamic data for the oleos and tyres. Dynamic results are determined from experimentation. The helicopter is lifted using a crane, then dropped at a range of configurations.

This allows the determination of stiffnesses and damping coefficients for the oleos and tyres using parameter estimation techniques.

This approach appears to be the one of the most detailed ship/helicopter dynamic models that has been published to date, unfortunately only limited direct data is given.

The Kaman SH-2F operating on US Navy frigates and destroyers is analysed by Wei et al [62, 63]. These papers deal primarily with the on-deck condition of the helicopter.

The aircraft is modelled in the six degrees of freedom. The main assumptions are that the helicopter equation of motions are linearised based on small angle assumptions, and the landing gear spring rates and damping coefficients are linear. Effect of the rotors running can be taken into account. Look up aerodynamic tables are used for the fuselage drag, and lift/drag caused by the non-rotating rotors.

The program identifies key limiting conditions such as aircraft sliding, or lifting of one main wheel. The papers look closely at the effect of different friction coefficients for the flight deck, yielding a large difference between a dry deck and a wet, oily deck. From this, ship lateral acceleration is identified as having a significant effect upon whether the aircraft will slide or not.

The program was proposed to be used onboard a ship with inputs of real time ship data and conditions such as wind speed and direction, which would indicate to the crew the suitability of helicopter on deck handling.

Tadros and Langlois [64] of Indel Technologies, the manufacturers of the RAST and the aircraft ship integrated secure and traverse (ASIST) systems, separate the landing phase into two main sections. Firstly, that of the helicopter in the air to touch-down, the second is the helicopter on the deck.

A Monte Carlo method is used to simulate the aircraft hover and landing phase. It can accommodate in the simulation a recovery assist cable, with or without a pilot model, with ship motion, steady wind and turbulence. From these inputs the landing dispersion patterns upon the flight deck can be obtained, including the landing velocities and orientations that can then be passed on to the next section.

The on-deck simulation consists of the oleos being modelled in great detail, oleo stiffness is modelled using ideal gas laws, with a multi-stage damping model being used to simulate each region of damping, with a friction model evaluating the force from seal friction and normal force contributions. Tyres have been modelled using linear stiffnesses and viscous damping, and also using an empirical model. External forces used in the model include rotor contributions, securing, fuselage drag, those caused by ship motions in the six degrees of freedom. This produces a very complete model, that is able to

determine helicopter security.

The author determines that an aircraft is insecure if a tyre slides, or when one oleo is at maximum extension and the other two at maximum compression, this provides stability criteria with which to work. Attention is given towards computational efficiency and stability, with the use of a complex integration approach that dynamically switches between integration methods according to the stiffness of the equations.

In the most recent publication [65], particular attention is given towards an acceleration quantity, which is based on LFE. It is noted that this significantly effects the stability of the helicopter on the flight deck.

Pedrazzi et al. [66] model the EH-101 *Merlin* and the NH90 on the flight deck of the proposed Horizon frigate. The approach used is based on commercial software specifically designed to solve multi-body dynamic problems. This software has been specifically customised for analysing the helicopter / ship interface.

Models have been created to simulate the helicopter up on touch-down, and for the period of time that the aircraft spends on deck, including the modelling of securing devices. Known non-linearities are modelled using numerical or graphical data curves for the oleos and tyres. Revolving and braking tyres are modelled, including a developed tyre friction model. This paper pays particular attention to the tyre model, as this is the predominant factor involved in on-deck manoeuvring. It describes the approach of using the automatic dynamic analysis of mechanical systems (ADAMS) software, and the benefits of such software can clearly be seen in the simplicity and speed involved in creating the models.

It can be seen from the work that has been carried out in this field, that some highly complex models have been formed. From Wei et al [62, 63] it can be seen that realistic results can be achieved without the need for large quantities of data derived from experimentation, or resulting in high computational demands.

3 Prediction of Quiescent Periods

3.1 Introduction

The aim of this area of the project was to develop a method that would give a ship motion prediction for the proceeding 15 seconds. This prediction should be of sufficient accuracy to determine motions levels that would prevent the helicopter from landing safely.

A quiescent period is the length of time in which certain quantities are within particular thresholds. In the case of a ship, these limits might be related to certain motions, their velocities or accelerations. In the case of aircraft landing on vessels, the thresholds are limiting values predetermined for the operational limitations of the helicopter. Determination of these periods in real time will provide the pilot with an indication as to when it will be safe to land on the ship.

This is important in many situations, as a warship maybe unable to achieve reduced motions by changing heading or speed, due to operational constraints. Combined with performing in high sea states, where quiescent periods are short and infrequent, precise determination is needed to take advantage of these durations of reduced motions for safe helicopter operability.

The suitable length of a quiescent period is dependent upon the performance and agility of the helicopter type which is to land upon the vessel, combined with the ability of the pilots. For a light to moderate size helicopter such as a *Lynx*, this period maybe as short as 6 to 8 seconds. This will provide sufficient time, for the helicopter to move from the familiar hover position above the side of the flight deck, to land and engage the deck securing device. For a larger aircraft such as the *EH-101* this time period will be significantly greater, possibly in the region of 15 to 20 seconds or more. Therefore a significant prediction time period is necessary to aid the landing of such large helicopters.

This chapter first describes approaches that are currently available to aid this motion prediction. It then continues to discuss wavelets, which have shown many benefits in other motion tracking and signal processing applications. A range of wavelet approaches have been investigated, with discussion as to their suitability for sea surface analysis and the prediction of quiescent periods.

3.2 Currently Available Methods

3.2.1 Pilot Judgement

This was the first method used for the prediction of quiescent periods, in the case of helicopters landing on small warships. From discussions with Royal Navy Lynx pilots [67], it was found to involve the pilot or observer analysing the current sea surface and ship direction to assess key wave components. From this, he can determine which wave components are likely to interact with the ship at a future point in time using his experience. Then, he determines whether the resultant ship motions in the future are likely to be excessive for the task of landing the helicopter, or whether the period of time until an excessive motion is adequate for the landing operation. This necessitates the pilots having a knowledge of the seakeeping characteristics of the vessel. Problems are caused by the high workloads placed upon the pilots, as he has to scan the sea surface, as well as fly the helicopter at such a critical point of the flight. This concept is unreliable at night and in low visibility conditions, seriously limiting the availability of this predictive system.

This approach is currently used by a majority of the navies around the world, if not all.

3.2.2 Fourier Transforms

A method has been used in Morris et al. [68] utilising fast Fourier transforms (FFT). The method assumes that it is possible to measure the present elevation of a one-dimensional sea surface, and analyses it with FFTs. These transforms are adapted to simulate the progression in time, which are then used to determine the sea elevations in the future, or to be able to determine the sea elevations at another point.

The use of Fourier transforms approaches compared to other methods are discussed in section 3.5.1.

3.2.3 Adaptive Predictors

This is a signal processing technique with numerous applications, one such naval architectural example is given in Broome and Pittaras [69], using ARMA *(Auto Regressive Moving Average)* filtering. Ship motions, such as roll have been modelled with this process. The approach uses data such as rudder angle, stabiliser angle and roll taken at discrete time intervals.

- The inputs to the ship motion system are rudder and stabiliser angles, and the output is the roll angle.

- Previous time interval values of rudder, stabiliser and roll angle and the subsequent value of rudder and stabiliser angles are combined to determine system parameters to equate to the subsequent roll angle. These system parameters are calculated to minimise system error.
- As the signal propagates in time, so the parameters are updated to maintain minimum system error.

When this method is utilised for the prediction of roll at a future epoch, the system parameters are held constant and the error is set to zero, as the future error cannot be determined. So as the prediction progresses, the new inputs to the system are the previous calculated roll values. Gradually the system error increases yielding inaccurate estimations. Therefore, this method is only suitable for relatively short time interval predictions, for roll this could be in the region of one roll period. For other motions such as heave and pitch, the approach yields far less accuracy due to the higher frequency of the responses. This approach adapts to the present situation and needs no prior ship characteristics, as these are accounted for in the system parameters.

A typical ARMA relationship is:

$$\varphi(t) + \sum_{i=1}^{n_a} a_i \varphi(t-i) = e(t) + \sum_{i=1}^{n_c} c_i e(t-i) \qquad (1)$$

$\varphi(t)$ measured roll angle
$e(t)$ system error
a_i, c_i system parameters
n_a, n_c represent the number of previous time step values to be incorporated in the analysis.

For a prediction of $\varphi(t)$ to be made, $e(t)$ is set to zero, this process is continued for increasing time predictions.

3.2.4 Energy Index (EI)

This approach is an empirical formulation relating ship motion data to desired motion limitations. The method determines the index value using ship accelerations, velocities and displacements as inputs, combined with predetermined parameters optimised for the current conditions.

A simplified version of the formulation is:-

$$EI = a_1\varphi^2 + a_2\dot{\varphi}^2 + a_3\theta^2 + a_4\dot{\theta}^2 + a_5V^2 + a_6\dot{V}^2 + a_7L^2 + a_8\dot{L}^2 \qquad (2)$$

a_i system parameters
φ roll angle
θ pitch angle
V vertical motion at the flight deck
L lateral motion at the flight deck

EI is a measure of the energy within the system, giving an indication as to the future possible rate of displacement of the ship given the hydrodynamic characteristics and the related operational limitations of the aircraft. If the energy index is high then it is unsafe to carry out the motion sensitive operation. This system is currently being explored by many navies as an aid to helicopter landing [70]. This type of approach has been detailed in [58].

3.3 Discrete Wavelets

Wavelets have shown to be of benefit to a number of signal processing applications with their properties of localising and identifying signal components. It is these benefits that could be beneficial to sea surface analysis, that of identifying key wave structures. And in the case of discrete wavelet analysis, vast computation gains are achievable through the method's efficiency.

The discrete wavelet transform (DWT) is an algorithm developed by Mallat [12], named the *Mallat pyramid algorithm.*

Wavelet coefficients are related to the following expressions:

$$a_{2^j+k} = 2^j \int_0^1 f(x) W(2^j x - k) dx \tag{3}$$

$$a_0 = \int_0^1 f(x)\phi(x)dx$$

The DWT is used to determine the wavelet coefficients a_0 to a_{2^j+k}, without the necessity to generate each value of the analysing wavelet $W(2^j x - k)$ and $\phi(x)$. This provides a considerable computational efficiency advantage.

These discrete wavelets are in a number of cases created from dilation equations. A complete description of these equations and their formation can be found in Newland [16].

Discrete wavelets are compact in the time domain, this means that the functions have a beginning and an end within that domain. As a consequence they are not compact in the frequency domain, therefore the function possesses an infinite frequency range.

A range of commonly adopted mother wavelets exist (defined in section 3.5) such as *Daubechies, Haar, Coiflet* and *Symmlet.* These are the basis functions from which all subsequent analysing functions are derived. A

mother wavelet has to conform to a number of criteria for it to be admissible as a discrete wavelet. Derivations of these criteria are listed in a number of publications such as [16].

The WaveLab [71] software was adopted for the investigation of discrete wavelets. This is a shareware toolbox of routines used within the MatLab environment [72]. This is only one of many currently available software packages, a number of which have been outlined in Bruce et al, [13].

A variety of different signal types were analysed with the WaveLab software, comparing the use of different wavelet family types on different signal types. A summary of the results is given in the following section.

3.3.1 Results

The first task was to find a wavelet type that would suit the application of analysing sea surface data. The most appropriate wavelet family proved to be, the *symmlet*, this was primarily due to its sinusoidal like, smooth nature.

Figure 2 is the discrete wavelet transformation of a sinusoidal wave train. Each level shown in the figure relates to a different scale of analysing function with the location of each function positioned upon that level.

A repeated pattern can be identified, also the position of each peak and trough can be approximated. The higher levels have negligible wavelet coefficients, this is due to the lack of higher frequency contributions, normally resulting from sharp discontinuities within a signal. This and the following figures give the individual coefficient magnitudes for each level of the analysed signal.

Figures 3 and 4 give the wavelet coefficients for a single wave component. The locality of the signal element can clearly be identified, though its exact position is difficult to distinguish due to the discretisation at the most significant contributing levels. The subsequent figures 5,6,7 and 8 show the progression of the wave component across the domain. It must be noted that the contributions within each level change considerably. This is due to the discretisation at the lower levels, being coarser than those at the high levels. There would be a similar outcome in the analysis of sea surface data extracted from a local remote sensing device. As the components would be of relatively low frequency to signal length ratio, in comparison to many other applications where wavelets are used. In these applications the elements of interest are usually of high frequency in comparison to signal length. This limits the applicability of such efficient wavelet approaches in this example.

Figure 9 is the wavelet transformation of a sea surface determined through wave spectra. Peaks in the original signal can be identified via magnitudes in the coefficients, though these are not easily isolated.

A major limitation of this technique is the choice of wavelet, the *symmlet* does not comprise of the same shaped components as the wave components under investigation. Therefore a wave component results in a range of wavelet coefficients to identify or reconstruct it.

3.3.2 Conclusions

As a consequence of the properties needed for the efficient performance of discrete wavelets, characteristics necessary for the analysis of sea surface data are lost, such as accurate location of a specific component within the space domain. This is due to limitations resulting from complying with the orthogonality criteria. To carry out the analysis of sea surface data, a more detailed wavelet algorithm approach is desired, which does not have the limitation of conforming to these criteria. As a consequence the efficiency will be vastly reduced, but the ability to locate features will be increased. This led to the study of discretised continuous wavelet transforms, which are discussed in section 3.5.

3.4 Harmonic Wavelets

3.4.1 Theory

Newland [21] formed a type of wavelet whose spectrum is band limited. It was discussed that wavelets formed from dilation equations, have refined frequency discrimination as the number of dilation coefficients increase. This is at the expense of computational efficiency. Therefore Newland pointed out that there may be advantages in forming a wavelet with a pre-defined frequency band. These wavelets were based on the following function:

$$w(x) = \frac{e^{i4\pi x} - e^{i2\pi x}}{i2\pi x} \tag{4}$$

Representations of this wavelet functions are graphical displayed in figures 10 and 11. Figure 10 is the plot of a real wavelet symmetric about the centre position and figure 11 that of a corresponding complex wavelet which is asymmetric about that point. From these, it can be seen that a wavelet component has the ability to distinguish signal element position, to a certain degree.

When level j and location k are applied to equation 4 it becomes,

$$w(2^j x - k) = \frac{e^{i4\pi(2^j x - k)} - e^{i2\pi(2^j x - k)}}{i2\pi(2^j x - k)} \tag{5}$$

j = level value
k = translation at level j scale

Therefore at level j the associated frequency band is $2\pi 2^j$ to $4\pi 2^j$.

Level -1, consists of the frequencies from 0 to 2 π, the function associated with this level is not a wavelet function as in equation 5, but a scaling function.

This scaling function is of the form:

$$\phi(x) = \frac{e^{i2\pi x} - 1}{i2\pi x} \tag{6}$$

As with other wavelets, harmonic wavelets have to conform to particular normalisation criteria. This has been outlined in [21].

The general expansion formulae for harmonic wavelets is therefore:

$$f(x) = \sum_{k=-\infty}^{\infty} a_{\phi,k}\phi(x-k) + \sum_{j=0}^{\infty}\sum_{k=-\infty}^{\infty} a_{j,k}w(2^j x - k) \tag{7}$$

Musical Wavelets

Musical wavelets are a more general expansion of harmonic wavelets, based on equation 4. The musical wavelet function is:

$$w_{m,n}(x) = \frac{e^{in2\pi x} - e^{im2\pi x}}{i(n-m)2\pi x} \tag{8}$$

The use of j to denote the levels has been superseded by the use of m and n. They represent a frequency band of $m2\pi$ to $n2\pi$ where $n > m$.

Musical wavelets must also maintain orthogonality. Wavelets from different levels are orthogonal, due to frequencies of one level not coinciding with those of another, a full proof is given in [21]. Wavelets from the same level are orthogonal if the interval by which one is translated in relation to the other is:

$$\frac{k}{n-m} \tag{9}$$

k is an integer value.

Complete derivations are given in [21, 22].

Wavelet Map

A major problem in analysing wavelet method calculations, is *'how to display the results?'*. One convenient method of achieving this is the wavelet map. This map is formed from the sum of the squared wavelet coefficients, in effect a measure of the energy, and is as follows:

$$\frac{1}{2^n}\sum_{r=0}^{2^n-1} x_r^2 = a_0^2 + \sum_{j=0}^{n-2}\frac{1}{2^j}\sum_{k=0} 2^j - 1\left(|a_{2^j+k}|^2 + |a^{2^n-2^j-k}|^2\right) + a_{N/2}^2 \qquad (10)$$

The maps given in the following section have been plotted with the x-axis denoting the energy location within the signal, with the y-axis corresponding to that of the level. Therefore the peaks identify the levels and positions of high energy.

3.4.2 Results

A series of routines where written in the MatLab language to carry out the wavelet transformations, data formation and visualisation. It was from these that the following figures were formed, based on the wavelet map described previously.

Figure 12 shows the harmonic wavelet map for the analysis of a sinusoidal wave train. The wave frequency of 0.1534 rad/sec lies within level 6. As the frequency is maintained over the entire signal duration, so this is reflected in the constant amplitude of level 6.

Figure 13 shows the musical wavelet map associated to level 6 for the same wave train used above, it can clearly be seen that the frequency of the signal has been confined to sub level 10.

The same datasets analysed by the discrete wavelets in section 3.3, were adopted for this analysis.

Figures 14 and 15 are wavelet maps of two different wave spectras. The first is based on a Bretschneider significant wave height ($h_{1/3}$) = 5.5m and a mean period (T) 12.4 sec (spectra 1), with the second being that based on a Bretschneider $h_{1/3}$ = 8m and T = 16 sec (spectra 2). The higher frequencies contributions are observed in the higher levels of figure 14 as would be expected. This is reflected in the more obvious low frequency components of the second spectra. The wavelet map also picks out the positions of apparently higher frequency packets. Musical wavelets can be used to give increased information from this type of signal.

This technique provides a method by which a sea surface maybe analysed to determine localised wave spectra of larger scale sea surface data, being more advantageous than short term Fourier transforms.

Figure 16 is a one-dimensional sea surface with the first half of the signal formed from spectra 1 and the second from spectra 2, with figure 17 illustrating its wavelet map. The energy distributions of the levels can clearly be seen to be different from one half of the signal to the other.

Figure 18 is the resulting harmonic wavelet map from a signal comprising of a series of four consecutive sinusoidal wave trains given in table 1.

Position	Frequency (rad/sec)
1	0.1534
2	0.2148
3	0.0920
4	0.1534

Table 1: Sinusoidal Frequencies

The wavelets isolate each wave train series, yielding the possible frequency range by way of the level, and also an approximation of its position. This identifies the harmonic wavelets major advantages due to the frequency discrimination.

A similar approach has been used in figures 19 and 20 with the data given in table 2. Only in this case, all the frequencies lie within one level, as can be seen in figure 19.

Position	Frequency (rad/sec)
1	0.1534
2	0.1718
3	0.1350
4	0.1534

Table 2: Sinusoidal Frequencies

Musical wavelets are therefore used to discriminate of the frequency content into finer frequency zones, as can be seen in figure 20.

Figures 21,23 and 25 denote a single sinusoidal wave component, moving across the time domain. The wavelets are able to identify its movement as can be seen in figures 22,24 and 26. The frequency content of the component has a wide range, therefore the signal has contributions in more than one wavelet level. The peak in level two has one of four possible positions due

to the discretisation in that level. As the level increases, so the number of positions in the domain increases.

3.4.3 Discussion

Harmonic wavelets do not yield the degree of localisation possible with other wavelet approaches investigated. They yield a good frequency content within a signal range, but the rate of decay of such a wavelet is low, accurate localisation is not possible. This is extremely limiting in the areas of analysis where reasonable localisation information is desired, such as that of short term sea surface analysis.

This type of approach was simple to implement through the use of software such as MatLab, where fast computations were achieved in comparison to other wavelet methods.

To have pre-defined frequency bands could be advantageous. This would be more appropriate for longer term sea surface analysis, where the user can afford to lose the position precision, due to the increased information gained through sufficient frequency discrimination. The user in this case is more interested in spectral content and magnitude with the range of its location and direction. This type of approach shows much promise over the use of short term Fourier transforms (defined in section 3.5). Unfortunately, it is not suitable for this specific application. This is reflected in harmonic wavelets abilities in analysing signals with relatively high frequency to signal length ratios, where vibration analysis is a prime example. In the case of short term sea surface analysis, the frequencies are relatively low in relation to the signal length placing much of the signal components in the lowest levels.

3.4.4 Conclusions

The harmonic wavelet type exhibits some of the same limitations encountered in the use of discrete wavelets, that of precise location discrimination and suitable component identification.

These wavelets exhibit properties that may make them suitable for longer term sea surface analysis, but not for the time scales and surface lengths under investigation in this case.

3.5 Continuous Wavelet Transforms

This type of technique had been adopted successfully for the analysis of sonar signals yielding the position of the reflecting object. This was made possible by analysing the returned signal with that of the transmitted. If a function could be found that was similar, if not the same as the signal components to be identified, then these components could be clearly recognised. It was with this in mind that these continuous wavelet transforms were selected for study.

Wavelet, as implies by the name, is a small wave. This wavelet forms a set of functions with which to analyse a signal. The basis function from which all others are formed is called the *Mother Wavelet.* From this all other analysing functions are created as scaled and/or translated (shifted in the time domain) versions of the original mother wavelet. Therefore only one basis function is required to form the entire set of analysing functions.

The continuous wavelet approach is less restrictive than other wavelet approaches, as it is not necessary to conform to the orthogonality conditions, as with DWT.

Even so, a mother wavelet must have the following properties:

- *to oscillate.* This allows the wavelet to be a *wave.*
- *decay rapidly to zero.* This produces a function that is small in duration.
- *integrate to zero.* Therefore has no zero frequency component.

This produces a function that is able to extract localised features from a signal. Therefore any function conforming to the above criteria could be used as a wavelet, but care is needed in using a wavelet suited to the signal being analysed.

The wavelet method described in this section is one of the most basic forms, a discretised version of the continuous wavelet transform (CWT). The method consists of multiplying the signal with a wavelet function, then summing it over the signal length to yield a value. The same process is then repeated, with the function being translated (figure 27) and scaled (figure 28) across the signal length, obtaining a value at each interval of scale and translation.

The continuous wavelet transform is of the form:-

$$W_{(a,b)} = \frac{1}{\sqrt{|a|}} \int_{x_{min}}^{x_{max}} f(x) g^* \left(\frac{x-b}{a} \right) dx \qquad (11)$$

- $f(x)$ is the original signal.
- $g(x)$ is the mother wavelet, the function by which all other subsequent functions are derived, by scaling and translating.
- $g^*(x)$ denotes the complex conjugate of the function.
- a is the scaling parameter, all wavelet functions are multiplied by $|a|^{-\frac{1}{2}}$ to maintain energy normalisation. This ensures that every subsequent wavelet possesses the same energy as that of the mother wavelet. This permits, easy comparisons of coefficients of vastly differing scales to be carried out.
- b is the translation.

The transform coefficient value found for each scale and translation is a measure of the correlation between the signal segment and the analysing function. The data derived from the signal for all scales and translations forms a two-dimensional matrix, as can be seen from figures 29 and 30. Therefore the higher frequency (small scale) wavelets identify the high frequency, local structures within the signal, whereas the large scale wavelets detect the lower frequency signal components. This process is known as wavelet decomposition. The data in this form can be processed, for example, to eliminate noise by rejecting the high frequency components, or to identify specific features within a signal, which can not be extracted directly from the original signal. So it can yield information that was masked by other signal components when part of the original signal.

The signal can be reconstructed from the wavelet coefficients using the inverse continuous wavelet transform (ICWT):-

$$f(x) = \frac{1}{C_g} \int_0^{n-1} \int_0^{n-1} \frac{1}{\sqrt{|a|}} \frac{W_{(a,b)}}{a^2} g\left(\frac{x-b}{a}\right) dx \tag{12}$$

$n = x_{max} - x_{min}$ is number of intervals

C_g is the admissibility constant that is a function of the mother wavelet, this is used to scale the reconstructed signal to correspond to that of the original. The condition verifies whether the wavelet is a finite energy function.

$$C_g = \int_{-\infty}^{\infty} \frac{|G(\omega)|^2}{|\omega|} d\omega \tag{13}$$

therefore it must satisfy:

$$C_g < \infty \tag{14}$$

C_g is the Fourier transform of g.

3.5.1 Comparison

The benefits of the wavelet approach can clearly be seen when compared to the commonly adopted signal processing techniques based on *Fourier Transforms (FTs)*. Fourier analysis is suitable for analysing stationary signals, that is a signal whose frequency components do not change with time. So they ascertain the frequency content over the entire signal length. This is the major restriction of FTs, in that it only provides frequency data.

Short Term Fourier Transforms (STFTs) have been used to overcome some of the problems of FTs and non-stationary signal analysis. This analysis assumes that a non-stationary signal can be broken down into smaller stationary segments. The signal is segmented into smaller portions with a suitable windowing function, the result is then Fourier transformed.

A window of infinite length will yield perfect frequency resolution, but provides no time information. As the window length is reduced, the time resolution improves, but as a consequence the frequency resolution decreases. It is assumed, that for STFT to be valid for non-stationary signals the window length must be small, therefore the theory limits the method to good time resolution at the expense of poor frequency resolution. Wavelets in fact give good frequency and poor time resolution for lower frequencies, with the opposite being true at the higher frequencies. Figure 30 shows this ability as the positions of the short wavelength signal components are well defined.

This weighting suits most signal types, as the high frequencies are of short duration, where localisation in the time domain is important, and vice-versa for the lower frequencies. STFT is unable to analyse lower frequency components over larger time scales, as this invalidates the small windowing condition used to approximate the stationary components from a non-stationary signal.

Therefore, wavelets are a signal processing tool that are able to analyse non-stationary signals, as it is possible to localise frequency components in the time domain. This is due to the use of localised functions, instead of the global functions used with FT, and partially overcomes the resolution problem of STFT described previously.

An example is given in figure 31, there is a base signal *(top left)* with its FFT *(top centre)* and wavelet coefficients *(top right)*. The base signal has a unit box function added to the start of the signal *(bottom left)*, with its corresponding FFT amplitudes *(bottom centre)* and wavelet coefficients

(bottom right). A comparison of the FFTs show that a small change to the signal can have a major effect on the amplitude of the frequency coefficients, whereas the addition of the square function only effects the local region of the wavelet plane. This is due to the FFT, resolving the addition of the square function over the entire signal frequency range. This prevents the tracking of wave components in the Fourier transform domain.

The mother wavelet function is of great significance, as this function can be chosen to suit the particular analysis. This provides great advantages over STFT, as it is possible to isolate local features directly from the signal, providing a suitable analysing function has been used.

3.5.2 Implementation

The key issue in using wavelet analysis is the form of the mother wavelet. It is necessary to select a function that best suits the elements being extracted from a signal. For analysing sea surfaces or any related data, such as ship motions, one cycle of a sinusoidal wave component was considered to be appropriate as a mother wavelet. The individual sinusoidal wave components conform to the conditions of being a function that oscillates, decays quickly to zero and has zero area. For the identification of a wave component, the best correlation would be achieved by use of a similar function. This can be seen from figure 32, the peak in the wavelet domain, yields the component location, as well as its frequency.

The *continuous discretised wavelet transform* has been chosen, due to its ability to extract the translation and scale information of a wave component. Other wavelet approaches investigated did not yield the accuracy of position, which are needed in order to track wave components.

The Progression of a Sea Surface

To prove that it is possible to progress a sea surface in time reliably using the wavelet method, the following technique has been evolved.

In this simple case, a set of data corresponding to random sea surface elevations in the space domain are to be analysed. The aim of this exercise is to predict the surface elevations at some future epoch.

The generated random sea surface is formed from a band limited section of the Bretschneider spectrum, this band limiting was used to make the graphical comparison between the original time progressed and that of the wavelet progressed signals easier. The spectrum time progressions were formed by advancing the frequency components through adaptation of the phase contributions. All wave components are propagating in the same di-

rection, therefore this method is analysing a uni-direction series of data in the space domain.

The original signal is analysed using CWT. The wavelet decomposition yields the wavelet coefficients for the signal, these values remain unchanged throughout the analysis. The functions used to disassemble the signal, are then progressed in time, to simulate the wave progression.

This is where a major problem arises, a wavelet function has a multiple frequency content. Wave phase speed of deep water sea waves is frequency dependent, governed by the equation:

$$c^2 \approx \frac{g}{k} \tag{15}$$

c denotes the wave phase speed, g gravitational acceleration and k wave number.

This results in time progressed wave components not being simple translated versions of the original, but having their forms drastically changed. So there is not a direct correspondence between an original wave component and a time progressed component.

This problem is not encountered in other forms of signal processing, such as sound waves travelling through a medium, as in these cases phase speed is constant. So a time progressed wave form is purely a translated version of the original.

In this case, each scale of wavelet function has to be progressed in time. This has been carried out using a FFT approach. The function is Fourier transformed, with each frequency phase component being adjusted to simulate a time progression. The new adapted function is then formed by the *Inverse Fast Fourier Transform (IFFT)* of the altered functions. Care has to be taken, in that the periodic nature of FFT can create periodic progressions. This effect can be eliminated by analysing the function in a larger domain placing signal lengths of zero amplitudes before and after the function length. The time progressed function can then be extracted.

The new adapted functions are now used in the ICWT procedure to construct the time progressed sea surface. The process of the ICWT is altered, as it does not use a mother wavelet to create the subsequent wavelet functions and this makes the process more demanding than in the original ICWT reconstruction. This approach therefore increases the processing time of the computation.

Figures 33,34,35,36 provide the results from such an analysis. The top diagram of figure 33 gives the original sea surface at time equal to zero, formed from spectral data. The centre diagram is the time progression of the top, this time progression is performed by adapting the phase of the spectral

data components. The lower diagram is the wavelet time progression of the original signal. Figures 34,35,36 also follow this style.

It can be seen from figure 33 with a time progression of 1 second, that the correlation between the actual progression and the wavelet progression are close, except for the underprediction at the start of the signal. This is caused by the inability to predict which components will be entering the system in the future. In this case, long wavelength components which have high phase speeds are moving into the signal domain with wavelets unable to forecast this. As a consequence, there exists a discrepancy between the two signals in the incoming wave region which is the left hand side of each figure.

Figure 34 shows the data from a 5 second progression. There is a close fit between both progressions. The wavelet prediction again breaks down at the incoming wave end of the signal, where it is unable to forecast which components will be entering the signal domain. Despite the prediction for the 0 - 30 (m) x range, the remaining signal is still reliable.

These trends are consolidated with increasing time progression, as can be seen from figure 35, time progression of 20 seconds and figure 36 time progression of 50 seconds. As time progression is increased, so the length of signal lost through the inability to predict which wave components are entering the system is increased. This length of signal is not only dependent on the duration of time prediction, but on which components will be entering the signal and at which point in time for a non-stationary signal being analysed.

Preliminary tests have been undertaken in order to extract wave component data from the wavelet plane. With a low number of wave components in the signal domain, component identification is possible, with tracking of each component also possible, even with the problems caused by the frequency dependent wave phase speed.

With increasing numbers of components in the domain, the process of component extraction becomes immensely complex. Superposition of components, makes separate identification not directly possible. Therefore a method needs to be sought that has the possibility of forefilling this task. The complexity of the process when applied to a realistic sea surface can clearly be seen from figure 37.

New Approach

The eventual objective of this work was to create a two-dimensional sea surface predictor, which could be linked to an additional system to determine ship motions into the future and thus providing information of available quiescent periods. The system could also be used to provide data to other

devices such as ship control systems, to aid the stabilisation or position keeping of a vessel. The idea behind this method is to build a system based on the philosophy of the method described in section 3.2.1. To identify wave components, track them, then progress each component on in time to form the predicted surface, with a continual check to verify the quality of the estimation. Instead of basing the prediction of the sea surface upon human judgement, a similar approach is made computationally.

The method is comprised of three stages:-

- Sea Surface Scanner: This is a remote sensing device that can scan an area of sea, yielding digital information of the surface elevation at a number of grid points upon that area. This data is passed on to the Sea Surface Predictor. Laser and other remote sensing technologies are currently being developed for this task.

- Sea Surface Predictor: The surface elevations for the range of grid points at one time step are analysed using a two-dimensional wavelet transform and the same approach is used for a number of subsequent time steps. By comparing the wavelet transform data of each time interval, wave positions, amplitudes and directions of significant wave components can then be extracted. From this, it will be possible to track each component in the transform plane.

  To predict where each wave component will be in the future demands progressing of the wave data, such as direction, position and amplitude extracted from this transform plane. Once all the wave components have been progressed in the wavelet domain, then reconstruction is executed. The outcome is the sea surface elevations at the grid points for future points in time. Continuous verification of the results with subsequent sea surface scans can be used to ensure reliable predictions.

- Ship Motion Predictor: This is linked to the sea surface predictor. Once the wave components have been identified and progressed, these components are used directly in the ship motion predictor to determine the future motions.

  This approach could use a pre-determined database of ship motions for each wavelet progressed component, which can be thought of as Wavelet Response Amplitude Operators. The database is created using a method that can calculate the ship response to an arbitrary wave shape. As the sea surface predictor identifies specific wave components, these elements are compared to the database to determine the magnitude of motion that the component will cause. This is completed

for each major wave component in the vicinity of the vessel, then the individual motions are summed to yield the expected ship motions. Therefore, quiescent periods may be predicted.

This method overcomes some of the limitations of linearity experienced by Response Amplitude Operators (RAO) [73]. The approach utilises the information directly from the sea surface predictor, without the need to determine the sea surface spectra. The number of wave components would be minimal, as only key components causing significant motions will be used.

The major drawback of this approach is extracting the wave component data, such as wave direction, wavelength and amplitude, whilst in the wavelet domain. A number of similar wave components, moving in different directions form a complex interactive problem in the wavelet plane, as the components superimpose. A process is needed that can separate out each component in the wavelet plane.

This approach may appear to be extremely over ambitious. It is considered that a similar technique to identify and track key areas of high wave energy rather than wave components would be more appropriate, essentially a de-sensitised version. This would operate directly from the wavelet plane, where the magnitudes in their current form relate to the energy content. This can only be adequately tested on actual sea surface data at a number of time steps. The author has been unsuccessful in finding a source for such data.

3.5.3 Other Possible Applications

De-Noising

One property of wavelets that is also exploited in other signal processing applications is their ability to de-noise a signal without significant loss of other signal components within the data. It is possible to eliminate the very high frequency noise components by reconstructing the signal from the wavelet coefficients, with the small scale wavelet coefficients equal to zero, this is known as thresholding.

In this case, the wavelet method has been used to analyse ship roll data over a period of time. It can be seen from figure 38a, that the signal has a high noise content. The signal is analysed with the wavelet method, the small scale transform coefficients are set to zero, then the signal is reconstructed from the altered coefficient matrix. It can be seen in figure 38b that the noise has been completely eliminated, with the underlying signal remaining intact.

The wavelets provide favourable results, when compared to many other de-noising schemes. Discrete wavelets are a more computationally efficient

waveleting method to de-noise a signal, due to their elimination of computational redunancies.

Waves in Shallow Water

From the previous discussions, it can be seen that wave component extraction in deep water is extremely complex, due to the extensive superposition of all the components, and the wave speed being a function of wavelength.

When analysing a shallow water problem with the same approach, these limitations no longer exist. As the water depth to wavelength ratio decreases the effect of frequency dependent phase speed decreases, this can be seen from the following wave phase speed equation:

$$c^2 \approx gh \tag{16}$$

where h denotes the water depth and $h < 0.03\lambda$ this is very shallow water.

Wave speed in shallow water is constant therefore wave component shape is consolidated.

Wavelet Response Amplitude Operators

This new approach of determining ship motion characteristics has some advantages over the RAO method.

The modelled vessel is motion tested for a number of elemental wave forms, i.e. wave height, component wavelength at various encounter frequencies and directions, forming the wavelet response amplitude operator (WRAO).

A typical encountered sea surface can then be analysed, with component wave forms being extracted by use of the wavelet method. The motions caused by each component are then determined from the WRAO. A summation of the components is then made to yield the resultant ship motions.

This method has the ability of accounting for some of the non-linearities caused during high magnitude ship motions, and this can be integrated into a realistic sea condition. This technique would not directly account for the historisis of the vessel, this would have to be considered to improve the ship motion prediction.

Further work is needed to thoroughly investigate this concept.

3.5.4 Conclusions

The key advantages of using CWT are that of identifying local signal details, their location, and its ability in analysing non-stationary signals, such as a

sea surface. It has been demonstrated that wavelets can be used to progress uni-dimensional sea surfaces in time. A description of this new proposed approach for the prediction of ship motions and quiescent periods has been given.

More research is needed to expand the basic example and results given, leading to the full implementation of two-dimensional sea surface time progression and determination of quiescent periods in ship motion. This is dependent on actual sea surface retrieved data rather than that created through numerical simulations. Especially, in respect to the identification, tracking and subsequent prediction of wave components in the wavelet domain. The limitations caused by the frequency dependent wave phase speed seriously complicates the process of extracting and tracking wave components.

This is where the identification of localised high energy areas and the tracking of them may be of greater interest.

Other applications utilising wavelets have been discussed, further investigation of these concepts are needed.

4 H_∞ Control

4.1 Introduction

Why H_∞? The objective of a ship roll controller is to reduce the major roll motions which are experienced in the region of a vessel's natural roll frequency. Therefore, an approach that permits the control designer to manipulate the controller in various ways in the frequency domain is important. The H_∞ methodology has the ability to generate robust and stable controllers, despite the differences between the idealised model and reality. This is the point at which many other methods become unreliable. *"Good multivariable feedback loop design boils down to achieving high loop (and possibly controller) gains in the necessary frequency range."* [74]. This is where an H_∞ control design process is superior to many other comparable approaches, such as PID, H_2 and LQG. It provides the user with a tool, where there is a great deal of direction over selecting these necessary frequency ranges and performance requirements. To take advantage of these benefits a higher degree of complexity is added to the control problem. The user not only has to set up the performance requirements, that are indicated by way of the weighting functions, but has to ensure that these functions do not conflict with the mathematical formulations, allowing a suitable controller or set of controllers to be determined.

The solutions to the H_∞ control problem are extremely intricate, demanding specific software to be used in order to derive easily controllers. The use of the Matlab software [72] and toolboxes [75] clearly identifies problems resulting from invalidating the highly sensitive numerics. With this knowledge, the model can be altered to a problem for which H_∞ controllers can be derived. This is particularily useful in the selection of valid weighting functions.

As a consequence of this, H_∞ control can be more difficult to implement than conventional methods, but this can result in more versatile and robust controllers.

4.2 H_∞ Theory

H_∞ control is so called because it uses the H_∞ norm to compare the performance of various functions. The H_∞ norm is a measure of the size or magnitude of a function. With this control method, the objective is to minimise this value for particular transfer functions. This concept will become more apparent in the following sections.

Such an H_∞ norm condition for a transfer function G can be defined as:

$$||G||_\infty = \sup_\omega \bar{\sigma}\left(G\left(j\omega\right)\right) \tag{17}$$

where sup stands for the supremum, $\bar{\sigma}$ is the largest singular value, such that:

$$\bar{\sigma}\left(A\right) = \max_{||x||=1} ||Ax|| \tag{18}$$

The supremum is the least upper bound, relating to the largest singular value of a frequency response matrix. This is a means of describing the performance of a system.

The following derivation is a state space representation of a transfer function, where the packed matrix notation has been used.

A transfer function of a system in state space matrix form. Using appendix A this can be written as:

$$G(s) = C(sI - A)^{-1}B + D \tag{19}$$

- A: the system matrix
- B: the input matrix
- C: the output matrix
- D: the feedforward matrix

When converted into a packed matrix form, equation 19 becomes:

$$G(s) = \left[\begin{array}{c|c} \mathrm{A} & \mathrm{B} \\ \hline \mathrm{C} & \mathrm{D} \end{array}\right] \tag{20}$$

This form is commonly used in control design and is a simplier means of defining the matrix content of the plant, due to its compact nature.

From figure 39, P represents the augmented plant, that is the system to be controlled. F represents the controller dynamics.

A system to be controlled can be given in the following form:

$$z = P_{11}v + P_{12}u \tag{21}$$
$$y = P_{21}v + P_{22}u \tag{22}$$
$$u = Fy \tag{23}$$

- v: the external inputs
- u: the control inputs
- y: the feedback signal
- z: the regulated outputs

4.2.1 Linear Fractional Transformation

From equations 21,22,23, the closed loop transfer function can be derived, which is the functional relationship between z and v.

Substituting equation 23 into equation 22 gives:

$$y = P_{21}v + P_{22}Fy \tag{24}$$

This means that y can be expressed in terms of the external inputs:

$$(I - P_{22}F)y = P_{21}v \tag{25}$$

Therefore, the control inputs can be given as:

$$y = (I - P_{22}F)^{-1}P_{21}v \tag{26}$$

Substituting equation 26 into equation 23:

$$u = F(I - P_{22}F)^{-1}P_{21}v \tag{27}$$

Substituting this in equation 21

$$z = P_{11}v + P_{12}F(I - P_{22}F)^{-1}P_{21}v \tag{28}$$

$$z = \left[P_{11} + P_{12}F(I - P_{22}F)^{-1}P_{21}\right]v \tag{29}$$

This results in the linear fractional transformation, the transformation matrix from v to z:

$$z = T_{zv}v \tag{30}$$

with:

$$T_{zv} = P_{11} + P_{12}F(I - P_{22}F)^{-1}P_{21} \tag{31}$$

4.2.2 Standard H_∞ Formulation

A state space representation of the plant can also be given as:

$$\begin{aligned} \dot{x} &= Ax + B_1 v + B_2 u \\ z &= C_1 x + D_{11} v + D_{12} u \\ y &= C_2 x + D_{21} v + D_{22} u \end{aligned} \tag{32}$$

Using the packed matrix form as per equation 20, this becomes:

$$G(s) = \left[\begin{array}{c|cc} \mathrm{A} & B_1 & B_2 \\ \hline C_1 & D_{11} & D_{12} \\ C_2 & D_{21} & D_{22} \end{array}\right] \tag{33}$$

This all leads to the standard H_∞ control problem that is based in the following equation:

$$||T_{zv}||_\infty < \gamma \tag{34}$$

The ∞ norm of the transfer function between z and v is given as:

$$||T_{zv}||_\infty = \left\| \begin{array}{c} W_1 S \\ W_2 F S \\ W_3 T \end{array} \right\|_\infty \tag{35}$$

where,

$$\begin{aligned} S &= (I + GF)^{-1} \\ T &= GF\,(I + GF)^{-1} \end{aligned} \tag{36}$$

- with S denoting the closed loop sensitivity
- T representing the complimentary sensitivity
- and FS denoting the control sensitivity.

The W_i denote the weightings, these functions are used to give the controller its required performance and are fundamental elements of the design process. These are described in more detail later in this section.

4.3 Simplified H_∞ Control Problem

This section gives a brief outline of the underlying theory used. The mathematics used in the H_∞ control process, is quite complex and has been tackled in other publications, such as [74].

This is based on a simplified H_∞ control problem, with the plant given as:

$$G(s) = \left[\begin{array}{c|cc} \mathrm{A} & \mathrm{B_1} & \mathrm{B_2} \\ \hline \mathrm{C_1} & 0 & \mathrm{D_{12}} \\ \mathrm{C_2} & \mathrm{D_{21}} & 0 \end{array}\right] \tag{37}$$

and the following assumptions applying:

- (A, B_1) is controllable and (C_1, A) is observable
- (A, B_2) is stabilisable and (C_2, A) is detectable
- D_{12} has full column rank and D_{21} has full row rank
- $D_{11} = 0$ and $D_{22} = 0$
- $D_{12}^T \left[\begin{array}{cc} C_1 & D_{12} \end{array}\right] = \left[\begin{array}{cc} 0 & I \end{array}\right]$
- $\left[\begin{array}{c} B_1 \\ D_{21} \end{array}\right] D_{21}^T = \left[\begin{array}{c} 0 \\ I \end{array}\right]$

The fundamental formulation involved in H_∞ control is the Algebraic Riccati Equation (ARE),

$$A^T X + XA + XRX + Q = 0 \tag{38}$$

The Hamiltonian matrix is used to find the solutions to the ARE, and is given as,

$$H = \left[\begin{array}{cc} A & -R \\ -Q & -A^T \end{array}\right] \tag{39}$$

with $R = BB^T$ and $Q = C^T C$, and assuming that **H** possesses no eigenvalues on the imaginary axis.

If X_1 is non-singular, then,

$$X = X_2 X_1^{-1} \tag{40}$$

denotes the complimentary property.

From equation 39 and 38, the H_∞ problem solution incorporates the following two Hamiltonian matrices:

$$H_{X_\infty} = \begin{bmatrix} A & \gamma^{-2}B_1B_1^T - B_2B_2^T \\ -C_1^TC_1 & -A^T \end{bmatrix} \tag{41}$$

$$H_{Y_\infty} = \begin{bmatrix} A^T & \gamma^{-2}C_1C_1^T - C_2C_2^T \\ -B_1^TB_1 & -A \end{bmatrix} \tag{42}$$

Resulting in the following ARE equations:

$$A^TX_\infty + X_\infty A + X_\infty\left(\gamma^{-2}B_1B_1^T - B_2B_2^T\right)X_\infty + C_1^TC_1 = 0 \tag{43}$$

$$AY_\infty + Y_\infty A^T + Y_\infty\left(\gamma^{-2}C_1^TC_1 - C_2^TC_2\right)Y_\infty + B_1B_1^T = 0 \tag{44}$$

The following three conditions must be met, for an acceptable controller to exist, such that $\|T_{zv}\|_\infty < \gamma$

$$\begin{array}{lll} H_{X_\infty} \in dom\,(\text{Ric}) & \text{and} & X_\infty = \text{Ric}\,(H_{X_\infty}) \geq 0 \\ H_{Y_\infty} \in dom\,(\text{Ric}) & \text{and} & Y_\infty = \text{Ric}\,(H_{Y_\infty}) \geq 0 \\ \rho\,(X_\infty Y_\infty) < \gamma^2 & & \end{array} \tag{45}$$

where,

- $dom(Ric)$ represents the domain of Ric comprising of the Hamiltonian matrices with the stability and complimentary properties.
- $Ric(i)$ denotes the Riccati equation possesses a stabilising solution.
- ρ represents the spectral radius, which is the maximum eigenvalue. i.e.

$$\rho(A) = \max_{1\leq i\leq n} |\lambda_i| \tag{46}$$

If these conditions are met, the controller can be given as,

$$F = \left[\begin{array}{c|c} A_F & B_F \\ \hline C_F & 0 \end{array}\right] \tag{47}$$

where,

$$A_F = A + \gamma^{-2} B_1 B_1^T X_\infty + B_2 C_F - B_F C_2 \quad (48)$$

$$B_F = \left(I - \gamma^{-2} Y_\infty X_\infty\right)^{-1} Y_\infty C_2^T \quad (49)$$

$$C_F = -B_2^T X_\infty \quad (50)$$

It must be borne in mind that the explanation given above relates to a simplified H_∞ control problem, in order to give the reader a background of the H_∞ theory adopted for this work.

4.4 Optimal - Sub-Optimal

The optimisation process is based on the T_{zv} function given in equation 31. If $||T_{zv}||_\infty$ is below a pre-determined value, γ and the closed loop system is stable for all admissible uncertainties, then a controller of this performance may be found. This will lead to the creation of a sub-optimal controller, as at this stage no attempt has been made to vary the magnitude of γ.

To achieve an optimum controller, γ has to be minimised. This is accomplished by decreasing γ to the point where no valid solution can be found. This is usually carried out by incrementally decreasing the magnitude of γ. As the optimal value is approached, the mathematical formulations become extremely sensitive, therefore great care and attention has to be given to the initial design formulation to eliminate any potential numerical problems. Adoption of a sub-optimal controller can be more beneficial in many cases, as the rigourous conditioning and numerical sensitivity associated with an optimal γ can be too restrictive forming a very conservative controller or even prevent a practical controller being derived.

4.5 Augmented Plant

The augmented plant is a complete description of the system for which a controller is to be designed. It contains a formulation of the nominal plant dynamics, and functions called weightings. These are used to characterise frequency properties of the system where high levels of control are desired or where there is uncertainty in the model definition. It is the augmented plant description that is the primary input into the Matlab package and its toolboxes [75].

The following equation defines the augmented plant for the simple fin roll controller.

$$P = \left[\begin{array}{c|c} \gamma W_1 & -\gamma W_1 G_{\varphi\alpha} \\ 0 & \gamma W_2 \\ 0 & \gamma W_3 G_{\varphi\alpha} \\ \hline I & -G_{\varphi\alpha} \end{array}\right] \tag{51}$$

4.6 Matlab

Matlab was selected at an early stage in this project, to be used as a tool for the development of the controllers. This was chiefly due to its associated Robust Control Toolbox [75]. This contains routines to carry out the H_∞ process to form controllers, as well as reduction routines, all within a well structured format.

The highly complex mathematical nature of the H_∞ problem is encompassed within a framework that enables the user to easily identify problems through set error statements, allowing ease of model development. This is beneficial in H_∞ controller design, in that determining augmented plants for which controllers can be found is problematic, due to the large number of conditions that must be satisfied. The plants must also maintain a sensible idealisation of the plant characteristics, this can easily be lost in the process of adapting weightings that satisfy all the control criteria. It is very easy to satisfy each of the conditions on their own, but to satisfy them simultaneously can be difficult, hence the use of the Matlab to simplify the process.

4.7 Robustness

A major benefit of the H_∞ control approach is in its ability to form robust and stable controllers despite the existence of modelling errors, uncertainties and system variations.

Modelling errors are always present in any controller design process. This is a result of the mathematical representation used to create the system idealisation, therefore in most cases model non-linearities are not appreciated; for a ship fin roll control system this would be the effects of the fins reaching the stops, or the effects of limiting fin rotation rates. It is also due to the simplifications used to create the idealisation, it can be extremely difficult to represent a complex physical system without resorting to elaborate mathematical formulations that are probably difficult to incorporate within a controller design process. Therefore, a balance has to be achieved between the model accuracy and the ease with which the idealised model can be incorporated and used within the design process.

H_∞ control designs result in relatively high order controllers. These can be quite complex to implement and lead to high computation demands. The controller can be reduced in order to acceptable levels, using the performance of the higher order controller as a guide with which to compare and manipulate the reduced order controller performance. A number of reduction methods exist, the use of these have been described in [74]. This route has advantages over alternative approaches, because the effects of important plant characteristics are incorporated within the controller prior to reduction and can be maintained through careful reduction.

Model uncertainties result from the differences between the modelled plant and the real system, some of these can be the consequence of difficulties in modelling known model behaviour within a mathematical framework which can then be implemented into a design method. Other uncertainties may result from unexpected system behaviour in particular conditions or in frequency ranges where model knowledge is low. In the case of a ship's behaviour, this could be related to vessel's performance in a large stern quartering seas.

Therefore any control approach must be able to cope with these differences. This is the area where H_∞ is of prime suitability in comparison to many other control approaches, in its robustness.

4.8 Weightings

One of the major design elements in the H_∞ design process is the selection of weighting functions, these are a means of forming a controller to specific performance objectives. This allows the designer to identify (principally in the frequency domain) particular areas where model accuracy is high leading to higher loop gains. These areas of high loop gain produce high fin activity potentially resulting in large motion reductions. For areas of uncertainty the loop gain can be reduced, in the case of ship roll control this may be at the very low and high frequencies where modelling is less accurate. This leads to the possibility of error rejection in specific frequency ranges, such as minimising the effects of sensor noise at high frequencies for a roll rate sensor. The weighting functions can also be used to emphasize or reduce the effects of particular signal content.

These weightings must be selected so that the control model satisfies the numerical solution criteria. This restricts the order and form of the weightings, so careful selection of these functions is critical. The selection of weightings does not follow a set routine, and is very application dependent. Therefore a full explanation for the problem of ship fin roll and LFE stabilisation has been given in chapter 6.

5 System Modelling

The first step in any control design process, is to create a nominal representation of the plant to be controlled. This leads to the question of which format to use to define the plant.

- Transfer function form
- State space representation

A major aim of this work is to create a LFE controller. LFE, is by its very nature composed of motions from three degrees of freedom. This makes modelling the system equations of motion using transfer function form problematic, necessitating the use of the state space approach.

The system equations of motion for sway, roll and yaw are given as:

$$\ddot{y} = \frac{F_2(t) - (a_{24}\ddot{\varphi} + a_{26}\ddot{\chi} + b_{22}\dot{y} + b_{24}\dot{\varphi} + b_{26}\dot{\chi} + c_{27}\alpha)}{m + a_{22}} \tag{52}$$

$$\ddot{\varphi} = \frac{M_4(t) - (a_{42}\ddot{y} + a_{46}\ddot{\chi} + b_{22}\dot{y} + b_{44}\dot{\varphi} + b_{46}\dot{\chi} + c_{44}\varphi + c_{47}\alpha)}{I_4 + a_{44}} \tag{53}$$

$$\ddot{\chi} = \frac{M_6(t) - (a_{62}\ddot{y} + a_{64}\ddot{\varphi} + b_{62}\dot{y} + b_{64}\dot{\varphi} + b_{66}\dot{\chi} + c_{67}\alpha)}{I_6 + a_{66}} \tag{54}$$

The added mass, damping and restoring coefficients a_{ij}, b_{ij} and c_{ij} are in this case calculated using the seakeeping software [10], and are described in detail in [4]. It is known that these coefficients are frequency dependent [76, 4], but over a frequency range close to the natural frequency are assumed to remain constant. These values are therefore determined for the vessel at the natural roll frequency.

The objective is to convert equations 52,53,54 into a state space representation, characterising the vessel's dynamics. Using Equation 52 as an example, it consists of the acceleration components of both roll $\ddot{\varphi}$ and yaw $\ddot{\chi}$ due to coupling. These terms have to be replaced by state variables.

This has been completed in the following example for equation 52, the same methodology has been used to derive the relationships for $\ddot{\varphi}$ and $\ddot{\chi}$ in terms of the state variables:

The state variables consist of:

$$
\begin{aligned}
x_1 &= \dot{y} \\
x_2 &= y \\
x_3 &= \dot{\varphi} \\
x_4 &= \varphi \\
x_5 &= \dot{\chi} \\
x_6 &= \chi
\end{aligned} \tag{55}
$$

To solve $\ddot{y}$ in terms of the state variables

$$
\dot{x}_1 = \ddot{y} \tag{56}
$$

$\ddot{\varphi}$ is to be defined in terms of the state variables and $\ddot{y}$.
Therefore equation 54 is substituted into equation 53.

$$
\begin{aligned}
(I_4 + a_{44} + \mathcal{A}a_{64})\,\ddot{\varphi} &= -(\ddot{y}(a_{42} + \mathcal{A}a_{62}) + \dot{y}(b_{42} + \mathcal{A}b_{62}) + \dot{\varphi}(b_{44} + \mathcal{A}b_{64})) \\
&- (\dot{\chi}(b_{46} + \mathcal{A}b_{66}) + \varphi c_{44} + \alpha(c_{47} + \mathcal{A}c_{67}))
\end{aligned} \tag{57}
$$

with,

$$
\mathcal{A} = \frac{-a_{46}}{I_6 + a_{66}} \tag{58}
$$

Equation 53 is substituted into equation 54, to give $\ddot{\chi}$ in terms of $\ddot{y}$.

$$
\begin{aligned}
(I_6 + a_{66} + \mathcal{B}a_{46})\,\ddot{\chi} &= -(\ddot{y}(a_{62} + \mathcal{B}a_{42}) + \dot{y}(b_{62} + \mathcal{B}b_{42}) + \dot{\varphi}(b_{46} + \mathcal{B}b_{44})) \\
&- (\dot{\chi}(b_{66} + \mathcal{B}b_{46}) + \varphi\mathcal{B}c_{44} + \alpha(c_{67} + \mathcal{B}c_{47}))
\end{aligned} \tag{59}
$$

with,

$$
\mathcal{B} = \frac{-a_{64}}{I_4 + a_{44}} \tag{60}
$$

When equations 57 and 59 are substituted into equation 52, $\ddot{y}$ becomes:

$$
\ddot{y} = \frac{\dot{y}Z_{\ddot{y}\dot{y}} + \dot{\varphi}Z_{\ddot{y}\dot{\varphi}} + \dot{\chi}Z_{\ddot{y}\dot{\chi}} + \varphi Z_{\ddot{y}\varphi} + \alpha Z_{\ddot{y}\alpha}}{Z_{\ddot{y}}} \tag{61}
$$

with,

$$\begin{aligned}\mathcal{P} &= I_4 + a_{44} + \mathcal{A}a_{64} \\ \mathcal{Q} &= I_6 + a_{66} + \mathcal{B}a_{46}\end{aligned} \tag{62}$$

and,

$$\begin{aligned}Z_{\ddot{y}\dot{y}} &= -b_{22} + \frac{a_{24}(b_{42} + \mathcal{A}b_{62})}{\mathcal{P}} + \frac{a_{26}(b_{62} + \mathcal{B}b_{42})}{\mathcal{Q}} \\ Z_{\ddot{y}\dot{\varphi}} &= -b_{24} + \frac{a_{24}(b_{44} + \mathcal{A}b_{64})}{\mathcal{P}} + \frac{a_{26}(b_{64} + \mathcal{B}b_{44})}{\mathcal{Q}} \\ Z_{\ddot{y}\dot{\chi}} &= -b_{26} + \frac{a_{24}(b_{46} + \mathcal{A}b_{66})}{\mathcal{P}} + \frac{a_{26}(b_{66} + \mathcal{B}b_{46})}{\mathcal{Q}} \\ Z_{\ddot{y}\varphi} &= \frac{a_{24}c_{44}}{\mathcal{P}} + \frac{\mathcal{B}a_{26}c_{44}}{\mathcal{Q}} \\ Z_{\ddot{y}\alpha} &= -c_{27} + \frac{a_{24}(c_{47} + \mathcal{A}c_{67})}{\mathcal{P}} + \frac{a_{26}(c_{67} + \mathcal{B}c_{47})}{\mathcal{Q}} \\ Z_{\ddot{y}} &= m + a_{22} - \frac{a_{24}(a_{42} + \mathcal{A}a_{62})}{\mathcal{P}} - \frac{a_{26}(a_{62} + \mathcal{B}a_{42})}{\mathcal{Q}}\end{aligned} \tag{63}$$

This is then combined within the state space matrices, to form the nominal system model on which the controller is to be developed.

This has also been carried out upon the $\ddot{\varphi}$ and $\ddot{\chi}$ components, yielding the following equations

$$\ddot{\varphi} = \frac{\dot{y}Z_{\ddot{\varphi}\dot{y}} + \dot{\varphi}Z_{\ddot{\varphi}\dot{\varphi}} + \dot{\chi}Z_{\ddot{\varphi}\dot{\chi}} + \varphi Z_{\ddot{\varphi}\varphi} + \alpha Z_{\ddot{\varphi}\alpha}}{Z_{\ddot{\varphi}}} \tag{64}$$

$$\ddot{\chi} = \frac{\dot{y}Z_{\ddot{\chi}\dot{y}} + \dot{\varphi}Z_{\ddot{\chi}\dot{\varphi}} + \dot{\chi}Z_{\ddot{\chi}\dot{\chi}} + \varphi Z_{\ddot{\chi}\varphi} + \alpha Z_{\ddot{\chi}\alpha}}{Z_{\ddot{\chi}}} \tag{65}$$

with,

$$\begin{aligned}\mathcal{D} &= -\frac{a_{26}}{I_6 + a_{66}} \\ \mathcal{E} &= -\frac{a_{62}}{m + a_{22}} \\ \mathcal{H} &= -\frac{a_{42}}{m + a_{22}} \\ \mathcal{J} &= -\frac{a_{24}}{I_4 + a_{44}}\end{aligned} \tag{66}$$

and,

$$
\begin{aligned}
\mathcal{F} &= m + a_{22} + \mathcal{D}a_{62} \\
\mathcal{G} &= I_6 + a_{66} + \mathcal{E}a_{26} \\
\mathcal{I} &= I_4 + a_{44} + \mathcal{H}a_{24} \\
\mathcal{K} &= m + a_{22} + \mathcal{J}a_{42}
\end{aligned} \tag{67}
$$

and,

$$
\begin{aligned}
Z_{\ddot{\varphi}\dot{y}} &= -b_{42} + \frac{a_{42}(b_{22} + \mathcal{D}b_{62})}{\mathcal{F}} + \frac{a_{46}(b_{62} + \mathcal{E}b_{22})}{\mathcal{G}} \\
Z_{\ddot{\varphi}\dot{\varphi}} &= -b_{44} + \frac{a_{42}(b_{24} + \mathcal{D}b_{64})}{\mathcal{F}} + \frac{a_{46}(b_{64} + \mathcal{E}b_{24})}{\mathcal{G}} \\
Z_{\ddot{\varphi}\dot{\chi}} &= -b_{46} + \frac{a_{42}(b_{26} + \mathcal{D}b_{66})}{\mathcal{F}} + \frac{a_{46}(b_{66} + \mathcal{E}b_{26})}{\mathcal{G}} \\
Z_{\ddot{\varphi}\varphi} &= -c_{44} \\
Z_{\ddot{\varphi}\alpha} &= -c_{47} + \frac{a_{42}(c_{27} + \mathcal{D}c_{67})}{\mathcal{F}} + \frac{a_{46}(c_{67} + \mathcal{E}c_{27})}{\mathcal{G}} \\
Z_{\ddot{\varphi}} &= I_4 + a_{44} - \frac{a_{42}(a_{24} + \mathcal{D}a_{64})}{\mathcal{F}} - \frac{a_{46}(a_{64} + \mathcal{E}a_{24})}{\mathcal{G}}
\end{aligned} \tag{68}
$$

and,

$$
\begin{aligned}
Z_{\ddot{\chi}\dot{y}} &= -b_{62} + \frac{a_{64}(b_{42} + \mathcal{H}b_{22})}{\mathcal{I}} + \frac{a_{62}(b_{22} + \mathcal{J}b_{42})}{\mathcal{K}} \\
Z_{\ddot{\chi}\dot{\varphi}} &= -b_{64} + \frac{a_{64}(b_{44} + \mathcal{H}b_{24})}{\mathcal{I}} + \frac{a_{62}(b_{24} + \mathcal{J}b_{44})}{\mathcal{K}} \\
Z_{\ddot{\chi}\dot{\chi}} &= -b_{66} + \frac{a_{64}(b_{46} + \mathcal{H}b_{26})}{\mathcal{I}} + \frac{a_{62}(b_{26} + \mathcal{J}b_{46})}{\mathcal{K}} \\
Z_{\ddot{\chi}\varphi} &= \frac{a_{64}c_{44}}{\mathcal{I}} + \frac{\mathcal{J}a_{62}c_{44}}{\mathcal{K}} \\
Z_{\ddot{\chi}\alpha} &= -c_{67} + \frac{a_{64}(c_{47} + \mathcal{H}c_{27})}{\mathcal{I}} + \frac{a_{62}(c_{27} + \mathcal{J}c_{47})}{\mathcal{K}} \\
Z_{\ddot{\chi}} &= I_6 + a_{66} - \frac{a_{64}(a_{42} + \mathcal{H}a_{26})}{\mathcal{I}} - \frac{a_{62}(a_{26} + \mathcal{J}a_{46})}{\mathcal{K}}
\end{aligned} \tag{69}
$$

The state equation:

$$
\dot{x} = Ax + Bu \tag{70}
$$

for this example becomes:

$$\begin{bmatrix} \ddot{y} \\ \dot{y} \\ \ddot{\varphi} \\ \dot{\varphi} \\ \ddot{\chi} \\ \dot{\chi} \end{bmatrix} = \begin{bmatrix} Z_{\ddot{y}\dot{y}}/Z_{\ddot{y}} & 0 & Z_{\ddot{y}\dot{\varphi}}/Z_{\ddot{y}} & Z_{\ddot{y}\varphi}/Z_{\ddot{y}} & Z_{\ddot{y}\dot{\chi}}/Z_{\ddot{y}} & 0 \\ 1 & 0 & 0 & 0 & 0 & 0 \\ Z_{\ddot{\varphi}\dot{y}}/Z_{\ddot{\varphi}} & 0 & Z_{\ddot{\varphi}\dot{\varphi}}/Z_{\ddot{\varphi}} & Z_{\ddot{\varphi}\varphi}/Z_{\ddot{\varphi}} & Z_{\ddot{\varphi}\dot{\chi}}/Z_{\ddot{\varphi}} & 0 \\ 0 & 0 & 1 & 0 & 0 & 0 \\ Z_{\ddot{\chi}\dot{y}}/Z_{\ddot{\chi}} & 0 & Z_{\ddot{\chi}\dot{\varphi}}/Z_{\ddot{\chi}} & Z_{\ddot{\chi}\varphi}/Z_{\ddot{\chi}} & Z_{\ddot{\chi}\dot{\chi}}/Z_{\ddot{\chi}} & 0 \\ 0 & 0 & 0 & 0 & 1 & 0 \end{bmatrix} \begin{bmatrix} \dot{y} \\ y \\ \dot{\varphi} \\ \varphi \\ \dot{\chi} \\ \chi \end{bmatrix} \quad (71)$$

$$+ \begin{bmatrix} Z_{\ddot{y}\alpha}/Z_{\ddot{y}} \\ 0 \\ Z_{\ddot{\varphi}\alpha}/Z_{\ddot{\varphi}} \\ 0 \\ Z_{\ddot{\chi}\alpha}/Z_{\ddot{\chi}} \\ 0 \end{bmatrix} \alpha$$

It is from this, that a majority of the nominal plants used for H_∞ control designs have been constructed.

To speed up this process, a Fortran program has been written to accept seakeeping motion files and determine values for equation 72.

5.1 Lateral Force Estimator (LFE)

LFE is essentially the acceleration in the plane of the deck for a particular point in the ship. This is the acceleration that may cause loss of balance of a crew member or make an object slide across the deck. As LFE increases with higher sea states, so the effectiveness of crew and the operation of shipborne systems diminishes.

Let y_d and z_d denote the lateral and vertical accelerations in the plane of the deck of a transverse ship section, this can be seen in figure 40. Therefore,

$$\begin{aligned} \ddot{y}_d &= \ddot{y}\cos\varphi + \ddot{z}\sin\varphi \\ \ddot{z}_d &= \ddot{z}\cos\varphi - \ddot{y}\sin\varphi \end{aligned} \quad (72)$$

These accelerations are combined with the gravity component resolved parallel and normal to the deck plane. As the roll angle increases, so the component due to gravity increases in the plane of the deck. These are the apparent accelerations perceived by an object in the plane of the deck and are given by:

$$\begin{aligned} \ddot{y}_p &= \ddot{y}_d - g\sin\varphi \\ &= \ddot{y}\cos\varphi + \ddot{z}\sin\varphi - g\sin\varphi \\ \ddot{z}_p &= \ddot{z}\cos\varphi - \ddot{y}\sin\varphi - g(1-\cos\varphi) \end{aligned} \tag{73}$$

When small amplitude motions are assumed, these can be reduced to:

$$\begin{aligned} \ddot{y}_p &= \ddot{y} - g\varphi \\ \ddot{z}_p &= \ddot{z} \end{aligned} \tag{74}$$

Therefore, LFE is the apparent acceleration in the plane of the deck.

The following equation, is a more general formulation taking into account the position within the ship.

$$LFE = \ddot{y} - z\ddot{\varphi} + x\ddot{\chi} - g\varphi \tag{75}$$

Therefore the magnitude of LFE is dependent upon location. The greater the lever from the centre of gravity (CG), the greater the potential value of LFE. This is the reason that the flight deck of a frigate has large LFE values, due to its aft position with a large lever to the CG combined with its height above the CG.

6 Controller Design

Motion stabilisation is a necessity on modern warships. As the need for ships to operate in more extreme environments increases, so the need to minimise the effects of these conditions is necessary. Fin stabilisation can reduce roll significiantly, leading to safer operation of the ship, reduced effects of motions upon the crew, and increased availability of shipborne systems such as the deployment of a helicopter.

Fin stabilisers are active, they need continuous control inputs to vary their angle of attack in order to produce a righting moment that will oppose the wave induced roll moment. Therefore the overall performance of the fin system is directly related to the quality of the controller used.

This chapter outlines the controller designs that were used to create the motion reducing controllers summarised in this thesis. The use of H_∞ as a candidate for an improved controller design method over classic methods has been discussed in a previous chapter.

6.1 Classic Roll

Three term control is often referred to as proportional, integral derivative PID control. The definition of the control is dependent upon the motion measuring device, whether it be a roll angle potentiometer, a roll rate sensor/gyro or accelerometers. In this discussion, proportional signifies the roll rate, integral the roll angle and derivative roll acceleration. Classic roll stabilisation controllers were often in the form of two term PD controllers. A typical control system consists of feedback of the roll motion and the roll velocity, as adopted by Dallinga [32].

The roll velocity component has the dominant effect in reducing roll motion. This is due to roll velocity always opposing roll motion, with a maximum at zero roll angle, where greatest fin angles would have significant roll reducing effects.

An approach for the formation of fin roll stabilisation controllers is outlined in Lloyd [4]. This is often termed the *frequency response method.* This technique is the basis for a large proportion of modern day ship fin controllers, and has therefore been used as the benchmark for comparison of other controller designs.

The formula for this roll stabilisation method can be given as

$$\frac{\alpha}{\varphi} = K_G \left[\frac{K_1 + K_2 s + K_3 s^2}{b_1 + b_2 s + b_3 s^2} \right] \tag{76}$$

where,

- α represents the demanded fin angle
- φ denotes the roll angle
- K_G represents the overall gain
- K_1, K_2 and K_3 are the roll angle and derivative sensitivites
- b_1, b_2 and b_3 are the fixed coefficients

The K_i sensitivites are selected to oppose the ship roll motion accounting for the phase difference, between the fin angle and ship roll. This necessitates a forced rolling test in order to determine the phase lag. Using the approach as detailed in appendix B, a relationship for sensitivities can be found. From this, a range of possible coefficients are calculated.

6.1.1 Selection of Control Coefficients

A range of possible sets of control coefficients with various sensitivity gain distributions were determined by using the method set out in appendix B. After comparative tests using the motion software [10], a set of coefficients biased towards the roll velocity component was selected as a typical classic roll controller. This gave good roll attenuating properties over a wide frequency range, and satisfies the condition of a high velocity contribution, as per [4, 32]. This includes a low K_1 contribution, which is necessary to prevent fin deflections resulting from zero frequency components due to loading conditions for example.

6.1.2 Classic LFE

In this section, the control of LFE is carried out using a similar method to that used for roll stabilisation given in [4]. The transfer function for classic roll control (equation 76) is used, by substituting LFE in place of the measured roll angle, LFE stabilisation may be attempted.

$$\frac{\alpha}{LFE} = K_G \left[\frac{K_1 + K_2 s + K_3 s^2}{b_1 + b_2 s + b_3 s^2} \right] \tag{77}$$

The procedure used for determining the control coefficients is that used by Tang and Wilson [3]. The controller was first tuned at the natural roll frequency with the overall gain being adjusted to maintain a specific rms fin angle for a particular sea spectrum condition. As with the work of Tang and Wilson, this produced a poor LFE controller. Therefore, the controller

was adjusted to other frequencies by adopting the same tuning process. This produced more satisfactory controllers for a tuning frequency lower than that of the natural roll, but comparative LFE reductions to the levels given in [3] were not achieved. This took quite a time and was a computationally expensive process, using essentially a trial and error method. The overall LFE attenuation of the LFE controller in this case was worse than the classic roll controller.

6.1.3 Search LFE

The method described above was essentially extended to form a global search mechanism, to obtain control coefficients for equation 77.

A matrix of values for the K_i control coefficients was set up, this consisted of an incremental set of values for each coefficient.

Therefore at each step, K_1, K_2, K_3 were selected. The set of sensitivities was then run through the motion program to determine the fin performance, this is linked into an iterative routine which calculates the ship motions given a particular fin response limit, where the overall gain K_G is calculated. If the ship motions are above a particular threshold or above the most favourable ship motion reduction achieved previously, then the new values are rejected, and the next increment is made to the sensitivity test matrix. If the values are the lowest, an *optimum*, then the sensitivities and their related motions are stored.

The search must cover a large range of values for each sensitivity in order to identify a global minima, not a localised value.

This type of approach is extremely computationally expensive. The major disadvantage of this method is the seakeeping code will type form the controller. The user needs to interpret the results in order to extract a controller that satisfies a magnitude of criteria, many of which are qualitative. This process did identify an LFE controller that had higher LFE attenuating properties than those determined through the tuning procedure. This approach essentially eliminates the *design process*, and necessitates careful checking of the final controllers.

6.2 H_∞ Controller Designs

The coefficients for all the controller designs listed below have been derived using the system equations of motions formulated using the software [10], and have been outlined in chapter 5.

The H_∞ controller design process comprises of two elements:

- The nominal plant description
- Weighting selection

The nominal plant description is a definition of the system to be controlled, in this case in state space format. The weightings are functions that are combined with the nominal plant representation to place more control emphasis in particular frequency ranges and less in others. These are combined in the following equation:

$$\mathbf{P} = \left[\begin{array}{c|c} \gamma W_1 & -\gamma W_1 G_{\varphi\alpha} \\ 0 & \gamma W_2 \\ 0 & \gamma W_3 G_{\varphi\alpha} \\ \hline I & -G_{\varphi\alpha} \end{array}\right] \tag{78}$$

This is to form **P**; the augmented plant for which the controllers will be determined. Therefore this section has been split into two parts, the first describes the nominal plant designs, and the latter outlines the weighting functions used.

6.2.1 Roll Controller Design

The following equation is a basic representation of the ship fin-roll model. The model only contains roll and its derivatives. The coupling between roll and the sway and yaw degrees of freedom is acknowledged, but as the contributions are not observable, a successful roll controller based on the full system equations would therefore be problematic to form, and necessitate the use of the three anti-symmetric DOFs and their derivative controller inputs.

$$\begin{bmatrix} \ddot{\varphi} \\ \dot{\varphi} \end{bmatrix} = \begin{bmatrix} Z_{\ddot{\varphi}\dot{\varphi}}/Z_{\ddot{\varphi}} & Z_{\ddot{\varphi}\varphi}/Z_{\ddot{\varphi}} \\ 1 & 0 \end{bmatrix} \begin{bmatrix} \dot{\varphi} \\ \varphi \end{bmatrix} + \begin{bmatrix} Z_{\ddot{\varphi}\alpha}/Z_{\ddot{\varphi}} \\ 0 \end{bmatrix} \alpha \tag{79}$$

$$Y = \begin{bmatrix} 1 & 0 \end{bmatrix} \begin{bmatrix} \dot{\varphi} \\ \varphi \end{bmatrix} \tag{80}$$

Grimble et al based Roll Controller

This controller design method is based on the design approach outlined in [5]. In that example, both the fins and the rudder were used for roll reduction. This has been reduced to that of a roll fin controller approach. It uses a transfer function based on the natural roll frequency and roll damping coefficient to model the nominal ship model. The formulation used and description of the method is given in appendix C. The approach has been

implemented during model tests outlined in chapter 8 including a numerical analysis.

6.2.2 LFE Controller Design

The primary aim of developing a new LFE controller design method is to provide a tool that can be used to create suitable control systems which will use a well structured process to derive controllers. This may then be used to produce reliable and stable controllers, that will provide good performance in a range of sea conditions.

As described earlier in this section, the previous LFE controllers were based on a method similar to that of the roll frequency response tuning. This was problematic, in the fact that the optimal frequency of tuning was not located at the natural roll frequency. Through a simple search routine, more appropriate controllers were achieved, but this method was extremely computationally intensive.

A number of LFE controller designs have been investigated, which ranged in complexity from a simplified system model based only on the roll and its derivative contributions, to a model where the controller uses roll, sway and yaw controller inputs. The following LFE controller was successfully implemented, more complex designs were attempted, without achieving suitable controllers. This resulted from modelling difficulties created by LFE and by comforming to the H_∞ assumptions.

LFE Controller based on Roll and its Derivatives

This controller is based on the ship's system motions coefficients of roll and its derivatives. These coefficients are determined at the roll natural frequency, and the nominal plant is given as:

$$\begin{bmatrix} \ddot{\varphi} \\ \dot{\varphi} \end{bmatrix} = \begin{bmatrix} Z_{\ddot{\varphi}\dot{\varphi}}/Z_{\ddot{\varphi}} & Z_{\ddot{\varphi}\varphi}/Z_{\ddot{\varphi}} \\ 1 & 0 \end{bmatrix} \begin{bmatrix} \dot{\varphi} \\ \varphi \end{bmatrix} + \begin{bmatrix} Z_{\ddot{\varphi}\alpha}/Z_{\ddot{\varphi}} \\ 0 \end{bmatrix} \alpha \tag{81}$$

$$Y = \begin{bmatrix} -z * Z_{\ddot{\varphi}\dot{\varphi}}/Z_{\ddot{\varphi}} & -z * Z_{\ddot{\varphi}\varphi}/Z_{\ddot{\varphi}} - g \end{bmatrix} \begin{bmatrix} \dot{\varphi} \\ \varphi \end{bmatrix} \tag{82}$$

where z denotes the vertical location.

6.3 Weightings

A key factor of the H_∞ control method is in the selection of the weighting functions. This is critical, as to whether a possible controller may be

found and also whether it relates to the system under investigation. Three weighting functions have been adopted in the case of the controllers described previously.

6.3.1 Sensitivity Weight Function

The sensitivity weighting is used to define the required controller performance. This has to be carried out with the nominal plant definition in mind. The control system must only counteract motions resulting from wave action and not that attributed to other factors such as loading conditions and wind strength and direction which result in a zero frequency roll angle component.

The weighting is therefore maximised in the region of the natural roll frequency, which is also the frequency at which LFE is at a maximum. As the frequency difference from this is increased, so the desired control should be reduced. This leads to the use of the following function:

$$W_1(s) = \frac{As}{\left(\frac{s}{\omega_\varphi}\right)^2 + \left(\frac{2Bs}{\omega_\varphi}\right) + 1} \tag{83}$$

where,
ω_φ denotes the natural roll frequency.
A denotes the amplitude parameter.
and B the bandwidth parameter.

6.3.2 Control Sensitivity Function

The control sensitivity is used to influence the control signal and hence is used to reduce the low frequency fin activity, this prevents fin motion to resist the roll induced by turning and wind loading for example. The fin servos are unable to achieve high frequency fin activity due to powering limitations, so the control signal is reduced at the high frequencies. This results in a system where the fins should be less likely to meet the displacement and rate limitations. As a consequence of this, system wear will be reduced. This leads to the use of this Butterworth filter like function:

$$W_2(s) = \frac{\left(\frac{s}{\omega_{l\alpha}} + C\right)\left(\frac{Cs}{\omega_{h\alpha}} + 1\right)}{\left(\frac{Cs}{\omega_{l\alpha}} + 1\right)\left(\frac{s}{\omega_{h\alpha}} + C\right)} \tag{84}$$

where C represents the control action amplitude in the range between ω_l and ω_h.

6.3.3 Complementary Sensitivity Function

The complementary weighting is used to influence the output signal. This function accounts for the existence of model uncertainties. These will be most dominate outside the natural roll frequency region, as the nominal plant dynamics are only strictly valid for the natural frequency zone and hence the use of a function of the form:

$$W_3(s) = D\frac{\left(\frac{s}{\omega_\varphi}+1\right)^2}{\left(\frac{Ds}{\omega_\varphi}+0.01\right)\left(\frac{0.01s}{\omega_\varphi}+D\right)} \tag{85}$$

where D represents frequency range where robustness is required.

These weightings are combined with the nominal plant, to form the augmented plant representation. As can be seen in chapter 9, is not necessary to utilise all the weightings to form valid controllers.

7 Experimentation

7.1 Introduction

Experimentation provided a fundamental tool with which to test a range of possible controller designs, which would compliment the use of numerical approaches. Model tests would provide data that relates to the roll attenuating performances of the full scale vessel fin stabilisation system. It is from this, that different controller design performances could be compared. The information could also be used to evaluate the accuracy and suitability of results from numerical analysis, being used to validate the motion software [10].

Dallinga [32] carried out a range of model experiments with a free running 4.5 metre model with controllable fins. This work investigated the hydrodynamic aspects of active fins, with only a simple controller being employed. Controller design methods have been investigated through in-service vessel operation. The major problems are caused by weather variation during sea trials, in Hickey et al [36] the rms roll values were relatively low, this makes the comparison of different controllers difficult.

An aim of this work was to develop a system using both hardware and software that could easily be adapted for use on a number of different scale model types. Therefore, the apparatus must be relatively compact and light weight, and can be powered from a small power source such as a car battery. The system based on the work of Nicholson and Pegrum [77] was developed to meet this criteria, with the additional advantage of being very adaptable. New controller designs can easy be implemented through the Labview software [78], allowing major alterations to be made to the controller design in relatively short periods of time.

This chapter outlines the experimental set up used and the approach taken to analyse the results.

7.2 Available Methods

The scope of the term Experimentation is extremely large. This has been broken down into three main catagories:-

- Full Scale Sea Trials
- Free running large models
- Smaller scale towed models

7.2.1 Sea Trials

- Sea trials are extremely expensive and time-consuming. The time necessary to encounter a significant range of conditions could be extremely large, therefore the tests are dictated by prevailing weather conditions.
- Wave-buoys or other such methods may be needed to extract sea surface/spectral data, to use as a measure of the encountered conditions.
- Safety issues arise, as some controllers may exhibit unstable behaviour in particular conditions, such as the first rudder roll stailisers [41] which in some cases were unstable at high speeds in stern quartering seas.
- A major benefit is that this is the *realistic condition*, needing no scaling or interpretation.

7.2.2 Free Running Models

- Large wave making tank facilities or lake/sea areas are necessary for this type of testing. With open water, the experiments are limited by the prevailing conditions, producing similar problems to those listed for sea trials. Large model basins can provide a range of wave heights and frequencies, even irregular seas, but an extensive range of tests would be quite costly.
- There is the need to control the rudders for directional control, whether it be by remote control or an autopilot. This would allow the testing of integrated control systems.
- The model is self propelled, and usually of large scale. This provides sufficient space and mass carrying ability for the associated systems for propulsion, steering and control.

7.2.3 Towed Models

- This method is quite cost effective, due to the use of smaller tank faciilities without the need for wave generation, and the use of smaller scale models.

- A large number of runs can be conducted per a day, due to the shorter tank settling times. This allows many controller variations to be tested, at a range of frequencies and equivalent wave slopes.
- It must be borne in mind that the model is only free to pitch, heave and roll. This restricts the coupling with sway and yaw that would be experienced on the full scale vessel.
- There are also scale effects caused by dissimilar Reynolds numbers between model and full scale. This principally affects the lift and drag of the foils due to boundary layer differences.
- The roll moment is induced on the model using a contra-rotating weight mechanism. This method assumes that there are no significant changes to the hydrodynamic effects.

The expense and time limitations of full scale sea trials led the author to adopt model experimentation, with the towed model approach being adopted for this study. This was due to its availability, and suitability for testing of a large number of configurations in a relatively short period of time.

7.3 Experimental Details

The experimental set up consisted of:-

A 1/45 scale model of a Leander class frigate, constructed in glass reinforced plastic (GRP). The model roll fitting pivot was positioned at the centre of gravity of model. The model consisted of a pair of controllable fins positioned at 755 mm forward of aft perpendicular. It was free of other roll reducing devices such as bilge keels and rudders, as these could significantly contribute to roll reduction, with the fins having a decreased contribution. The scale model had the dimensions given in table 3. The model can be seen in figure 41 with a body plan provided in figure 42.

Lwl	2.438m
Bwl	0.278m
Draught	0.100m
Mass	30.15 kg

Table 3: Model data

Two sets of fins were used during the experiments:-

Small fins, whose dimensions are given in table 4 which were directly Froude scaled from a frigate, and *large fins* with dimensions given in table 5 and shown in figure 43. These fins attenuated roll to levels more akin to the full size vessel, so were therefore used for the majority of the tests.

Span	35mm
Chord (root)	55mm
Chord (tip)	55mm
Chord (mean)	55mm
Thickness	6mm

Table 4: Small fin data

Span	52mm
Chord (root)	115mm
Chord (tip)	53mm
Chord (mean)	84mm
Thickness (root)	18mm
Thickness (tip)	8.5mm

Table 5: Large fin data

Each fin was fitted with a sandpaper strip at 25% aft of the leading edge on each surface to initiate turbulence.

The fin control system consisted of:-

- Two stepper motors, each rotating the corresponding fin using toothed sprockets and grooved belts.
- A potentiometer was mounted to the top of the port fin shaft, in order to provide fin angle measurement feedback to the control system. As the control system operates the fins in equal increments and in opposite directions, only the angle feedback of one fin was necessary.
- A roll angle potentiometer was built into the tow post heel fitting, providing a voltage that was used to verify that of the roll rate sensor.
- A roll rate sensor was positioned within the vessel, with the signal being sent to the control system. This device provides a similar signal to that of the roll rate gyros used on aboard the full size vessel.

- A contra-rotating weight mechanism was mounted on the deck, at approximately 275 mm forward of the tow fitting and is shown in figure 44. This imparted a sinusoidal roll moment on the vessel. The frequency of its oscillation was controlled by the user, and therefore an entire frequency roll moment range could be analysed.
- The terminal box is the unit into which both input and output signals are fed.
- The control / monitoring system was operated from a laptop computer using the National Instrument software package Labview [78] as can be seen in figure 45. A sampling rate of the order of 100 hertz was used for a majority of the controlled tests carried out. Average speed measurements were taken from the carriage data acquisition computer.

A diagram depicting the system is shown in figure 46.

The model tests were carried out at the Southampton Institute Towing Tank, shown in figure 47. This facility has the dimensions shown in table 6:

Overall Length	60m
Width	3.00m
Depth	1.8m
Max Carriage Speed	4.6 m/sec

Table 6: Towing tank data

7.4 Discussion

Various tests were carried out to provide data for the comparison of the different controllers and to obtain model characteristics, these are listed below:-

- Roll decrement
- Forced roll
- Contra-rotating weights
- Controlled fins

All tests were carried out with the rotating weight unit in location upon the model, with the weights positioned over the centreline to maintain zero static roll angle, when not in operation.

7.4.1 Roll decrement tests

The test involved heeling the model to a set angle, then removing the restraining moment to enable the model oscillate until it found its equilibrium. This was carried out at a set of model speeds to verify the effect of dynamic roll damping.

The roll decay tests were carried out for a full set of speeds for the large fins, this data is displayed in figure 48. The smaller fins were only tested at zero speed and at 0.5 m/sec. All the damping coefficient information is given in table 7.

Fin Type	Model Speed (m/sec)	Damping Coeff.
small	0.0	0.079
small	0.5	0.087
large	0.0	0.085
large	0.5	0.095
large	0.75	0.129
large	1.0	0.168
large	1.5	0.308

Table 7: Roll decay coefficients

Figure 48 clearly shows the increase in roll damping as model speed increases. The effect of adding the larger fins has slightly increased the roll damping, as would be expected with a larger fin area.

From these tests, the natural roll frequency of the model was found to be 3.3 rad/sec, determined from the average of the peak to peak periods.

A complete set of roll decay curves has been given in figures 49,50, 51,52,53,54 and 55.

7.4.2 Forced roll tests

These tests consisted of oscillating the fins about their mean position at various frequencies, whilst running at a range of model speeds. A maximum fin amplitude of 20 deg was used. Figure 56 shows the rms roll angle against fin frequency for the small fin configuration, with figure 57 relating to those of the larger fins.

It can be seen that roll angle increases with model speed. Therefore fin roll inducing effect increases with speed, this is consistent with theory.

It must be noted that even at relatively low speed, the large fins have a significant effect. Fins would usually be activated on a ship in a speed region of approximately 10 knots, this equates to the 0.75 m/sec. used for many of the tests.

It was from these tests in particular that the restricted roll reduction ability of the small fins was highlighted in comparison to the larger fins as can be seen in figure 58, therefore the large fins were selected as the fins to use for the controlled tests.

7.4.3 Contra-rotating weight tests

The model was run at a range of speeds with the large fins in their neutral position, with the rotating weight unit operating at various frequencies. This data is given in figure 59, it can be seen that roll angle decreases with speed as roll damping increases with model speed. The results from these tests were used as the datum for the uncontrolled roll motions used for the stabilised to unstabilised model comparisons.

7.4.4 Controlled fin tests

The model was run at a range of speeds with the large fins in the controllable mode, with the rotating weight unit operating at various frequencies. A range of different controllers were tested, both classic and H_∞. The results of these tests are given in chapter 9.

The majority of experimental data has been reduced to rms roll angle values for each run, in order to clearly view the results and to reduce the effects of errors.

7.4.5 Labview software

Labview is a powerful signal monitoring, control and processing package developed by National Instruments [78]. The project demanded selection of a suitable package or code to be used to control the fins. Programming languages such as Pascal were initially investigated. They were found to have the capability of efficient data processing, the major limitations were caused by the programming times to create new subroutines and introducing them to the code and validating the results. This lead to the adoption of an off-the-shelf product. This package offered a number of set routines, which could be easily integrated into any program. Compatibility problems found with

the other methods were overcome with this software, also offering the user real-time data plotting. The software was used to control the fins, with the relevant controllers whilst logging information such as fin angle and roll angle at set intervals. These datasets were then processed using programmed routines, to determine r.m.s. roll and fin angle for each run.

7.4.6 Fin scale effects

There exists some key scale effects to be appreciated in relating active fin model experiments to full scale results [79]. They are:-

- Reynolds Number Effects
- Fin-Hull Interactions

This resulted in the use of fins which were larger than directly Froude scaled model fins.

The issues of overall fin efficiency were not investigated during this study, but it must be noted that the overall performance of the fins would have been increased by reduction of the root gap, and the use of lower thickness-chord ratio foils.

What these model experiments have not modelled is the fin response associated with full scale operation. In that case, there is a significant fin lag due to the loadings and system response times and fin angle and rate limitations.

7.4.7 Conclusions

From this chapter, it can be seen that a system has been created that can be used as active roll fin stabiliser equipment on free running models, as well as its current use on towed small scale models. This is due to the compact and light nature of the apparatus.

Scale effects lead to the use of larger fins, these effects will reduce with increasing size of model.

The speeds adopted during these tests range from 0.5 to 1.0 m/sec (approximately 6.5 to 13 knots full scale), these adequately represent sampled working speeds for such a ship and fins. This type of stabiliser is normally initiated above 6 knots, above 13 knots in operational conditions the overall gain will be reduced using a function inversely proportional to speed. This is to maintain fin forces within the specified design range of the fin servos.

The frequency ranges tested contained the majority of large roll excited frequencies. Investigation of the effects of controllers outside this range has not been undertaken.

8 Experimental Results

This chapter presents the results from the towing tank tests, with trends being extracted and conclusions drawn. These results are also compared to those from the matching numerical model, using the motion software [10].

8.1 Three Term Fin Control

The PID controller was formed using the same tuning approach that would be adopted for a full size ship. The ship roll to fin angle phase was extracted from the forced roll tests with a value of natural roll frequency determined from roll decay tests.

Using the Lloyd [4] frequency response approach (outlined in Appendix B), a set of control coefficients were derived which were tuned to the ship response to fin movement, at the ship's natural frequency.

The coefficients were chosen to have a bias towards the roll velocity sensitivity, as this was indicated as having the most suitable overall roll reducing performance, outlined in [4, 23]. It was necessary to restrict the number of control coefficient conditions due to time restrictions, a number of conditions were briefly tested, with the control bias towards different derivatives. The large roll velocity coefficient performed well compared to the other coefficient sets. This supports its selection as the coefficients with which progress a full test matrix.

The figure 60 shows the rms roll angles for this controller at the three set speeds at a range of frequencies. It can be seen that there is a consistent trend between the different speeds.

Figure 61 shows the unstabilised / stabilised comparison for a range of frequencies at 0.5 m/sec. The roll reduction at frequencies below 3.75 rad/sec with the controlled fins can clearly be seen. Above this frequency, the fin performance deteriorates over that of the unstabilised case, this is the result of the controller phase not matching the model roll phase, in this region.

Figure 62 gives a comparison at 0.75 m/sec of the unstabilised case, to that of the PID controlled fin case, and to an example with the same control coefficients with an overall gain of $K_G = 3$. It can be seen again that the roll reduction of the original gain case is significant for frequencies less than 3.75 rad/sec. The increased gain example significantly out performs the original controller. This latter case is not realistic, when its fin activity is taken into consideration, as can be seen in figure 65.

Figure 63 represents a comparison at 1.0 m/sec. The increased roll reduction due to the higher speed can be seen when compared to the slower

previous examples. Roll reduction is maintained over a large range, converging to the unstabilised values at approximately 4.5 rad/sec.

Fin angles for the various PID control experiments are given in figures 64 and 65.

Figure 64 shows a comparison of the fin activity at a range of frequencies, for the three speeds. At lower speeds, the unstabilised roll is large, this decreases with speed due to dynamic damping. Therefore the fin demand and response are less at higher speeds, as can be seen in figure 64.

Figure 65 shows a comparison of the original controller with the increased gain controller. The high fin activity in the high frequency region is excessive, therefore this increased gain case would lead to excessive system wear and noise. This adds validity to the higher gain being inappropriate for roll control, and shows the original gain value provides reasonable fin behaviour.

A test matrix between frequencies of 2.0 and 6.0 rad/sec was adopted encompassing the area of greatest roll excitation, higher and lower frequencies were briefly tested. These resulted in low roll angles with very low fin activity with no unusual effects, therefore these were not incorporated in the complete test matrix. The testing of the controllers at frequencies outside this range of interest, would identify problems such as excessive fin activity at high frequencies, as would undesirable fin response due to static heel for instance.

The model tests were conducted at three set speeds 0.5, 0.75 and 1.0 m/sec, equating to approximately 6.5, 10 and 13 knots full scale respectively.

8.2 H_∞ Control

These controlled tests were also carried out using the same hardware set up and in the same conditions as those outlined in section 7.3. A typical fin and roll response achieved through H_∞ control is given in figure 66.

A range of controlled roll cases for a number of H_∞ control coefficients were carried out, the majority of which were at the intermediate model speed of 0.75 m/sec. This was necessary due to the limited time available for testing, with the need to investigate a number of different control coefficients. The various controllers $H_\infty i$ have each been designed using slightly different weighting variable values and overall gains.

Figure 67 shows the controllers to have significant roll reducing properties, when compared to the uncontrolled roll behaviour. This range of controllers was formed by adapting the variables in the controller design method, outlined in appendix C.

The general trend is for the medium to high frequency range to have significant roll attenuation, with the lower frequency range showing a slight

increase.

These results must be viewed with an appreciation of the fin activity in mind. The operator desires maximum roll reduction without excessive fin movement. Figure 68 shows the fin activity for the selected controllers compared to the realistic 3 term controller. The controller labelled $H_\infty 1$ shows excessive activity at the higher and lower frequencies, this is a result of excessive gain. $H_\infty 2$ and $H_\infty 6$ both show reasonable characteristics. It was from this, that $H_\infty 6$ was selected to be the controller with which to carry out a fuller investigation at the other test speeds.

Figure 69 gives the comparison of H_∞, 3 term and the uncontrolled at 0.5 m/sec, with figure 70 for that at 0.75 m/sec, and finally figure 71 for 1.0 m/sec.

The PID classic controller outperforms the H_∞ controller at the lower frequencies, below approximately 3.2 rad/sec. At every speed range, the roll angle at 2.0 rad/sec is slightly increased through $H_\infty 6$ control over the uncontroller case. For frequencies above 3.2 rad/sec the roll reduction effects are significantly below those achieved from the classic controller. These differences are in part due to the different tuning methods used to form the controllers. The classic controller was tuned to actual model frequency and phase information, whereas this phase information was calculated from a theoretical approach incorporated within the H_∞ design method.

The roll reduction in the vicinity of the natural roll frequency is more effective for the classic controller. This has been found to be the case in [6] from a numerical analysis, where roll reduction at the natural roll frequency was less favourable for the H_∞ controller, but outside this region significant gains where achieved.

Figure 72 shows the rms fin angle of each controller for a range of frequencies at the intermediate speed. It can be seen that the H_∞ controller has significantly less fin activity.

This data can be transformed into a non-dimensionalised form with respect to wave slope, and then applied to particular sea spectra conditions. This allows the comparison of the overall controller performances

Table 8 shows the rms roll angle and table 9 the rms fin angle values for the different controllers, simulating a sea state 5, Bretschneider, $T = 12.4$ and $h_{1/3} = 5.5$ m. The vessel is travelling at 10 knots in beam seas.

It can be seen that the controllers have similar roll reducing performances, though the H_∞ controller has significantly reduced fin activity. It must be borne in mind that the H_∞ control design method used has not been created using an optimised method, therefore it would be feasible to design these controllers to have improved performance characteristics in terms of

File	Speed m/sec	RMS Roll degs
Uncontrolled	0.5	3.335
Uncontrolled	0.75	3.068
Uncontrolled	1.0	2.815
PID	0.5	2.704
PID	0.75	2.253
PID	1.0	1.888
H_∞	0.5	2.583
H_∞	0.75	2.146
H_∞	1.0	1.838

Table 8: RMS Spectral Roll values for various stabilsed methods at 90° heading

File	Speed m/sec	RMS Fin Angle degs
PID	0.5	5.324
PID	0.75	4.483
PID	1.0	3.782
H_∞	0.5	4.857
H_∞	0.75	3.763
H_∞	1.0	3.126

Table 9: RMS Spectral Fin values for various stabilsed methods at 90° heading

roll attenuation, and even less fin activity. Therefore, these results do show promise for the H_∞ approach.

8.3 Comparison of experimental and numerical results

It can be seen from figure 73 the non-dimensionalised roll (using appendix D) to wave frequency plot, that the software identifies the peak frequency locations for the classic control case, and the separation of the uncontrolled and controlled results at low frequencies. The numerical results slightly over estimate the overall magnitudes.

Figure 74 gives the numerical/experimental comparison of the H_∞ controller. The convergence of the uncontrolled and controlled results at the lower frequencies can clearly be seen.

The numerical results relate to an unrestrained model, whereas the experimental setup restricted the yaw and sway degrees of freedom. This may account for the lower experimental values in comparison to the numerical results

It can be seen that the numerical program is able to reproduce reliable trends with which to investigate the performance of different controllers.

8.4 Conclusions

The roll reduction effects of the actively controlled fin stabilisers are large providing adequate control is applied. This proves the seakeeping benefits of such stabilising devices. Their capabilities increase with speed, this can be seen in the unstabilised / stabilised comparisons, given in figures 61,62 and 63.

The classic and H_∞ controllers produce similar roll attentuating levels, with the H_∞ control leading to reduced fin activity. This would be a major benefit on an actual ship, with reduced wear on the fin stabilisers. There is also the possible decrease in resistance, resulting from the lower fin incident angles, leading to reduced induced drag. The performance for the H_∞ controllers used were achieved without optimisation, therefore with further development increases should be obtained.

The experimental results have been used to validate successfully the numerical model.

9 Controller Results

9.1 Introduction

This chapter has been separated into two main sections. The first representing the results of roll controllers, then the second, LFE controllers.

The results have been summarised into two main figure types. The first is rms roll angle, fin angle and LFE at a range of headings. This has been principally carried for one sea spectra, outlining the overall controller performance. The second, non-dimensionalised (ND) roll and fin angle and LFE against wave frequency (roll and fin angle with respect to wave slope and LFE with respect to unit wave height). These represent the vessel on a 90° heading, and are used to identify any problem areas of the controller's operation. Such as undesirable fin activity at very high or low frequencies. Therefore, both plot types need to be analysed to quantify fully the quality of the controllers under consideration.

To enable all controllers to be compared on a like for like basis, the overall gain of each controller has been adjusted to achieve a maximum rms fin angle at any heading, of no greater than 8°. This is a similar condition to that adopted in the work of Tang and Wilson [3]. For these numerical tests the ship speed was 10 knots, which provided suitable fin-roll characteristics.

Systematic changes to the controller design have been made to investigate the envelope of H_∞ design method used, and these have been represented and discussed in the following section.

Tables 10 and 11 give details of the formation of each H_∞ controller discussed in this section, these are provided in more detail in appendix E. Descriptions of the weighting used have been given in section 6.3.

9.2 Roll Controllers

The overall effectiveness of the roll controllers can be seen in figure 75. There is a drastic reduction in roll motion as a result of the controlled fins. The classic controller has better performance for a heading range of 45° - 165° than the specifically designed H_∞ roll controller. A comparison of the fin activity of each controller, figure 81, shows similar overall rms fin response.

The frequency plots for the two controller types in figure 102 identify the greater roll attenuation of the H_∞ controller at frequencies below the natural roll frequency, with the opposite being the case above that range. From the fin response plot, figure 108, it can be seen that the desired design fin characteristics have been achieved with the H_∞ controller. The high frequency response is relatively low preventing fin wear, combined with a

low frequency response slightly lower than the classic controller comparison.

A number areas of the controller design necessitated investigation, such as:

- Sub-Optimal and Optimal Controllers
- Effect of Order Reduction
- Weighting Variation

9.2.1 Sub-Optimal and Optimal Controllers

It can be seen from figure 76 and 82, that the overall performance of the sub-optimal, $\gamma = 1$ controller is noticeably greater than that of the corresponding optimal controller. This results from the reduction of fin activity for headings greater than 45°. This is a consequence of the controller not reducing roll sufficiently in the region of significant spectral energy, as can be seen in figure 103, even though the lower frequency roll contributions are vastly reduced, with similar fin activity, figure 109.

9.2.2 Effect of Order Reduction

The order of the controllers plays a notable role in the ease with which a controller can be practically implemented. The lower the order, the easier it is to realise. This reduces the complexity of the controller itself, and decreases the effects of possible errors.

It can be seen in figures 77,83,104,110 that the performances of the different ordered controllers are extremely similar. This is the result of the balanced model reduction based on the Schur balanced reduction method [75]. From these results, a low order controller can be selected, with no significant loss of performance.

9.2.3 Weighting Variation

The form and number of weightings were varied, in order to determine their effects upon the controller characteristics. As described in a previous section, only certain functions maybe appropriate, as the augmented plant must satisfy a number of properties for a valid controller to be formed.

From figure 78, it can be seen that the various weighting gain changes have no effect on the overall roll reduction. It must be borne in mind, that the overall gain for each controller has been adjusted to achieve the rms 8° limiting fin response. The gain changes to W_1 and W_3 altered the overall

controller magnitudes proportionally by the same amount, whereas W_2 gain had little effect.

The equal performances can also be seen in figures 78,84,105,111.

Tests were carried out to reduce the number of weightings, this lead to the use of a *Cheap* control approach, similar to that used by [9], whereby $D_{12} = \varepsilon I$, with ε being relatively small; this satisfes the requirements of the Matlab software [72], allowing a valid controller to be found. It can be seen from figures 79 and 85 that the performance of this controller was significantly lower than that of the standard weighting controllers. This results from the frequency shift of the controller properties as displayed in figures 106,112.

The weighting that appeared to have a dominant effect on the controller design is W_1. Therefore the characteristics of this were varied in an attempt to improve the controller performance. Reduction of B, results in a more concentrated magnitude in the vicinity of the natural frequency.

From figure 80, the reduction of B (from section 6.3.1) can be seen to reduce the overall roll. This attentuation is attained with similar overall fin activity, as per figure 86. From figure 107, a roll reduction over a large frequency range can be seen, but there is a slight increase in fin response at the high frequencies with the lowering of B, seen in figure 113.

Name	W_1	W_2	W_3	**Description**
Roll 2	Yes	Yes	Yes	Optimal γ
Roll 5	Low Gain	Yes	Yes	Optimal γ
Roll 8	Yes	High Gain	Yes	Optimal γ
Roll 10	Yes	Yes	High Gain	Optimal γ
Roll 13	Yes	No	Yes	$\gamma = 1$, Low Order
Roll 15	Yes	No	Yes	Optimal γ, Low Order
Roll 16	Yes	No	Yes	Optimal γ, High Order
Roll 17	Yes	No	No	Optimal γ, $D_{12} = \varepsilon$
Roll 20	Yes	No	Yes	Optimal γ
Roll 21	Yes	No	Yes	Optimal γ, $B = 0.5$
Roll 22	Yes	No	Yes	Optimal γ, $B = 0.05$
Roll 23	Yes	No	Yes	Optimal γ, $B = 0.01$

Table 10: Formation of H_∞ roll controllers

9.3 LFE Controllers

A similar investigation to that applied to the roll controllers was carried out on the LFE controllers. Included in this analysis, are the results of the LFE controller derived using the simple search routine.

The first major point of interest in figure 91, was the overall performance of the H_∞ LFE controller reducing roll more effectively than the roll controllers tested. This was most apparent for headings less than 90°. A similar approach had been used to create the H_∞ roll controllers, without such a favourable roll attenuating performance. The controller derived using the search routine has a low response at 75°, but significantly higher roll response at other headings in comparison to the other controllers. The fin activities given in figure 96 show that they have similar activities, with a reduction for H_∞ LFE controllers for headings greater than 90°.

It can be seen in figure 101, that the H_∞ LFE controllers were superior in LFE reduction in comparison to the roll controllers over the entire heading range. This was one of the essential aims of this work, to create an improved LFE controller. The search LFE controller produced poor LFE control, apart from the heading angle of 75°, where its performance was of the order of the H_∞ LFE controller.

From the frequency plots of figures 118,123,128, the roll reduction of the LFE controller below 0.6 rad/sec is far greater than that of the roll controller. The performance converges to that of the unstabilised case at approximately 1.2 rad/sec, resulting from the lack of fin activity above that range. This was one of the criteria of the design process, to reduce the higher frequency fin motion. The disadvantage of the classic roll controller, is that it increases the LFE above approximately 0.65 rad/sec, although it did significantly reduce LFE in the region of the natural roll frequency. The LFE controller does not increase LFE as notably as the roll controller. In fact, its value converges to the unstabilised case at the higher frequencies.

9.3.1 Effects of Order Reduction

From figures 87,92,97 it can be seen that controller order makes little difference to the controllers overall performance. The high order controller has a slight increase of fin activity above 1.4 rad/sec from figure 119, this is not exhibited by the lower order controller. As a result, the LFE reductions remain very similar up to 1.4 rad/sec, as can be seen from figure 124 and 114.

Name	W_1	W_2	W_3	Other
LFE 3	Yes	Yes	Yes	Optimal γ, High Order (5)
LFE 4	Yes	Yes	Yes	Optimal γ, Mid Order (4)
LFE 5	Yes	Yes	Yes	Optimal γ, Low Order (3)
LFE 6	Yes	Yes	No	Optimal γ
LFE 10	Yes	No	Yes	$\gamma = 1$
LFE 11	Yes	No	Yes	Optimal γ
LFE 12	Yes	No	Yes	Optimal γ, $B = 0.5$
LFE 13	Yes	No	Yes	Optimal γ, $B = 0.05$
LFE 14	Yes	No	Yes	Optimal γ $B = 0.01$

Table 11: Formation of H_∞ LFE controllers

9.3.2 Sub-Optimal and Optimal Controllers

The roll (figure 89), fin (figure 94) and LFE (figure 99) overall responses for the controller with $\gamma = 1$ and the optimal controller are quite similar. The sub-optimal controller has slightly improved LFE reduction compared to the optimal controller over the entire heading range. This is an effect from the shift of the fin activity in the 0.05 rad/sec - 0.8 rad/sec region (figure 121), which results in increased LFE values in that range (figure 126 and 116).

9.3.3 Weighting Variation

The elimination of particular weightings made very little overall difference, as can be seen in figures 88,93,98.

The variation of W_1 made very little difference to the roll (figure 90) and fin (figure 95) response, though the rms LFE (figure 100) was reduced with decreasing B. This was also the case for the roll controllers. The difference is caused by a slight reduction of LFE in the 0.5 - 0.8 rad/sec region.

These effects of weighting variation can also be seen in figures (115,117, 120,122,125,127).

9.4 Conclusions

- The classic roll controller has slightly better roll attentuation than the specifically designed H_∞ roll controller. The design properties of reduced low and high frequency fin activity have been achieved.
- Selection of γ is important, a near optimal controller may not necessarily result in the best overall controller performance, due to the resultant

controller being over conservative.

- Lowering the order of the controllers in the case of the roll controller to an order of 3 and an order of 4 for the LFE controller, does not affect the controllers overall performance.

- The variation of the weightings has been carried out to select the most appropriate combination. This appears to be W_1 and W_3, but the differences between a majority of the various combinations is relatively small. Rejection of W_2 cannot be fully investigated through this type of analysis, testing with instrument noise in the time domain would be a more suitable means of testing the effects of this function.

- The results discussed and graphical displayed in this section, are a selection of the most appropriate controllers designed and tested. This was also dictated by the rigourous requirements that had to be met to satisfy the H_∞ theory and the Matlab software and toolboxes demands, this resulted in very few valid controller designs.

- It can be seen, that an improved LFE controller has been developed. More rigourous testing is needed to explore its limitations, and to highlight its benefits.

- The H_∞ controllers have all been formed using a structured design method. The method was found to be robust in its ability to determine suitable controllers.

- The roll reducing ability of the H_∞ LFE controller was found to significantly out perform all the roll controllers tested. This is in part due to the reduction of fin activity at higher frequencies for the H_∞ controller, allowing a higher overall gain controller to be applied. This advantage is increased, by the controllers performance at lower frequencies being significantly better than the other controllers, leading to improved rms LFE reductions.

- These controllers have only been tested using a frequency domain approach. A further examination with a time domain approach may highlight problem areas resulting from system non-linearities or noise for example.

10 Ship / Helicopter Dynamic Modelling

10.1 Introduction

This chapter introduces the dynamic modelling of the ship / helicopter interface, and how it has been adopted as a tool with which to evaluate various ship motion control schemes. The process used to develop the model is outlined, with validation carried out to verify its suitability as an design tool.

This dynamic model is of prime importance to complete this research. Previous chapters have discussed a range of fin stabiliser control designs. So this model provides a means to evaluate the overall performance benefits of helicopter on-deck stability of the various designs and configurations.

A number of different methodologies have been used to study the dynamics of the ship helicopter interface by other researchers, as discussed in chapter 2. These models range in complexity and their areas of application, from simple on deck models [63], or those developed using commercial software [66] to highly intricate airborne, landing and on-deck models [60].

The dynamic modelling of the ship/helicopter interface is a means of simulating the motions and forces experienced by the helicopter during the landing phase, and in the subsequent duration whilst on deck.

This type of analysis is an important aid in the determination of operational limits for specific aircraft on particular ship types. At present, helicopter operational limits are determined from tests at sea, these trials are extremely expensive and time consuming. They are also dictated by the weather, meaning only a few different operating conditions can be investigated thoroughly. Therefore, a complete operational envelope for a specific ship/helicopter combination is extremely problematic to create.

This dynamic modelling approach permits the analysis of a large number of operational conditions, with a number of different scenarios, such as operating in any sea state, for a range of different wind directions, and predominate wave directions, without the associated risks inherent in actual onboard testing. The approach can also be used to test concepts, such as verifying helicopter radome and missile clearances, forces exerted on securing equipment, and to analyse structural loading scenarios.

It must be borne in mind that helicopters operating from small warships in the North Atlantic during winter do have a limited operational availability. Any gain in availability would be of significant advantage, both for tactical reasons and for operator safety. A reliable dynamic ship/helicopter interface model can be used to explore different effects, i.e. reductions in particular ship motions, to increase the availability of the shipborne aircraft. Methods of reducing ship motions have been discussed in previous chapters.

One of the global aims of this work is to improve methods of ship motion control, in order to reduce specific motions at the flight deck. This will have the effect of increasing the aircraft's availability to higher sea states, as well as augmenting the overall safety of helicoper operations.

10.2 Modelling

To achieve an accurate representation of the dynamic ship/helicopter interface, each major associated element of the system has to be understood to a sufficient accuracy. Therefore the model has been broken down into the following main sections:-

- Oleos: these are the shock absorbers and spring configurations linking the wheels to the airframe, that damp the landing loads.
- Tyres.
- Entrapment and Handling Devices.
- Aerodynamics.
- Ship Motions.

10.2.1 Oleos

Realistic modelling of the oleos is extremely important, as they provide the greatest contribution to helicopter motion reduction and damping as the helicopter lands and whilst it is upon the deck prior to handling. This necessitates the use of an accurate oleo model, exhibiting the same characteristics as those of the nominal helicopter adopted within this investigation, in this case it is the *Lynx*.

The oleo characteristics are highly non-linear, especially for the *Lynx*. These can be described using the following figures. Figure 129 denotes the oleo static reaction. This yields the compression force within the unit as a function of the oleo closure measurement. From this figure it can be seen that there are three major regions, the first A-B, denotes the compression of the first air- spring within the system. This is of low stiffness, it prevents abrupt forces being transmitted during the initial wheel touch down phase and allows the extension of the undercarriage during take off. At B, the first air spring bottoms out.

The second section B-C, is the range where only a small oleo closure occurs. This is due to the damper unit taking the compression. This zone allows the helicopter to remain stable on the moving flight deck, maintaining

a constant ride height. It allows easier re-fuelling and re-arming, even with the addition of increased load weight to the aircraft. The final section C-D is the region where the second, stiffer air spring breaks in. This provides a high percentage of the arresting force during the landing phase.

Figure 130 illustrates the damping characteristics of the oleo arrangements. It consists of a three phase compression system using an orifice stack and a more detailed explanation is provided in [80]. The role of the dampers is to absorb the landing reactions of the helicopter rapidly, but not at such a rate as to cause damage to the aircraft structure. Each region A-B, C-D, E-F is where the next orifice size in the stack is used to provide the damping, therefore supplying a greater damping rate.

The characteristics of the oleo stiffnesses have been obtained from [80], the damping characteristics have been derived using [81], and by varying the magnitudes and investigating the effects directly upon the dynamic model, this is also verified by [82].

10.2.2 Tyres

The significance of this element of the system is directly related to that of the stability of the helicopter whilst on the flight deck. This is the characteristic of the tyres against sliding.

The tyres have been modelled as linear stiffness and damping components. This is primarily due to the lack of available data. Other dynamic models [64, 66] have used non-linear equations to model the tyre characteristics. As the tyre compression in the vertical plane will have an effect for the characteristics in the horizontal plane. (Such a non-linear approach could very easily be incorporated into the model at a later date, as and when the data becomes available. Though at present, the current linear model produces no unusual results.)

The tyre orientation has been accounted for in the model. As the stiffness in each plane is different.

The tyre dynamics become increasingly important when manoeuvring of the helicopter is considered. This is an added consideration to complicate the dynamic model which has been examined in [83], as a prime aim of this research was to analyse the stability of the helicopter post landing and not for the entire handling phase, simulation of manoeuvring was not necessary. Therefore, the wheels have been modelled with brakes on.

The friction coefficients between the flight deck and the helicopter tyres are of prime importance in the aspect of sliding. Values for these coefficients have been given in reference [62, 63], for a range of flight deck conditions from worn, wet and oily decks, to a new dry flight deck, this data is given in

table 12. [80] gives a slightly higher maximum coefficient, which takes into account modern deck treatments.

Flight Deck Condition	Friction Coefficient
Oily	0.15
Wet	0.3
Worn	0.5
Dry	0.7
Dry with Modern Treatments	0.8

Table 12: Flight Deck Friction Coefficients

10.2.3 Entrapment Devices

Modelling of entrapment and handling devices is of relevance, as they enhance the stability of the helicopter on the flight deck. The design of the *Lynx*, has accounted for the inclusion of the Harpoon decklock on frigates to provide a down pull of approximately one third of the helicopter weight, in order to increase stability to both sliding and toppling. The inclusion of the deck lock into the numerical model is therefore vital. The theory and subsequent computer program gives the user the ability to select whether the deck lock is used or not. The inclusion of other securing devices types can be made easily, which could yield information as to the most suitable entrapment arrangement.

The model showed that improvements in helicopter stability to both sliding and toppling were gained by the use of the deck lock. Values of static stability angles are given in table 13. The helicopter is defined as sliding, when one tyre exceeds the deck friction limit; the toppling condition is met when one wheel leaves the deck. These limits were investigated with the helicopter positioned parallel to the ship's centreline on a dry deck. Then the deck was heeled to achieve a pre-determined roll angle, from this analysis the limits were found. Roll angle was increased using a linear ramp until it reach a specified value.The stability limits are given in table 13. These showed similar values to those given in [80]. The values were also confirmed as being typical values by [84].

10.2.4 Aerodynamics

The aerodynamic forces contribute considerably to the external loading of the system and therefore greatly affect the stability of the helicopter in its

Stability Condition	Without Decklock	With Decklock
Sliding	17.0 deg	22.0 deg
Toppling	22.3 deg	29.8 deg

Table 13: Stability Limit Angles (no other external forces)

exposed position on the flight deck. As can be seen from previous research [61], modelling of the airflow in the proximity of the flight deck is still to be fully implemented.

There are the loads created by three main helicopter components:

- Fuselage.
- Main Rotor.
- Tail Rotor.

The fuselage contributes a high quantity of loading due to drag, which is based on airflow around bluff bodies [79]. The two sets of rotors have the forces created during their operation as they are lift generating devices, and drag loadings exerted when not rotating.

In this investigation, a reasonable quantitative interpretation of the aerodynamic load is needed, to represent adequately aircraft on-deck stability limits.

The fuselage drag is resolved as a point load, in the direction of the apparent wind, in the plane of the flight deck. This is acknowledged as being rather crude, but it is simple to implement and possible with the current available data.

A look-up table of aerodynamic forces and centre of pressures, for a range of apparent wind speeds and directions can also be input for both the fuselage and the rotors. These may be obtained from published data, or determined through experimental wind tunnel results or CFD based techniques.

In the case of the *Lynx*, once the helicopter has touched down, negative collective is possible, where the main rotor can create a negative thrust, pushing the helicopter downwards and hence increasing its stability on the deck. This has also been implemented as part of a dynamic rotor model. This effect has not been investigated in this document.

Ship motions also contribute significantly to the effect of the aerodynamic forces, particularly from a rotor lift view point. Reference [65] points out that increased roll angle orientates the helicopter lift from the main rotor in an

increasing tranverse direction, reducing the stability of the helicopter on the flight deck, whilst the rotors are in operation.

Fuselage drag is given with wind parallel to the ship deck, apparent wind to rotors is given parallel to the mean sea surface, therefore ship roll and pitch have a significant effect on the resultant forces.

10.2.5 Ship Motions

The ship motions have a predominant environmental effect on the stability of the helicopter. A successful model needs adequate modelling of all the six degrees of freedom, as accelerations from each degree of freedom (DOF) will have a significant effect on the aircraft.

The dynamic program has the ability to accept a range of different motion cases:

- Sinusoidal ship motions.
- Spectral ship motions.
- Actual motions.

The computer program has been designed to determine the shipborne helicopter response to sinusoidal ship motions. This enables the dynamic helicopter model to be validated with simple inputs. It was found from this that the model behaviour was as expected. The frequency, amplitude and phase variation of each DOF motion is obtainable.

It is possible to input the ship motions in a seaway, using spectral ordinate inputs, along with the frequency contributions of amplitude and phase. In this case, the motion characteristics have been derived using the Wolfson Unit Seakeeping Package [85] based on a strip theory approach, to yield heave and pitch contributions. The seakeeping software [10] was used to derive the roll, yaw and sway contributions. From this, analysis of the helicopter operating in a range of sea states and wave direction conditions is plausible.

The program can also accept actual or computed ship motion time histories and this could be used as part of a further validation exercise, but primarily to subject the model to motions from the real environment. This would overcome the limitations caused by the linearity of the ship motion simulations used, to create more accurate results at the higher sea states, where non-linearities can have a significant effect. This point has led Tadros et al [86] to implement a non-linear ship motion code within the ship/helicopter dynamic model.

The computer program [10] also derives the RAOs for vessels with active stabilisation from roll fin stabilisation to rudder LFE stabilisation, adopting the active control to counteract roll or LFE, as has been described in previous chapters. Baitis and Tadros [23, 65] to name but a few, acknowledge LFE as being a dominant ship motion affecting helicopter stability criterion, using this facility the controllers performance as a function of helicopter loading or improved stability can be quantified.

Alternative ship/helicopter criteria are also incorporated within the program, such as helicopter slide and toppling limitations.

10.2.6 Helicopter

The nominal helicopter used in this investigation is broadly based on the Westland *Lynx*. This helicopter was chosen, due to the quantity of data to be found upon it. Also the aircraft has been specifically adapted for shipborne operations. A wide range of information and data upon the helicopter is given in [80], and through [82] and [84].

The helicopter fuselage is modelled as a rigid body. The helicopter equations of motion are for a full six degree of freedom system which includes coupling.

The use of small angle approximations were rejected at an early stage of the analysis, as the assumptions created modelling difficulties. This problem became greater, as more complex components were modelled upon the helicopter. This was also due to the need for the model to be suitable for a range of helicopter types. The nominal helicopter is relatively stiff upon the deck, whereas other shipborne helicopters may undergo motions that exceed the small angle approximation. At present, this has not affected the computational demands, as has been seen in previous investigations [62, 63], where real time calculations were desired.

10.2.7 Theory

The system equations of motions were formed in the following way:

The forces and the moments created by the oleos and tyres based on the aircraft state in the previous time step are calculated.

- $_H$ denotes at the Helicopter centre of gravity.
- $_T$ motion at the Tyre position.
- $_O$ motion at the Oleo position.

- $_i$ denotes which tyre or oleo, 1,2 or 3.

A representation of the helicopter is given in figure 131.
The contributions for the forces are as follows:

$$x_{iT} = x_H - l_i(1 - \cos\theta_H) + d_i \sin\theta_H - l_i(1 - \cos\chi_H) - s_i \sin\chi_H \tag{86}$$

$$\dot{x}_{iT} = \dot{x}_H - \dot{\theta}_H l_i \sin\theta_H + \dot{\theta} d_i \cos\theta_H - \dot{\chi}_H l_i \sin\chi_H - \dot{\chi}_H s_i \cos\chi_H \tag{87}$$

$$F_X = m\ddot{x}_H + \sum_{i=1}^{n} c_{iTx}\dot{x}_{iT} + k_{iTx}x_{iT} \tag{88}$$

$$y_{iT} = y_H - d_i \sin\varphi_H - s_i(1 - \cos\varphi_H) + l_i \sin\chi_H - s_i(1 - \cos\chi_H) \tag{89}$$

$$\dot{y}_{iT} = \dot{y}_H - \dot{\varphi}_H(d_i \cos\varphi_H + s_i \sin\varphi_H) + \dot{\chi}_H(l_i \cos\chi_H - s_i \sin\chi_H) \tag{90}$$

$$F_Y = m\ddot{y}_H + \sum_{i=1}^{n} c_{iTy}\dot{y}_{iT} + k_{iTy}y_{iT} \tag{91}$$

$$z_{iO} = z_H - l_i \sin\theta_H - d_i(2 - \cos\theta_H - \cos\varphi_H) + s_i \sin\varphi_H \tag{92}$$

$$\dot{z}_{iO} = \dot{z}_H - \dot{\theta}_H(l_i \cos\theta_H + d_i \sin\theta_H) + \dot{\varphi}_H(s_i \cos\varphi_H - d_i \sin\varphi_H) \tag{93}$$

$$F_Z = m\ddot{z}_H + \sum_{i=1}^{n} c_{iOz}\dot{z}_{iO} + k_{iOz}z_{iO} \tag{94}$$

For the moments:

$$\begin{aligned}
L_{i\theta z} &= l_{iO}\cos\theta_H + d_{iO}\sin\theta_H \\
L_{i\varphi z} &= s_{iO}\cos\varphi_H - d_{iO}\sin\varphi_H \\
L_{i\theta x} &= d_{iT}\cos\theta_H - l_{iT}\sin\theta_H \\
L_{i\chi x} &= -s_{iT}\cos\chi_H - l_{iT}\sin\chi_H \\
L_{i\varphi y} &= -d_{iT}\cos\varphi_H - s_{iT}\sin\varphi_H \\
L_{i\chi y} &= l_{iT}\sin\chi_H - s_{iT}\cos\chi_H
\end{aligned} \tag{95}$$

$$
\begin{aligned}
M_\theta = I_\theta \ddot{\theta}_H \quad &+ \quad \sum_{i=1}^{n} L_{i\theta x}(c_{iTx}\dot{x}_{iT} + k_{iTx}x_{iT}) - \sum_{i=1}^{n} L_{i\theta z}(c_{iOz}\dot{z}_{iO} + k_{iOz}z_{iO}) \\
M_\varphi = I_\varphi \ddot{\varphi}_H \quad &+ \quad \sum_{i=1}^{n} L_{i\varphi y}(c_{iTy}\dot{y}_{iT} + k_{iTy}y_{iT}) + \sum_{i=1}^{n} L_{i\varphi z}(c_{iOz}\dot{z}_{iO} + k_{iOz}z_{iO}) \\
M_\chi = I_\chi \ddot{\chi}_H \quad &+ \quad \sum_{i=1}^{n} L_{i\chi x}(c_{iTx}\dot{x}_{iT} + k_{iTx}x_{iT}) \\
&+ \quad \sum_{i=1}^{n} L_{i\chi y}(c_{iTy}\dot{y}_{iT} + k_{iTy}y_{iT})
\end{aligned} \tag{96}
$$

Calculation of the external forces into the system, from the ship motions and aerodynamic loadings are evaluated relating to the current ship state and position. This is dependent on which ship motion option is selected, and the degree of complexity of the aerodynamic simulation. The forces exerted from entrapment and handling devices are evaluated at this stage. The effect of gravity is also accounted for as an external loading.

For x, y or z:

$$
F_X = F_X(Aero) + F_X(Ship) + F_X(Grav) + F_X(Entr) \tag{97}
$$

For θ, φ or χ:

$$
M_\theta = M_\theta(Ship) + M_\theta(Aero) \tag{98}
$$

These forces and moments are then combined to form the system equations of motions. This consists of six simultaneous equations.

$$
\ddot{x}_G = \frac{F_X(Aero + Ship + Grav + Entr) - \sum_{i=1}^{n} c_{iTx}\dot{x}_{iT} + k_{iTx}x_{iT}}{m} \tag{99}
$$

$$
\ddot{\theta}_H = \frac{M_\theta(Aero + Ship) - \sum_{i=1}^{n} L_{i\theta x}(c_{iTx}\dot{x}_{iT} + k_{iTx}x_{iT}) + \sum_{i=1}^{n} L_{i\theta z}(c_{iOz}\dot{z}_{iO} + k_{iOz}z_{iO})}{I_\theta} \tag{100}
$$

The Runge-Kutta-Merson method is used to integrate the system equations, to yield the displacements and velocities of the helicopter at the next time step. This operation is repeated for every time step. A sensitivity study of time step length was carried out on the model and only when the oleos

entered the high stiffness regions was a short step necessary, a typical application of this is during a landing when very high loads are applied. For the example of a drop test 100 Hz was used, this provided sufficient detail and accurate modelling of the oleo dynamics. The ship motion time histories of 30 minutes used time steps of 10 Hz, the longer time step was found suitable as in such conditions the oleos did not enter their high stiffness regions and this resulted in relatively efficient solution times.

Program

The code for the dynamic interface model has been written in FORTRAN utilising Nag routines for pre-defined processes, such as the integration method.

The Runge-Kutta-Merson method has been adopted for the integration technique. This is a fourth order plus scheme. It was selected as it provides reasonable accuracy, for computational cost. It is relatively insensitive to initial conditions, where a stable result will still be approached. This has been tested at a range of different initial conditions, with consistent, stable results being achieved. The direct method is not suitable for stiff systems. So far, this has not proved to be a problem. If, with alternative model properties this becomes apparent, then the adoption of an alternative Runge-Kutta approach suitable for stiff systems has been included in the program. References to the Runge-Kutta and other possible integration techniques may be found in [87].

The integration technique in this example has to be used twice. This is because it is formulated to solve first order differential equations, in this case, the solutions to second order differential equations are needed. This is carried out by reducing the second order differential to two first order differential equations. This can be seen from the following equations.

$$m\ddot{x} + c\dot{x} + kx - F_X = 0 \tag{101}$$

$$\begin{aligned} y_1 &= x \\ y_2 &= \dot{x} \end{aligned} \tag{102}$$

$$\begin{aligned} y_1' &= y_2 \\ y_2' &= \frac{-cy_2 - ky_1 + F_X}{m} \end{aligned} \tag{103}$$

10.2.8 Results

A full validation exercise has been carried out on the dynamic model, in conjunction with continuous model verification that has been ongoing throughout the development of the program.

The first set of figures give the results from a numerical drop test. The modelled helicopter is given an initial downwards velocity of $3.0m/sec$, typical of a landing scenario. This simulates the helicopter dynamics as the aircraft lands, but in this example the forces from the rotors and ship motions have been ignored. From this simulation, the resulting motions and forces can be analysed.

Figure 132 gives the vertical displacement at the helicopter CG. The displacement increases at an initially high rate, this lies within the area of low oleo stiffness. When the oleos are compressed into the higher stiffness zone, the rate of displacement reduces. The final arresting is carried out in the $0.32m$ displacement region, this is the area where oleo stiffness increases to relatively high values. A slight recoil is observed, but significantly damped out after one cycle.

Figure 133 shows the pitch response during this drop test. The position of the two aft oleos force the compression of the forward oleo, resulting in the helicopter pitching forwards.

This is also reflected in the oleo load results given in figure 134. The loads in oleos 2 and 3, are equal, due to the symmetric nature of the helicopter and the drop condition. With the forward oleo 1 resisting far more load than either aft oleo.

Overall, the numerical drop test yielded results that would be expected during such an experiment.

The second series of figures correspond to the helicopter on a ship undergoing sinusoidal roll motion. The helicopter was first set at its equilibrium condition, then the sinusoidal motions were applied.

The helicopter responses in a sinusoidal manner, this is observed in the helicopter roll response (figure 135).

The oleo load (figure 136) follows the sinusoidal pattern, the port and starboard oleo loads oppose each other, with the roll inducing a change in vertical displacement. The tyre transverse loads (figure 137) show duplicate results for the aft tyres, with an increased load for the forward tyres.

The final test was to induce realistic ship motions upon the helicopter. The following figures are those obtained for an approximation of sea state 5, Bretschneider wave spectra, $T = 12.4sec$ and $h_{1/3} = 5.5m$. Five degrees of ship motion were modelled, with that of surge being ignored.

The initial disturbance is caused by the initial application of the ship motion loadings, but this is damped out rapidly. This effect can be reduced by applying the loadings using a ramp type function. Figure 138 shows the helicopter heave following the flight deck motions, this is comparable to the roll output (figure 139). The loads of the oleos (figure 140) and the tyre in the transverse direction (figure 141) show consistent results. The differences in the tyre loads, between the aft tyres denoted as 2 and 3, and the forward 1, are caused by the lever each has to the CG, as the forward tyre arrangement is further from the CG. This would result in a low load, but there are two aft tyre arrangements sharing the force.

It can be seen from the previous figures that the model yields reasonable, logical results. These results have also compared favourably with the views of [82] and [84].

10.3 Stabilised Ship Motion Dynamic Effects

This section presents the results of the effects of different stabilised ship conditions upon helicopter loadings and stability, using the motions determined from the computer program [10] during the controller analysis. Three conditions have been selected to test. The first being that of the unstabilised ship. The second, classic roll control, this provided reasonable roll reductions. And finally, H_∞ LFE control, this gave superior roll and LFE attenuation. All these motions relate to a heading of 60°, which corresponds to the heading of maximum LFE.

The results were determined for the helicopter mounted on the flight deck, 36.0 m aft of CG and 5.0 m above CG. This is the same position as that used for the LFE controller design. A Bretschneider spectra of $T = 12.4sec$ and $h_{1/3} = 5.5m$ has been applied. The rms roll and LFE values for each control method are given in table 14, and a section of the roll history plot for each condition is provided in figure 144. The effects of the controllers on roll reduction can clearly be seen.

It can be seen from figure 142, that the loads exhibited in the deck plane are of an order lower than that perpendicular, resulting in an oleo load. This results from the weight of the aircraft. It must be borne in mind, that lowest oleo loads coincide with the highest in plane loads, as can be seen from the figure. Roll and LFE stabilisation increase the working range of the helicopter on the flight deck, this can be seen from the rms loads given in table 15, with the lower motions of the LFE controller leading to lower loads. To prove that these results were not dependent upon the spectra selected, a similar analysis was carried out with a JONSWAP, $T = 9sec$ and $h_{1/3} = 4.0m$, representing a moderate to high sea state in coastal waters. These results are given in table 16, and are similar to those achieved with the initial spectra, despite a shorter wave period.

The magnitudes of the deck plane wheel loads over a time period have been given in figure 143. It can clearly be seen that the loads resulting from the ship being unstablised are significantly greater than for the controlled conditions. This is again reflected in figure 145, where the friction coefficient and oleo load to deck plane wheel load ratio shows the low values for the unstabilised case. This plot is effectively a measure of the helicopters stability, the higher the value, the greater the stability of the aircraft at that moment. If, the function falls below 1.0, then a wheel would have lost grip and slide upon the deck, therefore breaking the stability criteria. In the case of the unstabilised condition, this occurs at 87 seconds. For such an analysis to be carried out, a sufficient length of simulation must be computed in order to gain a statistically valid selection. A friction coefficient of 0.3 has been used.

This has been adopted, as in such a sea state the deck would probably be wet, and therefore corresponds to the coefficients given in [63].

The differences between the classic roll and H_∞ LFE stabilisation loadings is approximately 8%. The reduced rms roll and LFE motions created by LFE control, has lead to lower loads.

When the helicopter is in an equilibrium position on the flight deck, ship motions do not significantly compress the oleos. This results from the relatively high stiffnesses of these spring type elements in this condition, which is necessary for the helicopter to maintain a constant ride height when arming/disarming and refuelling. Therefore, the helicopter once settled from the landing phase, exhibited relatively stiff properties for the ship motions levels experienced at this moderate sea state.

For off centreline locations, heave motion dominates the displacement perpendicular to the deck plane. This results in very similar oleo loads between the different control configurations. The controlled fins only have a significant effect on the anti-symmetric DOFs. Therefore, the controller effects on helicopter stability can be analysed primarily with the inplane deck loads.

The results used to determine the rms values, were carried out over a time period of 30 minutes, in order to have a valid statistical sample. These loads may initially appear to be relatively low, but it must be borne in mind that effects resulting from wind loading associated from such a sea state could vastly increase the loads applied in the deck plane.

Control Condition	rms Roll degs	rms LFE m/sec^2
Unstabilised	5.582	1.132
Roll Stabilised	1.661	0.386
H_∞ LFE Stabilised	1.202	0.344

Table 14: Various Control Condition Motion Data

Control Condition	Av. rms Load N	% Diff.
Unstabilised	1352.2	0.0
Roll Stabilised	796.6	41.1
H_∞ LFE Stabilised	731.9	45.9

Table 15: Average rms Wheel Load in the deck plane

Control Condition	Av. rms Load N	% Diff.
Unstabilised	1377.7	0.0
Roll Stabilised	762.6	44.6
H_∞ LFE Stabilised	715.2	48.1

Table 16: Average rms Wheel Load in the deck plane for Jonswap Spectra

From this it can be concluded that the LFE controller has the effect of reducing in deck plane loadings upon the helicopter. This will translate to increased helicopter operability in more severe environments. More extreme sea states need to be tested, to investigate the working limits of each controller. This necessitates the use of alternative non-linear, time domain seakeeping approaches or the inclusion of actual ship data, as the seakeeping program [10] will be inappropriate due to its linear assumptions.

11 Conclusions

- A major aim of this project was to determine methods with which to increase the overall effectiveness of helicopters operating from warships. This has been accomplished by minimising ship motions by way of a H_∞ LFE controller. This controller exhibited improved performance over the conventional type controllers frequently used on modern day vessels.

- An experimental set up has been adapted that can be used to test roll controllers on a range of model ship types. The Labview package has been used to create control software. The equipment was tested on a towed small scale model, but can also be used for free running model tests. The control equipment was used successfully to test classic PID and H_∞ roll controllers using a towed model and a contra-rotating weight mechanism to induce the roll moment. The data provided from these tests was used to validate the ship motion software, that was then used to test new controllers numerically. The software results were found to compare well with the experimental data, this provided reassurance in the accuracy of this numerical tool.

- A H_∞ LFE controller has been developed that produced both good roll and LFE attenuation using a structured approach, out performing the classic PID equivalent. This was an improvement on the frequency response based approach used previously to investigate LFE control.

- The H_∞ control method proved to have advantages over more conventional approaches resulting from careful design. This benefitted motion attenuating performance and lead to properties such as reduced higher frequency fin activity. A major benefit of the H_∞ approach is in the ability to provide control activity in desirable frequency zones, and less in others. This allows the user to emphasise the control in regions where the system description is considered accurate, and to diminish it in areas that are not.

- A numerical dynamic model of a helicopter on the flight deck was developed in order to test the effects of ship motion reduction on helicopter stability. The model contains representations of non-linear oleos, tyres, wind, ship motions and decklocks, so it can be used to determine helicopter operational limits due to wind and ship motions, effects of decklocks and other entrapment devices for example. Using this dynamic

model, controlled ship motions were found to reduce significantly helicopter loadings and therefore increase aircraft on deck stability, with the H_∞ LFE controller resulting in lower loads than the comparable classic roll controller.

- Globally, a route has been created that allows ship roll and LFE controllers to be derived, tested numerically to determine the resultant ship motions and to measure the overall effect of the reduced motions on the helicopter on-deck stability. This produces a relationship between the controller and the eventual helicopter performance.

- The work of Grimble et al [5] was used as a base line from which to develop further roll and LFE controllers. This was also used to form the H_∞ controllers that were tested experimentally. From these experiments, similar overall roll attenuating performances were achieved between the two control approaches.

- An investigation of H_∞ controller order reduction was carried out. This proved that controller order could be reduced to acceptable levels for practical application, without significant loss of the controllers characteristics. This was carried out using the ship motion which is frequency domain based. It would be valuable to carry out the same comparison with a time domain non-linear analysis.

- A number of weighting functions were attempted, due to the numerical sensitivity of the H_∞ method, only specific functions are admissible. The frequency domain ship motion package did not permit analysis of non-linear effects. It is acknowledged, that to gain a full appreciation of the H_∞ controller performances, a time domain analysis is necessary. This would allow the effects of unmodelled dynamics such as fin displacement, rate limits, sensor and external noise upon the various controllers to be extensively studied.

- A Bretschneider spectra of 12.4 sec mean period and 5.5 metres has been used as a typical North Atlantic spectra. To avoid this particular spectra misleading the overall conclusions of the controller results, other spectra values were applied. This made little difference to the overall relatively results. The differences in the frequency content of the classic roll and H_∞ LFE controllers is quite different, therefore the comparative results will not change within a realistic range of spectra periods.

- The controller order reduction techniques appeared to work satisfactorily, with very little control action loss. This was also apparent in comparing the controllers frequency responses. This is beneficial, as lower order controllers are far simpler to implement from a practical aspect.

- A number of wavelet methods have been investigated as a means of determining periods of quiescent periods, and found to be quite limited for this task. To progress this area of research, data from a localised sea surface over a time scale are necessary to explore any concept, as the use of simulated data is extremely restrictive. Wavelet use for other marine applications have been identified.

12 Scope of Further Work

The process used to quantify the controller motion attenuating performances is based on a frequency domain approach. This limits its use as a complete analysis tool, as it is unable to model the effects of limiting fin displacements and rates, fin stops and noise inputs. Also, the linear motion assumption is only valid for moderate sea states. Therefore, more rigourous verification processes are necessary to explore fully the characteristics of each controller, this can be accomplished using non-linear, time domain ship motion methods. With such a tool, the controllers described in this document could be tested to a greater extent.

The designed H_∞ controllers in this document have only been compared to a PID frequency response controller. Other control methods may produce greater motion reductions with which to compare new designs. Therefore, attention could be given towards the implementation of other control strategies such as non-linear adaptive control.

The ship/helicopter dynamic model has been designed with a modular format in mind. This allows the simple inclusion of new elements into the system, without disruption to the existing components. Improvements that could be used to develop the model further are:

- Improved modelling of the aerodynamic model, especially due to the effect of the ship and superstructure on modifying the airflow over the flight deck.
- Inclusion of other current entrapment devices within the model.
- To attempt to include helicopter on-deck manoeuvring, resulting from aircraft handling. This would provide information as to the appropriateness of various handling concepts and increase the envelope of the dynamic models applicability.

This could then be used to determine helicopter operational limits, with a comparison to the actual operational limits derived from full scale trials.

Many improvements to the model experimental setup are possible, to make the system more versatile.

- Due to the ongoing modifications and improvements made to the system during its lifetime, could be made more compact and lighter. Therefore the electronics could be transferred solely to printed circuit boards (PCBs), and contained within a watertight unit to prevent any ingress of water and damage.

- The system capacity will be modified to incorporate the larger motors needed for larger scale models.
- The adaption of the system for rudder motion stabilisation will also be a important addition to the system.
- Development of new controllers within the Labview environment will also be appropriate, to test new control variations.

These new properties will vastly increase the flexibility of the current system.

Model testing of various controllers to date has been quite limited. Therefore, increased experimentation will provide more information to improve experimental approaches. In addition, other key areas of fin stabiliser use maybe investigated, such as the increase drag contributions from active appendages and optimal fin placement.

References

[1] M. P. Prince and P. A. Wilson. Helicopter handling and entrapment. Ship science report no. 96, University of Southampton, March 1996.

[2] M. P. Prince and P. A. Wilson. A review of helicopter entrapment and handling systems used by navies around the world. In *RINA Conf. WARSHIP '97, Air Power at Sea*, London, 1997.

[3] A. Tang and P. A. Wilson. LFE stabilisation final report. Ship Science report no. 61, University of Southampton, March 1993.

[4] A. R. J. M. Lloyd. *Seakeeping: Ship Behaviour in Rough Weather.* Ellis Horwood Ltd., 1989.

[5] M. J. Grimble, M. R. Katebi, and Y. Zhang. H_∞ based ship fin-rudder roll stabilisation design. In *Proc.* 10^{th} *Ship Control Systems Symp.*, volume 5, Ottawa, Canada, 1993.

[6] A. Agarwal. H_∞ robust control technology applied to the design of a combined steering/stabiliser system for warships. In *Proc.* 11^{th} *Ship Control Systems Symp.*, volume 1, Southampton, UK, 1997.

[7] D. S. Desanj, D. C. Donha, M. R. Katebi, and M. J. Grimble. H_∞ adaptive controllers for auto-pilot applications. In *Proc.* 11^{th} *Ship Control Systems Symp.*, volume 1, Southampton, UK, 1997.

[8] R. Piché, S. Pohjolainen, and T. Virvalo. Design of robust controllers for position servos using H_∞ theory. *Proc. Instn. Mech. Engrs.*, 205:299–306, 1991.

[9] J. Stoustrup, G. Aglietti, E. Rogers, R. S. Langley, and S. B. Gabriel. H_∞ controllers for the rejection of microvibration disturbances. In *Proc.* 5^{th} *European Control Conference*, Karlsruhe, Germany, 1999.

[10] Dept. of Ship Science, University of Southampton. *Modified Seakeeping Software*, 1999.

[11] I. Daubechies. The wavelet transform, time-frequency localisation and signal analysis. In *IEEE Trans. Information Theory*, volume 36, 1990.

[12] S. Mallat. A theory for multiresolution signal decomposition: The wavelet representation. *IEEE Trans. Pattern Analysis and machine intelligence*, 11, 1989.

[13] A. Bruce, D. Donoho, and H. Y. Gao. Wavelet analysis. In *IEEE Spectrum*, October 1996.

[14] A. Graps. An introduction to wavelets. *IEEE Computational Science and Engineering*, 2(2), 1995.

[15] D. A. Jay and E. P. Flinchem. Wavelet transform analyses of non-stationary tidal currents. In *IEEE Proc.* 5^{th} *working conf. on current measurement*, volume 5, February 1995.

[16] D. E. Newland. *An Introduction to Random Vibrations, Spectral and Wavelet Analysis.* Longman, 3^{rd} edition, 1993.

[17] D. E. Newland. Wavelet theory and applications. In *Proc.* 3^{rd} *Intl. Congress on Air- and Structure-Borne Sound and Vibration*, Montreal, Canada, 1994.

[18] O. Rioul and M. Vetterli. Wavelets and signal processing. In *IEEE signal processing magazine*, October 1991.

[19] L. G. Weiss. Wavelets and wideband correlation processing. In *IEEE Signal Processing Magazine*, January 1994.

[20] R. K. Young. *Wavlet theory and its applications.* Kluwer Academic Publishers, 1993.

[21] D. E. Newland. Harmonic wavelet analysis. In *Proc. R. Soc.*, volume 443, London, 1993.

[22] D. E. Newland. Harmonic and musical wavelets. In *Proc. R. Soc.*, volume 444, London, 1994.

[23] A. E. Baitis, D. A. Woolaver, and T. A. Beck. Rudder roll stabilisation for coast guard cutters and frigates. *Naval Engineers Journal*, May 1983.

[24] R. Graham. Motion induced interruptions as ship operability criteria. *Naval Engineers Journal*, March 1990.

[25] A. R. J. M. Lloyd. The operational effectiveness of the shipborne naval helicopter. *Journal of Naval Science*, August 1986.

[26] K. Monk. A warship roll criterion. In *Trans. RINA*, volume 128, London, October 1987.

[27] A. Tang and P. A. Wilson. An investigation into lateral force estimator (LFE) stabilisation using the rudder. Ship Science report no. 51, University of Southampton, April 1992.

[28] A. E. Baitis and L. V. Schmidt. Ship roll stabilization in the US Navy. *Naval Engineers Journal*, May 1989.

[29] J. van Amerongen, P. G. M. Van Der Klugt, and J. B. M. Pieffers. Model tests and full-scale trials with a rudder roll stabilization system. In *Proc. 7^{th} Ship Control Systems Symp.*, volume 1, Bath, UK, 1984.

[30] R. T. Schmitke. The influence of displacement, hull form, appendages, metacentric height and stabilisation on frigate rolling in irregular seas. In *SNAME Ship Technology and Research (STAR) symp.*, California, USA, 1980.

[31] M. T. Sharif, G. N. Roberts, S. A. French, and R. Sutton. Lateral force stabilisation: A comparison of controller designs. In *Proc. 10^{th} Ship Control Systems Symp.*, volume 5, Ottawa, Canada, 1993.

[32] R. P. Dallinga. Hydromechanic aspects of the design of fin stabilisers. In *Trans. RINA*, volume 193, 1993.

[33] W. W. Zhou, D. B. Cherchas, S. Calisal, and A. Tiano. A new approach for adaptive rudder roll stabilisation control. In *Proc. 9^{th} Ship Control Systems Symp.*, volume 1, Maryland, USA, 1990.

[34] S. Grahlmann. Neurofuzzy based control of ships operating in disturbed water. Project report, Dept. of Electronics and Computer Science, University of Southampton, May 1998.

[35] R. Sutton, G. N. Roberts, and S. R. Dearden. Design study of a fuzzy controller for ship roll stabilisation. *Electronics and Communications Engineering Journal*, July/August 1989.

[36] N. A. Hickey, M. J. Grimble, M. A. Johnson, M. R. Katebi, and R. Melville. Robust fin roll stabilisation of surface ships. In *Proc. 36^{th} Conf. on Decision and Control*, San Diego, USA, 1997.

[37] R. Taggart. Anomalous behaviour of merchant ship steering systems. *Marine Technology*, April 1970.

[38] W. E. Cowley and T. H. Lambert. The use of the rudder as roll stabiliser. In *Proc. 3^{rd} Ship Control Systems Symp.*, volume 2, Bath, UK, 1972.

[39] W. E. Cowley and T. H. Lambert. Sea trials on a roll stabiliser using the ship's rudder. In *Proc.* 4^{th} *Ship Control Systems Symp.*, volume 2, Netherlands, 1974.

[40] J. B. Carley. Feasibility study of steering and stabilising by rudder. In *Proc.* 4^{th} *Ship Control Systems Symp.*, volume 2, Netherlands, 1974.

[41] A. R. J. M. Lloyd. Roll stabilisation by rudder. In *Proc.* 4^{th} *Ship Control Systems Symp.*, volume 2, Netherlands, 1975.

[42] F. F. Van Gunsteren. Analysis of roll stabiliser performance. *Intl. Shipbuilding Progress*, May 1974.

[43] D. R. Broome. An integrated ship control system for CS Manchester Challenge. In *Trans. RINA*, volume 121, 1979.

[44] H. Eda. A digital simulation study of steering control with effects of roll motions. In *Proc.* 5^{th} *Ship Control Systems Symp.*, volume 3, Annapolis, USA, 1978.

[45] P. H. Whyte. A note on the application of modern control theory to ship roll stabilisation. In 18^{th} *ATTC*, Maryland, USA, 1977.

[46] A. E. Baitis, T. R. Applebee, and T. M. Mcnamara. Human factors considerations applied to operations of the FFG-8 and Lamps MK III. *Naval Engineers Journal*, May 1984.

[47] P. G. M. Van Der Klugt. Rudder roll stabilization: The Dutch solution. *Naval Engineers Journal*, May 1990.

[48] C. G. Kallström. Control of yaw and roll by a rudder/fin stabilisation system. In *Proc.* 6^{th} *Ship Control Systems Symp.*, Ottawa, Canada, 1981.

[49] C. G. Kallström. An integrated rudder control system for roll damping and course maintenance. In *Proc.* 9^{th} *Ship Control Systems Symp.*, volume 3, Maryland, USA, 1990.

[50] M. Blanke, P. Haals, and K. K. Andreasen. Rudder roll damping experience in Denmark. In *Intl. Federation of Automatic Control IFAC workshop on Expert Systems and Signal Processing in Marine Automation*, Lygby, Denmark, 1989.

[51] D. C. Powell. Rudder roll stabilisation - a critical review. In *Proc.* 9^{th} *Ship Control Systems Symp.*, volume 2, Maryland, USA, 1990.

[52] M. R. Katebi, M. A. Johnson, and M. J. Grimble. The design of rudder roll stabilisation control system using the LQG stochastic optimal approach. In *Intl. Federation of Automatic Control IFAC Workshop on Expert Systems and Signal Processing in Marine Automation*, Lygby, Denmark, 1989.

[53] G. N. Roberts and S. W. Braham. Warship roll stabilisation using integrated control of rudder and fins. In *Proc. 9^{th} Ship Control Systems Symp.*, volume 1, Maryland, USA, 1990.

[54] R. Sutton. A linguistic self-organising controller for rudder induced warship roll stabilisation. In *Proc. 9^{th} Ship Control Systems Symp.*, volume 1, Maryland, USA, 1990.

[55] A. R. J.M̃. Lloyd. Ship motions, wind and the helicopter. In *Royal Aeronautical Society RAS/RINA symp. Helicopters and the Marine Environment*, London, June 1982.

[56] J. Val Healey. The prospects for simulating the helicopter/ship interface. *Naval Engineers Journal*, March 1987.

[57] P. J. F. O'Reilly. Aircraft/deck interface dynamics for destroyers. *Marine Technology*, 24(1), 1987.

[58] B. Ferrier, H. Polvi, and F. A. Thibodeau. Helicopter/ship analytic dynamic interface. In *Advisory Group for Aerospace Research and Development AGARD Conf. Proc. 509*, 1991.

[59] A. M. Arney, J. Blackwell, and R. A. Feik. Modelling the helicopter/ship dynamic interface. In *Proc. Australian Aeronautical Conf.*, Melborne, Australia, 1989.

[60] A. M. Arney, J. Blackwell, L. P. Erm, and N. E. Gilbert. A review of Australian activity on modelling the helicopter/ship dynamic interface. In *Advisory Group for Aerospace Research and Development AGARD Conf. Proc. 509*, 1991.

[61] J. Blackwell, A. M. Arney, N. E. Gilbert, and T. T. Truong. Modelling the helicopter/ship dynamic interface for the *Seahawk*/FFG-7. In *5^{th} Australian Aeronautical Conf.*, Melborne, Australia, 1993.

[62] F. S. Wei, E. Baitis, and W. Meyers. Analytical modelling of SH-2F helicopter shipborne operation. In *Advisory Group for Aerospace Research and Development AGARD Conf. Proc. 509*, 1991.

[63] F. S. Wei, E. Baitis, and W. Meyers. Analytical modelling of SH-2F helicopter shipborne operation. *Journal of Aircraft*, 29(5), 1992.

[64] A. R. Tadros and R. G. Langlois. Helicopter/ship dynamic interface. In *RINA Conf. WARSHIP '97, Air Power at Sea*, London, 1997.

[65] A. R. Tadros, G. Sopher, and R. G. Langlois. A new approach for passive securing at landing and powered handling of helicopters onboard small ships. In *RINA Conf. WARSHIP '98, Surface Warship: The Next Generation*, London, 1998.

[66] C. Pedrazzi, G. Barbieri, and B. Spanghero. ARCHIMEDES: The Riva Calzoni helicopter/ship dynamic interface modelling software. In *RINA Conf. WARSHIP '97, Air Power at Sea*, London, 1997.

[67] Royal Navy Lynx Pilots. Correspondence and meetings, 1996-8.

[68] E. L. Morris, H. K. Zienkiewicz, M. M. A. Pourzanjani, J. O. Flower, and M. R. Belmont. Techniques for sea state predictions. In 2^{nd} *Int. conf. Manoeuvring and Control of Marine Craft*, Southampton, UK, 1992.

[69] D. R. Broome and A. Pittaras. Ship motion predictions. In 9^{th} *Int. conf. Offshore Mechanics and Arctic Engng. OMAE*, Houston, USA, 1990.

[70] R. Bruce Lumsden and B. Ferrier. Along side analysis of Type 23 ship motion as a function of mechanical and dynamic limits of an EH-101-like helicopter using the landing period designator helicopter recovery device. In *American Helicopter Society AHS,* 51^{st} *Annual Forum Proc.*, Fort Worth, USA, 1995.

[71] J. Buckheit, S. Chen, D. Donoho, I. Johnstone, and J. Scarle. *WaveLab.* Standford University and NASA-Ames research center, 1995.

[72] The Math Works Inc. *MATLAB: Reference Guide*, 1992.

[73] M. St. Denis and W. J. Pierson. On the motions of ships in confused seas. In *Trans SNAME*, volume 61, 1953.

[74] K. Zhou and J. C. Doyle. *Essentials of Robust Control.* Prentice-Hall International Inc., 1998.

[75] The Math Works Inc. *Robust Control Toolbox Guide*, 1992.

[76] R. T. Schmitke. Ship sway roll and yaw in oblique seas. In *Trans. SNAME*, volume 86, 1978.

[77] N. R. Nicholson and M. R. Pegrum. Design and development of a digital control system for active fin stabilisers fitted to a towing tank model. Technical report, Vosper Thornycroft Marine Products Ltd., Hydraulic Power Division, September 1997.

[78] National Instruments. *Labview: user, function and reference guides*, 1997.

[79] S. F. Hoerner and H. V. Borst. *Fluid - Dynamic Lift.* Hoerner Fluid Dynamics, 1975.

[80] Westland. The design of helicopters for small ships and in particular the Westland naval Lynx. Technical report, Westland Helicopters Ltd., 1979.

[81] S. Newman. Notes on the development of the Westland WG13 helicopter for naval use. Dept. Aeronautics and Astronautics, University of Southampton.

[82] DERA Bedford. Private communications.

[83] A. J. Gray. A helicopter decklock: The minimum tension for stability. Master of Philsophy, Heriot-Watt University, March 1994.

[84] MacTaggart Scott. Private communications.

[85] Wolfson Unit M.T.I.A. *Symmetric Motion Seakeeping Software*, 1993.

[86] A. R. Tadros, J. S. Pawlowski, and R. Bruce Lumsden. A new non-linear time-domain ship motion prediction program and its effect on helicopter/ship dynamic interface analysis. In *RINA Conf. WARSHIP 2000, Warships for Amphibious Operations and Minewarfare*, London, 2000.

[87] G. Hall and J. M. Watt. *Modern numerical methods for ordinary differential equation.* Academic Press, London, 1980.

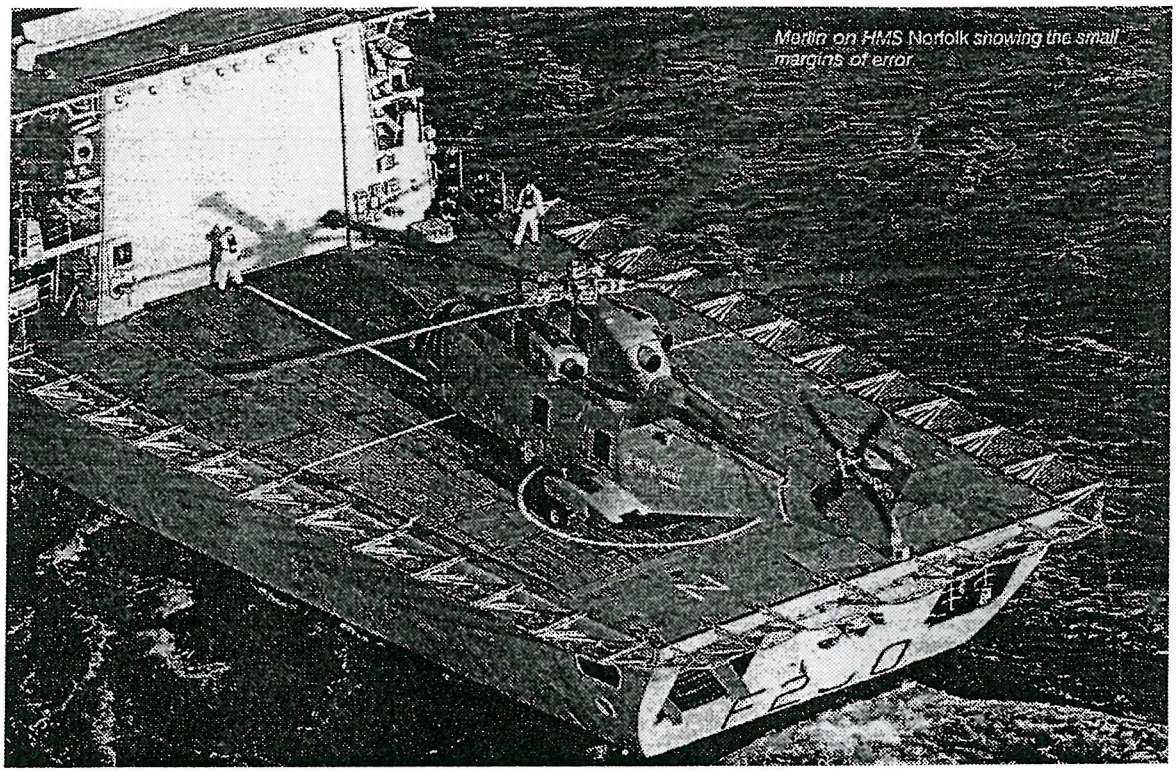

Figure 1: Photograph of Type 23 Frigate with 'Merlin' Helicopter

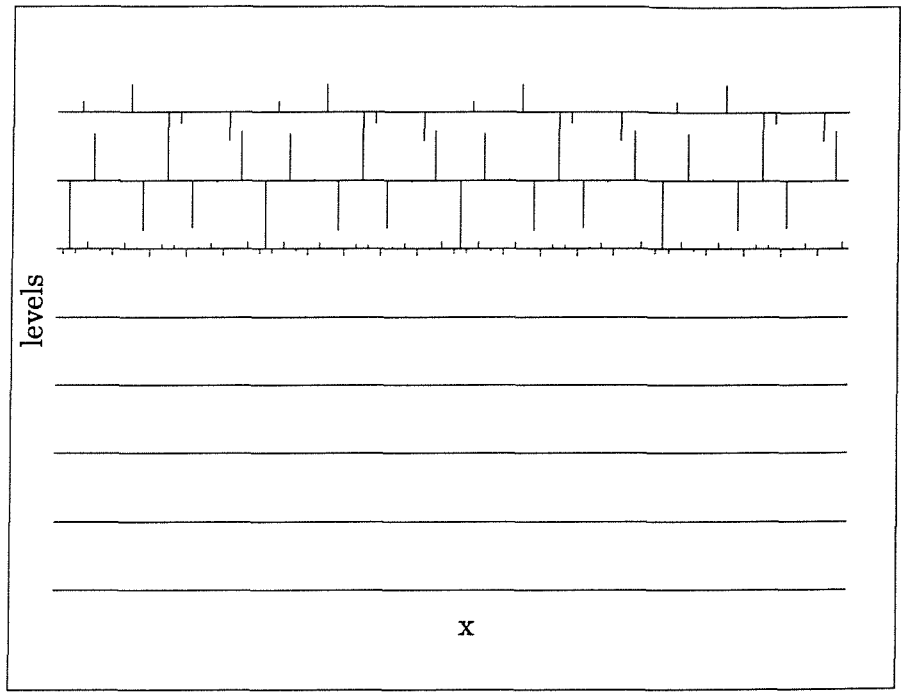

Figure 2: Dilation wavelet transformation, sinusoidal wave train

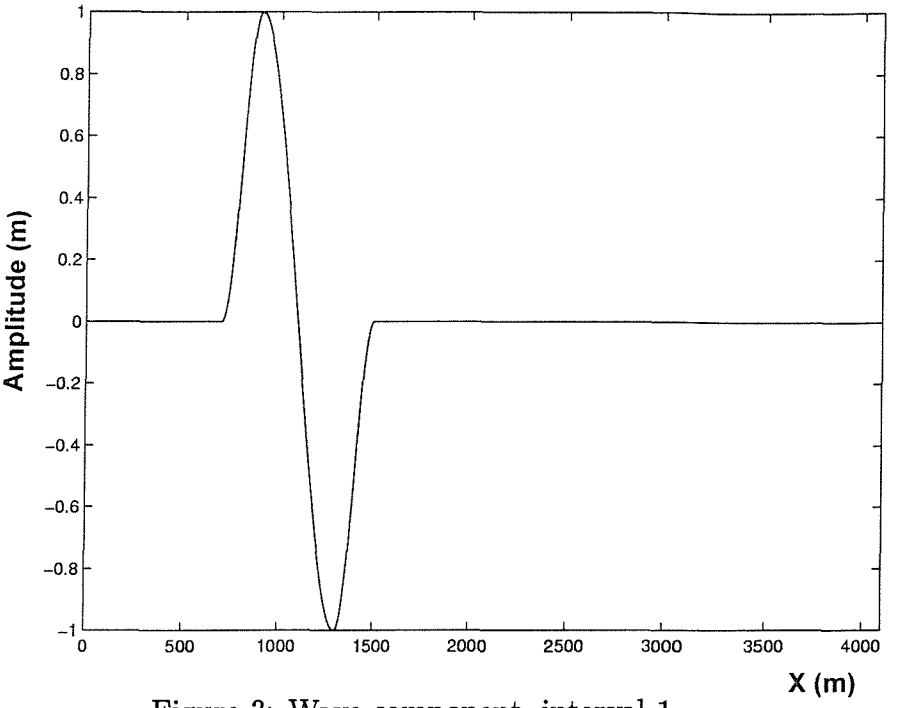

Figure 3: Wave component, interval 1

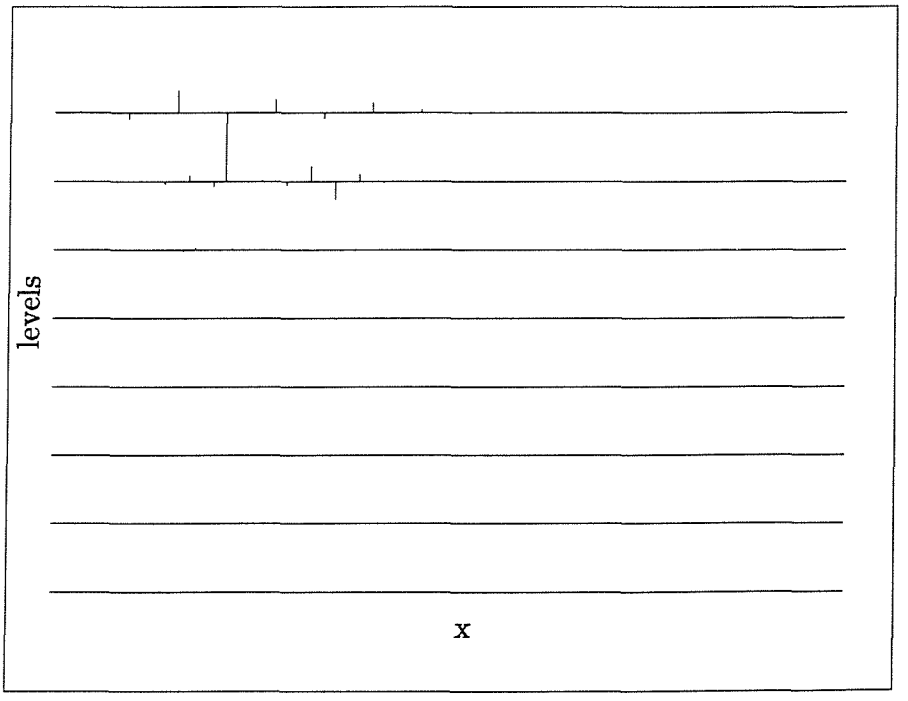

Figure 4: Dilation wavelet transformation, wave component interval 1

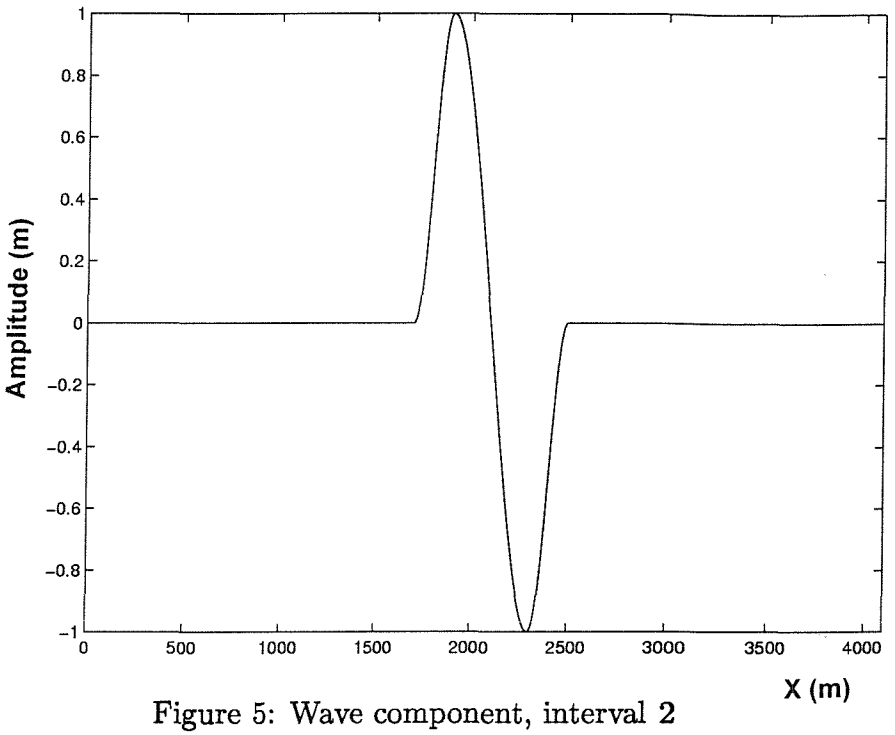

Figure 5: Wave component, interval 2

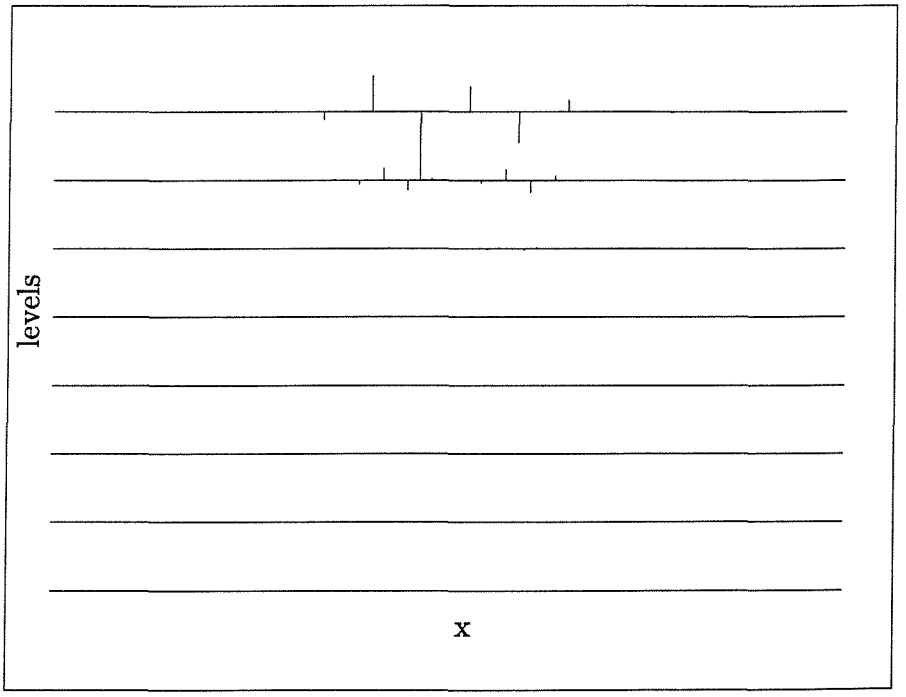

Figure 6: Dilation wavelet transformation, wave component interval 2

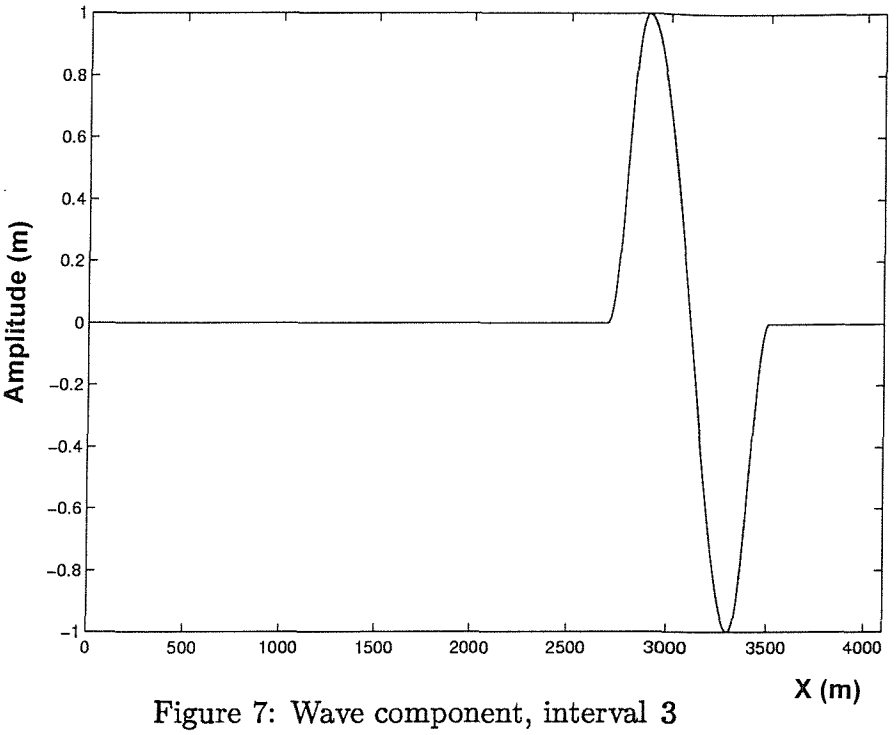

Figure 7: Wave component, interval 3

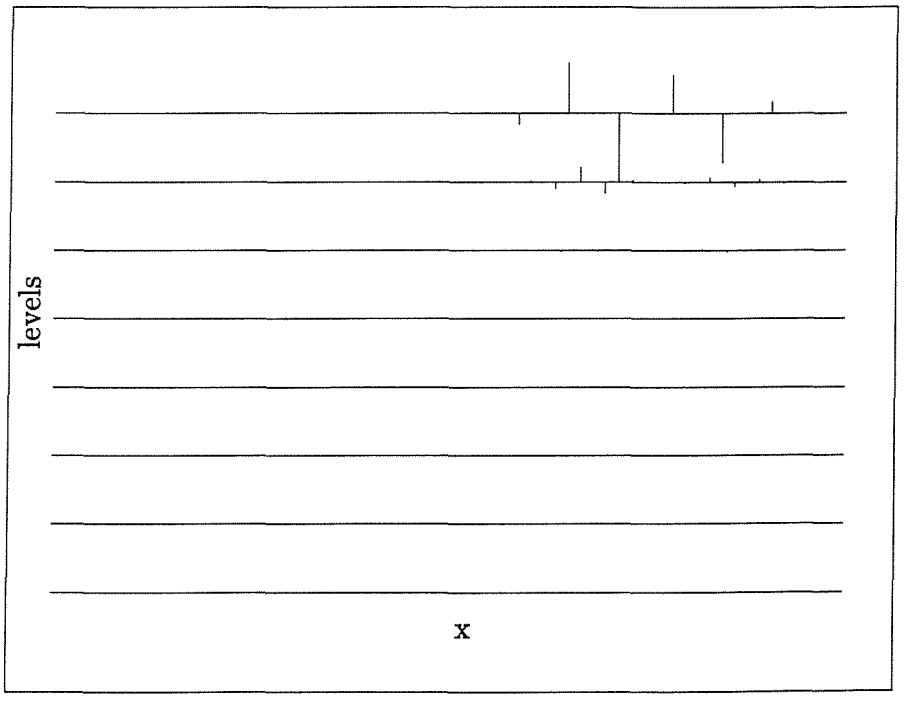

Figure 8: Dilation wavelet transformation, wave component interval 3

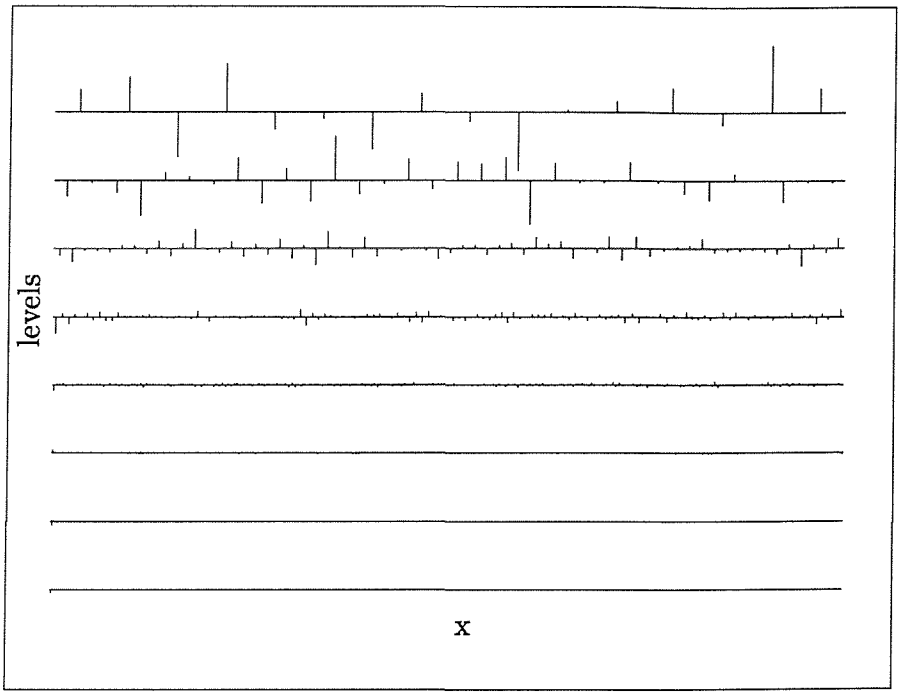

Figure 9: Dilation wavelet transformation, wave spectra 1

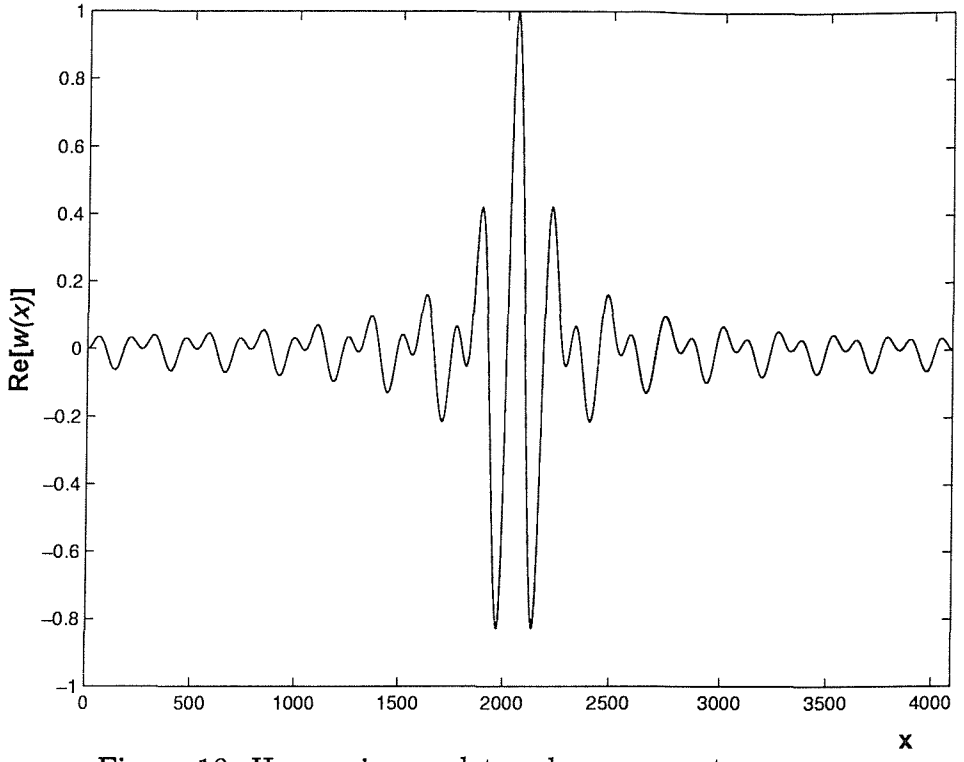

Figure 10: Harmonic wavelet real component

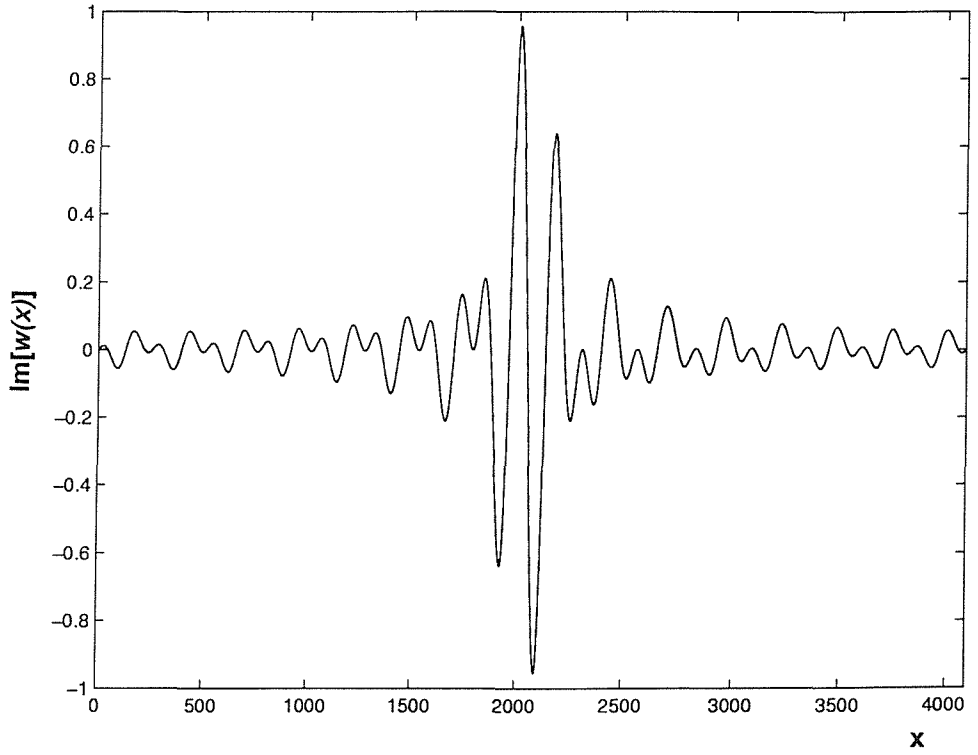

Figure 11: Harmonic wavelet imaginary component

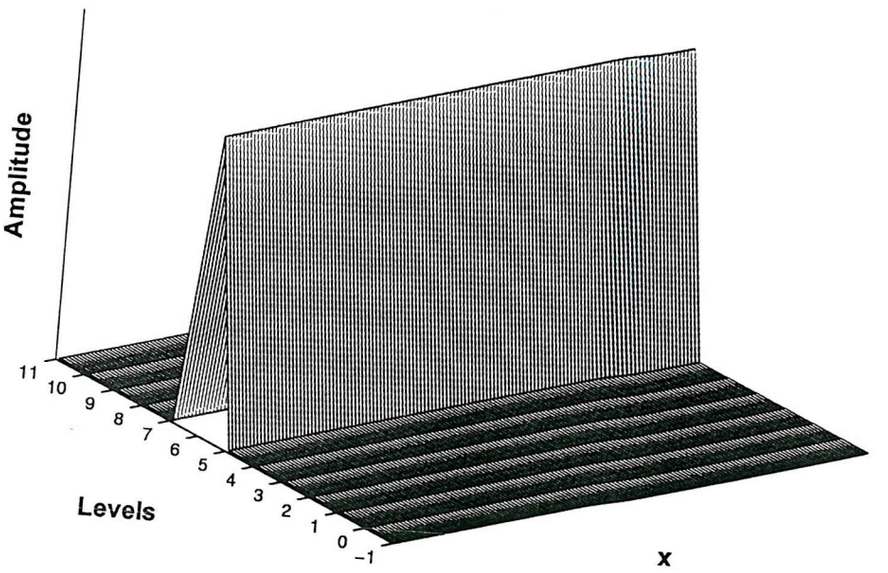

Figure 12: Harmonic wavelet map, sinusoidal wave train

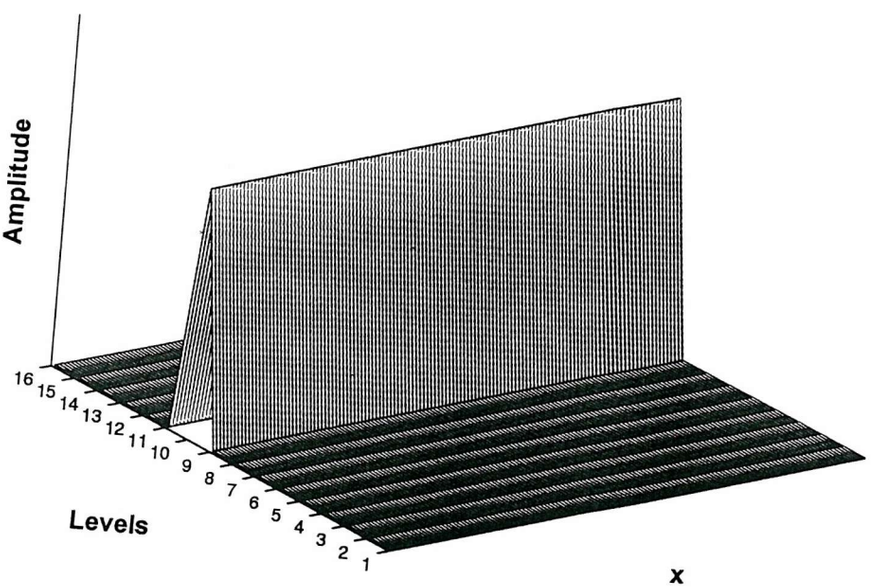

Figure 13: Musical wavelet map, sinusoidal wave train

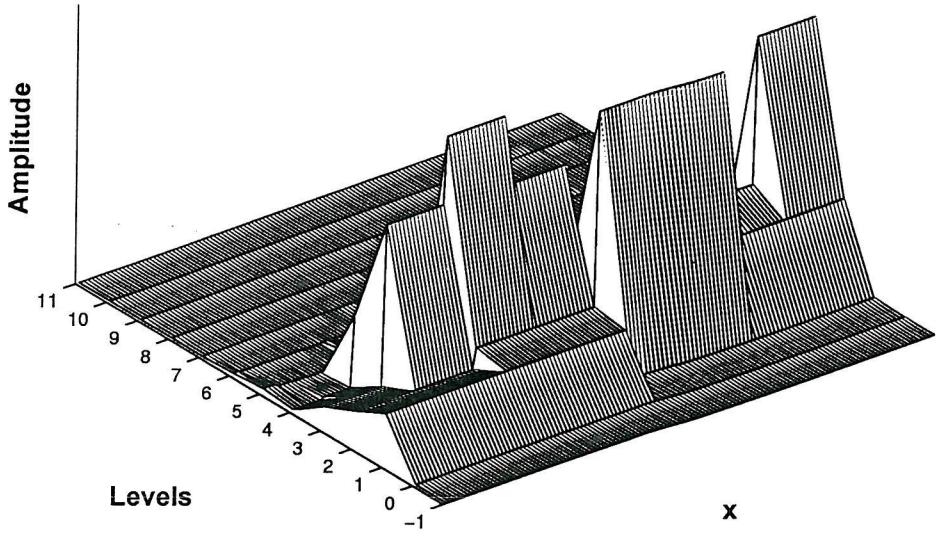

Figure 14: Harmonic wavelet map, wave spectra 1

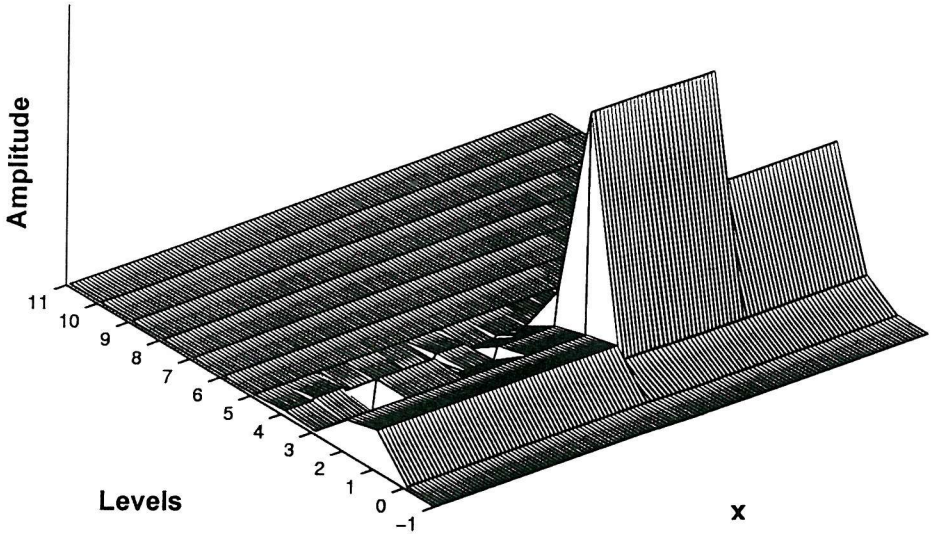

Figure 15: Harmonic wavelet map, wave spectra 2

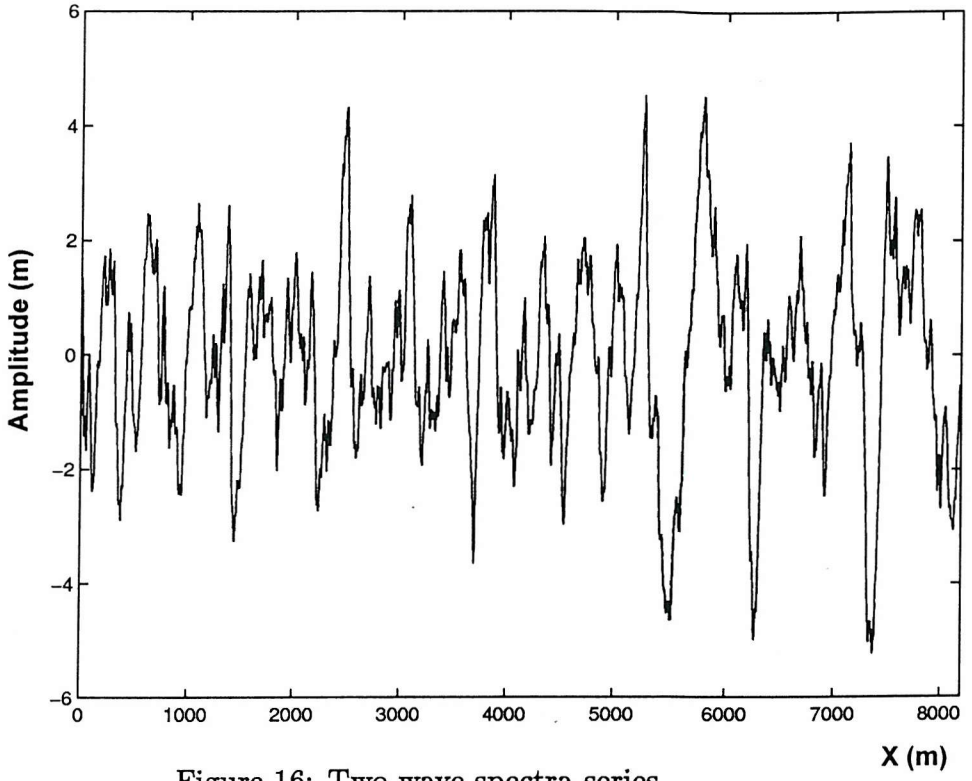

Figure 16: Two wave spectra series

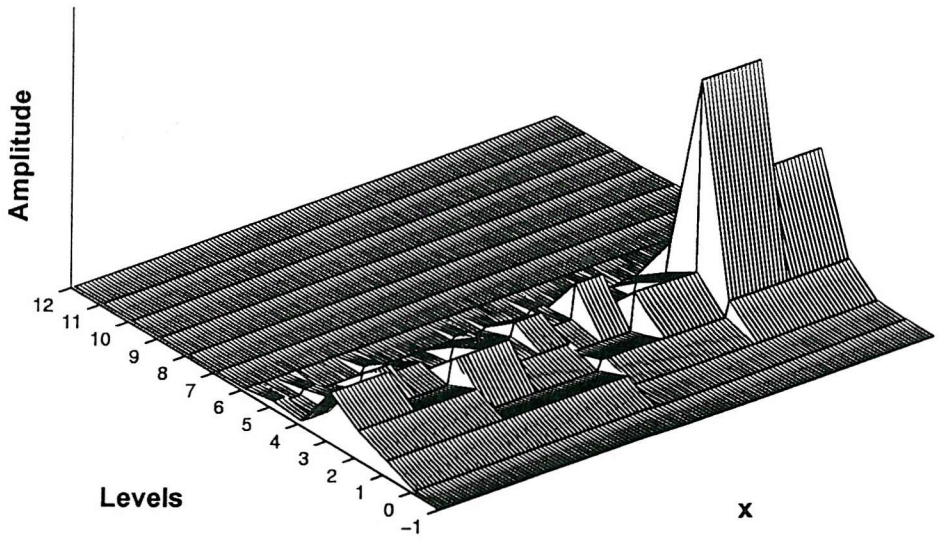

Figure 17: Harmonic wavelet map, Two wave spectra series

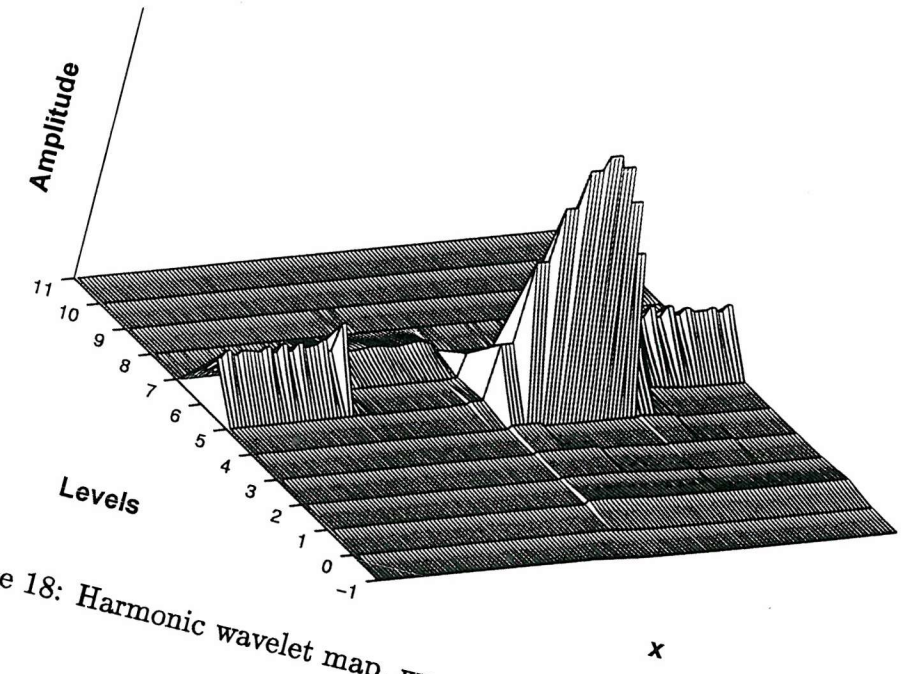

Figure 18: Harmonic wavelet map, wave train components

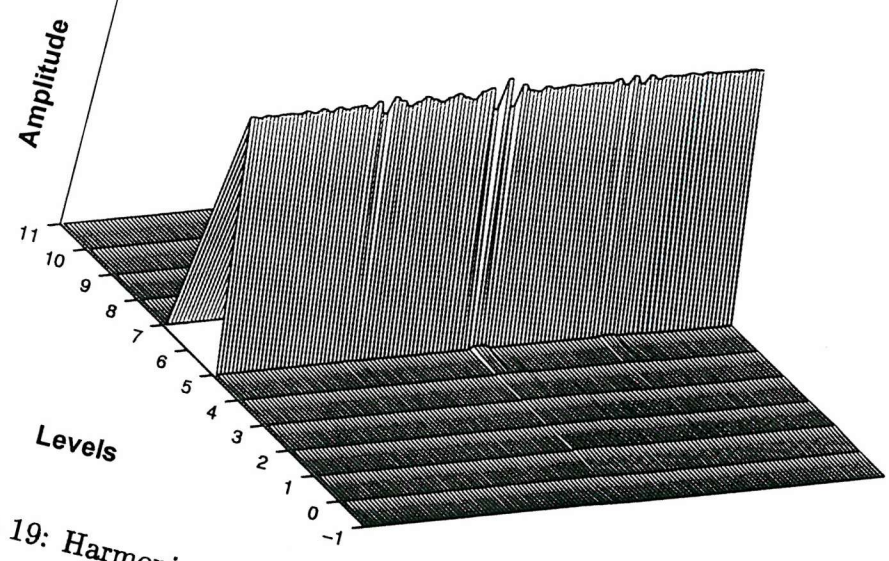

Figure 19: Harmonic wavelet map, wave train components

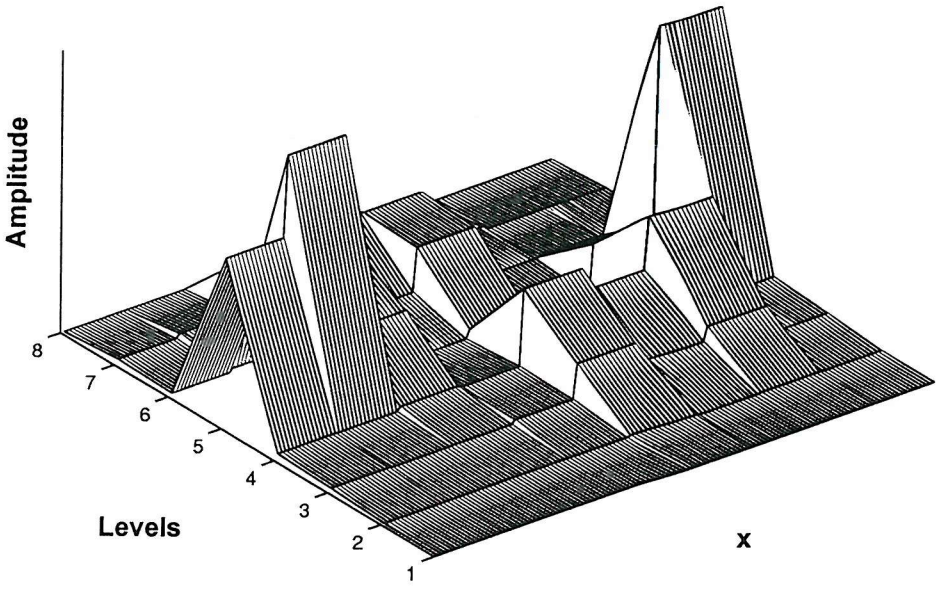

Figure 20: Musical wavelet map, wave train components

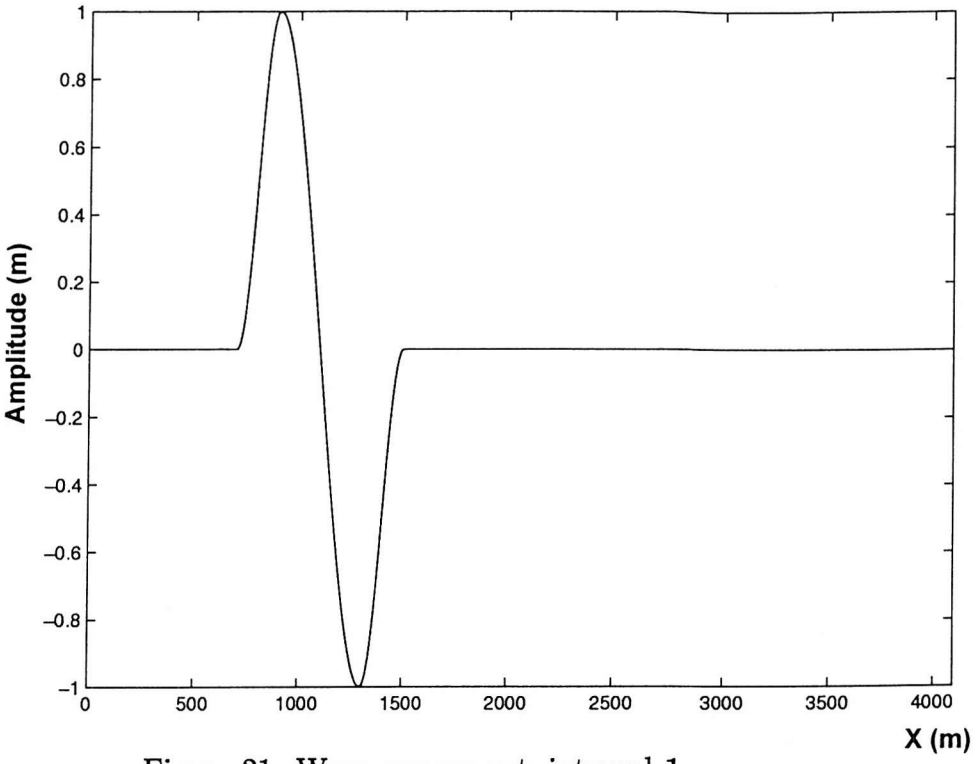

Figure 21: Wave component, interval 1

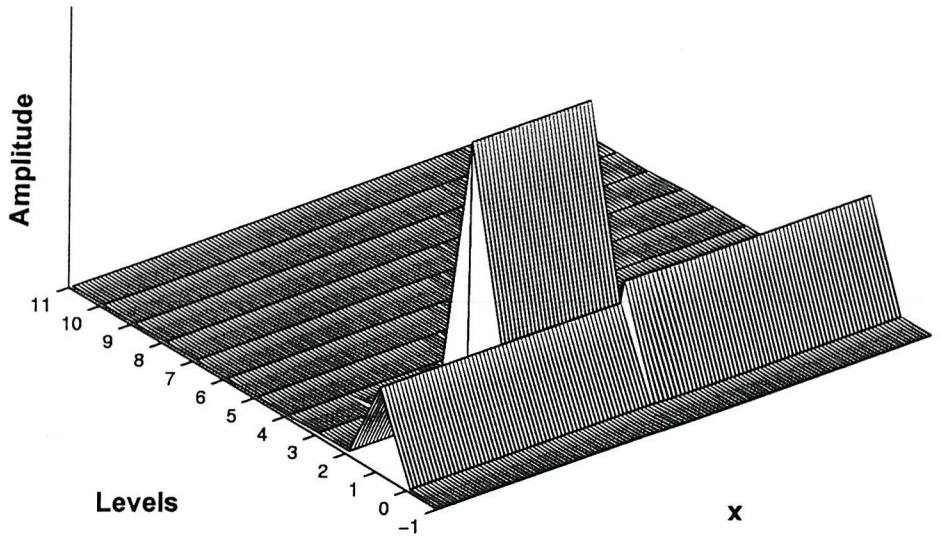

Figure 22: Harmonic wavelet map, wave component interval 1

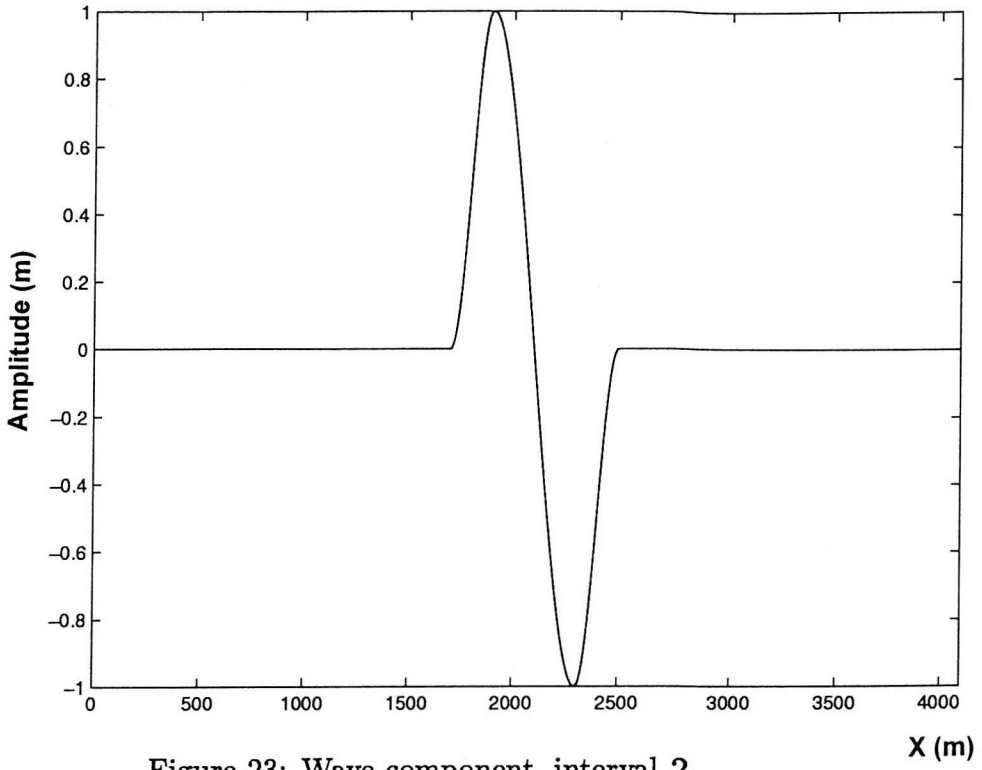

Figure 23: Wave component, interval 2

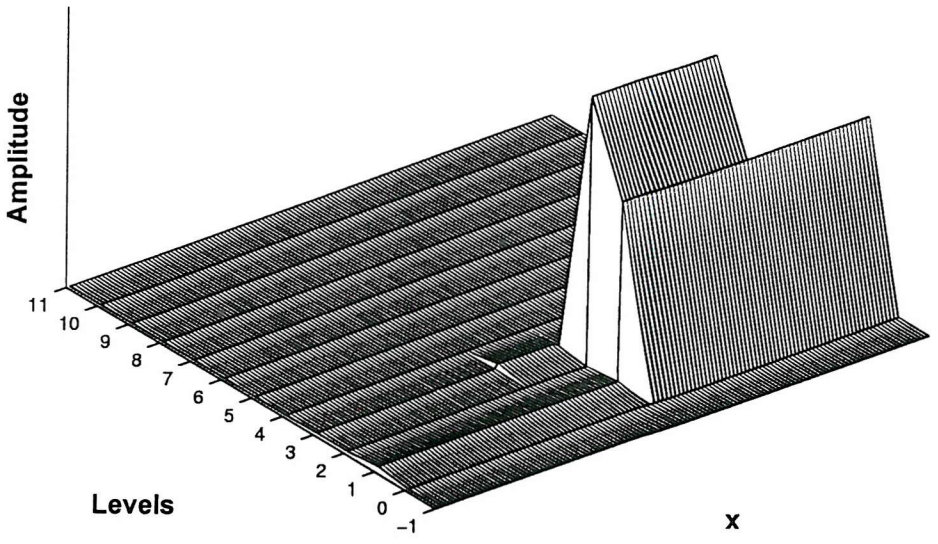

Figure 24: Harmonic wavelet map, wave component interval 2

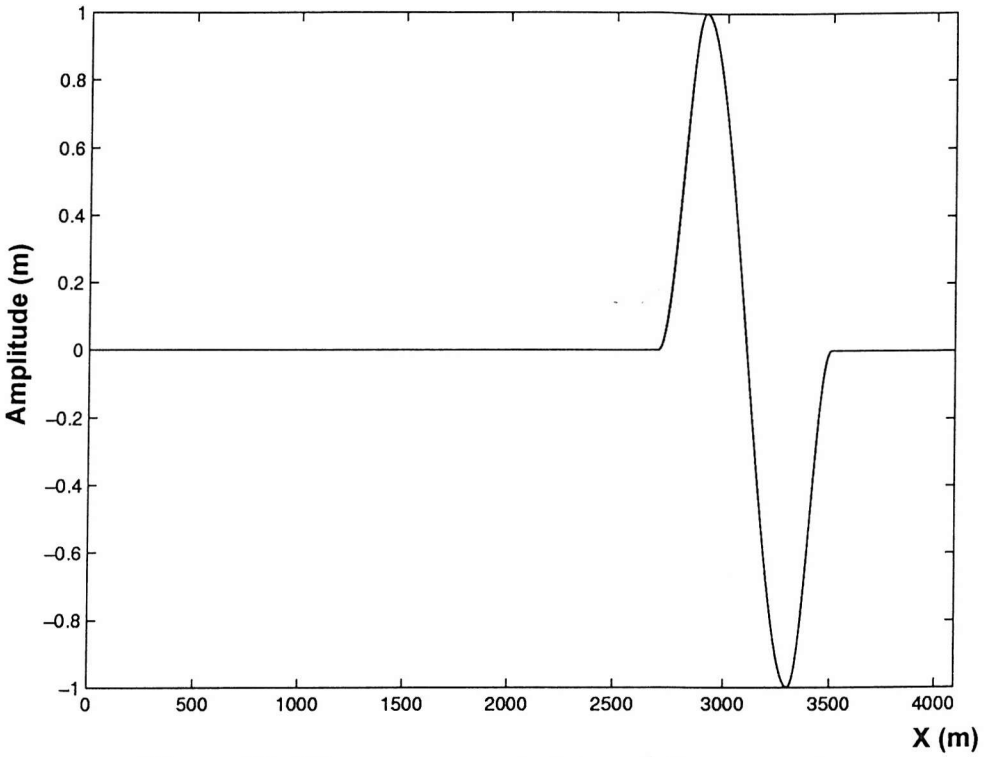

Figure 25: Wave component, interval 3

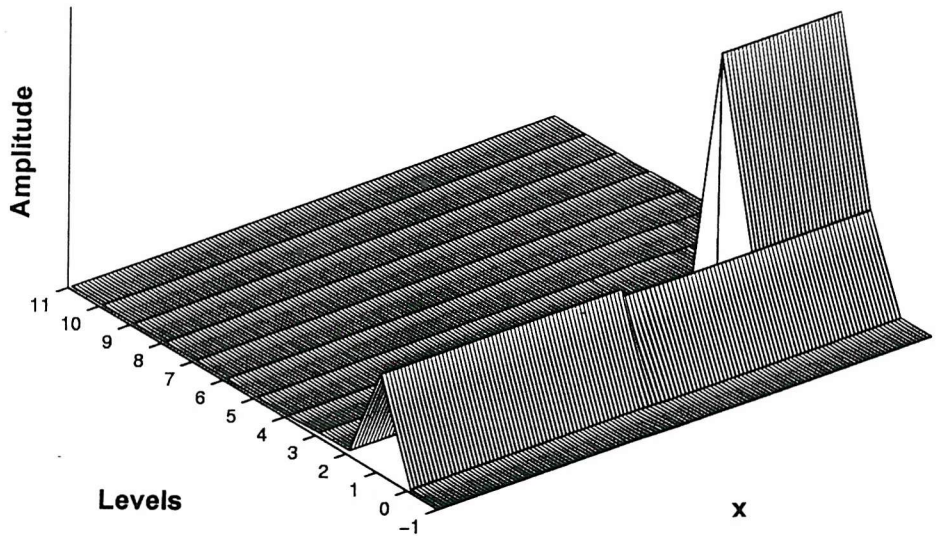

Figure 26: Harmonic wavelet map, wave component interval 3

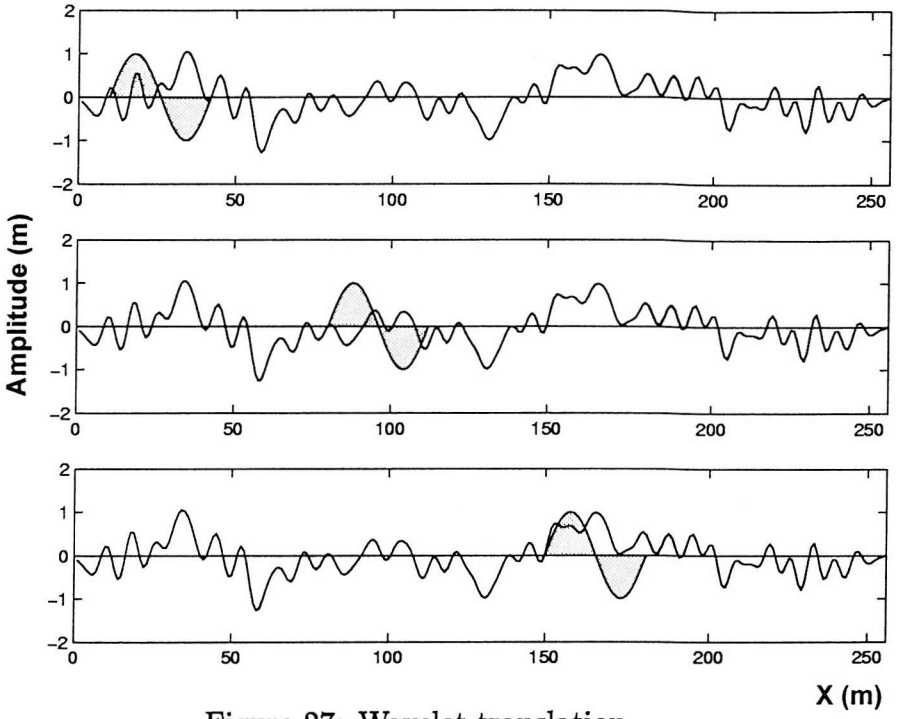

Figure 27: Wavelet translation

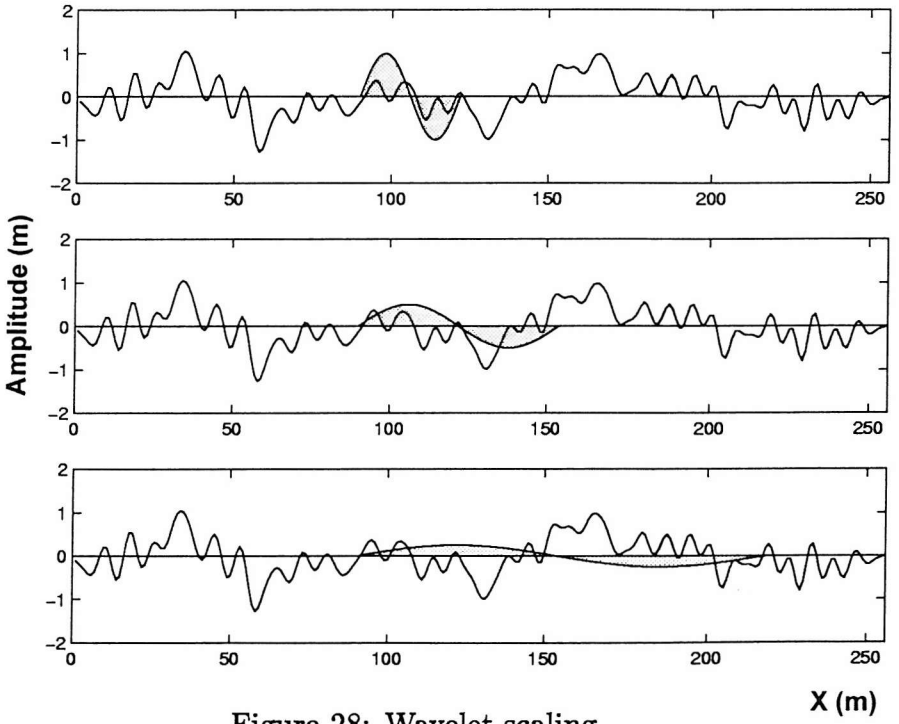

Figure 28: Wavelet scaling

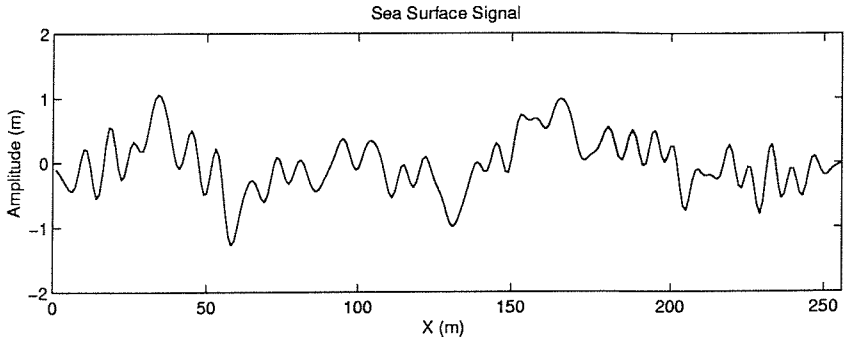

Figure 29: Sea surface signal

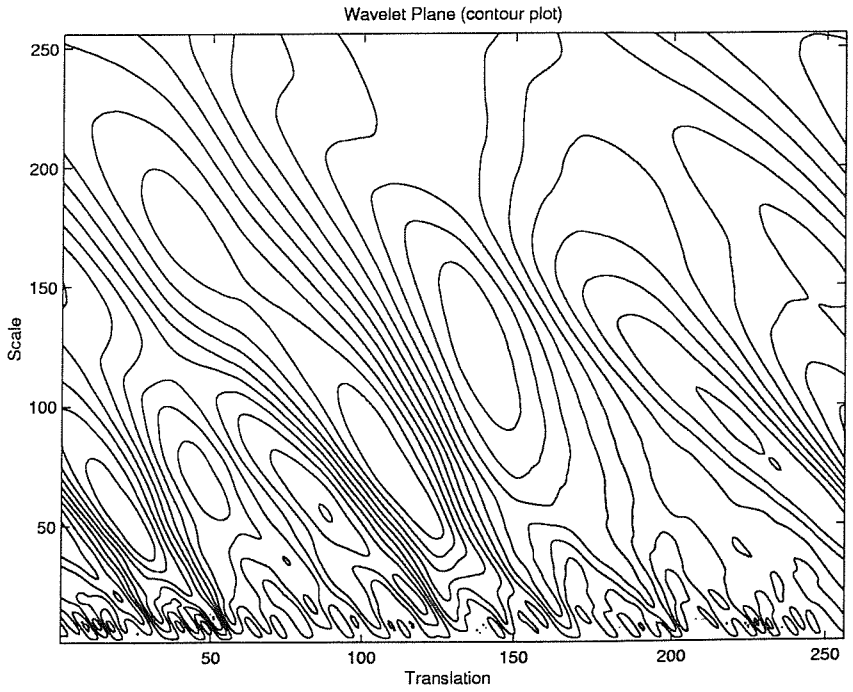

Figure 30: Wavelet decomposition, sea surface

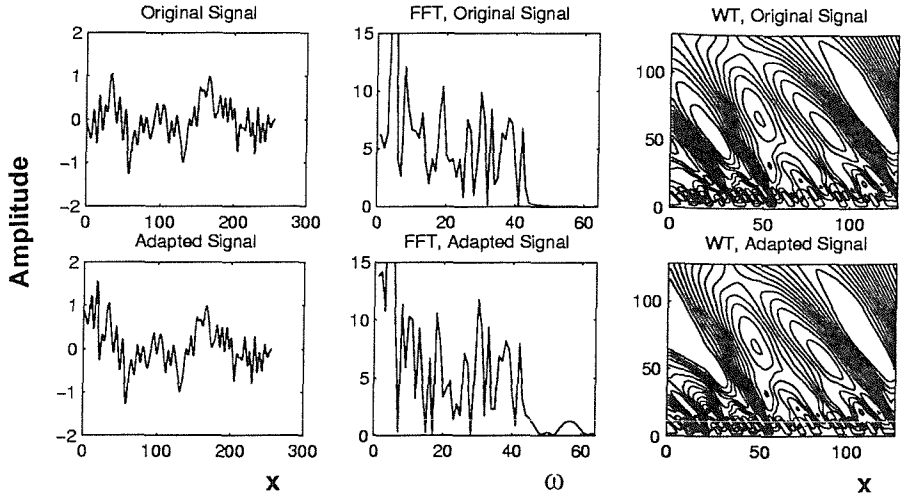

Figure 31: Wavelet FFT comparison

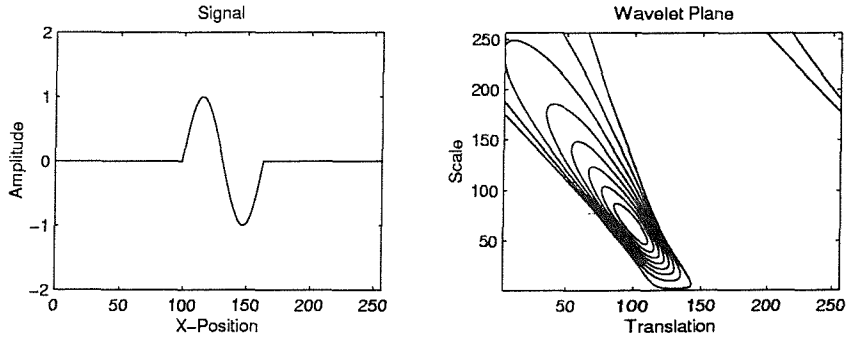

Figure 32: Wavelet decomposition, single wave component

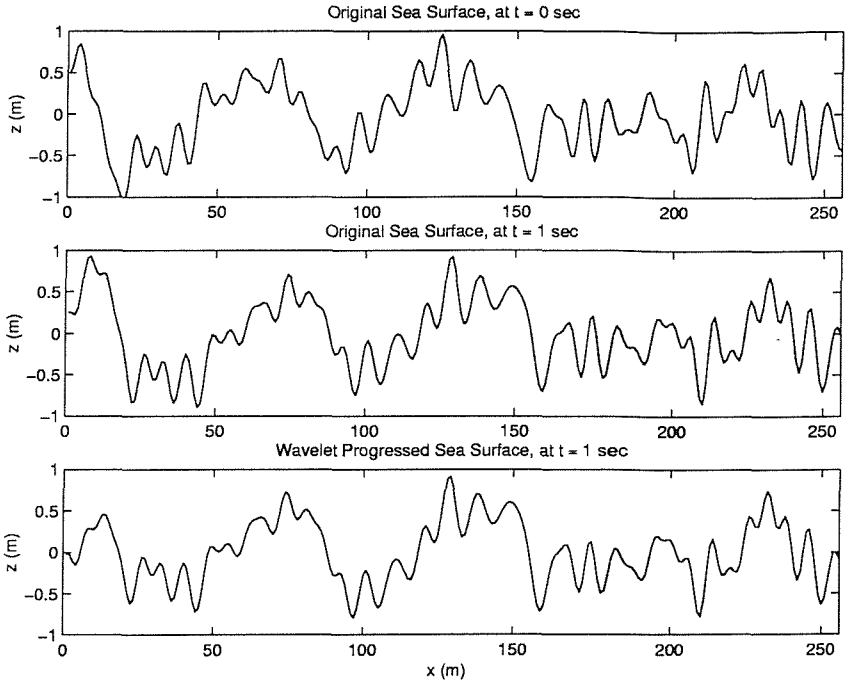

Figure 33: Wavelet progression, t = 1 sec

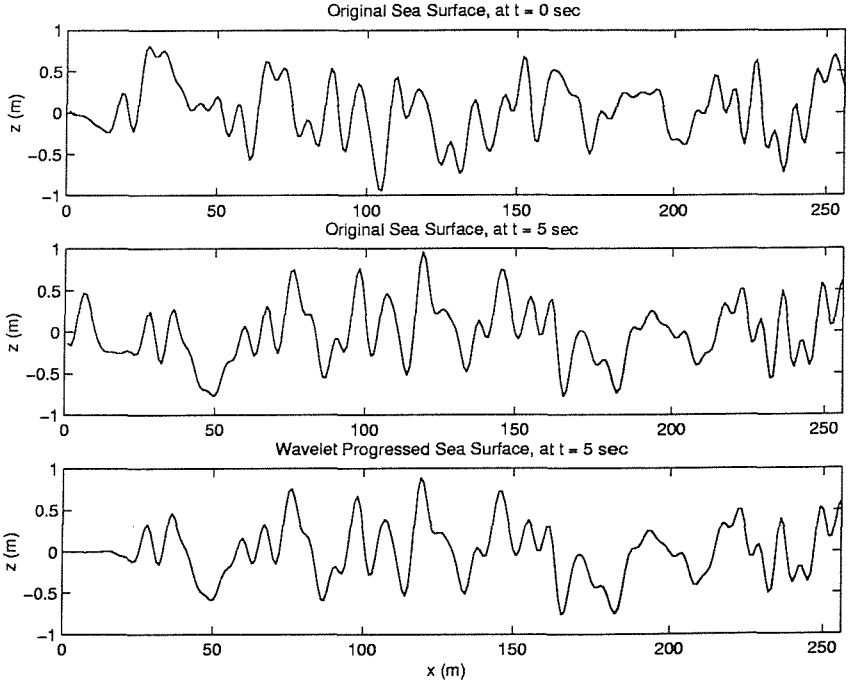

Figure 34: Wavelet progression, t = 5 sec

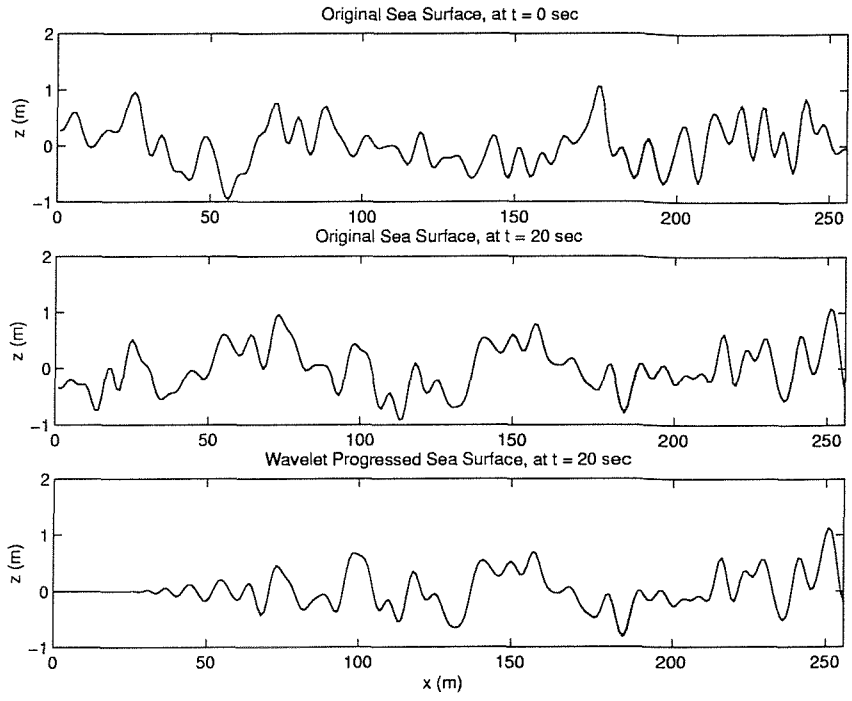

Figure 35: Wavelet progression, t = 20 sec

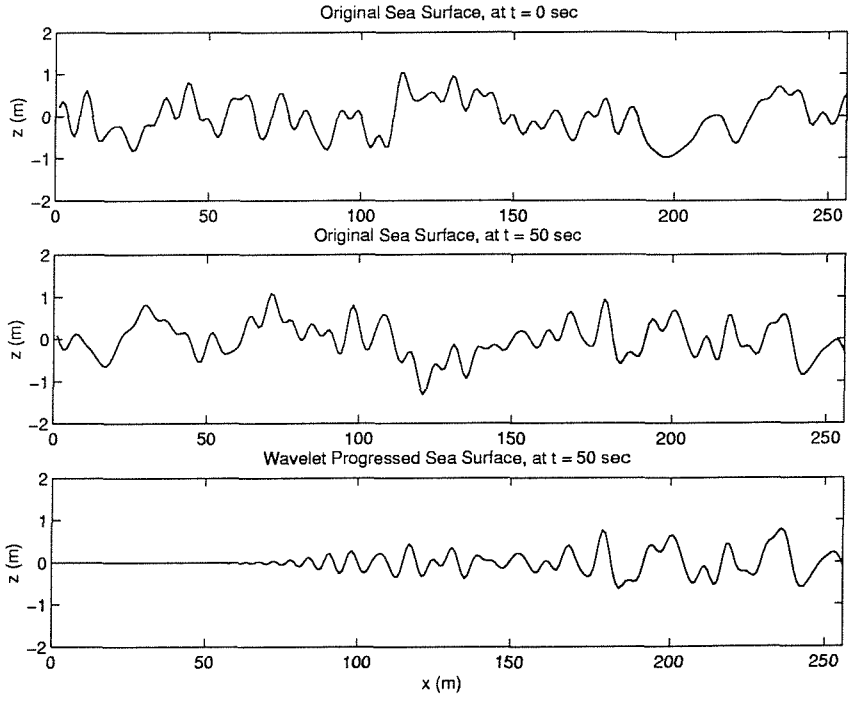

Figure 36: Wavelet progression, t = 50 sec

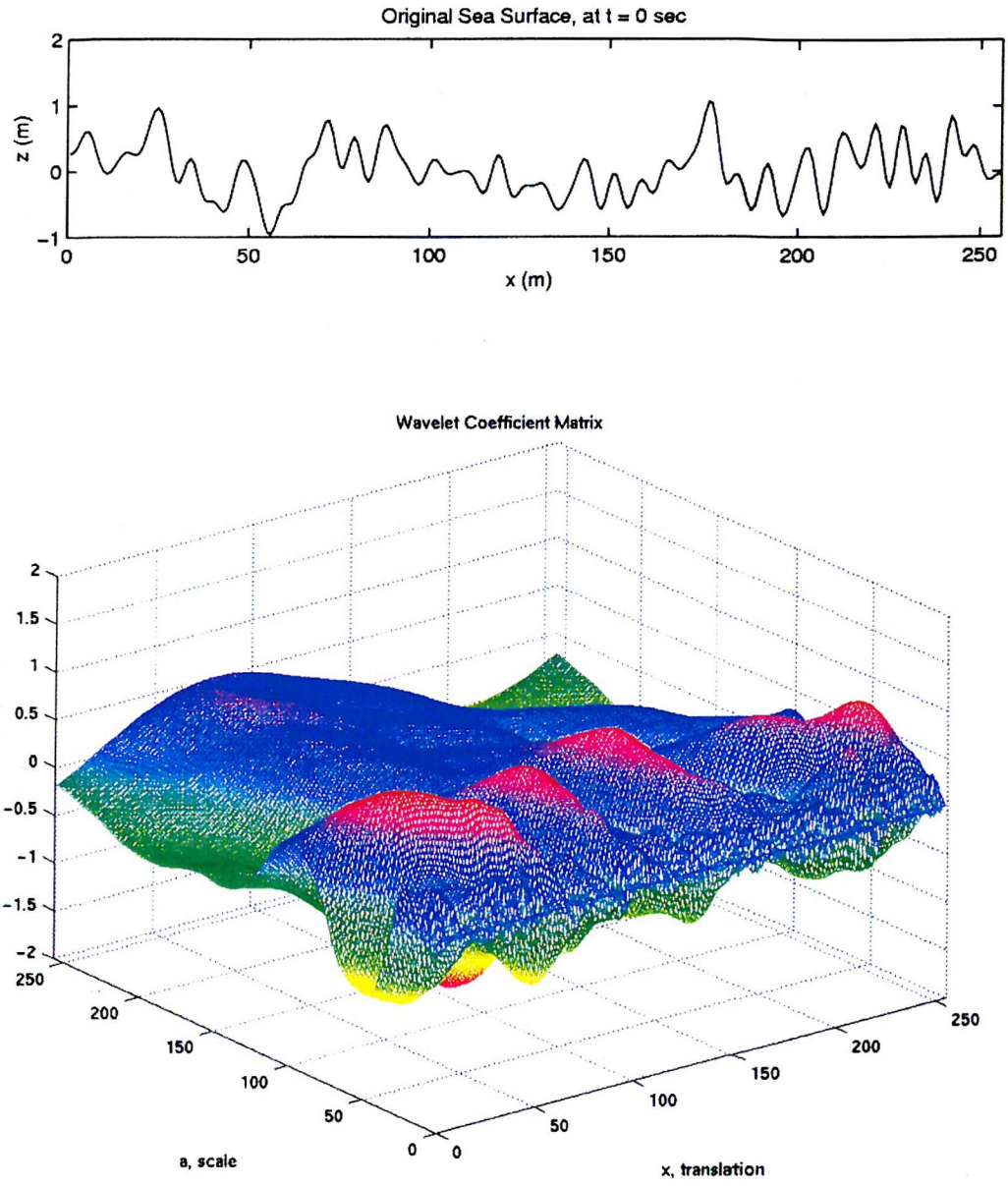

Figure 37: Wavelet transform map

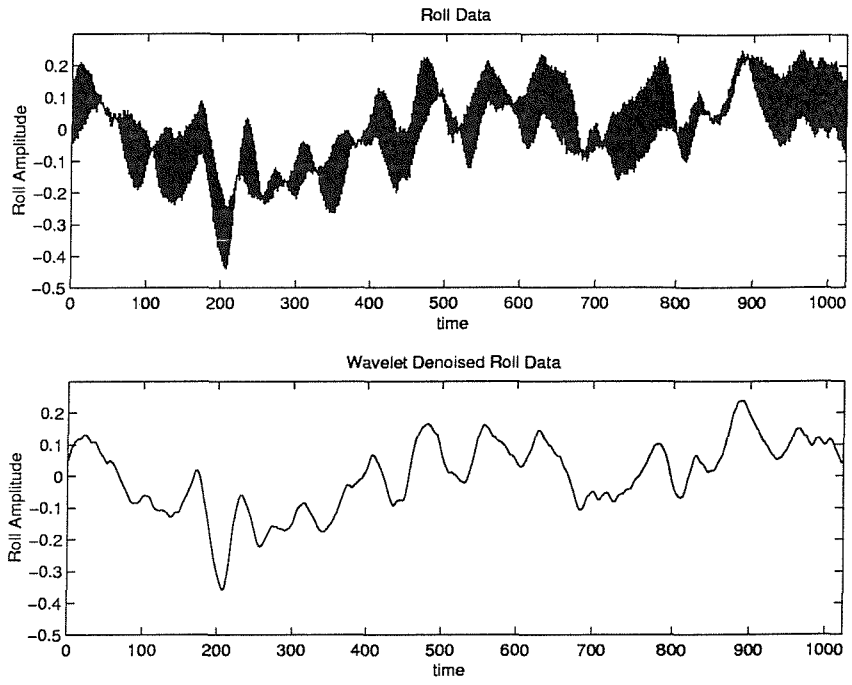

Figure 38: Wavelet denoising

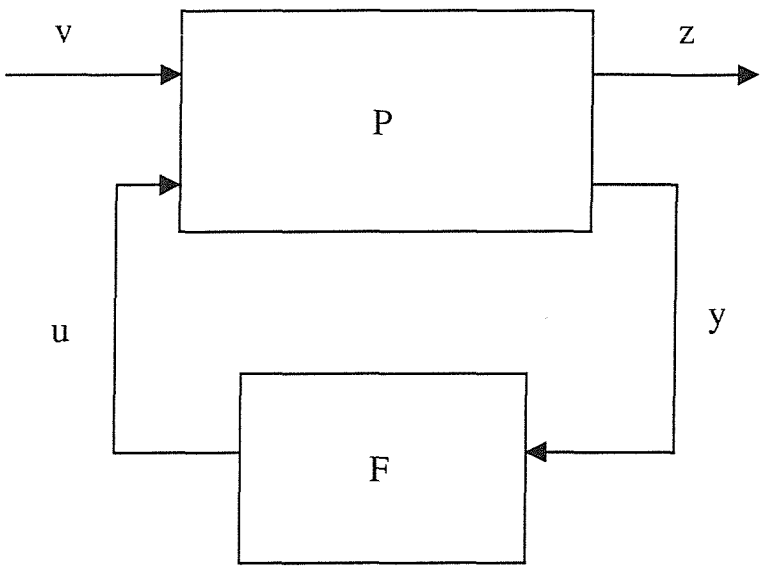

Figure 39: Representation of H_∞ Control Problem

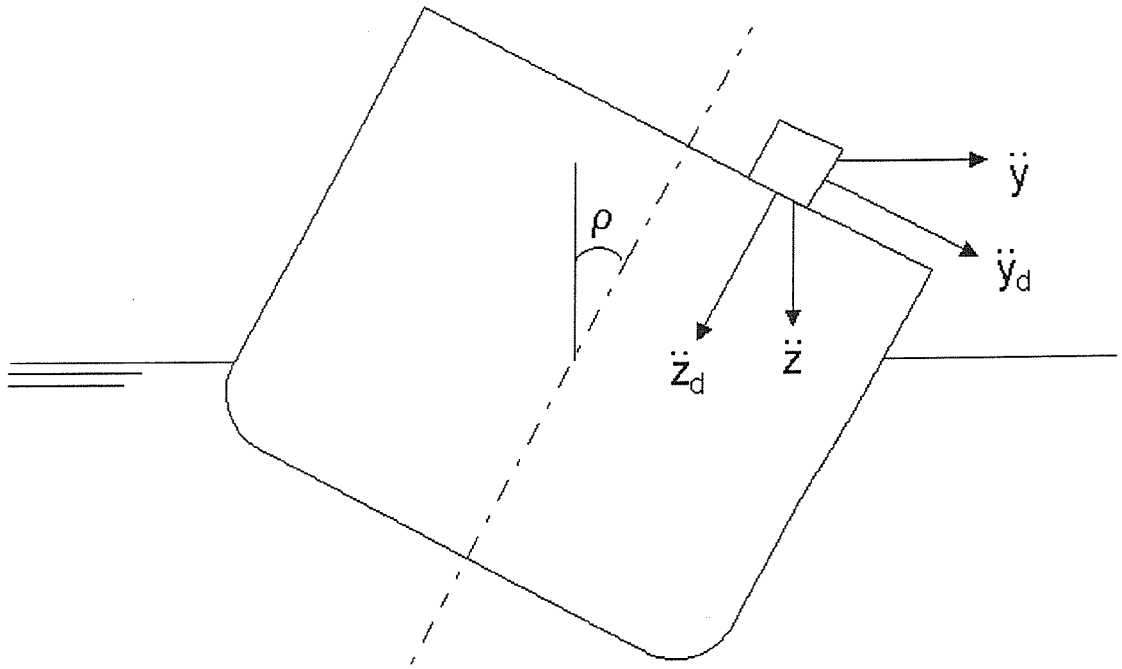

Figure 40: Representation of accelerations

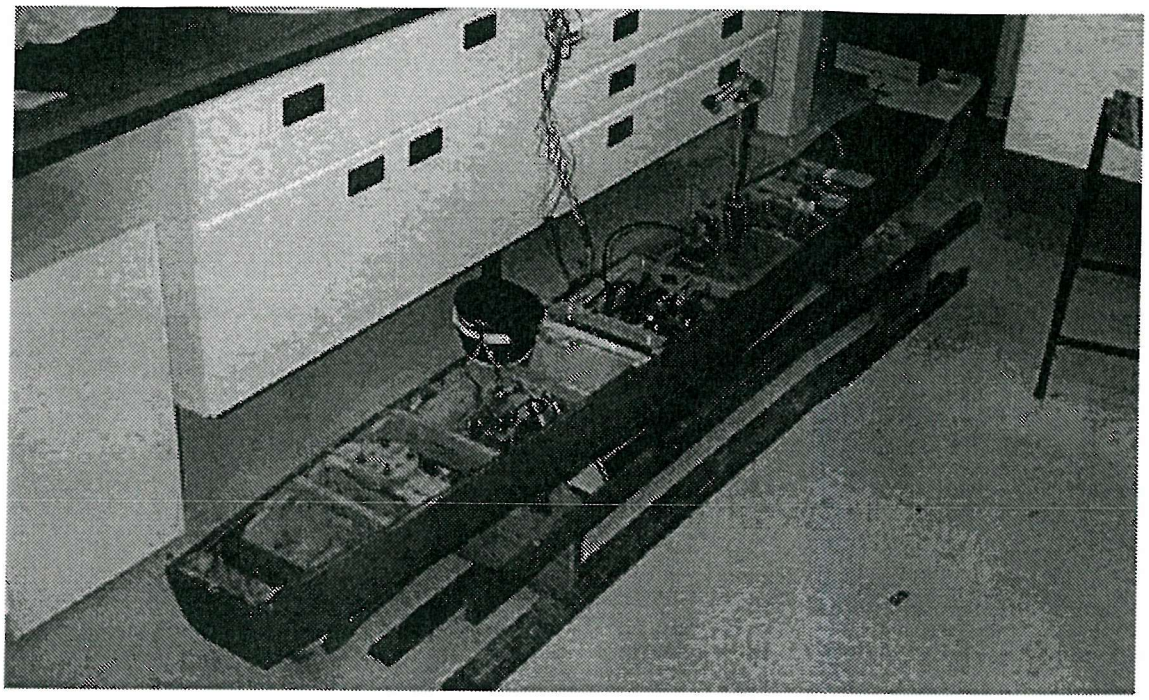

Figure 41: Photograph of Frigate Model

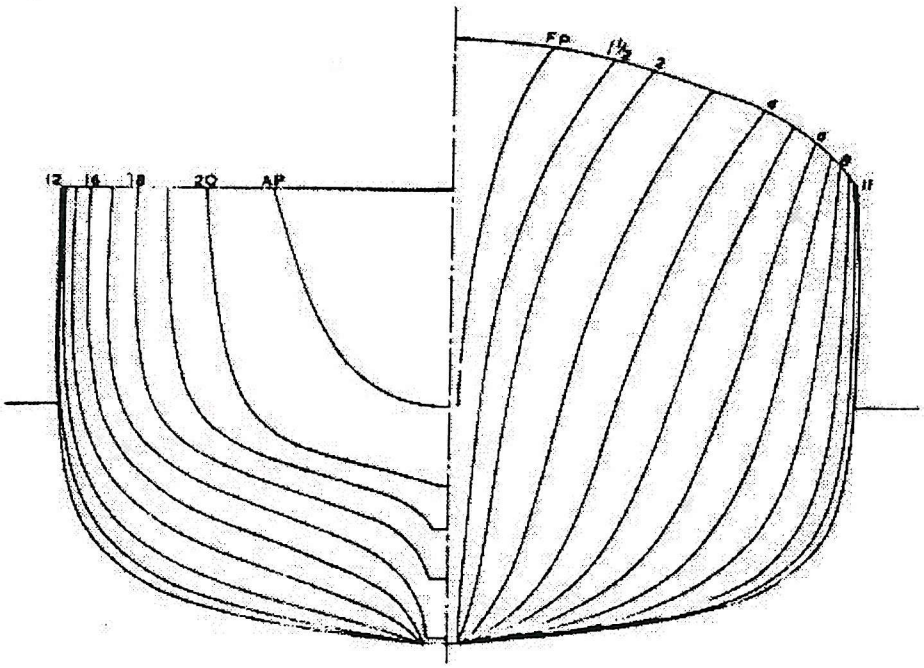

Figure 42: Body Plan of Frigate

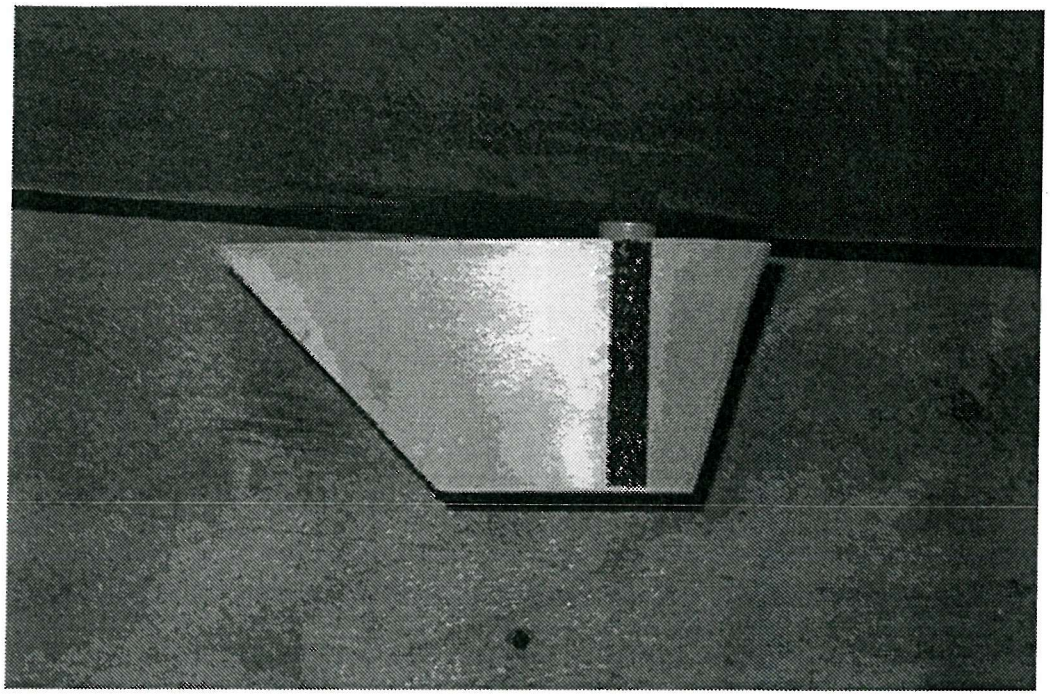

Figure 43: Photograph of a Large Stabilising Fin

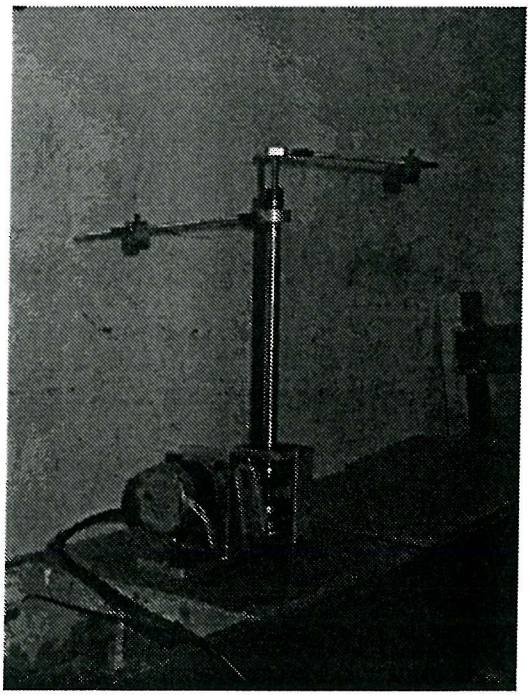

Figure 44: Photograph of the Contra-Rotating Weight Mechanism

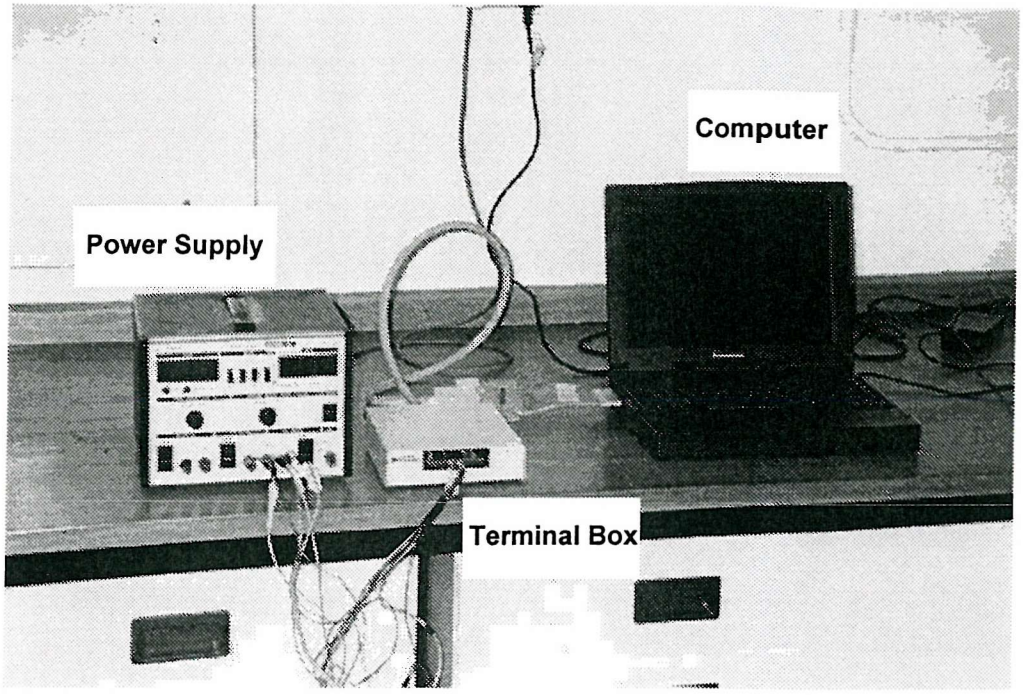

Figure 45: Photograph of the Hardware

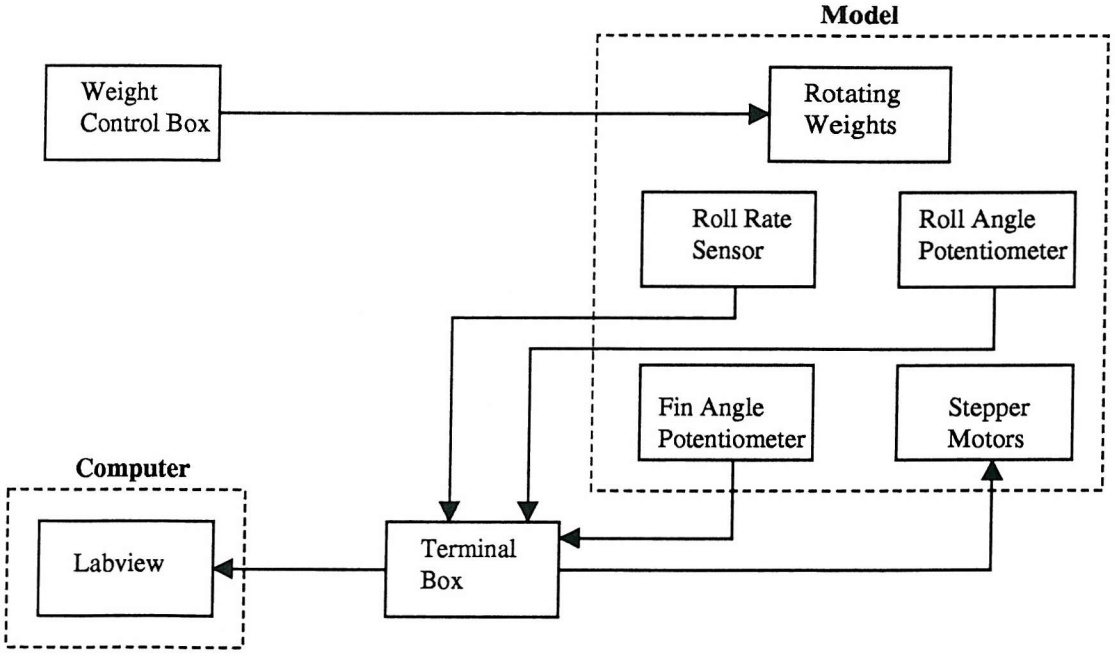

Figure 46: Schematic representation of experimental set up

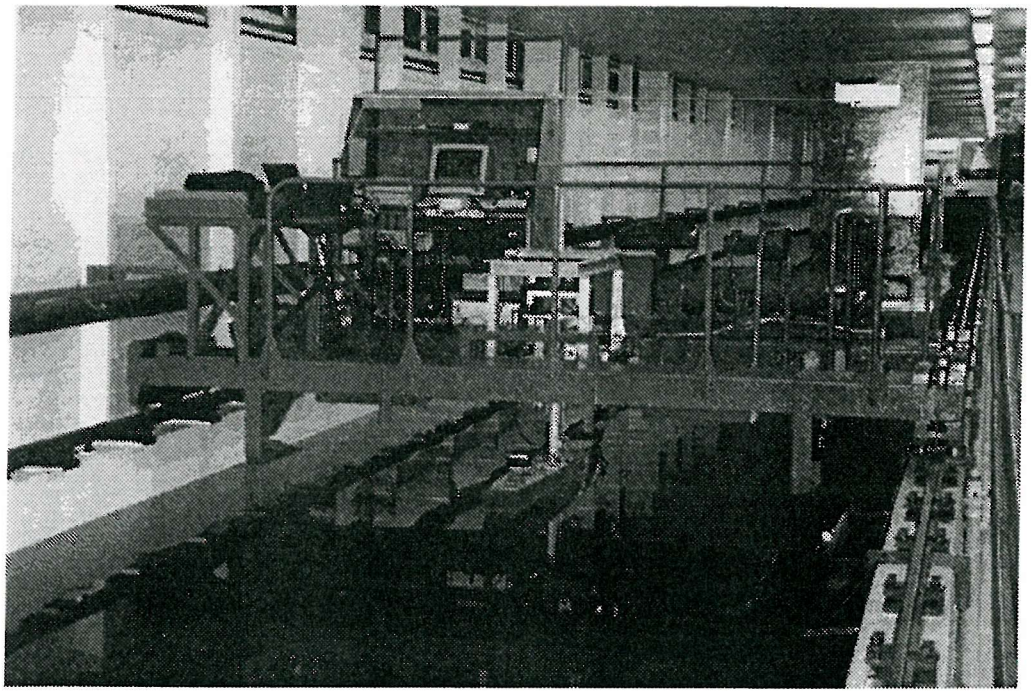

Figure 47: Photograph of the Towing Tank Facility

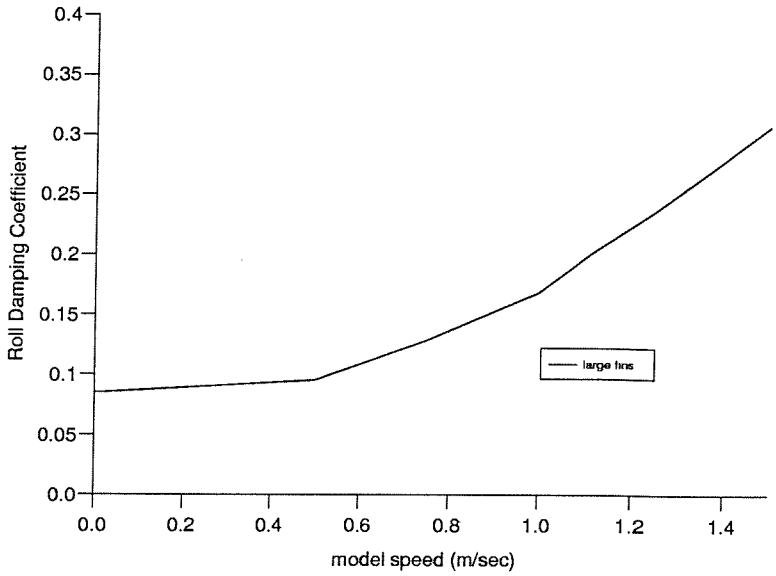

Figure 48: Roll damping coefficients, model with large fins

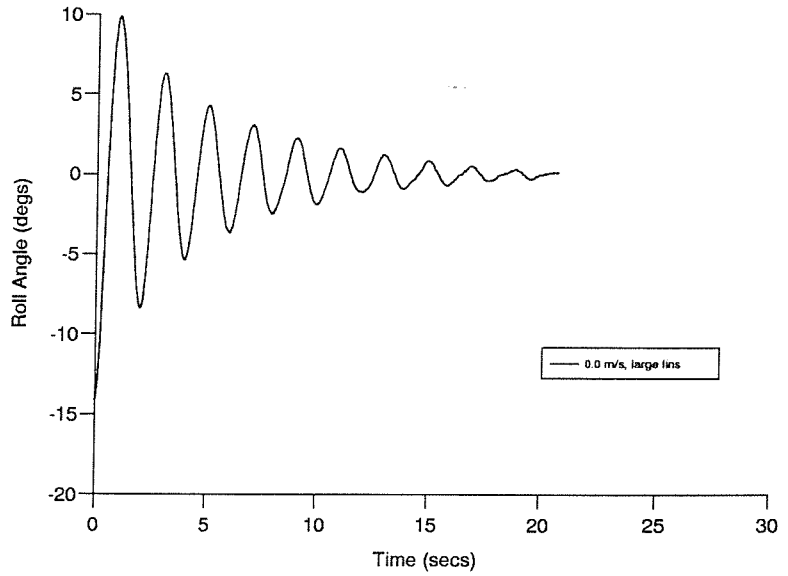

Figure 49: Roll decay curve, model with large fins at 0.0 m/sec

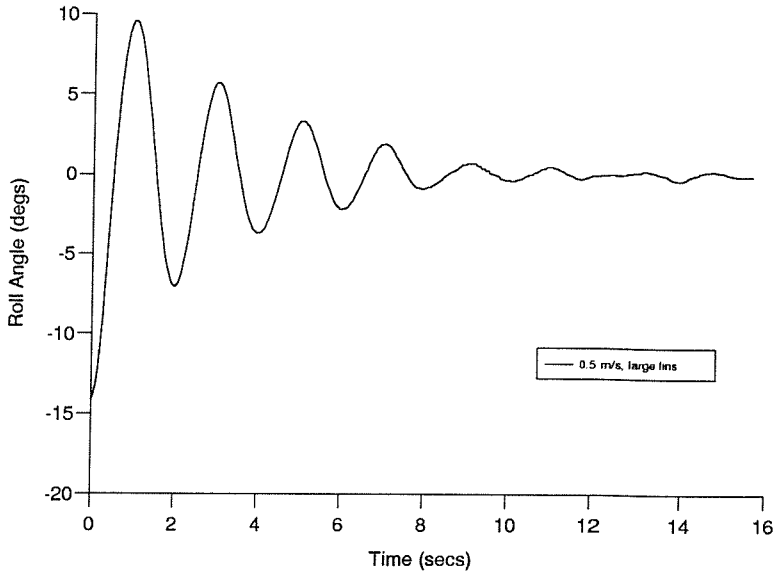

Figure 50: Roll decay curve, model with large fins at 0.5 m/sec

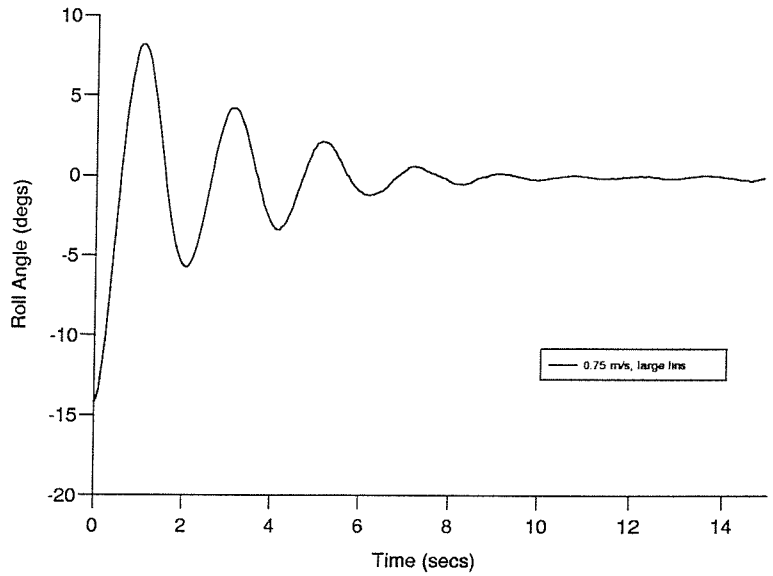

Figure 51: Roll decay curve, model with large fins at 0.75 m/sec

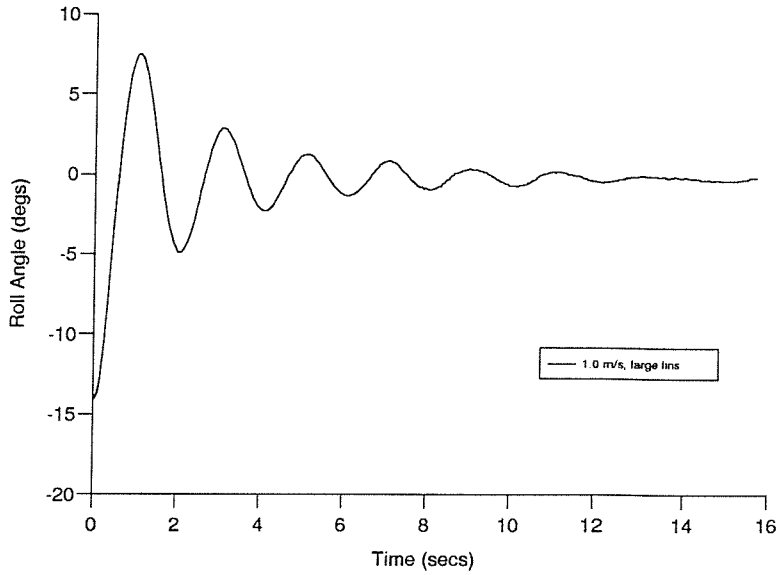

Figure 52: Roll decay curve, model with large fins at 1.0 m/sec

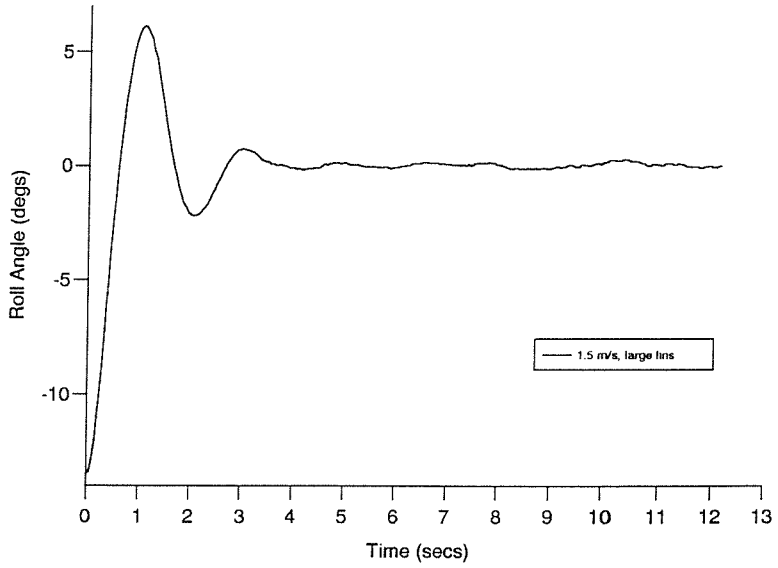

Figure 53: Roll decay curve, model with large fins at 1.5 m/sec

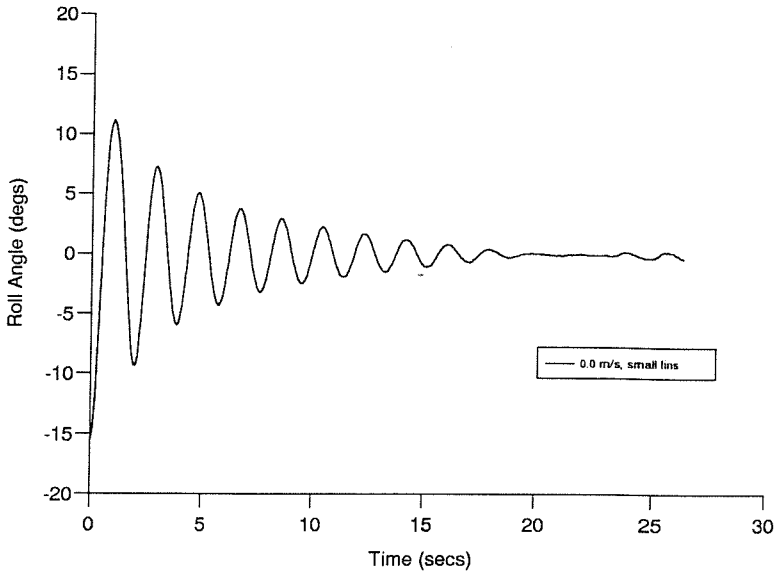

Figure 54: Roll decay curve, model with small fins at 0.0 m/sec

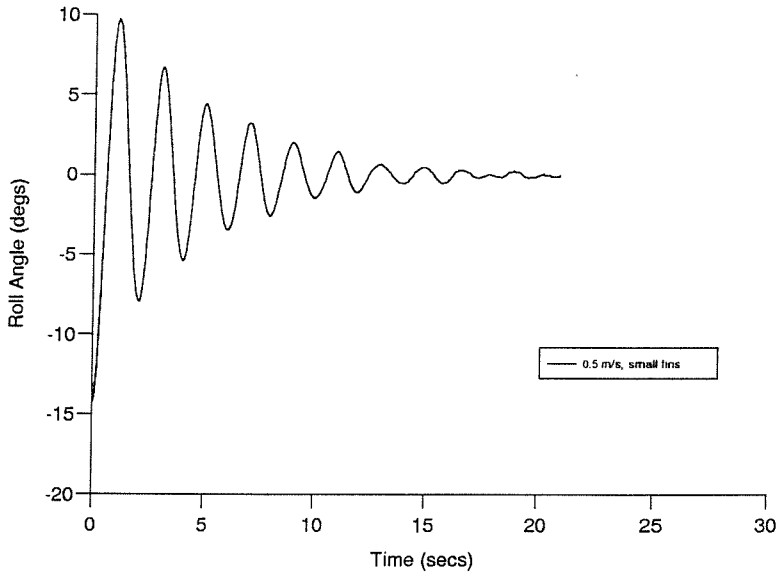

Figure 55: Roll decay curve, model with small fins at 0.5 m/sec

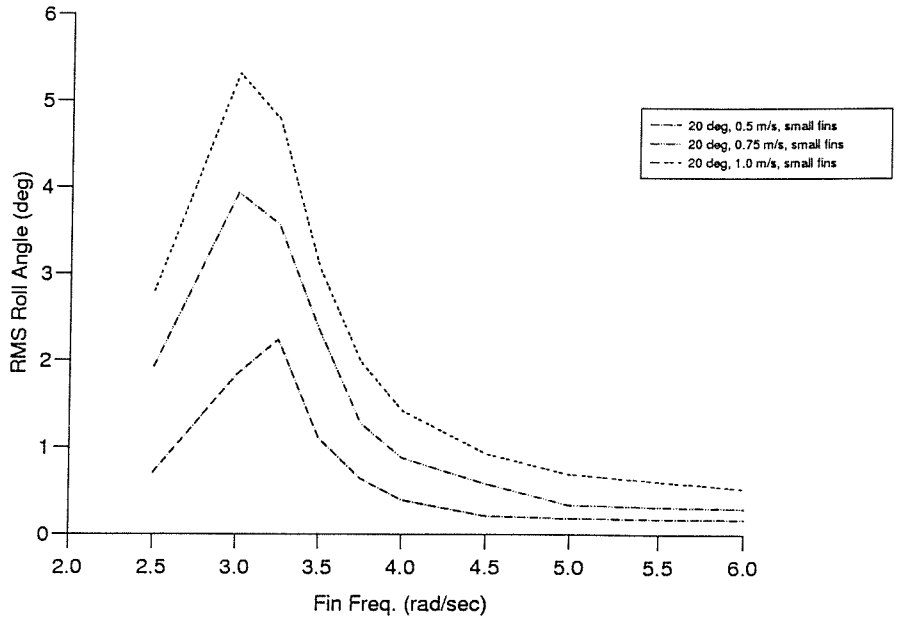

Figure 56: RMS roll angle, sinusoidal fin movement at various speeds, small fins

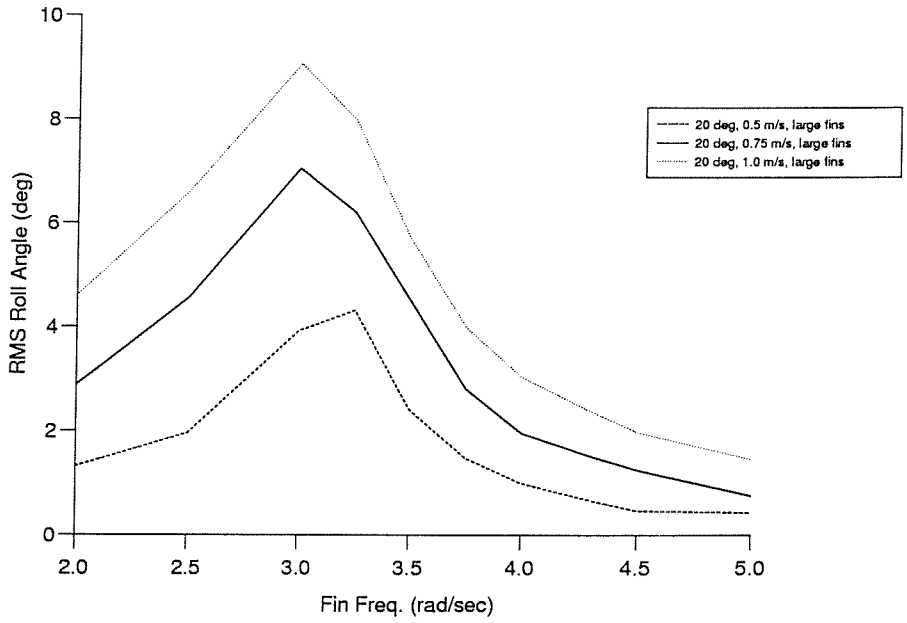

Figure 57: RMS roll angle, sinusoidal fin movement at various speeds, large fins

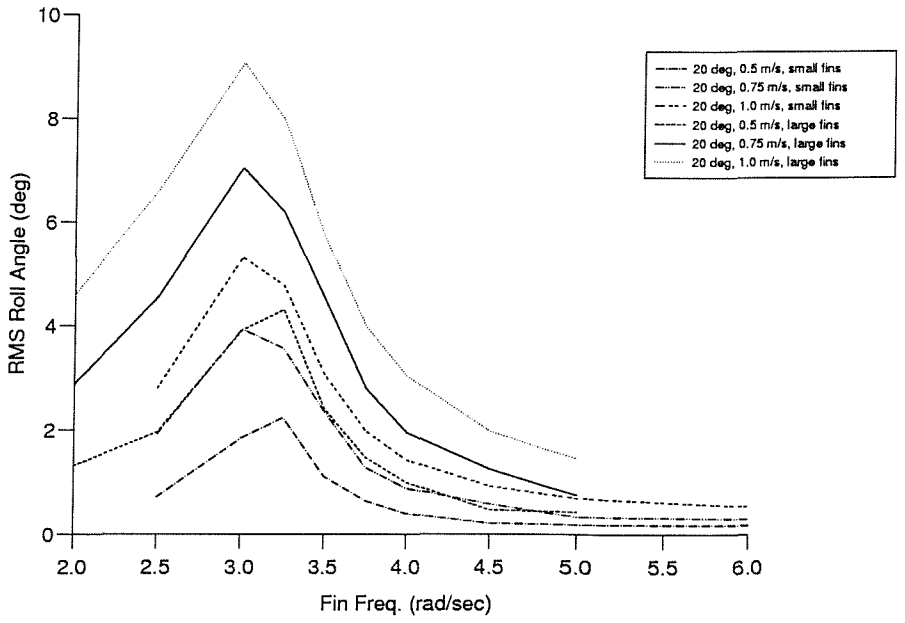

Figure 58: RMS roll angle, sinusoidal fin movement at various speeds

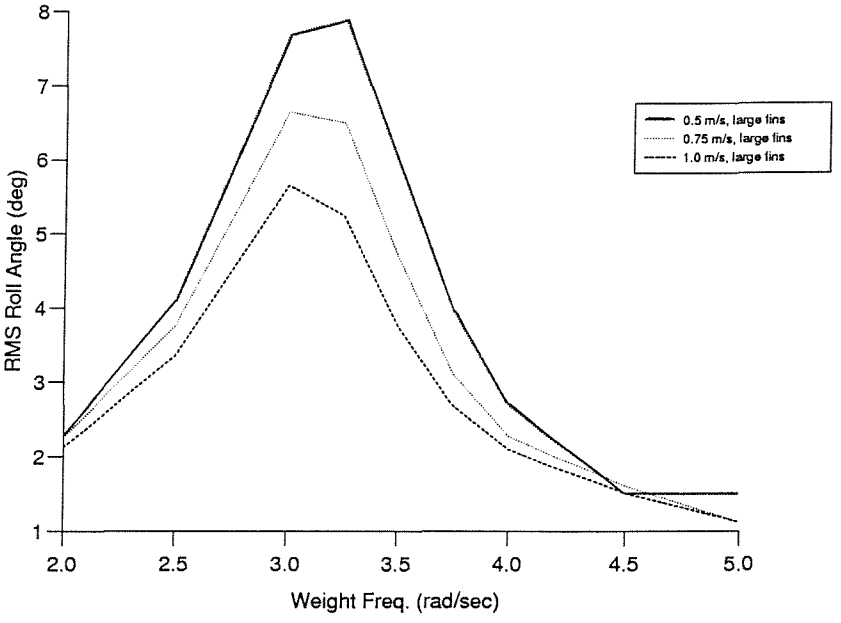

Figure 59: RMS roll angle, rotated weights at various model speeds

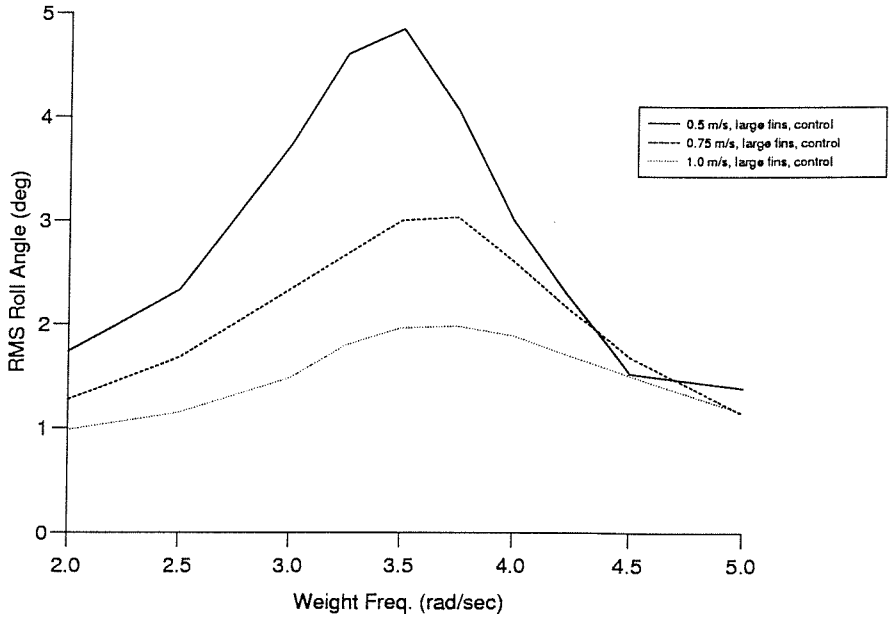

Figure 60: RMS roll angle, PID control at various speeds

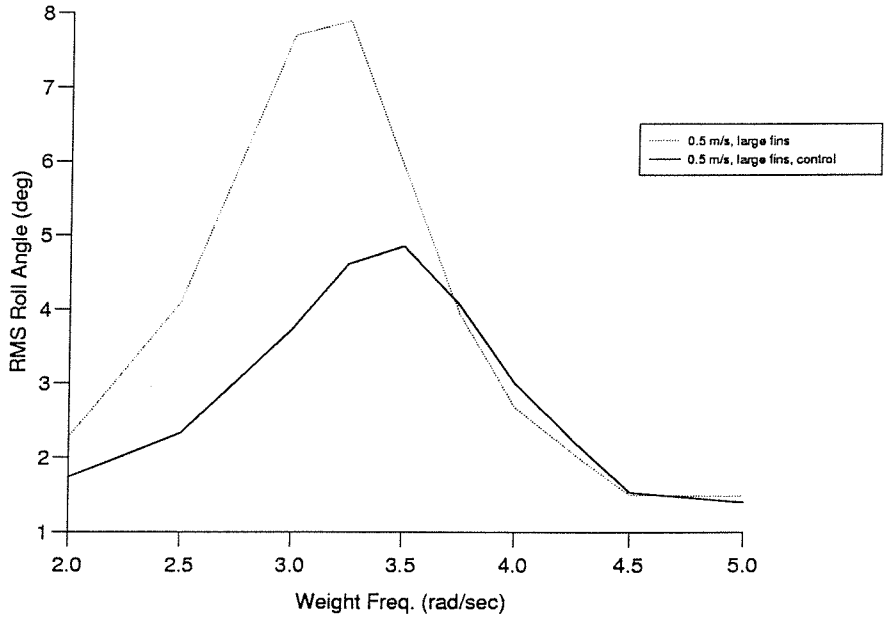

Figure 61: RMS roll angle, PID control comparison, 0.5 m/sec

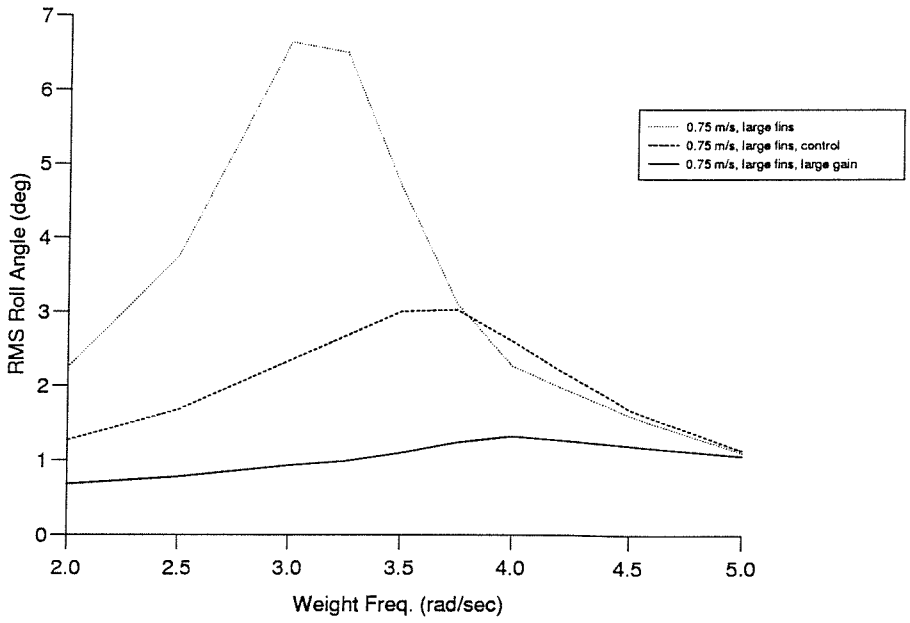

Figure 62: RMS roll angle, PID control comparison, 0.75 m/sec

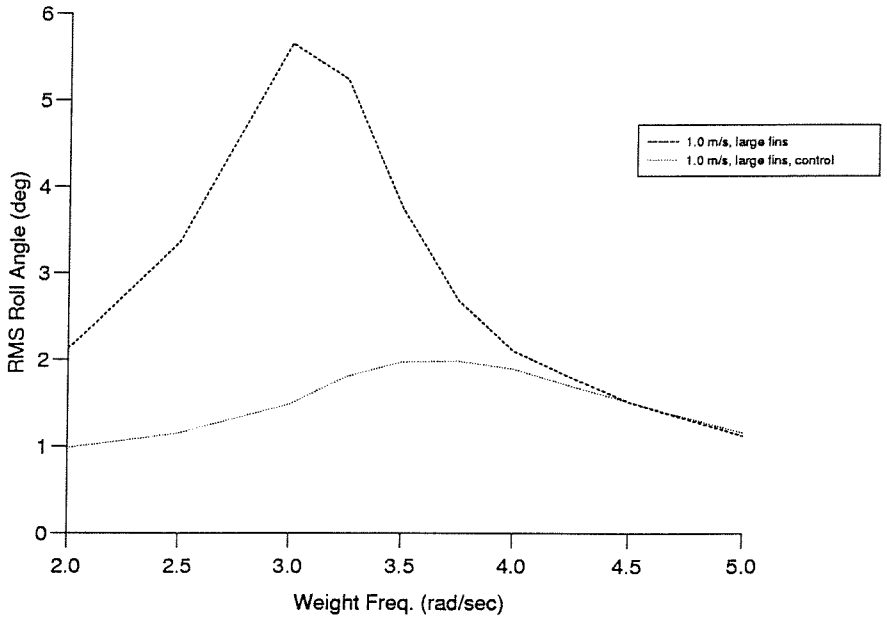

Figure 63: RMS roll angle, PID control comparison, 1.0 m/sec

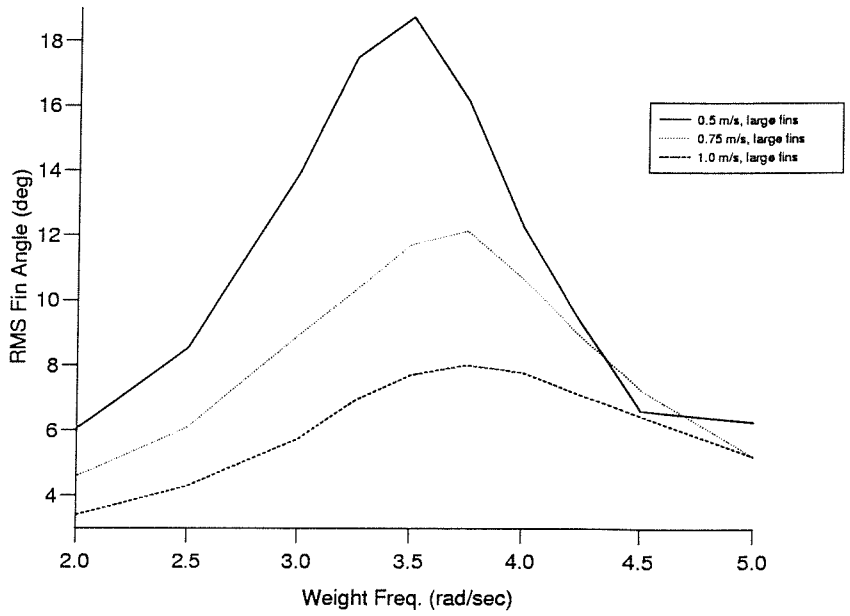

Figure 64: RMS fin angle, PID control at various speeds

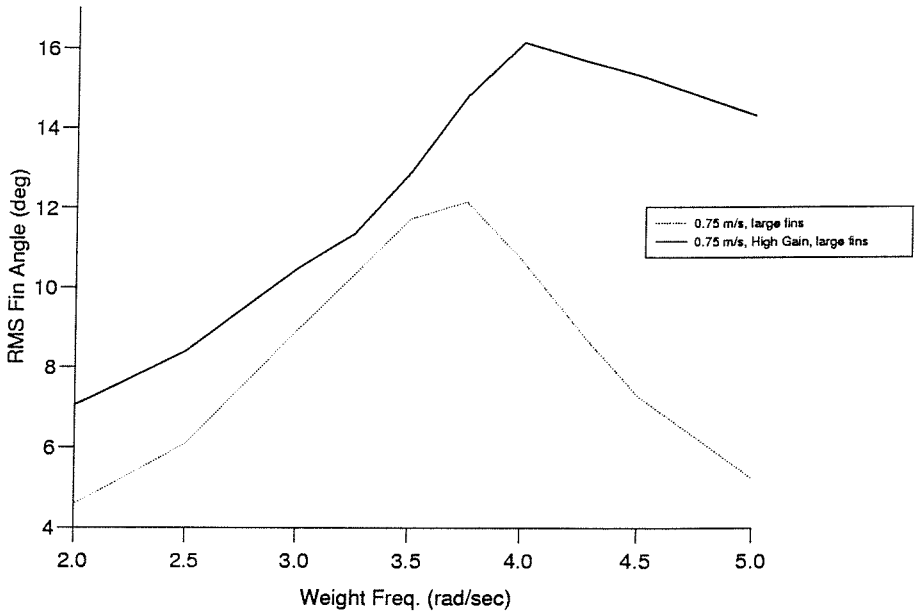

Figure 65: RMS fin angle, low versus high gain, 0.75 m/sec

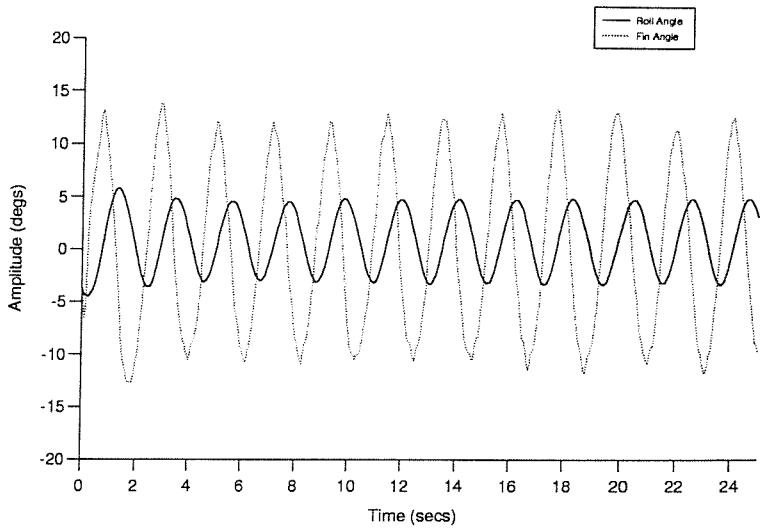

Figure 66: Typical H_∞ control roll and fin response

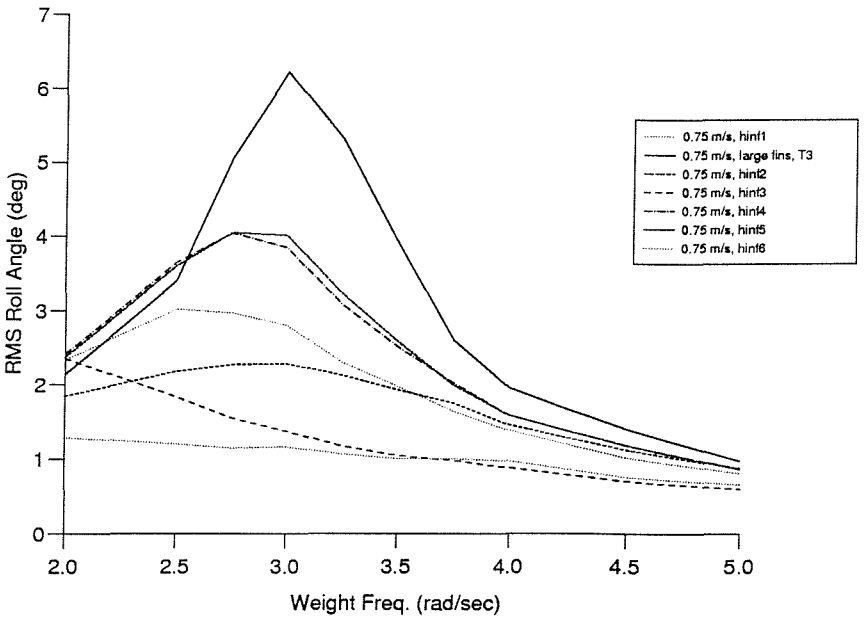

Figure 67: RMS roll angle, H_∞ control, 0.75 m/sec

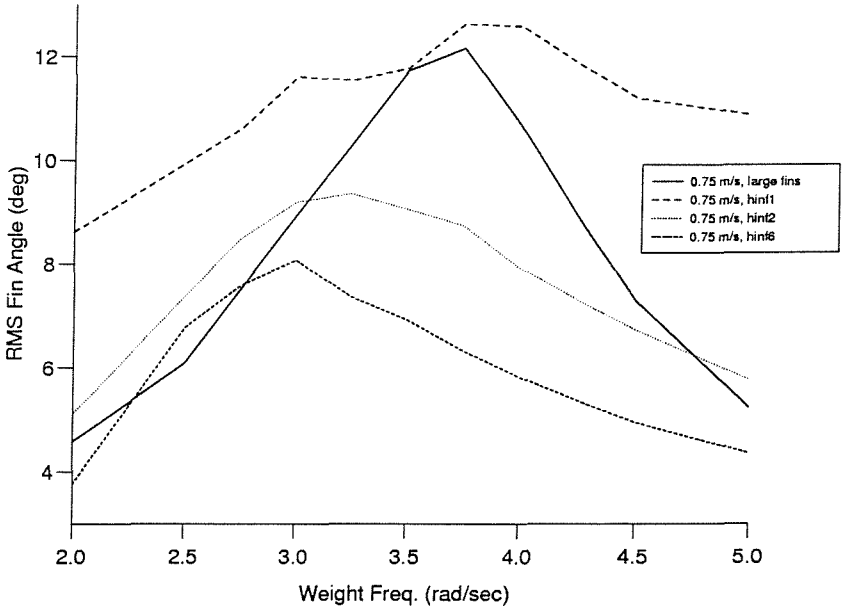

Figure 68: RMS fin angle, control comparison, 0.75 m/sec

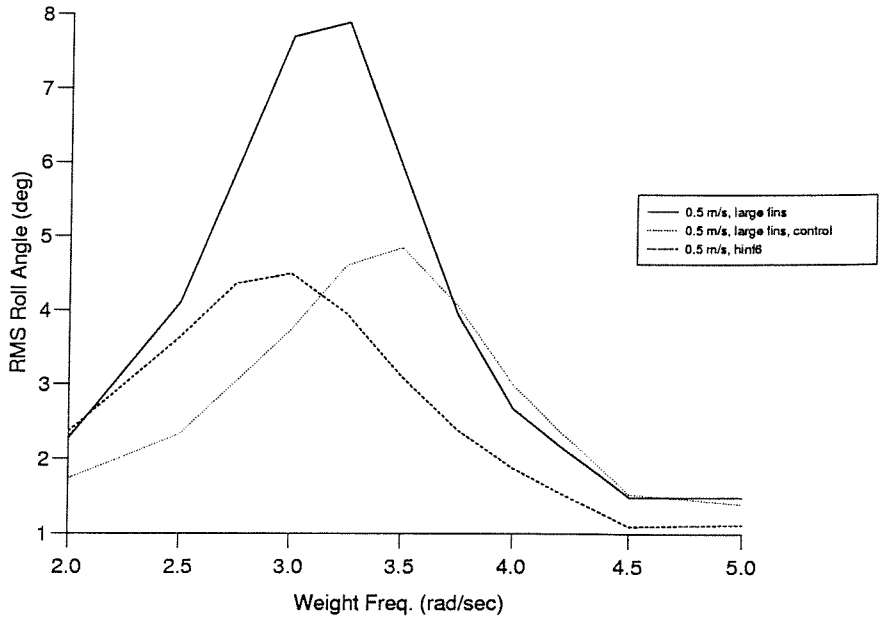

Figure 69: RMS roll angle, control comparison, 0.50 m/sec

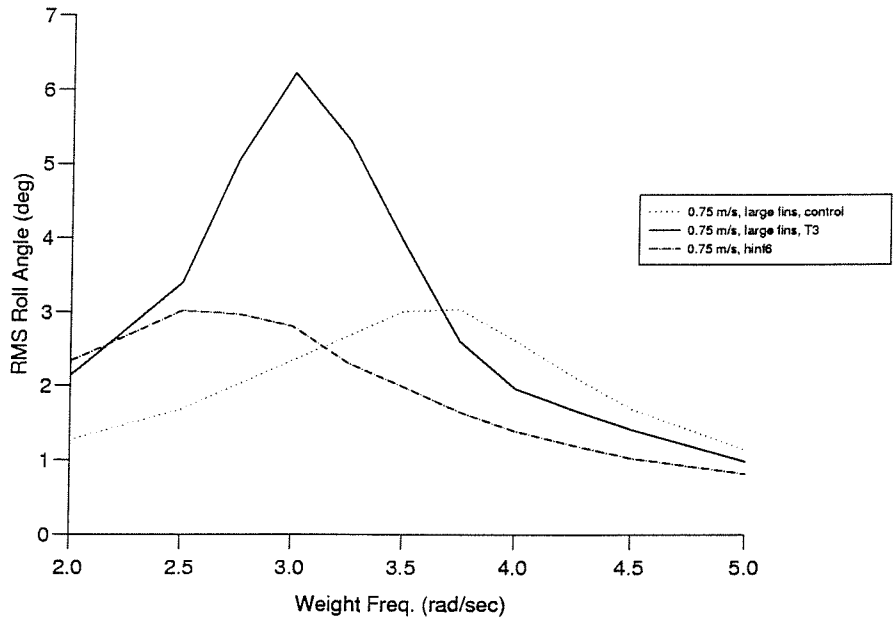

Figure 70: RMS roll angle, control comparison, 0.75 m/sec

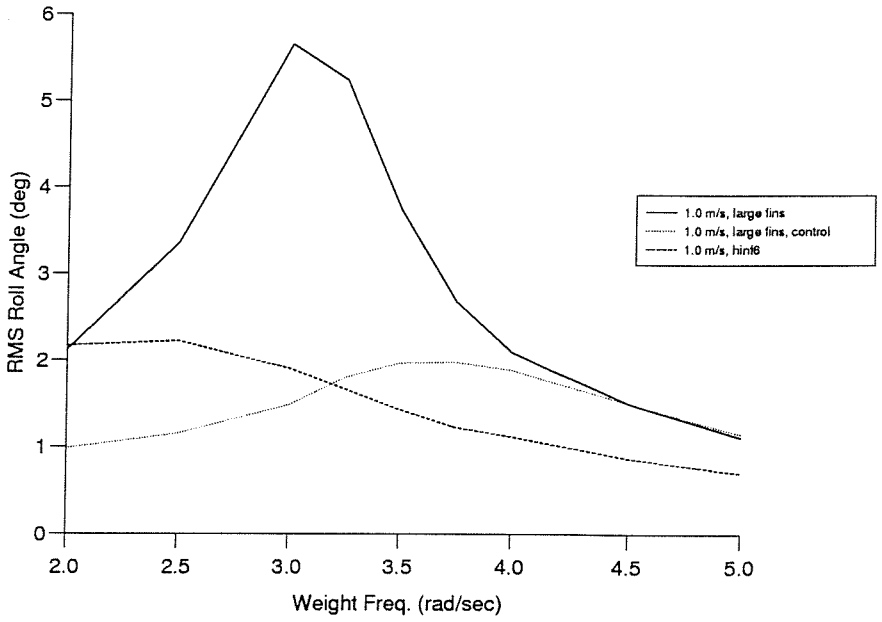

Figure 71: RMS roll angle, control comparison, 1.00 m/sec

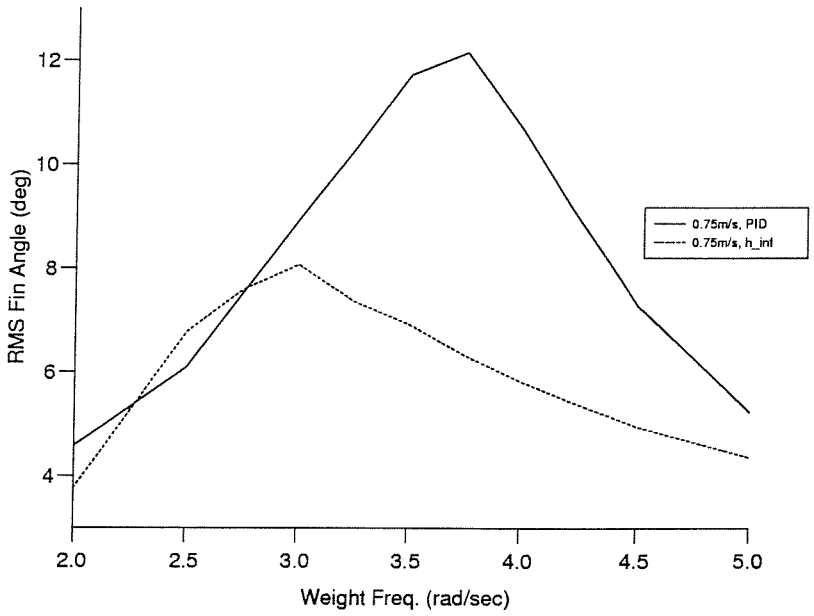

Figure 72: RMS fin angle, control comparison, 0.75 m/sec

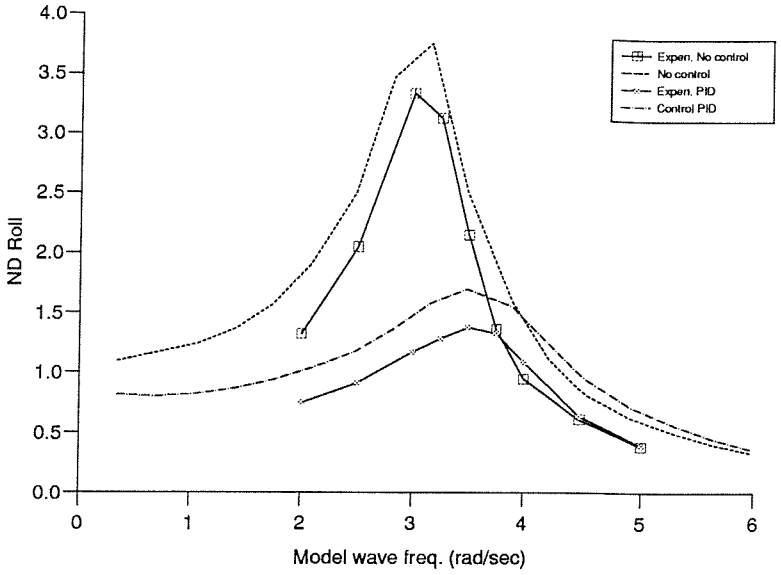

Figure 73: RMS roll angle, PID, Experiment v Software, 0.75 m/sec

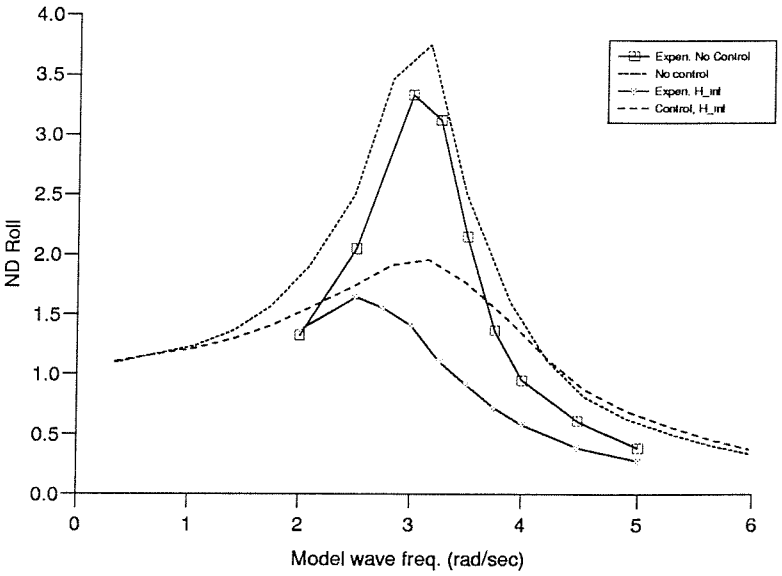

Figure 74: RMS roll angle, H_∞, Experiment v Software, 0.75 m/sec

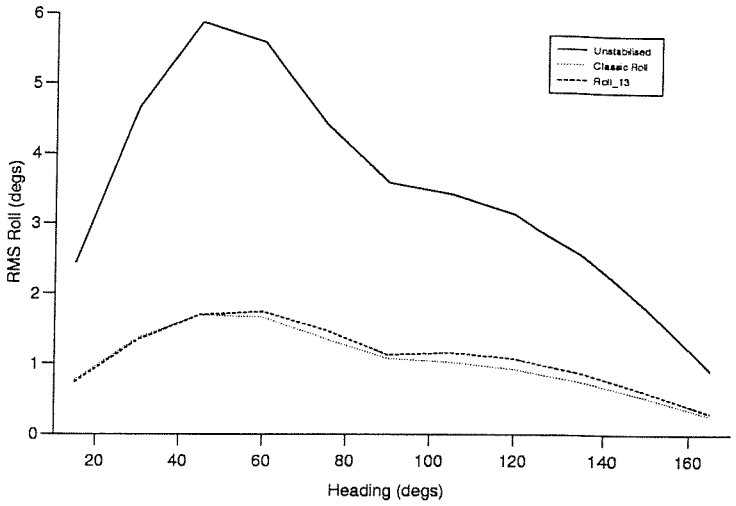

Figure 75: RMS Roll, Overall Controller Performance, spectra 1

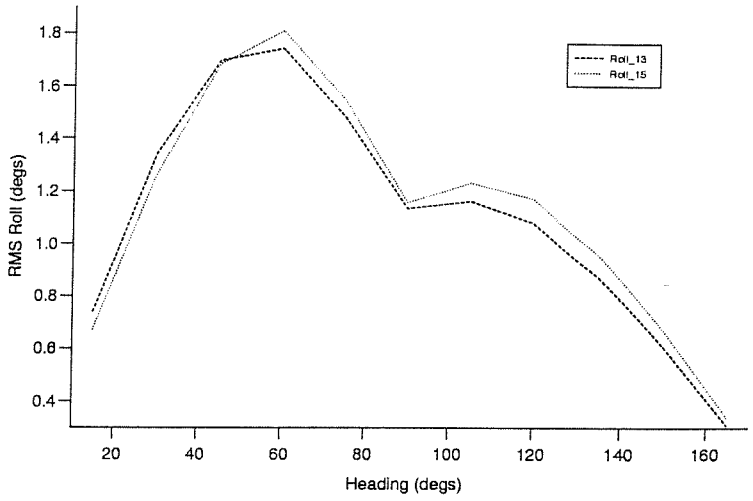

Figure 76: RMS Roll, Sub/Optimality, spectra 1

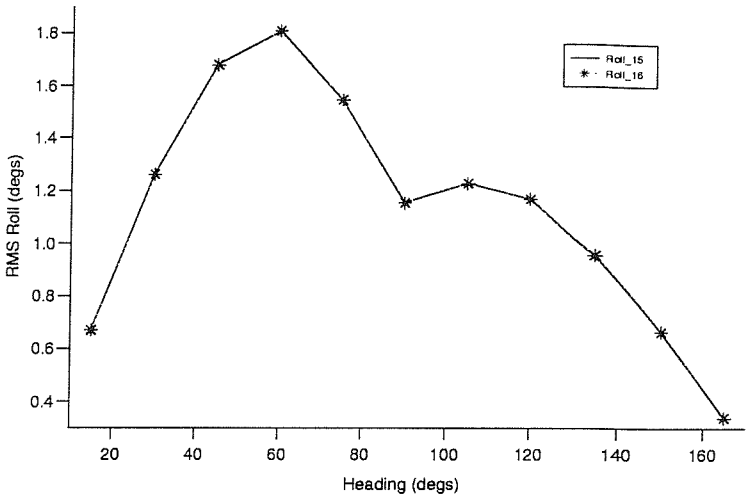

Figure 77: RMS Roll, Effect of Controller Order, spectra 1

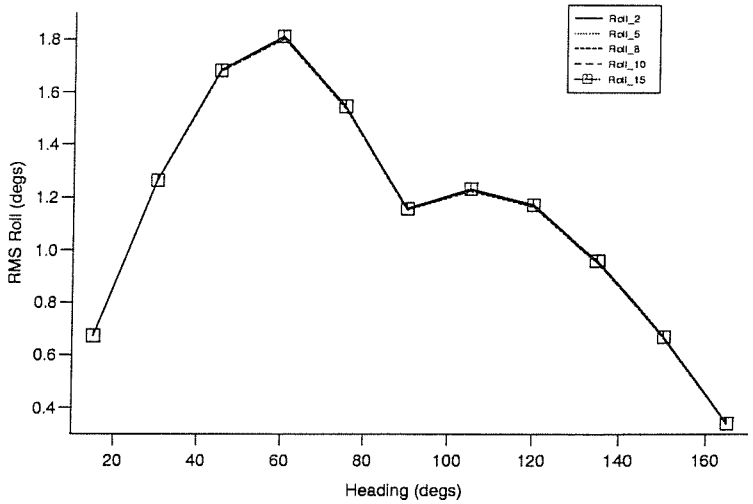

Figure 78: RMS Roll, Weighting Variation, spectra 1

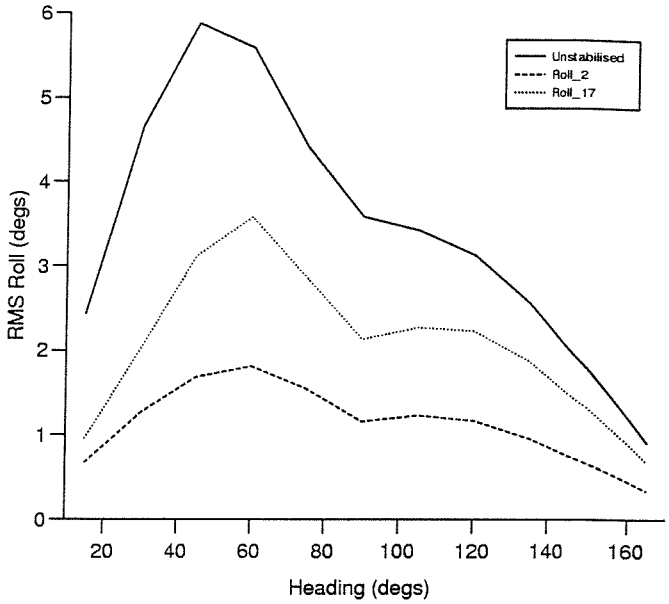

Figure 79: RMS Roll, Weighting Variation, spectra 1

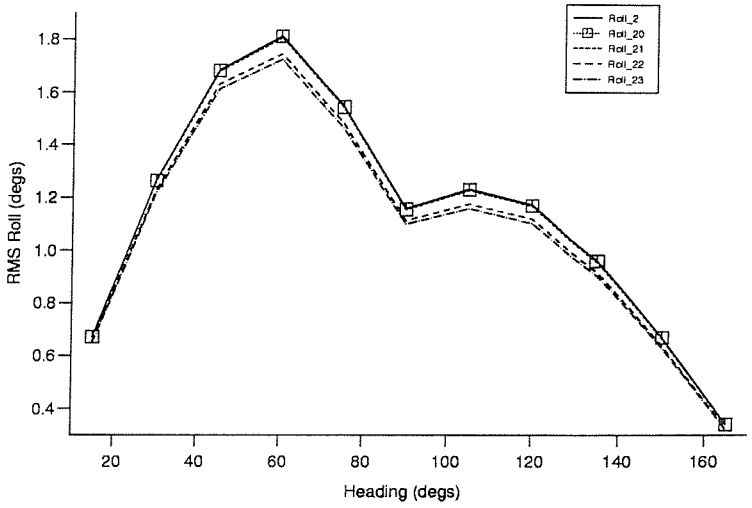

Figure 80: RMS Roll, Weighting Variation, spectra 1

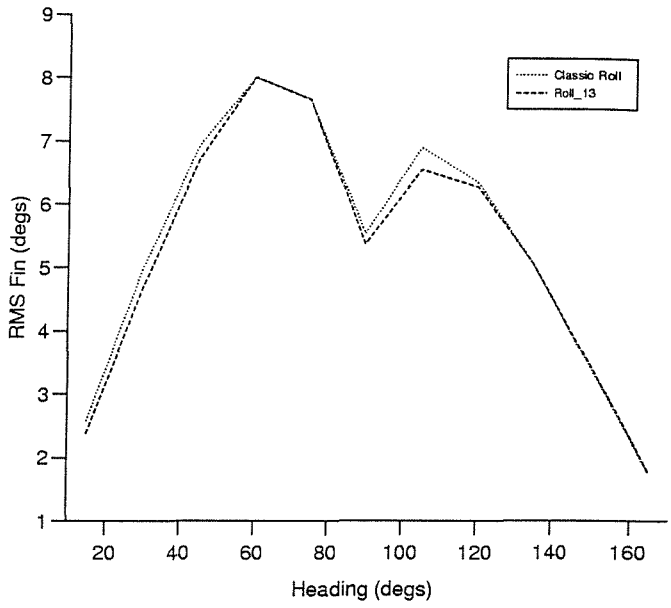

Figure 81: RMS Fin, Overall Controller Performance, spectra 1

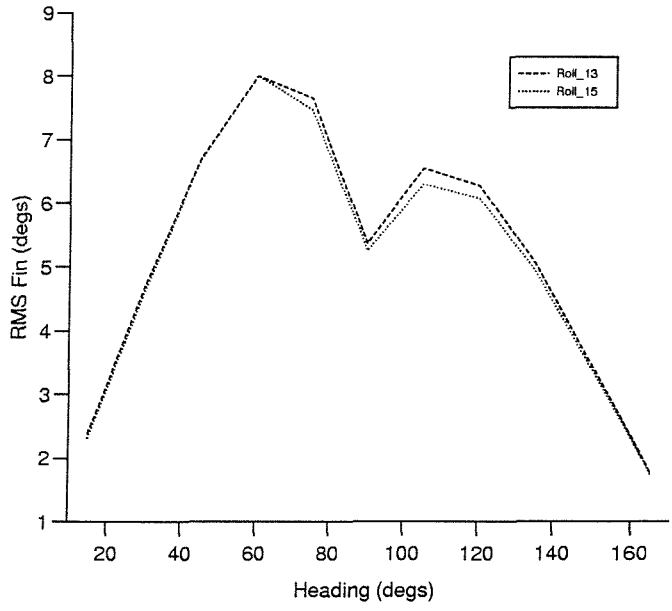

Figure 82: RMS Fin, Sub/Optimality, spectra 1

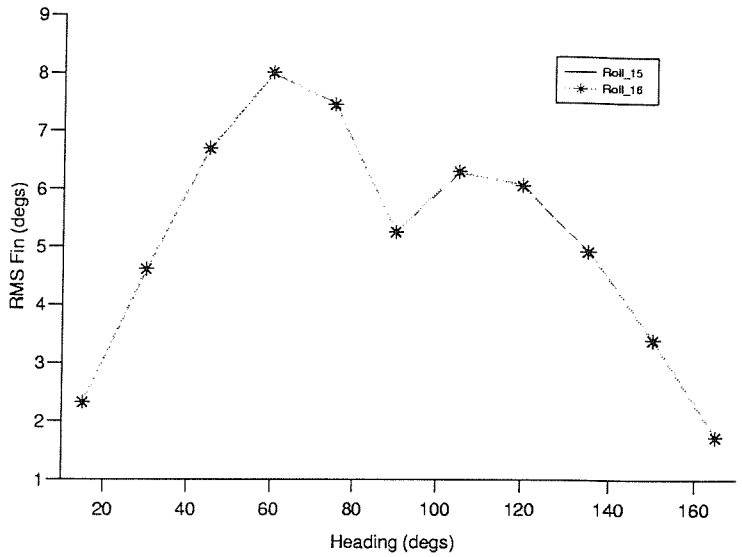

Figure 83: RMS Fin, Effect of Controller Order, spectra 1

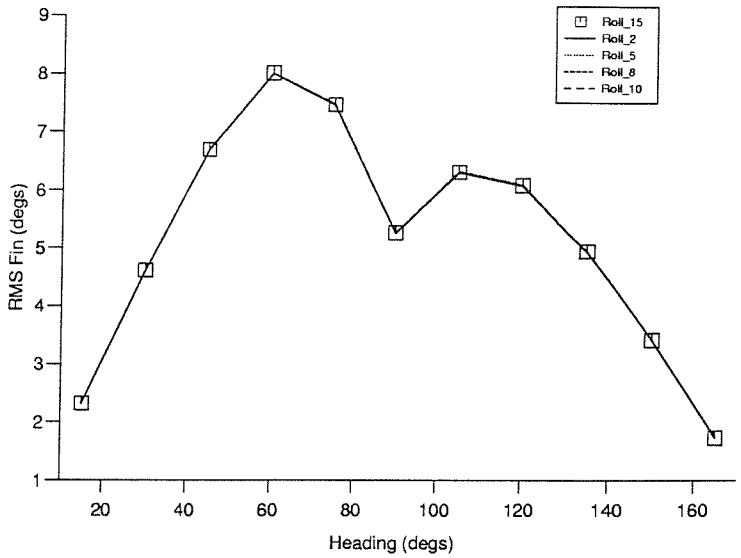

Figure 84: RMS Fin, Weighting Variation, spectra 1

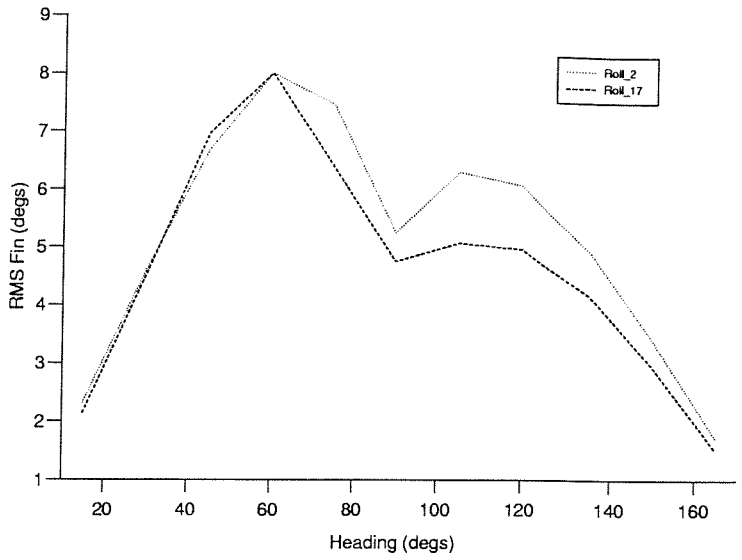

Figure 85: RMS Fin, Weighting Variation, spectra 1

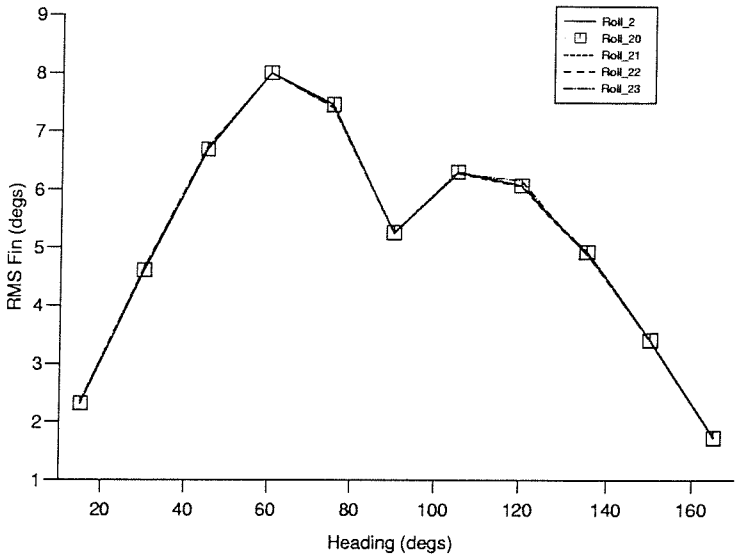

Figure 86: RMS Fin, Weighting Variation, spectra 1

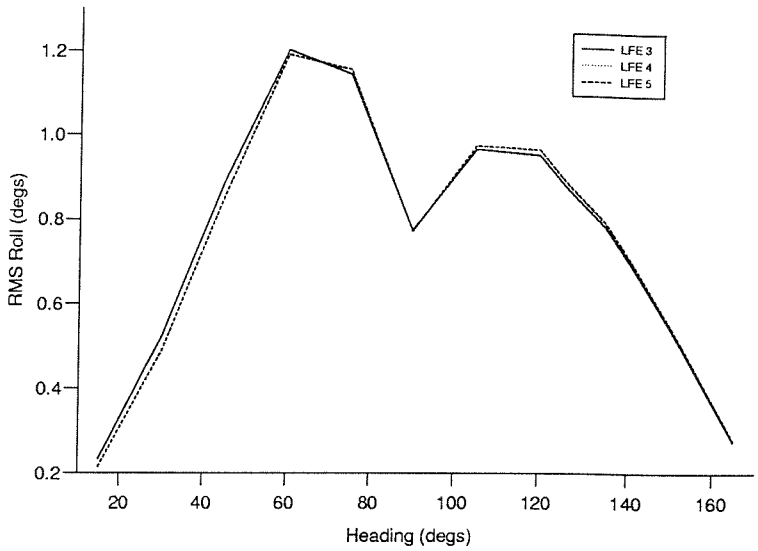

Figure 87: RMS Roll, LFE Controllers, Effects of Controller Order, spectra 1

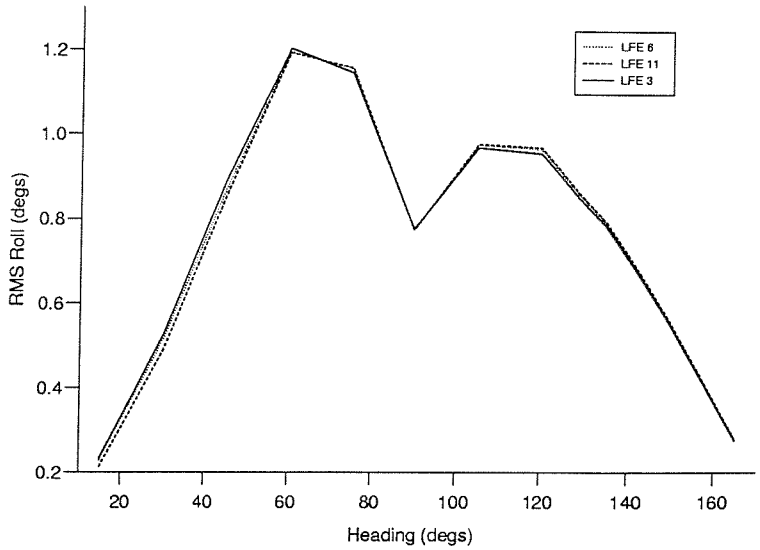

Figure 88: RMS Roll, LFE Controllers, Weighting Variation, spectra 1

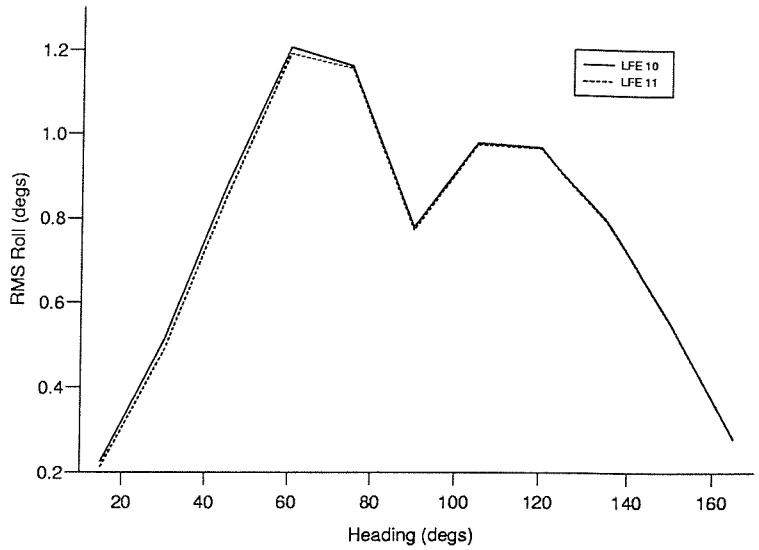

Figure 89: RMS Roll, LFE Controllers, Sub/Optimality, spectra 1

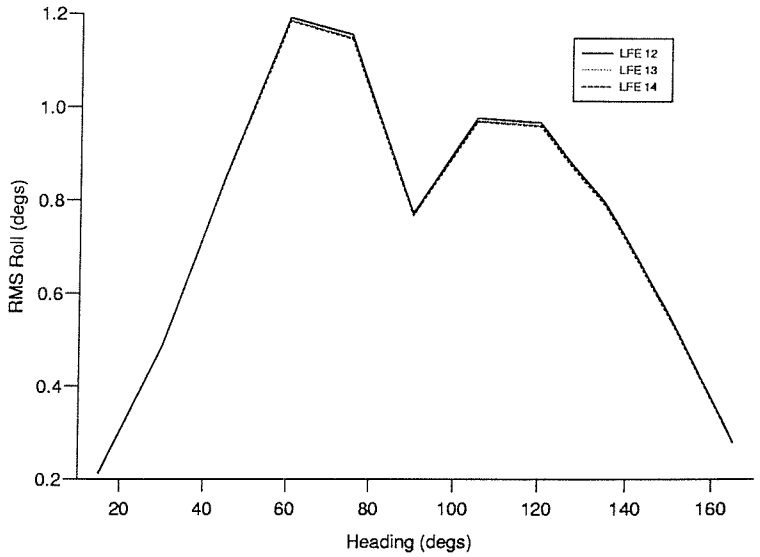

Figure 90: RMS Roll, LFE Controllers, Weighting Variations, spectra 1

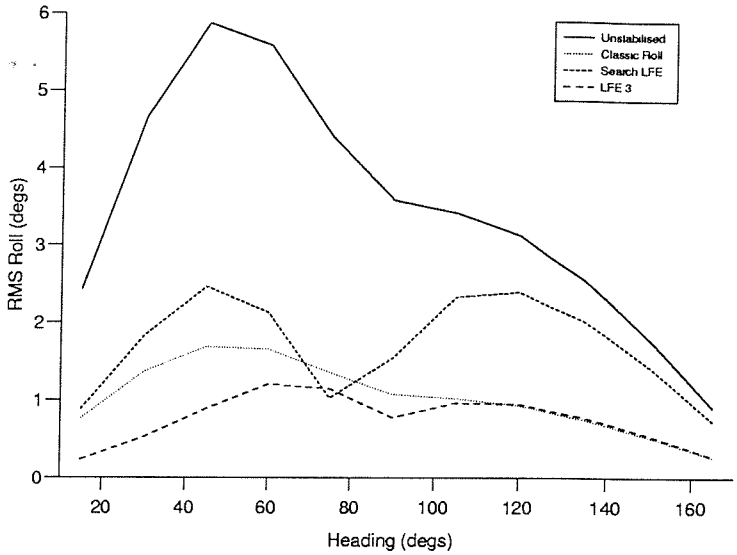

Figure 91: RMS Roll,LFE Controllers, Overall Performance, spectra 1

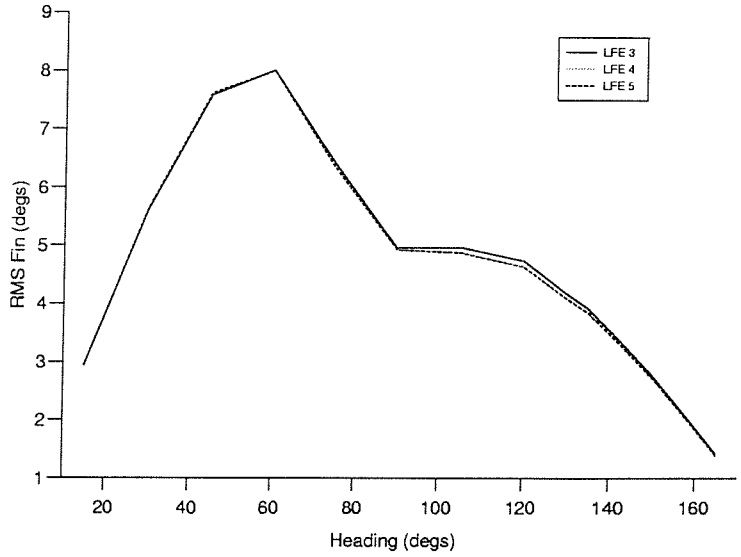

Figure 92: RMS Fin, LFE Controllers, Effects of Controller Order, spectra 1

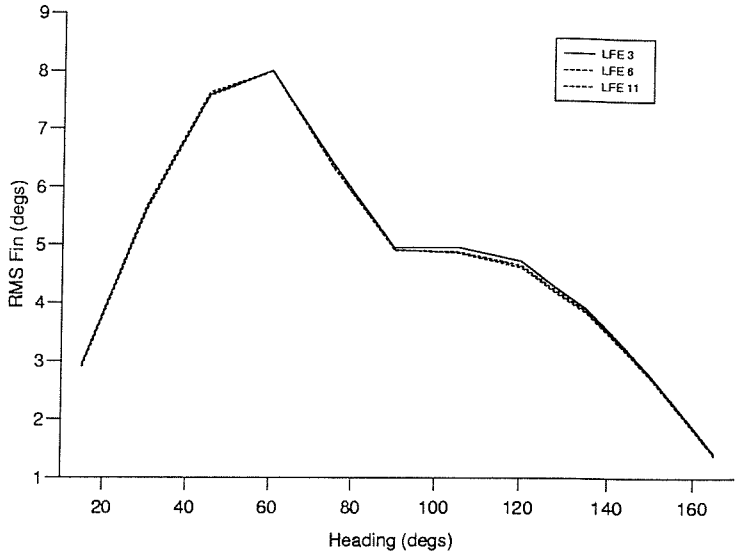

Figure 93: RMS Fin, LFE Controllers, Weighting Variations, spectra 1

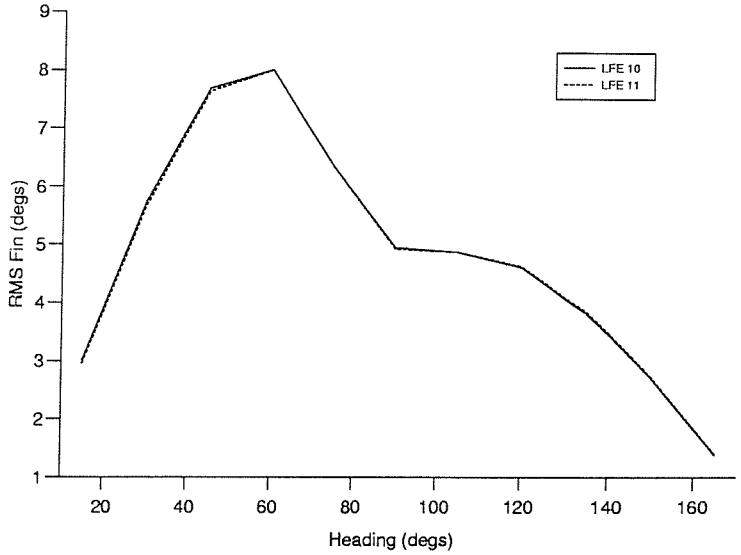

Figure 94: RMS Fin, LFE Controllers, Sub/Optimality, spectra 1

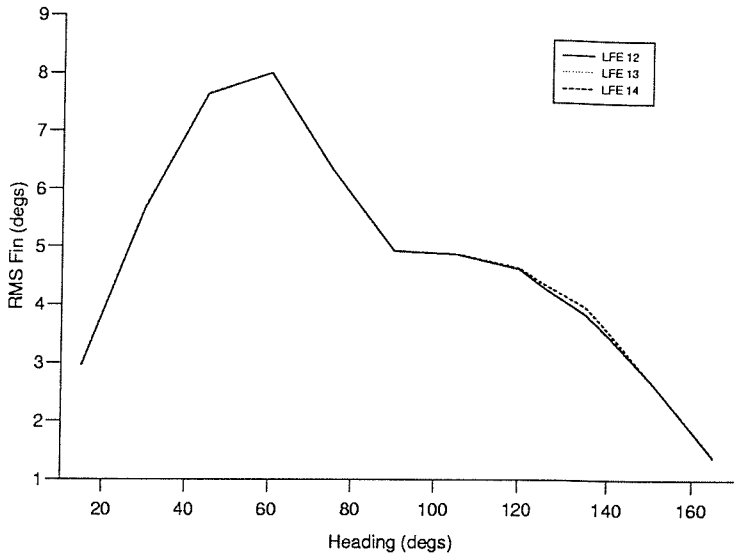

Figure 95: RMS Fin, LFE Controllers, Weighting Variations, spectra 1

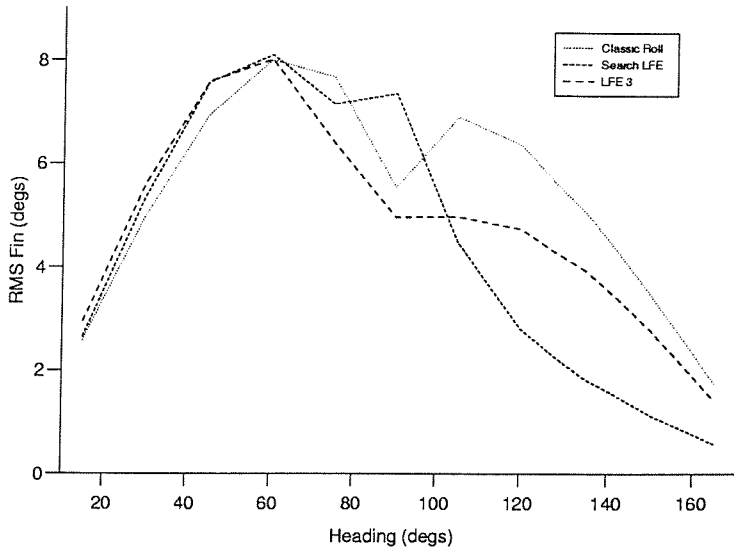

Figure 96: RMS Fin, LFE Controllers, Overall Performance, spectra 1

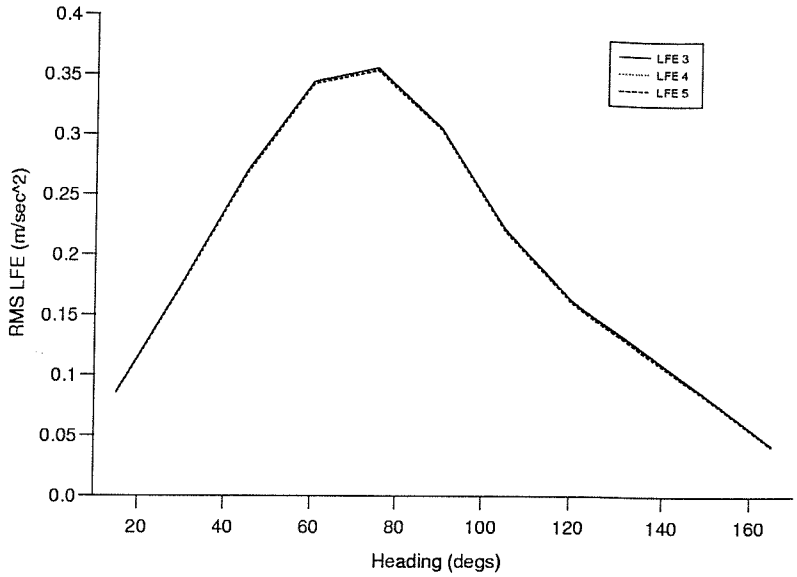

Figure 97: RMS LFE, LFE Controllers, Effects of Controller Order, spectra 1

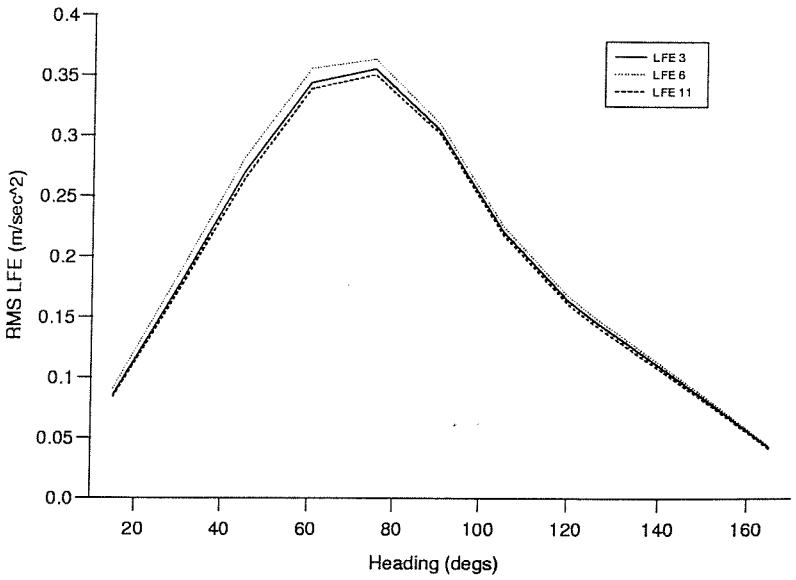

Figure 98: RMS LFE, LFE Controllers, Weighting Variations, spectra 1

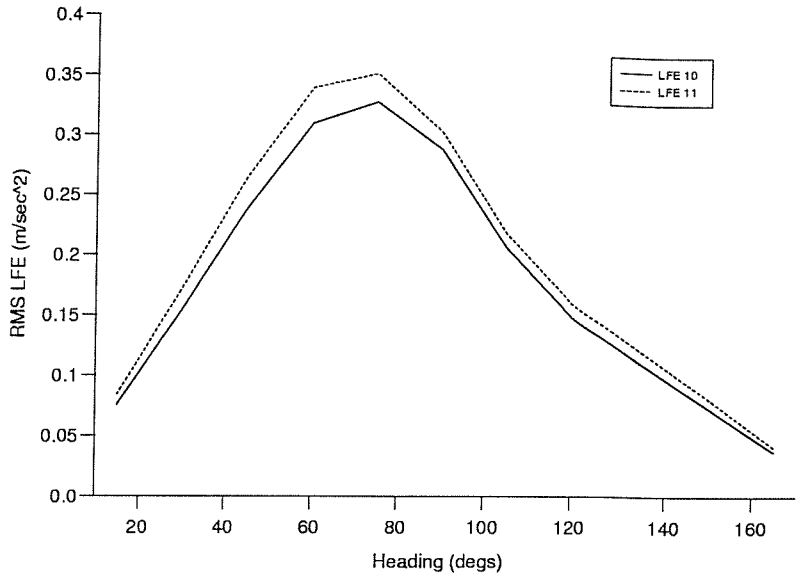

Figure 99: RMS LFE, LFE Controllers, Sub/Optimality, spectra 1

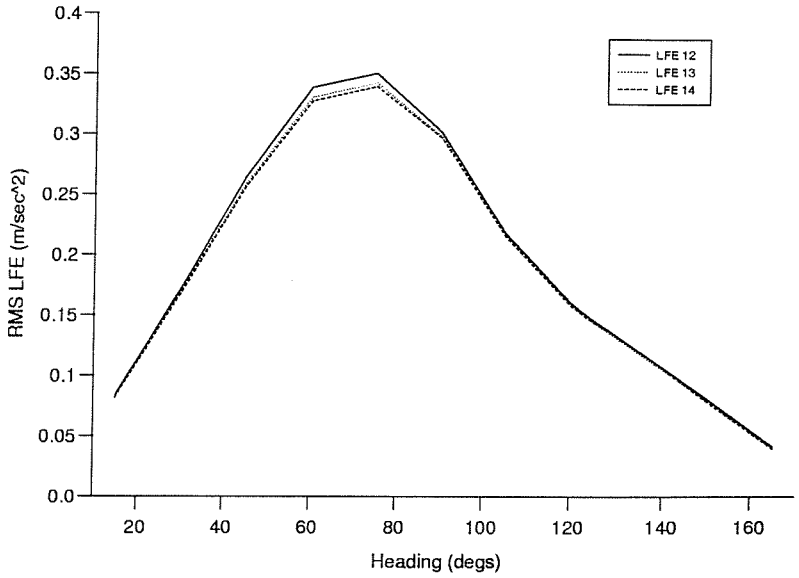

Figure 100: RMS LFE, LFE Controllers, Weighting Variations, spectra 1

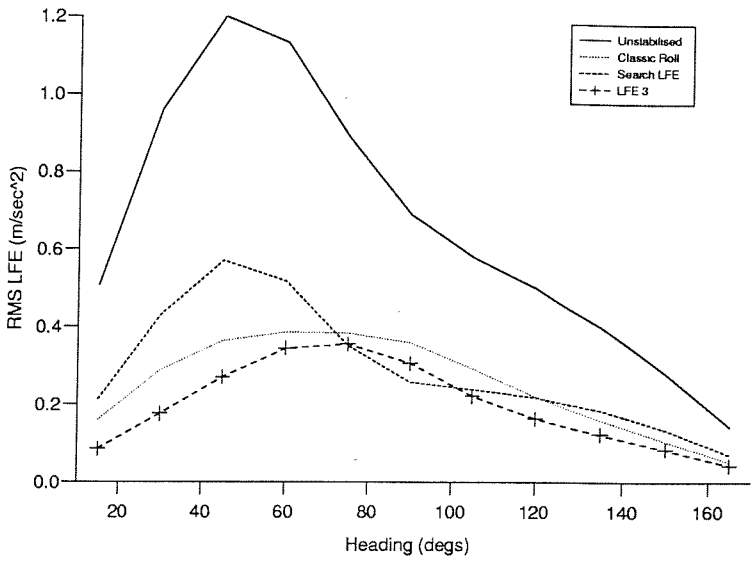

Figure 101: RMS LFE, LFE Controllers, Overall Performance, spectra 1

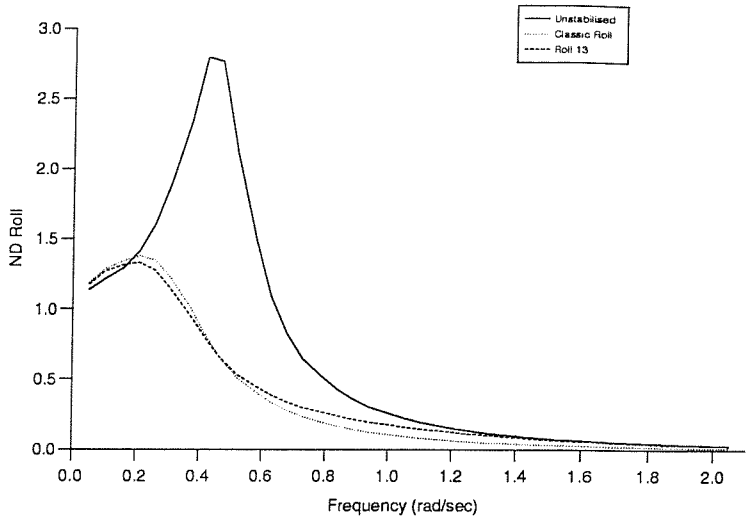

Figure 102: ND Roll, Overall Controller Performance

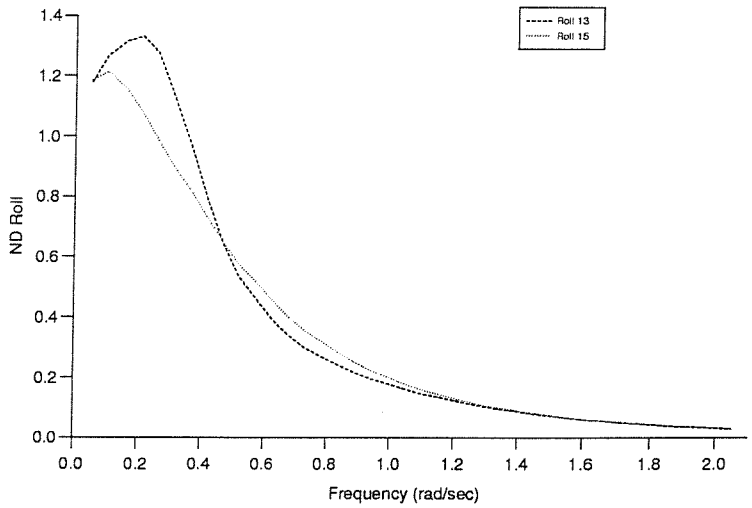

Figure 103: ND Roll, Sub/Optimality

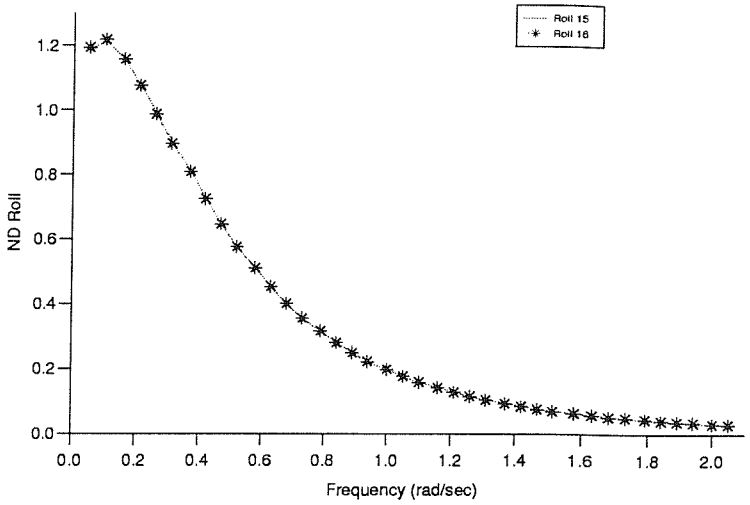

Figure 104: ND Roll, Effect of Controller Order

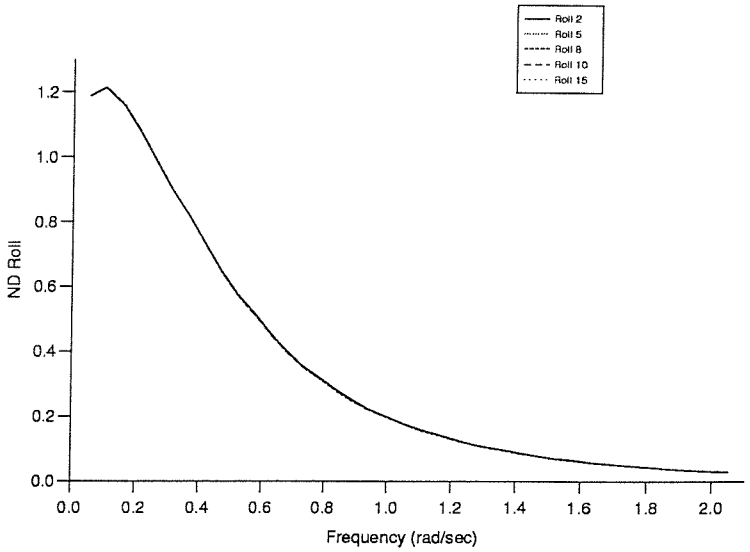

Figure 105: ND Roll, Weighting Variation

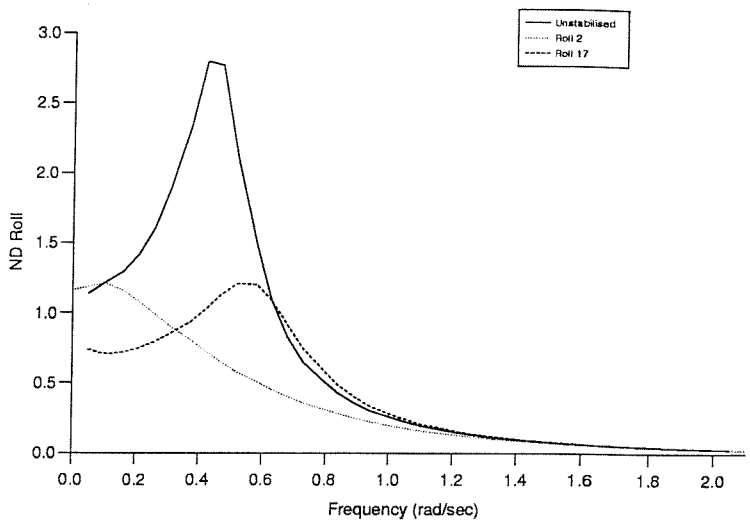

Figure 106: ND Roll, Weighting Variation

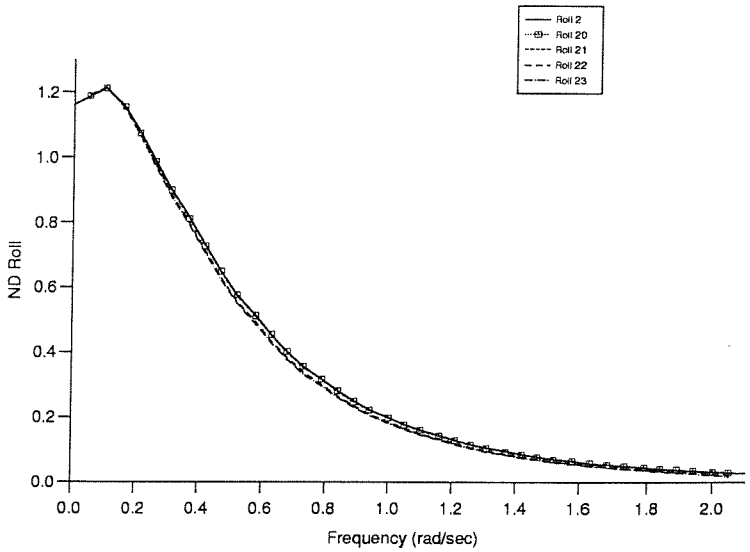

Figure 107: ND Roll, Weighting Variation

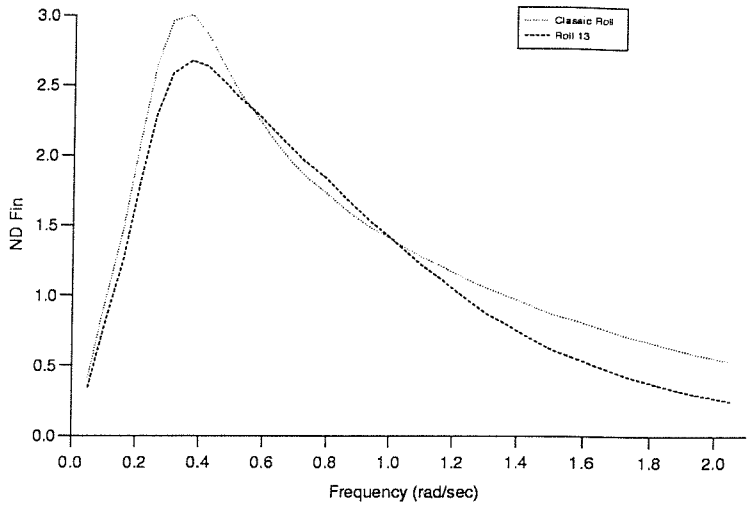

Figure 108: ND Fin, Overall Controller Performance

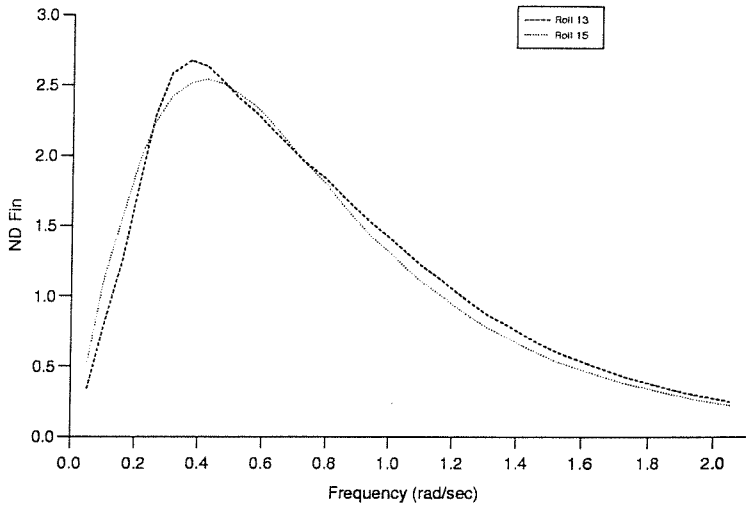

Figure 109: ND Fin, Sub/Optimality

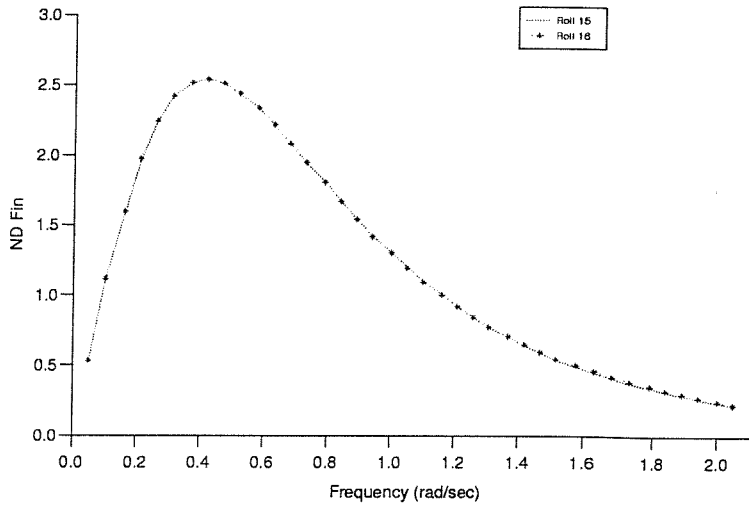

Figure 110: ND Fin, Effect of Controller Order

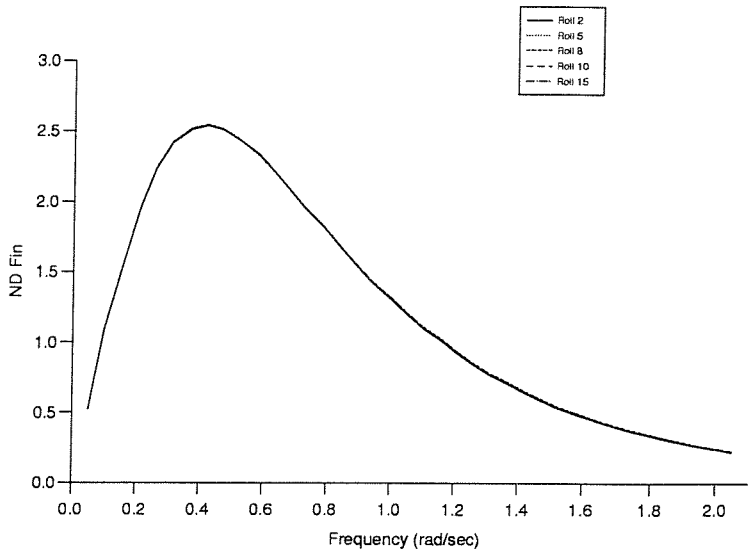

Figure 111: ND Fin, Weighting Variation

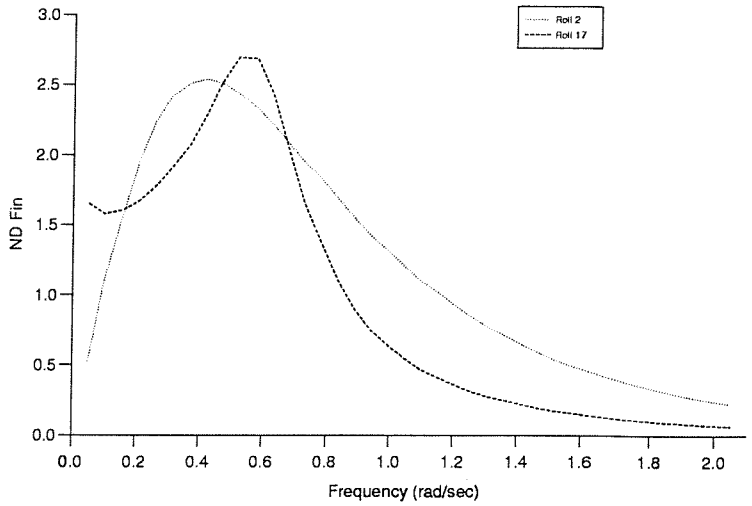

Figure 112: ND Fin, Weighting Variation

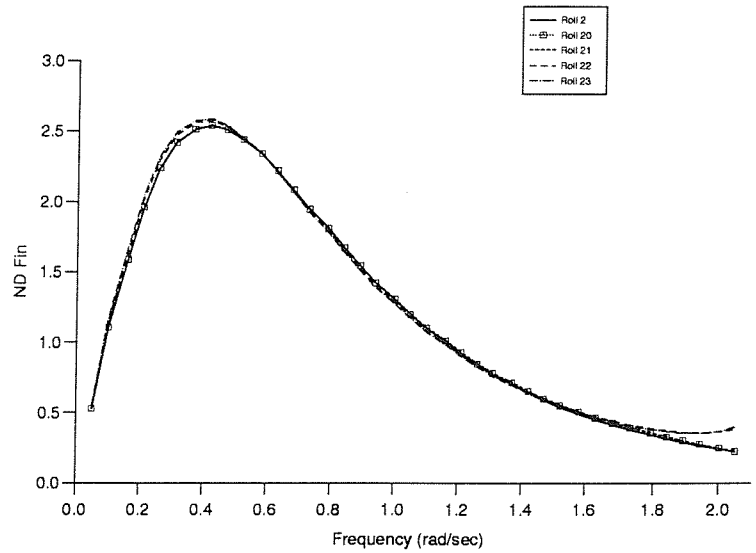

Figure 113: ND Fin, Weighting Variation

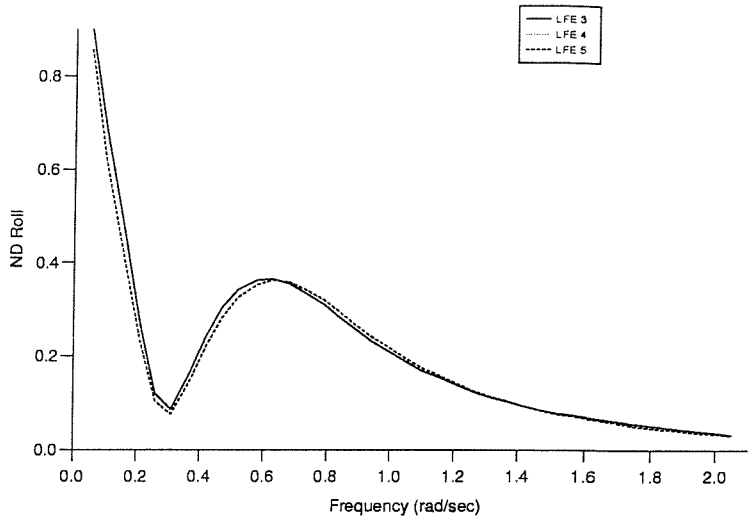

Figure 114: ND Roll, Effects of Controller Order

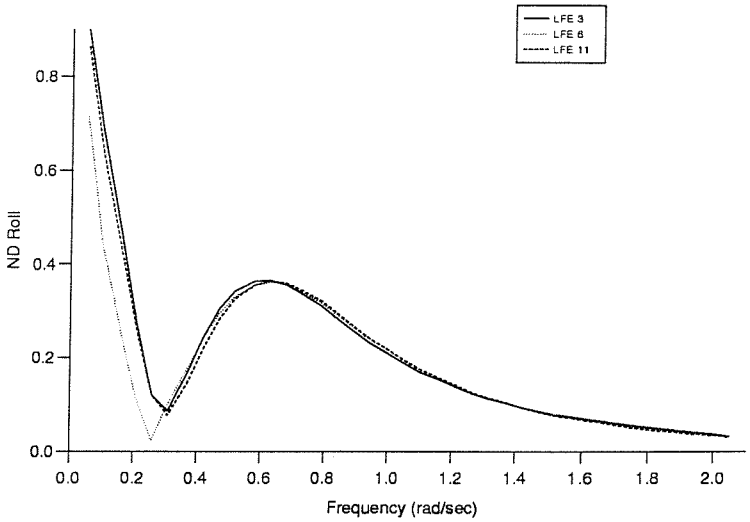

Figure 115: ND Roll, Weighting Variation

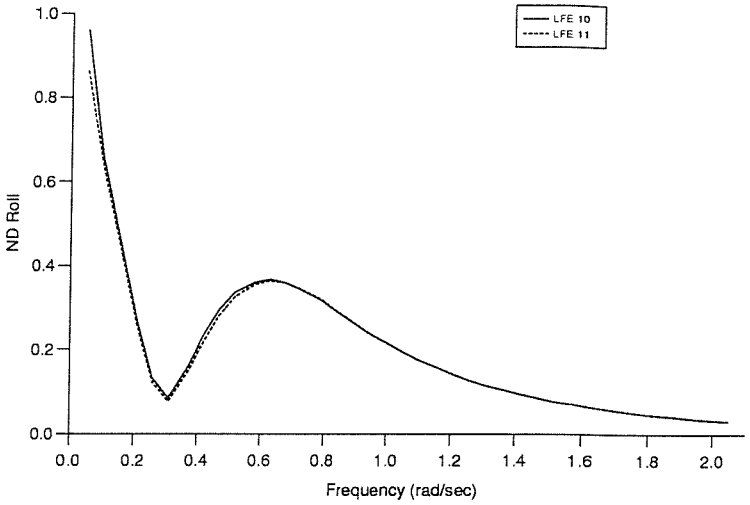

Figure 116: ND Roll, Sub/Optimality

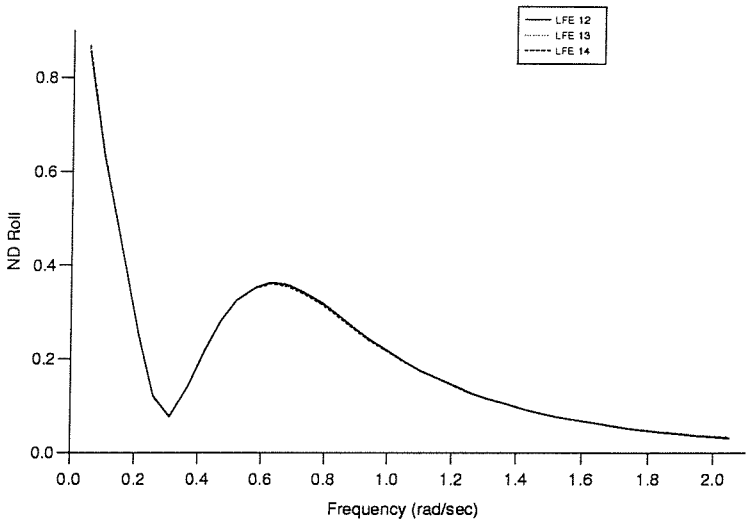

Figure 117: ND Roll, Weighting Variation

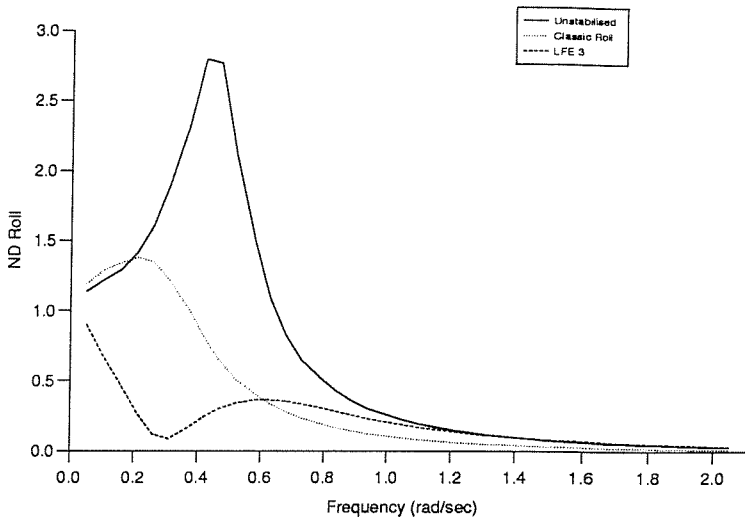

Figure 118: ND Roll, Overall Performance

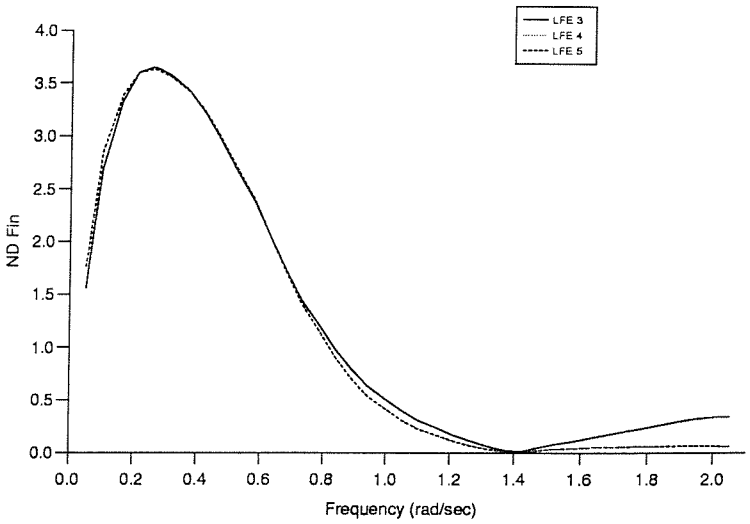

Figure 119: ND Fin, Effects of Controller Order

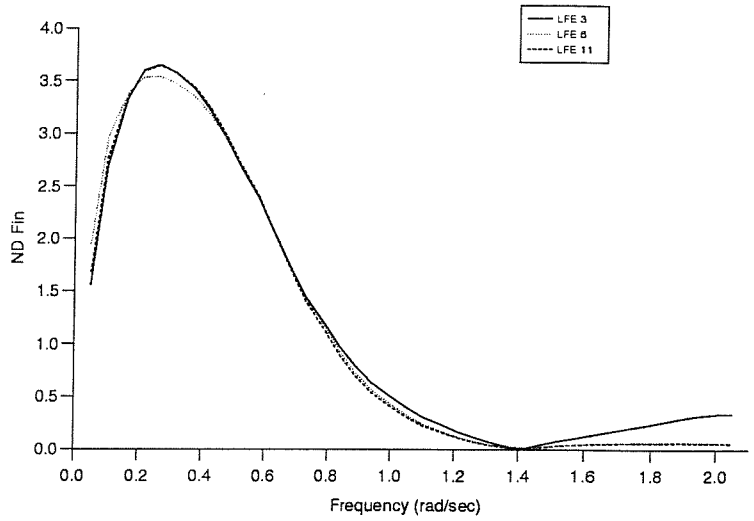

Figure 120: ND Fin, Weighting Variation

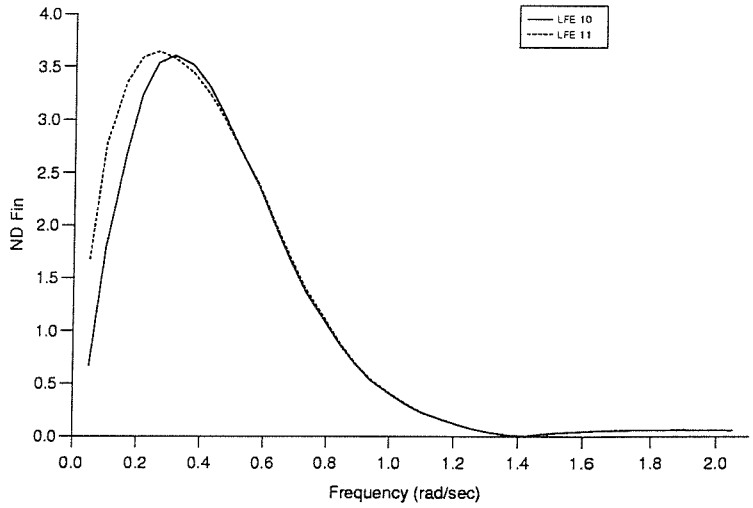

Figure 121: ND Fin, Sub/Optimality

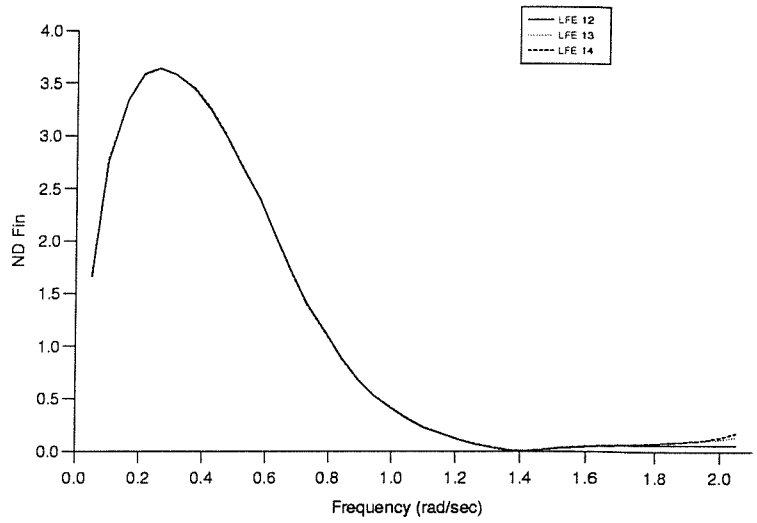

Figure 122: ND Fin, Weighting Variation

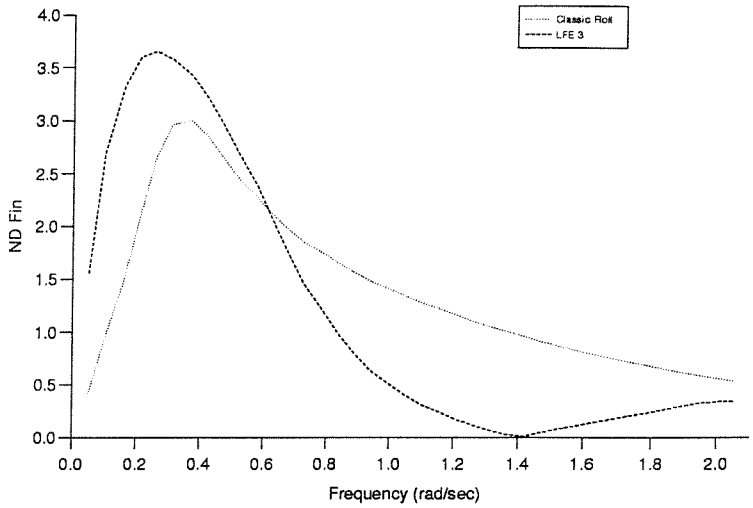

Figure 123: ND Fin, Overall Performance

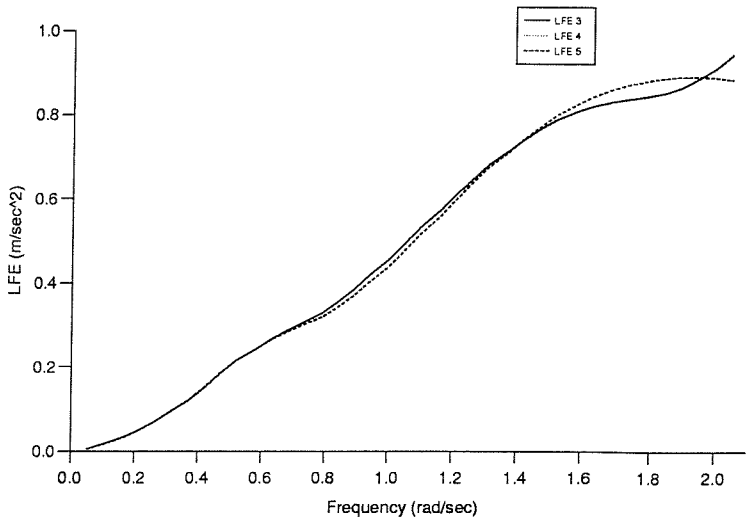

Figure 124: LFE, Effects of Controller Order

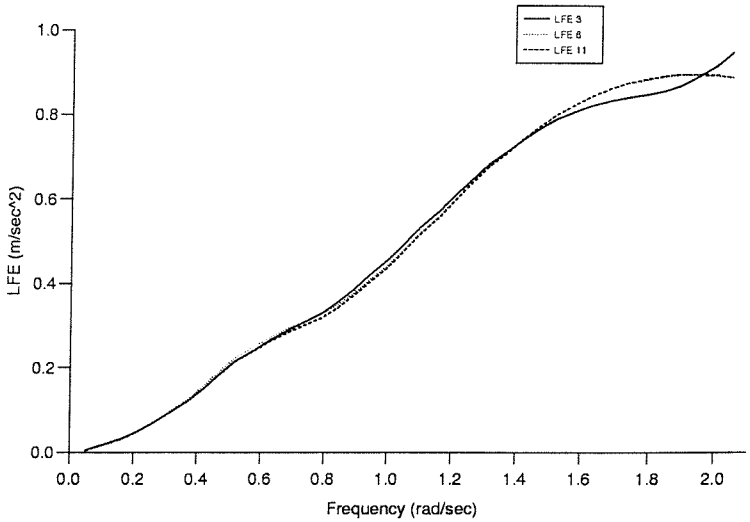

Figure 125: LFE, Weighting Variation

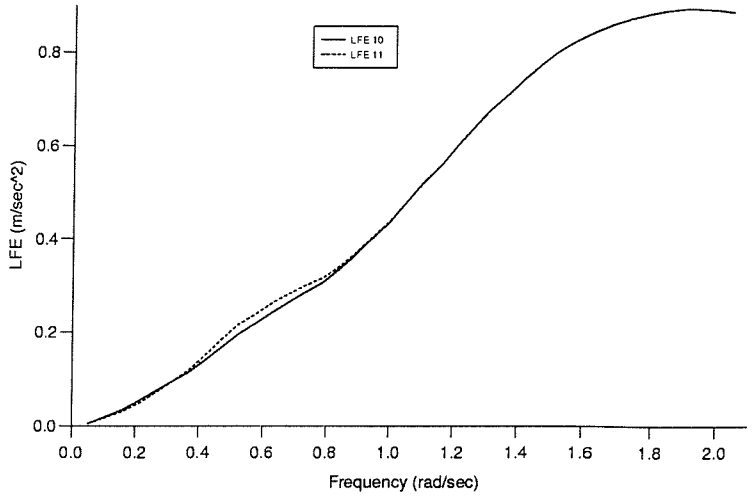

Figure 126: LFE, Sub/Optimality

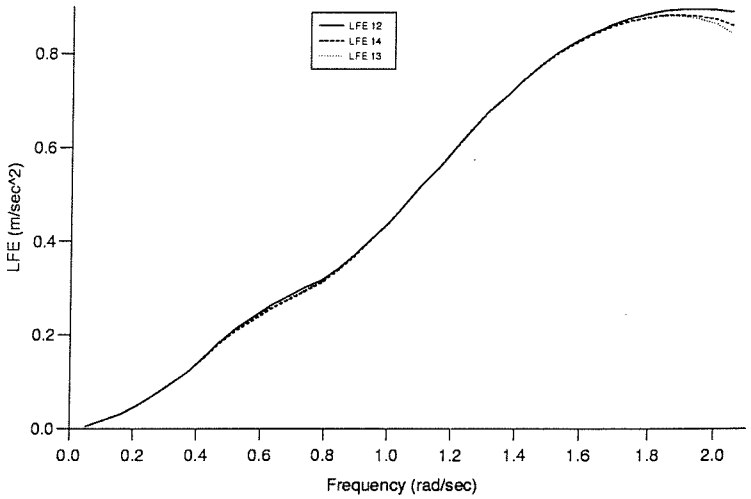

Figure 127: LFE, Weighting Variation

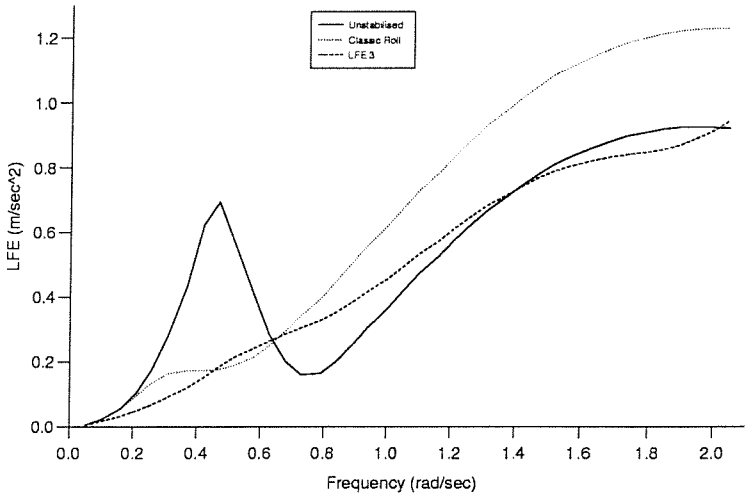

Figure 128: LFE, Overall Performance

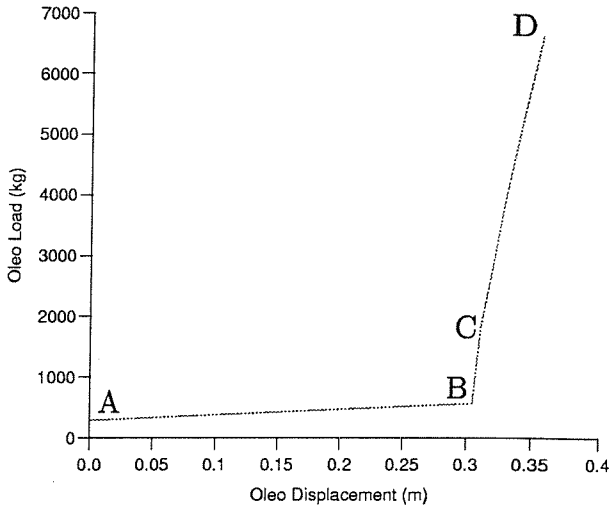

Figure 129: Static Oleo Reaction

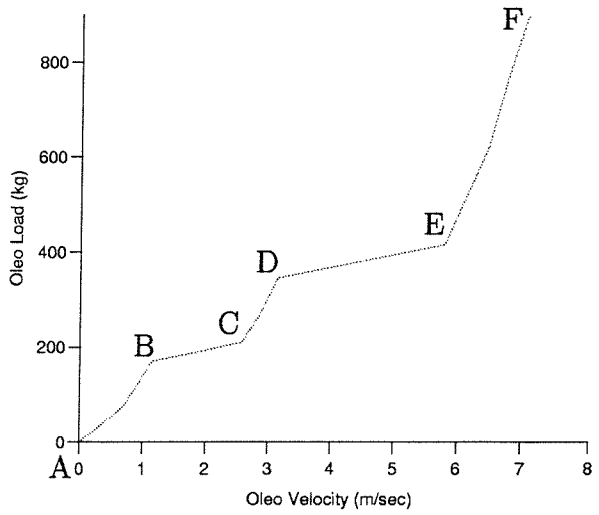

Figure 130: Dynamic Oleo Damping

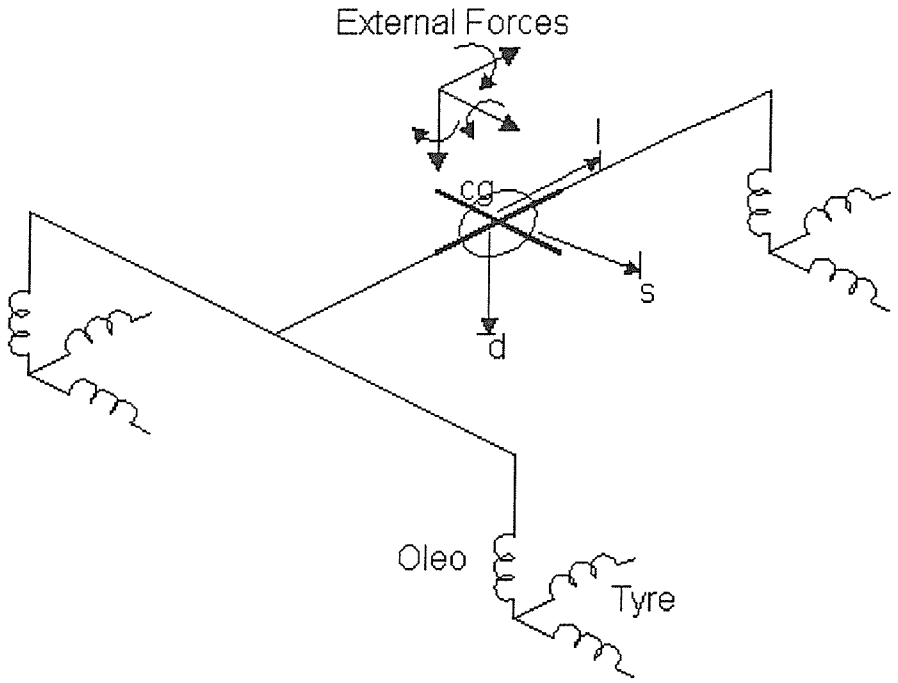

Figure 131: Representation of helicopter model

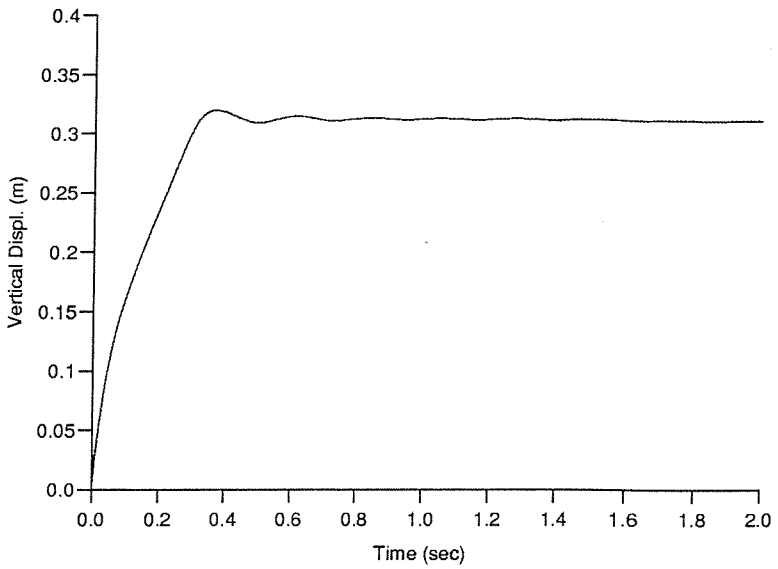

Figure 132: Helicopter Vertical Displacement, Drop Test

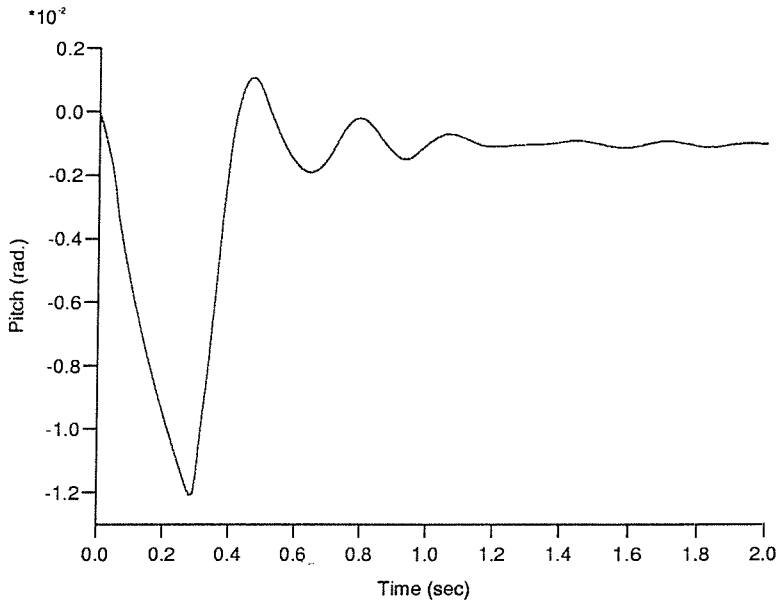

Figure 133: Helicopter Pitch, Drop Test

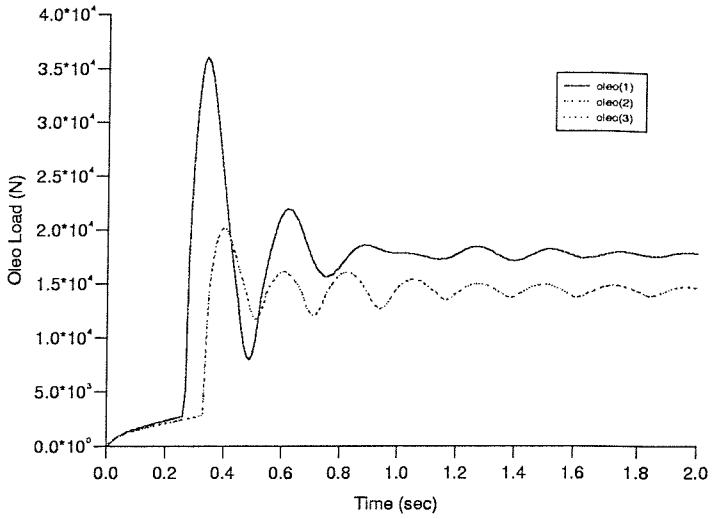

Figure 134: Oleo Loads, Drop Test

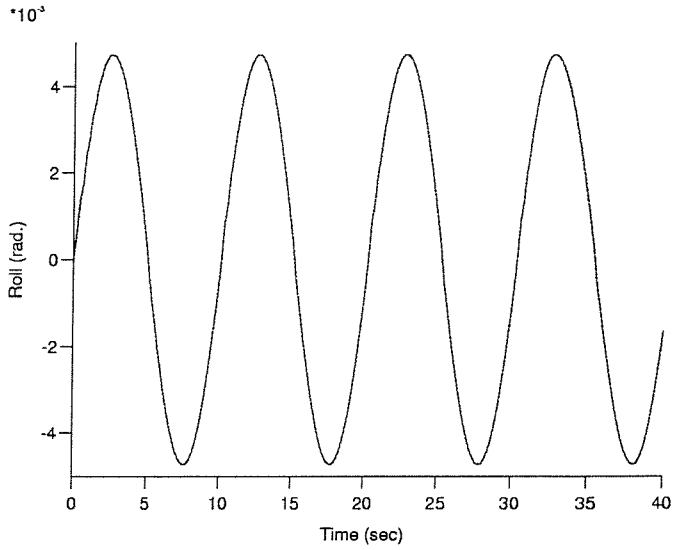

Figure 135: Helicopter Roll, Sinusoidal ship roll

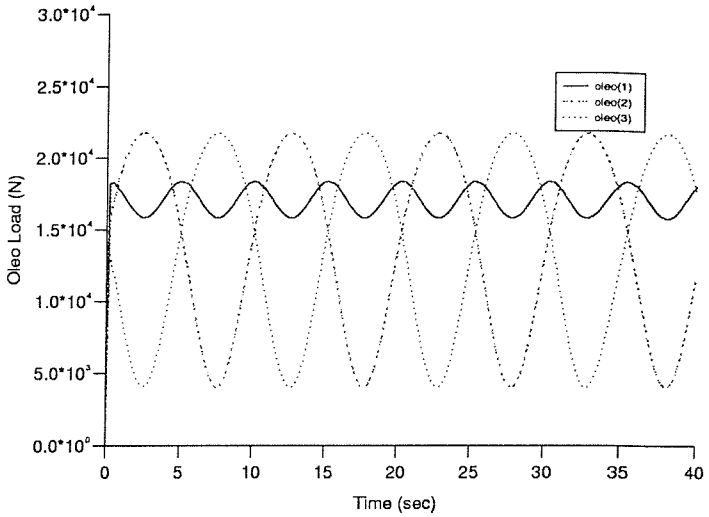

Figure 136: Oleo Loads, Sinusoidal ship roll

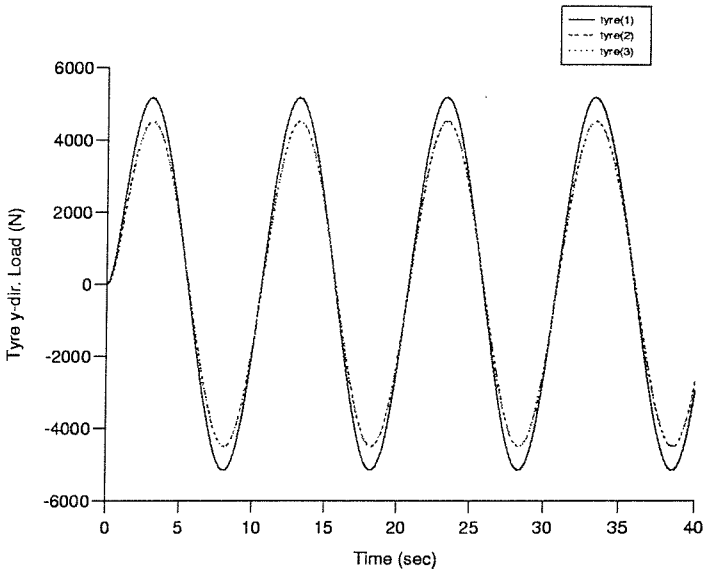

Figure 137: Transverse Tyre Loads, Sinusoidal ship roll

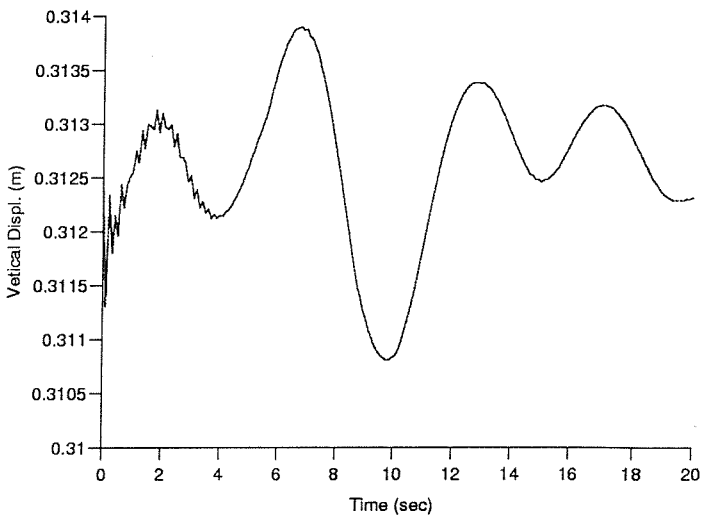

Figure 138: Helicopter Vertical Displacement, Irregular ship motions

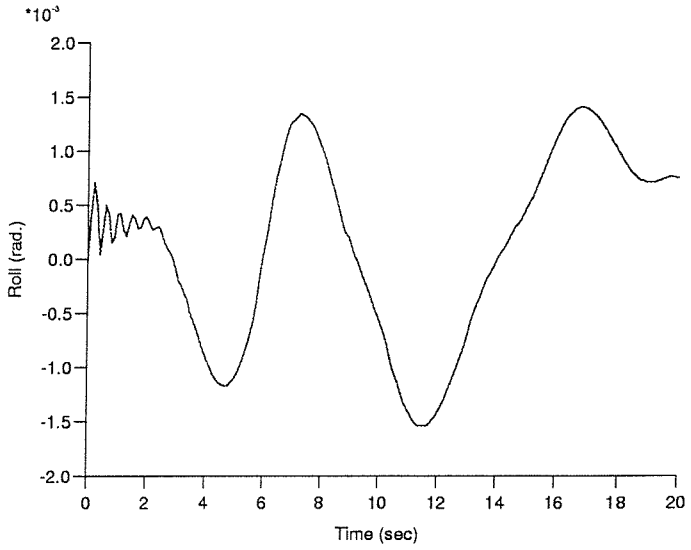

Figure 139: Helicopter Roll, Irregular ship motions

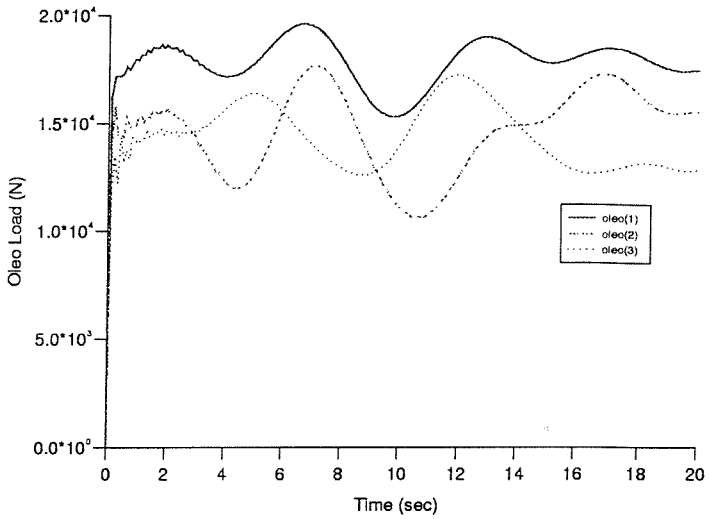

Figure 140: Oleo Loads, Irregular ship motions

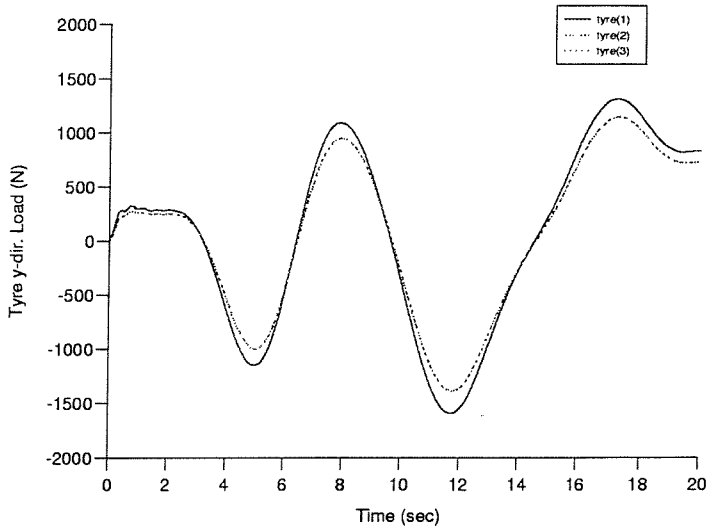

Figure 141: Transverse Tyre Loads, Irregular ship motions

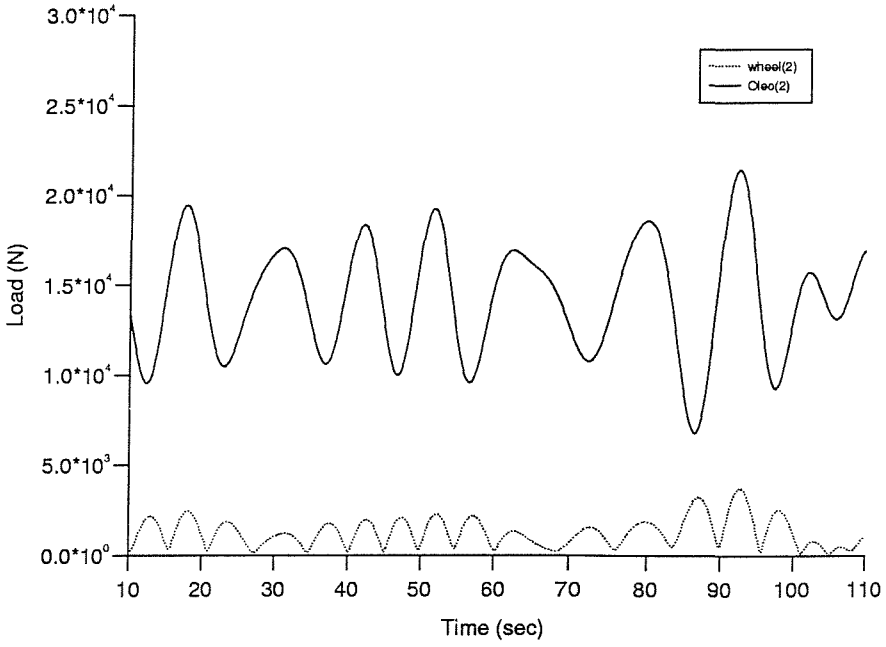

Figure 142: Unstabilised: Wheel Horizontal Load and Oleo Vertical Load

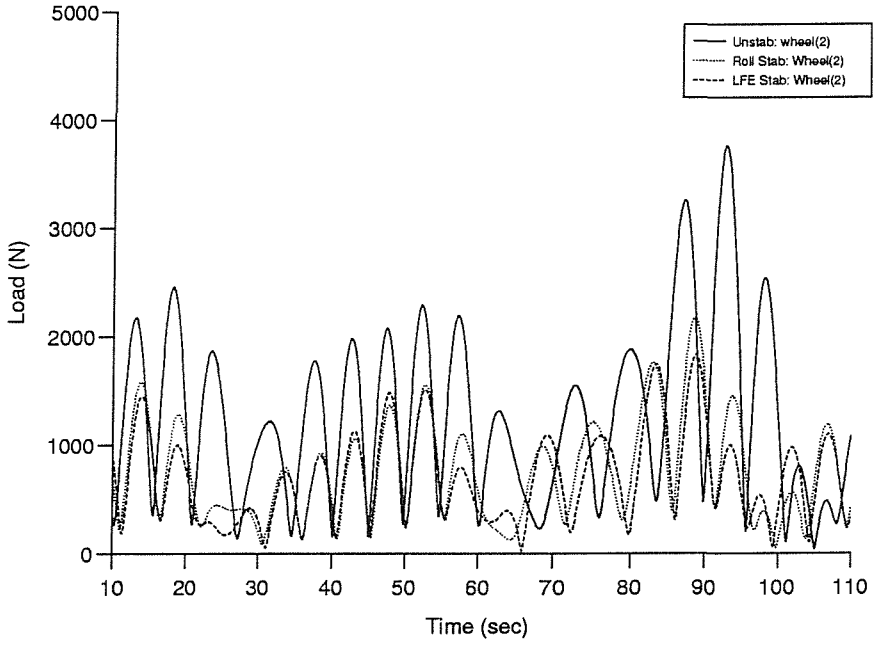

Figure 143: Effect of Stabilisation on Wheel Horizontal Load

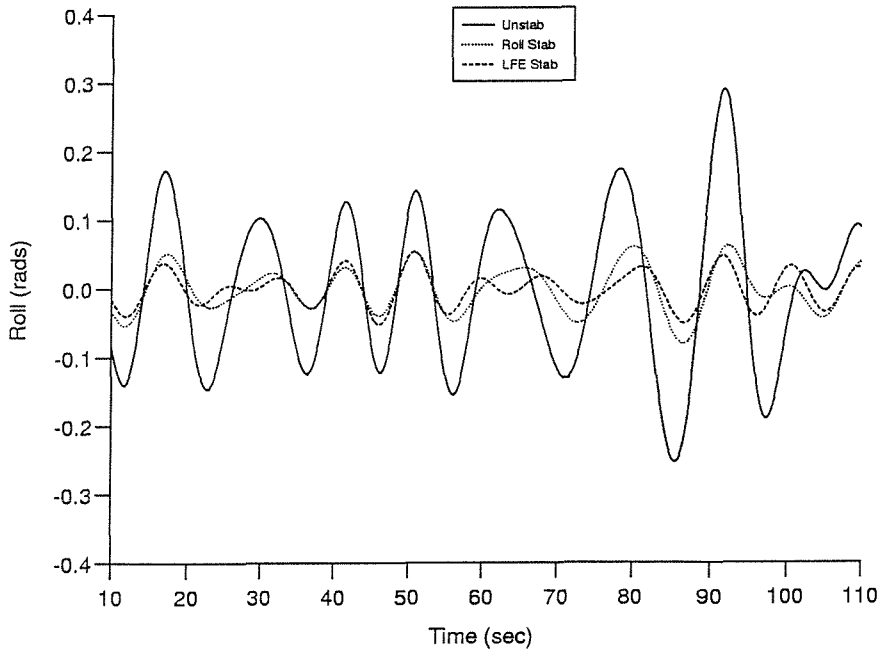

Figure 144: Roll for each Stabilisation

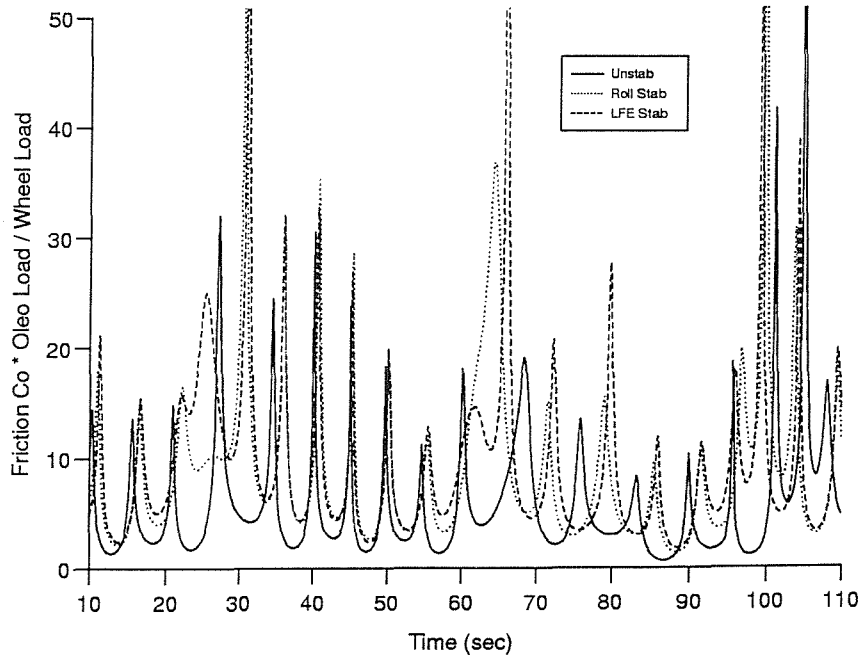

Figure 145: Friction Coefficient * Oleo Load / Wheel Load Ratio

A State Space to Transfer Function Matrix

The state and output equations for a system in space space form is

$$\begin{aligned} \dot{X} &= AX + BU \\ Y &= CX + DU \end{aligned} \tag{104}$$

Taking the Laplace transforms with the initial condition $X(0) = 0$, these become

$$sX(s) = AX(s) + BU(s) \tag{105}$$

and,

$$Y(s) = CX(s) + DU(s) \tag{106}$$

Equation 105 can be re-arranged to give

$$X(s) = (sI - A)^{-1}BU(s) \tag{107}$$

By substituting 107 into equation 106

$$Y(s) = \left[C(sI - A)^{-1}B + D\right]U(s) \tag{108}$$

Therefore, the transform function matrix is

$$G(s) = C(sI - A)^{-1}B + D \tag{109}$$

B Selection of Classic Roll Control Coefficients

The objective of the fin control system is to ensure that the roll moment created by the fins opposes the roll moment created by the incident waves or in the experiments described in section 8.1, the moment created by the rotating weights.

The phase difference between the action of the fins and the roll motion resulting in the ship must be accounted for. Therefore, the control system has to send the desired fin angle signal at a particular phase in advance of the desired restoring moment. This phase lag is dependent upon wave frequency. Therefore, the phase lag at the natural roll frequency is used to determine the relevent controllers, as it is at this frequency that maximum roll occurs and at which roll reduction is most desired.

This phase lag can be given as:-

$$\varepsilon_c = \varepsilon_s + \varepsilon_{fs} \tag{110}$$

ε_s ship phase

ε_{fs} fin servo phase

ε_c represents the phase lag between the control signal and the ship roll. This is is measured from forced roll experiments.

The predominant phase contributions are created from the ship ε_s and fin servo system elements ε_{fs}.

The classic control system is characterised by the following equation.

$$\frac{\alpha}{\varphi} = K_G \left[\frac{K_1 + K_2 s + K_3 s^2}{b_1 + b_2 s + b_3 s^2} \right] \tag{111}$$

with α fin angle and φ roll angle

By substituting:-

$$s = i\omega_{nat}$$

ω_{nat} natural roll frequency

Then the controller phase is given as:-

$$\varepsilon_c = \tan^{-1}\left(\frac{K_2\omega_{nat}}{K_1 - K_3{\omega_{nat}}^2}\right) - \tan^{-1}\left(\frac{b_2\omega_{nat}}{b_1 - b_3{\omega_{nat}}^2}\right) \tag{112}$$

if,

$$\tan\varepsilon = \frac{K_2\omega_{nat}}{K_1 - K_3{\omega_{nat}}^2} \tag{113}$$

Therefore,

$$\varepsilon = \tan^{-1}\left(\frac{b_2\omega_{nat}}{b_1 - b_3{\omega_{nat}}^2}\right) - \varepsilon_s - \varepsilon_{fs} \tag{114}$$

From this, the relationships between the control coefficients is,

$$K_2 = \frac{K_3\tan\varepsilon}{\omega_{nat}}\left(\frac{K_1}{K_3} - {\omega_{nat}}^2\right) \tag{115}$$

By careful selection of 2 of the coefficients, the third can be found. This provides the user with some command over the controller performance. From this, caution is needed in selecting a suitable overall gain value K_G.

C H_∞ Roll Controller

A ship roll stabilisation system has been formed using a H_∞ polynomial control approach, that adopts a design methodology similar to that given by Grimble et al [5]. In this example, only the fins are used as an active stabilising devices.

The first stage in any control problem is to derive a representation of the system. This has been performed for a roll stabilisation system as can be from figure 146.

This list constitutes each major element to be accounted for in the system model:-

- Fin servo
- Roll Dynamics
- External Disturbances
- Rate sensor

Representations of the properties of each of these elements can be described in transfer function form, and are as follows.

Fin Roll Rate

The control system adopted in this example uses the roll rate feedback signal, therefore the form of the equations is as follows:-

$$G_{\dot{\varphi}\alpha} = K_{\dot{\varphi}\alpha}\omega_\varphi \frac{\frac{s}{\omega_\varphi}}{\left(\frac{s}{\omega_\varphi}\right)^2 + \frac{2\zeta_\varphi s}{\omega_\varphi} + 1} \tag{116}$$

ω_φ roll natural frequency.
ζ_φ roll damping coefficient.
$K_{\dot{\varphi}\alpha}$ fin - roll rate gain.

The roll damping coefficient is speed dependent, therefore this must be tuned to the actual ship velocity. These values can be obtained from experimentation, or maybe approximated through the following expression:-

$$\zeta_\varphi = \zeta_{\varphi S} + \zeta_{\varphi D}\frac{U}{U_{op}} \tag{117}$$

$\zeta_{\varphi S}$ stationary damping coefficient (zero speed).

$\zeta_{\varphi D}$ dynamic damping coefficient.
U actual ship speed
U_{op} operational ship speed

Fin servo

Figure 147 shows a diagram of the actuator dynamics.

The fin servo functions have been represented using:-

$$\begin{aligned} \tau_\alpha \frac{d\alpha}{dt} + \alpha &= \alpha_d \\ |\alpha| &\leq \alpha_{max} \\ \left|\frac{d\alpha}{dt}\right| &\leq \dot{\alpha}_{max} \end{aligned} \tag{118}$$

α_{max} maximum achievable fin angle.
$\dot{\alpha}_{max}$ maximum achievable fin angle rate.

It can be seen that, the known fin non-linearities can be modelled with respect to fin angle and fin angle rate.

Roll Rate Sensor

The following transfer function has been used to model the roll rate sensor, this simulates the effect of the devices frequency range. The output is a near constant function of the input in the range between the frequency limits, outside that the output magnitude reduces. This results in a band pass type filter, as used in [5].

$$G_{\dot{\varphi}\dot{\varphi}}(s) = \left[\frac{(\omega_l + \omega_h)\, s}{(s + \omega_l)(s + \omega_h)}\right]^2 \tag{119}$$

ω_h upper frequency limit
ω_l lower frequency limit

Wave Roll

These are the external disturbances resulting from interaction with waves. The magnitude of roll motion is dependent upon wave height and encounter frequency, which can be determined with wave spectra data. In this example,

the Bretschneider spectra has been adopted. When combined with the roll rate dynamics, an indication of the roll rate in a seaway can be formed.

Various spectra can be substituted into this formulation, in addition to varying the sea state parameters. The wave induced roll is calculated from:-

$$\varphi_{wave} = \frac{1}{s} G_{\dot{\varphi}\alpha} G_{wave}(s)\,\omega \tag{120}$$

$$G_{wave}(s) = \frac{h_{\frac{1}{3}} K_{wave} \sin\phi}{L\left(1 - \frac{2U\omega}{g}\cos\phi\right)} \left[\frac{\frac{s}{\omega}}{\left(\frac{s}{\omega}\right)^2 + \frac{s}{\omega} + 1}\right]^2 \tag{121}$$

ϕ wave encounter angle.
L ship length.
$h_{\frac{1}{3}}$ significant wave height.
ω wave frequency.
U ship speed.

Wind Roll

This has been taken into consideration, as it can result in static heel angles that need to be accounted for in any system simulation.

$$\varphi_{wind} = K_{wind}\left(\frac{V_{wind}}{U}\right)^2 \sin\phi_{wind} \tag{122}$$

V_{wind} wind velocity relative to ship.
ϕ_{wind} assumed to equal ϕ wave encounter angle.

All of the above can be used to assist in the formation of the weighting functions and to approximate the nominal plant.

The key factor of the H_∞ control method is in the selection of the weighting functions. This is critical, as to whether a possible controller maybe found and also whether it relates to the system under investigation. Three weighting functions have been adopted in this example.

Sensitivity Weight Function

This function is used to specify the desired performance of the controller. In this example, that is the required roll attenuation. The system should not react against the stable heel angle caused by wind loading or other factors such as the vessel loading condition. This function is used to define the

frequency region, in the vicinity of the natural roll frequency where maximum roll reduction is required. Outside this region, the system should be prevented from increasing roll.

The sensitivity function is minimised within the natural frequency range. As a result of this, the control system is able to successfully operate in a range of conditions.

$$W_1(s) = \left(\frac{2B}{1-\frac{A}{100}}\right)\frac{s}{\left(\frac{s}{\omega_\varphi}\right)^2 + \left(\frac{2Bs}{\omega_\varphi}\right) + 1} \tag{123}$$

A percentage peak reduction.
B bandwidth parameter.

Control Sensitivity Function

Control sensitivity is related to the fin activity. High and low frequency components are attenuated by the controller. High frequency components are undesirable as they are unachievable, limited by the maximum fin rate $\dot{\alpha}_{max}$ and would result in excessive system wear. The low frequency components, are not necessary as the resulting fin response can be relatively ineffective.

$$W_2(s) = \frac{\left(\frac{s}{\omega_{l\alpha}} + C\right)\left(\frac{Cs}{\omega_{h\alpha}} + 1\right)}{\left(\frac{Cs}{\omega_{l\alpha}} + 1\right)\left(\frac{s}{\omega_{h\alpha}} + C\right)} \tag{124}$$

C control action in the range between ω_l and ω_h.

Complementary Sensitivity Function

This weighting function is minimised outside the natural frequency region, this is a result of uncertainties in the model formation, such as those resulting from speed variations and non-linear distortions.

$$W_3(s) = D\frac{\left(\frac{s}{\omega_\varphi} + 1\right)^2}{\left(\frac{Ds}{\omega_\varphi} + 0.01\right)\left(\frac{0.01s}{\omega_\varphi} + D\right)} \tag{125}$$

D represents frequency range where robustness is required.

These weightings are combined with the nominal plant, to form an augmented plant representation.

Figure 146 shows a representation of the closed loop system dynamics.

The system disturbances form the following relations:-

$$\varphi = S(\varphi_{wav} + \varphi_{win} + \varphi_{aut}) - T\varphi_{ins} \tag{126}$$

$$\alpha = -R(\varphi_{wav} + \varphi_{win} + \varphi_{aut} + \varphi_{ins}) \tag{127}$$

R = Control sensitivity
S = Closed loop sensitivity
T = Complementary sensitivity

Which have the following relationships:-

$$S = (1+L)^{-1} \tag{128}$$
$$T = SL \tag{129}$$
$$R = CS \tag{130}$$

The open loop transfer function is of the form:-

$$L = G_{\dot{\varphi}\dot{\varphi}} G_{\dot{\varphi}\alpha} G_{\alpha\alpha} C_{\alpha} \tag{131}$$

Eqn. 131 in reality is highly non-linear. In the frequency bandwidth over which the ship roll is significant, the roll rate and fin servo dynamics can be assumed to be constant. That reduces the open loop transfer function to:-

$$L = G_{\dot{\varphi}\alpha} C_{\alpha} \tag{132}$$

The roll angle contributing disturbances are given as:-

$$d = \varphi_{wav} + \varphi_{win} + \varphi_{aut} \tag{133}$$

It is assumed that this has a spectral density of:-

$$S_d(s) = W_1(s) W_1^T(-s) \tag{134}$$

With sensor disturbances being given as:-

$$n = \varphi_{ins} \tag{135}$$

With a spectral density of:-

$$S_n(s) = W_n(s) W_n^T(-s) \tag{136}$$

From this, a set of norm conditions can be applied that the controller must be optimised to.

The purpose of the controller is to reduce the roll significantly in the vicinity of the natural roll frequency without increasing roll for disturbances outside this region. This leads to the following norm condition:-

$$||W_1 S(C)||_\infty \leq 1/\gamma \tag{137}$$

A norm condition that limits the control activity to the natural roll frequency region is given by:-

$$||W_2 R(C)||_\infty \leq 1/\gamma \tag{138}$$

with

$$W_2(s)W_2^T(-s) = S_n(s) + S_d(s) \tag{139}$$

The ability of the sensor to provide an accurate measure of roll angle is given by the norm condition of:-

$$||W_n T(C)||_\infty \leq 1/\gamma \tag{140}$$

Δ is assumed to be the model uncertainty, this is adopted in a multiplicative manner to give:-

$$||W_\Delta^{-1}\Delta||_\infty \leq 1 \tag{141}$$

The stability and performance is regulated with the following norm condition:-

$$||W_\Delta T(C)||_\infty < 1 \tag{142}$$

The conditions eqn. 140 and eqn. 142 can be combined, resulting in a single norm condition.

$$|\gamma W_3(s)| \geq max\left(|\gamma W_n(s)|, |W_\Delta(s)|\right) \tag{143}$$

The following norms are then used to characterise the system.

$$\begin{aligned} ||W_1 S(C)||_\infty &\leq 1/\gamma \\ ||W_2 R(C)||_\infty &\leq 1/\gamma \\ ||W_3 T(C)||_\infty &\leq 1/\gamma \end{aligned} \tag{144}$$

The following condition encompasses all of the previously derived norm conditions:-

$$||F(C,\gamma)|| \leq 1 \tag{145}$$

with:-

$$F(C,\gamma) = \begin{bmatrix} \gamma W_1 S(C) \\ \gamma W_2 R(C) \\ \gamma W_3 T(C) \end{bmatrix} \tag{146}$$

It must be noted that in all the previous equations:-

$$\gamma > 0 \tag{147}$$

The augmented plant is formed as:-

$$P = \left[\begin{array}{c|c} \gamma W_1 & -\gamma W_1 G_{\dot{\varphi}\alpha} \\ 0 & \gamma W_2 \\ 0 & \gamma W_3 G_{\dot{\varphi}\alpha} \\ \hline I & -G_{\dot{\varphi}\alpha} \end{array}\right] \tag{148}$$

From this the H_∞ problem can be solved.

The mathematic background of the H_∞ control method is quite intensive and involves solving relatively large matrix Ricatti equations. These are very numerically sensitive, therefore careful selection of weighting functions is critical.

D Equivalent Wave Slope

This section gives the conversion to determine the equivalent wave slope for the contra- rotating weight mechanism.

The moment induced by the weight mechanism is:-

$$M = M_0 \left(1 + \frac{h\omega^2}{g}\right) \sin(\omega t) \tag{149}$$

M_0 is the moment induced by the weights at 90° to the centreline. h is the vertical distance between tow post heel fitting (model centre of gravity) and the rotating weights.

From this, the non-dimensional wave slope can be given the following relationship:-

$$\alpha(\omega) = \alpha_0 \left(1 + \frac{h\omega^2}{g}\right) \tag{150}$$

α_0 is the static heel angle with the weights at 90° to the centreline.

The dimensionalised wave slope is given as:-

$$\alpha(\omega) = \omega^2 \alpha_0 \left(1 + \frac{h\omega^2}{g}\right) \tag{151}$$

E Controller Transfer Functions

The following transfer functions relate to the controllers defined in chapter 9, tables 10 and 11.

$$ROLL2 = \frac{17.7407s^2 + 1.7364s - 0.0229}{s^3 + 1.2088s^2 + 0.3754s + 0.0139} \tag{152}$$

$$ROLL5 = \frac{12.2652s^2 + 1.4059s - 0.0189}{s^3 + 1.1963s^2 + 0.3754s + 0.0165} \tag{153}$$

$$ROLL8 = \frac{16.8903s^2 + 2.0153s - 0.0255}{s^3 + 1.1994s^2 + 0.3806s + 0.0170} \tag{154}$$

$$ROLL10 = \frac{12.4452s^2 + 1.3267s - 0.0181}{s^3 + 1.1985s^2 + 0.3664s + 0.0153} \tag{155}$$

$$ROLL13 = \frac{7.2557s^2 + 19.0154s - 0.4105}{s^3 + 2.1004s^2 + 1.9758s + 0.3122} \tag{156}$$

$$ROLL15 = \frac{17.8117s^2 + 1.7369s - 0.0235}{s^3 + 1.2057s^2 + 0.3563s + 0.0140} \tag{157}$$

$$ROLL16 = \frac{5.9s^5 6865.1s^4 + 846.8s^3}{s^6 + 382.3478s^5 + 481.5772s^4 + 219.2497s^3 \quad +1405.3s^2 + 0.3s - 0.0001} \tag{158}$$
$$+102.3655s^2 + 16.7149s + 0.0093$$

$$ROLL17 = \frac{1.0201s^2 + 0.0895s + 0.0001}{s^3 + 511.2834s^2 + 55.3382s + 0.0120} \tag{159}$$

$$ROLL20 = \frac{17.8900s^3 + 2.2496s^2 + 3.6025s}{s^4 + 1.2522s^3 + 0.5738s^2 + 0.2622s + 0.0430} \tag{160}$$

$$ROLL21 = \frac{8.6589s^3 + 1.1174s^2 + 1.7147s}{s^4 + 1.2432s^3 + 0.5744s^2 + 0.2565s + 0.0423} \tag{161}$$

$$ROLL22 = \frac{8.9174s^3 + 1.0869s^2 + 1.8253s}{s^4 + 1.1564s^3 + 0.4693s^2 + 0.2465s + 0.0437} \tag{162}$$

$$ROLL23 = \frac{9.0661s^3 + 1.1145s^2 + 1.8559s}{s^4 + 1.1305s^3 + 0.4286s^2 + 0.2413s + 0.0437} \tag{163}$$

$$LFE3 = \frac{26s^4 - 27721s^3 - 3330s^2 - 5666s + 13}{s^5 + 1511s^4 + 1294s^3 + 17754s^2 + 2614s + 3684} \tag{164}$$

$$LFE4 = \frac{-18.3700s^3 - 1.8740s^2 - 3.6420s + 0.0193}{s^4 + 0.8348s^3 + 11.7391s^2 + 1.5563s + 2.3525} \tag{165}$$

$$LFE5 = \frac{-18.3801s^2 - 0.1028s - 0.0320}{s^3 + 0.7400s^2 + 11.4649s + 0.3246} \tag{166}$$

$$LFE6 = \frac{-7.4482s^4 - 2235.2s^3 - 227.27s^2 - 451.95s + 10.074}{s^5 + 50.467s^4 + 39.365s^3 + 766.33s^2 + 111.03s + 160.38} \tag{167}$$

$$LFE10 = \frac{-0.0870s^4 - 101.1190s^3 - 10.6290s^2 - 19.7662s + 0.5017}{s^5 + 8.5594s^4 + 18.1196s^3 + 88.6598s^2 + 15.9504s + 17.5407} \tag{168}$$

$$LFE11 = \frac{-5.9s^4 - 6865.1s^3 - 843.0s^2 - 1406.9s + 0.5}{s^5 + 382.0s^4 + 345.4s^3 + 4315.9s^2 + 643.8s + 895.5} \tag{169}$$

$$LFE12 = \frac{-1.7s^4 - 1980.2s^3 - 242.4s^2 - 405.7s + 0.3}{s^5 + 226.4s^4 + 209.0s^3 + 2554.9s^2 + 382.0s + 530.0} \tag{170}$$

$$LFE13 = \frac{-2.7s^4 - 3150.2s^3 - 386.7s^2 - 645.6s + 0.3}{s^5 + 351.5s^4 + 286.3s^3 + 3947.1s^2 + 236.0s + 824.2} \tag{171}$$

$$LFE14 = \frac{-6.7s^4 - 7743.4s^3 - 953.2s^2 - 1587.2s + 0.1}{s^5 + 853.8s^4 + 648.7s^3 + 9576.5s^2 + 223.6s + 2004.7} \tag{172}$$

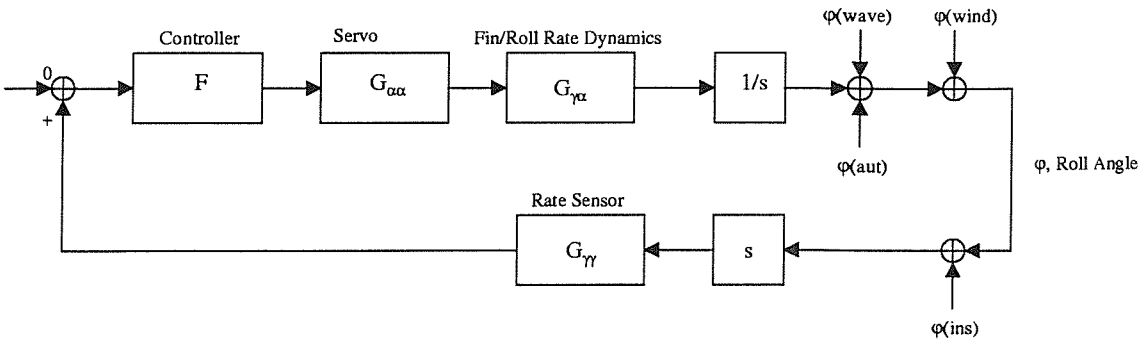

Figure 146: Flow Digram of a Roll Stabilisation System

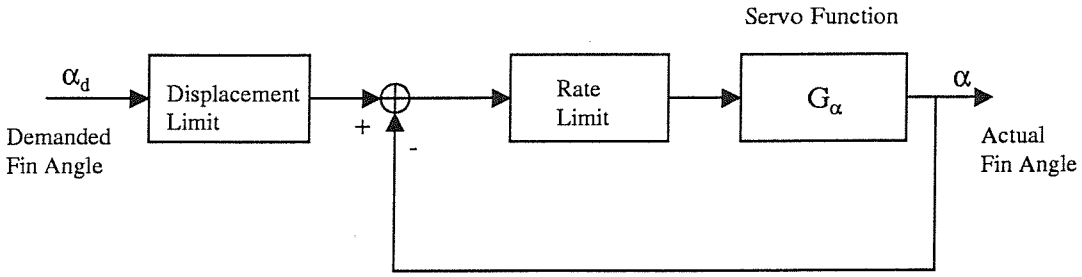

Figure 147: Flow Digram of the Fin Servo Dynamics